

Modeling of CO₂ Absorption from Gas Mixtures Using Chemical Absorbents in Adiabatic Packed-Beds

by

Rui Wang

B.S. Petroleum Engineering, China University of Petroleum, 2017

Submitted to the Graduate Faculty of
The Swanson School of Engineering in partial fulfillment
of the requirements for the degree of
Master of Science in Petroleum Engineering

University of Pittsburgh

2019

UNIVERSITY OF PITTSBURGH
SWANSON SCHOOL OF ENGINEERING

This thesis was presented

by

Rui Wang

It was defended on

July 5, 2019

and approved by

George E. Klinzing, Ph.D., Instructor
Department of Chemical and Petroleum Engineering

Hseen Baled, Ph.D., Assistant Professor
Department of Chemical and Petroleum Engineering

Thesis Advisor: Badie I. Morsi, Ph.D., Professor
Department of Chemical and Petroleum Engineering

Copyright © by Rui Wang

2019

Modeling of CO₂ Absorption from Gas Mixtures Using Chemical Absorbents in Adiabatic Packed-Beds

Rui Wang, M.S.

University of Pittsburgh, 2019

A five-components comprehensive mathematical model for CO₂ absorption from different gaseous mixtures by aqueous solutions of AMP (2-amino-2-methyl-1-propanol) and sodium glycinate (NaGly) in a countercurrent adiabatic packed-bed absorber was developed. The model was implemented in MATLAB 2017b and used to predict, among others, the profiles of CO₂ absorption efficiency, CO₂ loading, and gas-phase and liquid-phase temperatures. The model predictions were first validated using four different runs of the AMP experimental data by Tontiwachwuthikul et al. (1992). In general, the model predicted the experimental data with good accuracy.

The validated model was used to predict the behavior of a small-scale (0.1 m ID) packed-bed absorber with (13 mm ceramic Berl Saddle) for CO₂ capture from a CO₂-air gaseous mixture using SG under identical inlet conditions to those of AMP. A direct comparison between the two absorbents showed that AMP has higher CO₂ absorption efficiency and CO₂ loading than those of SG due to the former's greater reaction rate constant (k_2) under similar temperatures.

The validated model was also used to conduct a parametric study to investigate the behavior of a large-scale (1.5 m ID) absorber packed with 13 mm ceramic Berl Saddle for CO₂ capture from CO₂-N₂ gaseous mixtures using AMP and SG. The system pressure, liquid temperature, superficial liquid and gas velocities, CO₂ mole fraction and packing type were varied in this study. The model predictions indicated that increasing system pressure, liquid temperature,

superficial liquid and gas velocities, and CO₂ mole fraction led to increasing the CO₂ absorption efficiency and CO₂ loading by both absorbents. This behavior was related respectively to the increase of the gas-residence time, reaction rate constants, gas-liquid mass transfer coefficients and the wetted specific area of the packing used. Among these variables, system pressure appeared to have the strongest effect on CO₂ absorption efficiency. Also, the Metal Pall Ring 25 mm random packing with the largest specific wetted area showed the highest CO₂ absorption efficiency when compared with those of the other four packings used.

Table of Contents

Nomenclature	xvi
Acknowledgment.....	xix
1.0 Introduction and Background	1
1.1 CO₂ Capture Methods.....	8
1.1.1 Physical Methods.....	8
1.1.2 Chemical Methods.....	10
1.2 CO₂ Packed-Bed Absorbers.....	16
1.3 Gas-liquid Mass Transfer in Packed-Beds.....	20
1.4 Flooding in Countercurrent Packed-Bed Absorbers	27
1.5 Pressure Drop and Liquid Holdup	33
2.0 Objective	37
3.0 Model Development for CO₂ Absorption in an Adiabatic Packed-Bed.....	40
3.1 Model Assumptions	41
3.2 Model Equations	41
3.2.1 Material Balance	42
3.2.1.1 Material Balance in the Gas-Side.....	43
3.2.1.2 Material Balance in the Liquid-Side	46
3.2.2 Energy Balance.....	48
3.2.2.1 Energy Balance in the Gas-Side	48
3.2.2.2 Energy Balance in the Liquid-Side	50
3.2.3 Solution Method	54

3.3 Model Equation Parameters.....	56
3.3.1 Gas Mixture Density	57
3.3.2 Gas Mixture Viscosity.....	58
3.3.3 Gas Mixture Thermal Conductivity	59
3.3.4 Gas/Gas Diffusivity	61
3.3.5 Gas/Liquid Diffusivity	63
3.3.6 Henry’s Law Constant.....	65
3.3.7 Liquid/Liquid Diffusivity	67
3.3.8 Heat of Absorption.....	68
3.3.9 Water Vapor Pressure	69
3.3.10 Latent Heat of Water Vaporization.....	70
3.3.11 Reaction Mechanism.....	70
3.3.12 Reaction Rate Constant	71
3.3.13 Mass Transfer Coefficients.....	73
3.3.14 Heat Transfer Coefficients	74
4.0 Validation of the Model Predictions Using the Data by	
Tontiwachwuthikul Et Al. [93] for AMP	77
4.1 Equation Parameters for CO₂-AMP System	77
4.1.1 Heat Capacity of the Gases Used	77
4.1.2 Viscosity of the Gases Used	79
4.1.3 Thermal Conductivity of the Gases Used	81
4.1.4 Density of AMP Aqueous Solutions.....	83
4.1.5 Viscosity of AMP Aqueous Solutions	85

4.1.6	Surface Tension of AMP Aqueous Solutions	87
4.1.7	Heat Capacity of AMP Aqueous Solutions	89
4.2	Comparison Between Model Predictions and the Data by Tontiwachwuthikul Et Al. [93]	92
4.3	Model Predictions of CO ₂ Absorption from CO ₂ -Air Mixtures Using SG	100
4.3.1	Equation Parameters for CO ₂ -SG System	100
4.3.1.1	Diffusivity of CO ₂ in SG Aqueous Solution	100
4.3.1.2	Henry's Law Constant of CO ₂ in SG in Water Solution.....	101
4.3.1.3	Density of SG Aqueous Solutions	103
4.3.1.4	Viscosity of SG Aqueous Solutions.....	104
4.3.1.5	Surface Tension of SG Aqueous Solutions	106
4.3.1.6	Heat Capacity of SG Aqueous Solutions	107
4.3.2	Model Predictions of CO ₂ Absorption Using SG and Comparison with AMP	110
5.0	Prediction of the Behavior of a Large-Scale Absorber.....	120
5.1	Effect of System Pressure	121
5.2	Effect of Liquid Temperature	128
5.3	Effect of Superficial Liquid Velocity	134
5.4	Effect of CO ₂ Mole Fraction in the Inlet Gas Feed	140
5.5	Effect of Packing Type	146
5.6	Comparison Between the Performance of AMP and SG Absorbents	152
6.0	Concluding Remarks	156
7.0	Future Work.....	159

Bibliography 160

List of Tables

Table 1-1: A Typical Flue gas Composition [26]	6
Table 1-2: Different Amines and Amino Acids for CO ₂ Absorption	16
Table 1-3: Correlations for Predicting Mass Transfer Coefficients in Countercurrent Packed-beds	24
Table 1-4: Packing Used in Gas Absorbers [115]	27
Table 1-5: Flooding Correlations in Countercurrent Packed-bed Absorbers [117].....	29
Table 1-6: Values of Characteristic Parameters of Packings for Billet and Schulte's Equation [108]	34
Table 1-7: Values of Characteristic Parameters of Packings for Stichlmair's Equation [125]	35
Table 3-1: Critical Temperature, Critical Pressure and Acentric Factor for the Gases Used [127]	58
Table 3-2: Typical Gases Boiling Point.....	60
Table 3-3: Atomic Diffusion Volume and Diffusion Volume of Typical Molecules [133].....	62
Table 3-4: Association Parameters of Different Solvents.....	67
Table 3-5: Characteristics of Different Packings.....	74
Table 4-1: Inlet Stream Conditions Used in Our Model.....	93
Table 4-2: Inlet Stream Conditions Used in the Validated Model for CO ₂ -SG Solutions	111
Table 5-1: Inlet Stream Conditions Used in the Large-Scale Absorber	121
Table 5-2: Effect of Pressure on the Absorber Performances.....	122
Table 5-3: Effect of Liquid Temperature on the Absorber Performances	128
Table 5-4: Effect of Superficial Liquid Velocity on the Absorber Performances	134

Table 5-5: Effect of CO ₂ Mole Fraction on the Absorber Performances	140
Table 5-6: Effect of Packing Type on the Absorber Performances	147
Table 5-7: Inlet Parameters for AMP and SG Aqueous Solution Used.....	152

List of Figures

Figure 1-1: Global Surface Temperature From 1901-2015 [4]	1
Figure 1-2: Greenhouse Gas Emission Sources [7]	2
Figure 1-3: History of CO ₂ Emission due to Fossil Fuel Combustion [11].....	3
Figure 1-4: Precombustion CO ₂ Capture Process [19]	4
Figure 1-5: Postcombustion CO ₂ Capture from Flue Gas [19].....	6
Figure 1-6: A Schematic of a Typical Chemical Absorption Process [42].....	11
Figure 1-7: Amino Acid (a) and Zwitterion Structure (b)	14
Figure 1-8: Packed Column Structure Arrangement [92].....	17
Figure 1-9: Experimental set-up for CO ₂ Chemical Absorption by Tontiwachwuthikul et al. [100]	19
Figure 1-10: A Schematic of Two-Film Theory Schematic Plot.....	21
Figure 1-11: Leva's Pressure Drop Correlation [118]	32
Figure 3-1: Schematic of the packed-bed absorber.....	40
Figure 3-2: Schematic Plot of Control Volume	42
Figure 3-3: Gas-Side Control Volume.....	44
Figure 3-4: Liquid Side Control Volume.....	46
Figure 3-5: Algorithm for Gas Absorption in Packed-bed Absorber [98].....	55
Figure 3-6: Correlated CO ₂ Diffusivity as a Function of Temperature and AMP Concentration	65
Figure 3-7: Correlated CO ₂ Henry's Law Constant as a Function of Temperature and AMP Concentration	66
Figure 3-8: Comparison Between the Reaction Rate Constant (k_2) for AMP and SG [144, 145]	72

Figure 4-1: Heat Capacity of Gases as a Function of Temperature	79
Figure 4-2: Viscosity of Gases as a Function of Temperature.....	81
Figure 4-3: Thermal Conductivity of Gases as a Function of Temperature	83
Figure 4-4: Density of AMP Aqueous Solutions as a Function of Their Mole Fractions	85
Figure 4-5: Viscosity of AMP Aqueous Solutions as a Function of Their Mole Fractions.....	87
Figure 4-6: Surface Tension of AMP Aqueous Solutions as a Function of Their Mole Fractions	89
Figure 4-7: Heat Capacity of AMP Aqueous Solutions as a Function of Their Mole Fractions..	91
Figure 4-8: Comparison Between CO ₂ Loading of Experimental Data [93] and Model Predictions	95
Figure 4-9: Comparison Between Liquid Temperature of Experimental Data [93] and Model Predictions	96
Figure 4-10: Model Predictions of Gas Temperature	97
Figure 4-11: Comparison Between CO ₂ Mole Fraction of Experimental Data [93] and Model Predictions	98
Figure 4-12: Predicted Enhancement Factor and Hatta Number Along the Absorber	99
Figure 4-13: Correlated CO ₂ Diffusivities in SG Aqueous Solutions	101
Figure 4-14: Correlated Henry's Law Constant for CO ₂ in SG Aqueous Solutions	102
Figure 4-15: Density of SG Aqueous Solutions as a Function of Their Mole Fractions.....	104
Figure 4-16: Viscosity of SG Aqueous Solutions as a Function of Their Mole Fractions	105
Figure 4-17: Surface Tension of SG Aqueous Solutions as a Function of Their Mole Fractions	107
Figure 4-18: Heat Capacity of SG Aqueous Solutions as a Function of Their Mole Fractions .	109
Figure 4-19: CO ₂ Absorption Efficiency Using AMP and SG	113

Figure 4-20: CO ₂ Mole Fraction Profiles Using AMP and SG	114
Figure 4-21: CO ₂ Loading Profiles Using AMP and SG	115
Figure 4-22: Liquid Temperature Profiles Using AMP and SG	116
Figure 4-23: Gas Temperature Profiles using AMP and SG	117
Figure 4-24: Enhancement Factor Profile Using AMP and SG.....	118
Figure 4-25: Hatta Number Profiles Using AMP and SG	119
Figure 5-1: Effect of Pressure on CO ₂ Absorption by AMP Aqueous Solutions (A, B, C, D)...	124
Figure 5-2: Effect of Pressure on CO ₂ Absorption by AMP Aqueous Solutions (E, F, G, H) ...	125
Figure 5-3: Effect of Pressure on CO ₂ Absorption by SG Aqueous Solutions (A, B, C, D)	126
Figure 5-4: Effect of Pressure on CO ₂ Absorption by SG Aqueous Solutions (E, F, G, H).....	127
Figure 5-5: Effect of Liquid Temperature on CO ₂ Absorption Using AMP Aqueous Solutions (A, B, C, D).....	130
Figure 5-6: Effect of Liquid Temperature on CO ₂ Absorption Using AMP Aqueous Solutions (E, F, G, H)	131
Figure 5-7: Effect of Liquid Temperature on CO ₂ Absorption Using SG Aqueous Solution (A, B, C, D)	132
Figure 5-8: Effect of Liquid Temperature on CO ₂ Absorption Using SG Aqueous Solutions (E, F, G, H)	133
Figure 5-9: Effect of Liquid Velocity on CO ₂ Absorption by AMP (A, B, C, D)	136
Figure 5-10: Effect of Liquid Velocity on CO ₂ Absorption by AMP (E, F, G, H).....	137
Figure 5-11: Effect of Liquid Velocity on CO ₂ Absorption by SG (A, B, C, D).....	138
Figure 5-12: Effect of Liquid Velocity on CO ₂ Absorption by SG (E, F, G, H)	139

Figure 5-13: Effect of CO ₂ Mole Fraction on Absorber Performance using AMP Aqueous Solutions (A, B, C, D).....	142
Figure 5-14: Effect of CO ₂ Mole Fraction on Absorber Performance using AMP Aqueous Solutions (E, F, G, H)	143
Figure 5-15: Effect of CO ₂ Mole Fraction on Absorber Performance using SG Aqueous Solutions (A, B, C, D).....	144
Figure 5-16: Effect of CO ₂ Mole Fraction on Absorber Performance using SG Aqueous Solutions (E, F, G, H)	145
Figure 5-17: Effect of Packing Type on CO ₂ Absorption Using AMP Aqueous Solutions (A, B, C, D).....	148
Figure 5-18: Effect of Packing Type on CO ₂ Absorption Using AMP Aqueous Solutions (E, F, G, H).....	149
Figure 5-19: Effect of Packing Type on CO ₂ Absorption Using SG Aqueous Solutions (A, B, C, D).....	150
Figure 5-20: Effect of Packing Type on CO ₂ Absorption Using SG Aqueous Solutions (E, F, G, H).....	151
Figure 5-21: Comparison Between AMP and SG (A, B, C, D).....	154
Figure 5-22: Comparison Between AMP and SG (E, F, G, H)	155

Nomenclature

a	Specific packing area	(m^{-1})
a_w	Specific wetted packing area	(m^{-1})
C	Concentration	mol/m^3
C_p	Heat Capacity	$(\text{J}/\text{mol}/\text{K})$
D_c	Column diameter	(m)
d_{eq}	Equivalent diameter of the packing	(m)
d_p	Diameter of packing Particle	(m)
D	Diffusivity	(m^2/s)
E	Enhancement factor	$(-)$
E_1	First-order enhancement factor	$(-)$
E_i	Instantaneous enhancement factor	$(-)$
g	Acceleration due to gravity	(m/s^2)
G	Superficial gas molar velocity	$(\text{mol}/\text{m}^2/\text{s})$
G'	Superficial gas mass velocity	$(\text{kg}/\text{m}^2/\text{s})$
G_B	Superficial gas molar velocity of inert gas	$(\text{mol}/\text{m}^2/\text{s})$
Ha	Hatta number	$(-)$
He	Henry's law constant	$(\text{Pa}\cdot\text{m}^3/\text{mol})$
ΔH	Heat of reaction	(J/mol)
ΔH_{LV}	Latent heat of vaporization	(J/mol)
k_L	Liquid side mass transfer coefficient	(m/s)

k_G	Gas side mass transfer coefficient	(mol/Pa/ m ² /s)
k_2	Reaction rate constant	(m ³ /mol/s)
L	Superficial liquid molar velocity	(mol/m ² /s)
L'	Superficial liquid mass velocity	(kg/m ² /s)
M	Molecular weight	(g/mol)
P	Pressure	(Pa)
Pr	Prandtl number	(-)
R	Gas constant	(m ³ Pa K ⁻¹ mol ⁻¹)
Sc	Schmidt number	(-)
St	Stanton number	(-)
St_H	Stanton number for heat transfer	(-)
T	Temperature	(K)
u	Superficial velocity	m/s
X_2	Mole fraction of absorbents in solution	(-)
y	Mole fraction of gas component	(-)
Y	Molar ratio between single gas and inert gas	(mol/mol)

Greek Letters

α	Loading, mol CO ₂ /initial Amine or Amino acid	(-)
β_L	Liquid hold up	(-)
γ	Stoichiometric number	(-)
ρ	Density	(kg/m ³)
ν	Kinetic viscosity	(m ² /s)

μ	Dynamic viscosity	(Pa.s)
λ	Thermal conductivity	(W/m/K)
σ	Surface tension	(N/m)
ε	Packing porosity	(-)
ϵ_G	Gas hold up	(-)

Subscripts

A	CO ₂
B	Inert Gas (i.e. Air or N ₂)
P	Product
R	Absorbent (i.e. AMP or SG)
S	H ₂ O
L	Liquid
G	Gas

Acronyms

AMP	2-amino-2-methyl-1-propanol
IL	Ionic liquid
SG	Sodium glycinate

Acknowledgment

First and foremost, I would like to thank my advisor Professor Badie I. Morsi for giving me a great opportunity to do research in the area which I'm interested in. I feel grateful for his tremendous inspiration, mentoring, and selfless guidance to me to thoroughly learn and think. I would like to thank Professors George Klinzing and Hseen Baled for serving at my defense committee.

Thanks to all the Reactor and Process Engineering Laboratory (RAPEL) research group members (Dr. Omar Basha, Mr. Husain Ashkanani, Ms. Sudesna Banerjee) for helping and sharing their research experiences with me. I also would like to thank all the professors who taught me and all the staff who helped me at the Department of Chemical and Petroleum Engineering, University of Pittsburgh.

To Qiudi Meng, thank you for all your love and firm support.

Last but not least, I would like to present my gratitude to my parents and grandparents. Thank you all for your nurture and persistent encouragement.

1.0 Introduction and Background

Global warming has dramatic effects on humans and the environment [1], such as irregular precipitation patterns, frequent droughts and heat waves, strong and intense hurricanes, 1-4 feet rise of sea level, and vanishing ice in the Arctic [2]. The global average temperature has been rising fast in the past decades [3]. Based on the earth's temperature in 1901,

Figure 1-1 shows the temperature is anomalously fluctuating since the industrial revolution [4] and by the end of 20th century to present time, the rise of the earth's surface temperature has been far above that of the pre-industrial period.

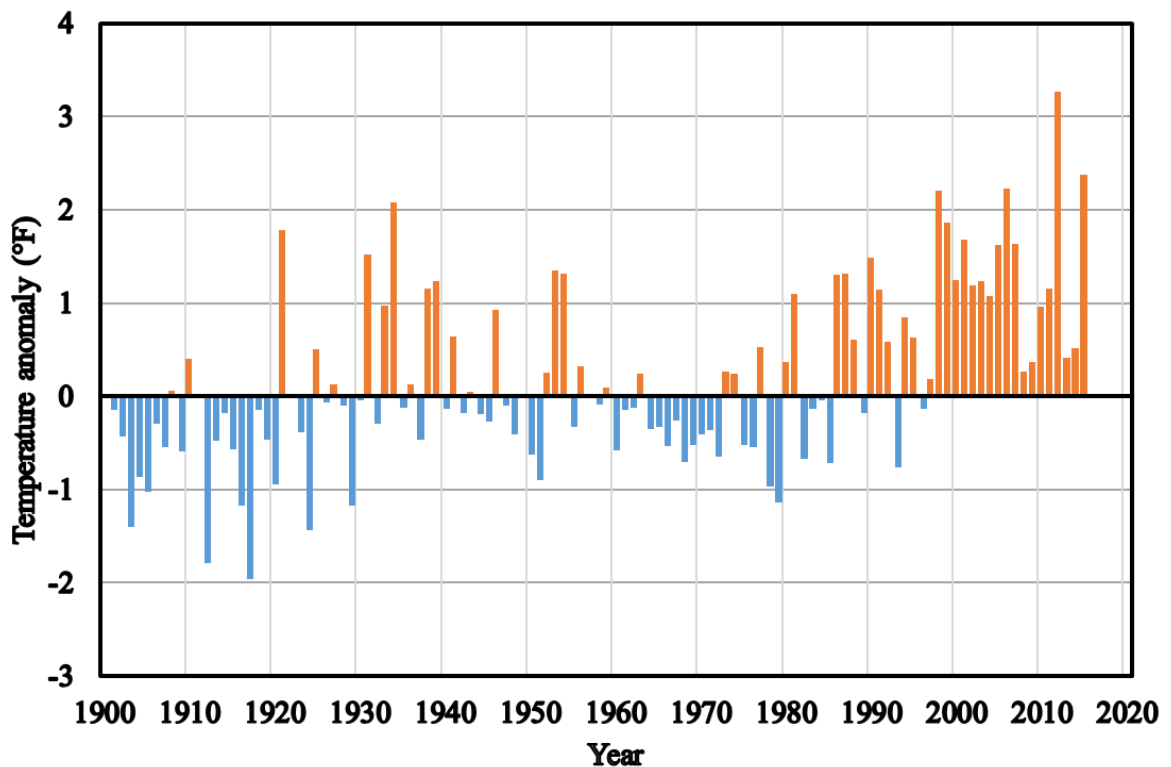


Figure 1-1: Global Surface Temperature From 1901-2015 [4]

This anomaly of temperature changes have been linked to the rise of the atmospheric concentrations of greenhouse gases (GHGs), including carbon dioxide (CO₂), methane (CH₄), and nitrogen oxides (NO_x) due mainly to anthropogenic human activities [5]. Among these GHGs, CO₂, produced by burning fossil fuels, is the most abundant [6], while CH₄ is more potent as a GHG than CO₂. According to IPCC report [7], Figure 1-2, shows that 65% of CO₂ emission comes from fossil fuels and industrial processes.

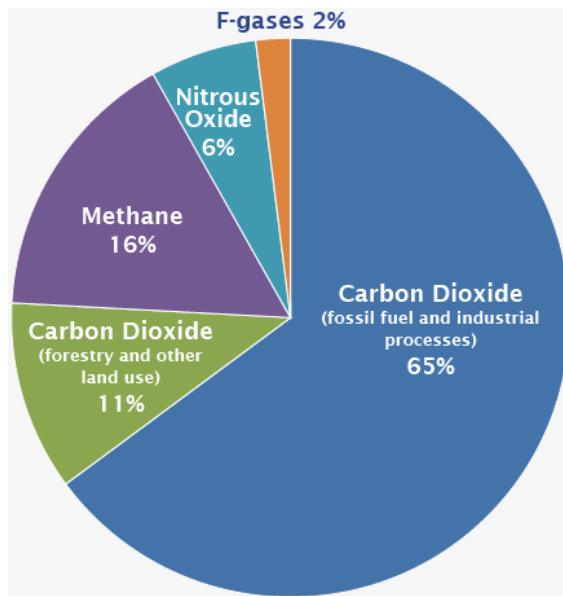


Figure 1-2: Greenhouse Gas Emission Sources [7]

Figure 1-3 shows that increasing the worldwide energy demand for fossil fuels leads to an increasing trend of CO₂ emissions. According to EIA International Energy Outlook, the use of fossil fuels will continue to overtake renewable energy as the main primary energy source for the next few decades [8]. Power generation and other industrial processes, such as cement industries,

are the largest source of CO₂ emissions. Coal is widely used for power generation and releases approximately twice as much CO₂ as natural gas for each unit of electricity generation [9, 10].

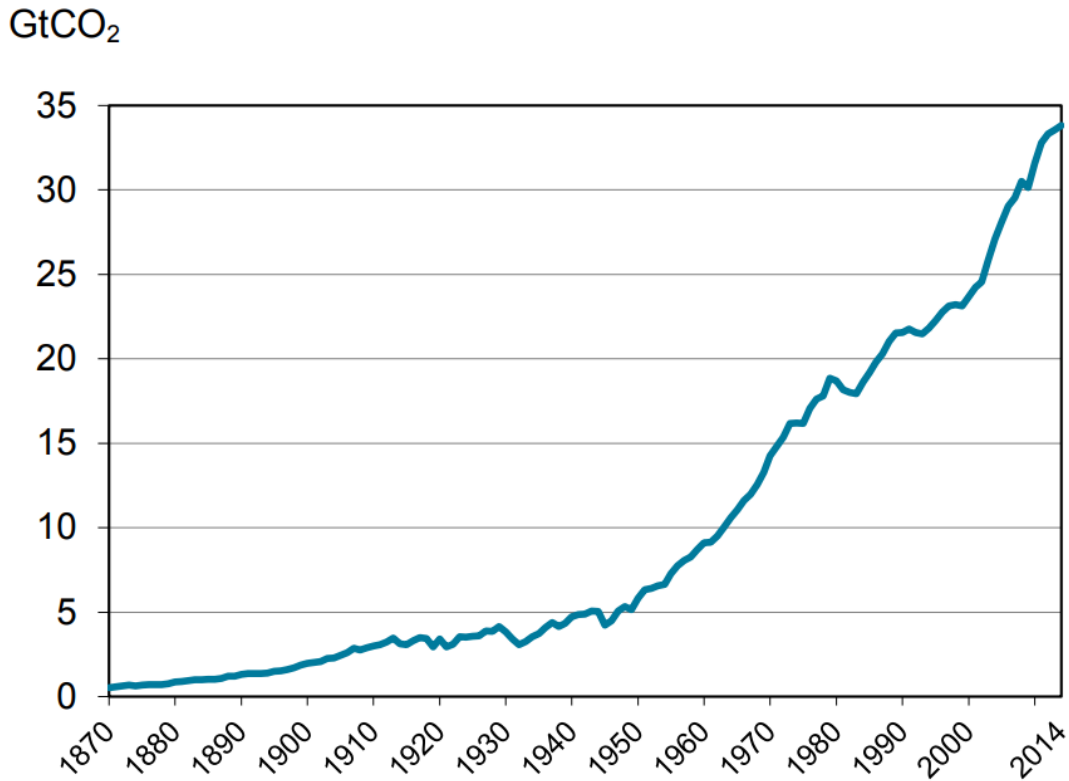


Figure 1-3: History of CO₂ Emission due to Fossil Fuel Combustion [11]

In 2009, Meinshausen et al. [12] reported that if the CO₂ annual emission could not be limited to 50 Gt, global temperature is very likely to increase by 2 °C. In the effort to mitigate CO₂ emission in 2015, the US government planned to cut more than 1,300 metric tons of carbon emission by 2025 [13]. The fact is CO₂ capture and sequestration approach is attractive, since it would allow coal to be used without radically contributing to GHG effects [14, 15]. For its carbon

capture and sequestration (CCS) program, the US government aims at capturing 90% of CO₂ from power plants and industrial processes without substantially increasing the cost of electricity.

CO₂ capture refers to selective removal of CO₂ from fuel gas and flue gas streams. The main processes for carbon capture include: (1) oxy-combustion, (2) precombustion and (3) postcombustion [16, 17]. Oxy-combustion process uses highly concentrated oxygen as the primary oxidant to achieve complete combustion of the coal and accordingly the flue gas stream produced is rich of CO₂ and can be directly captured and sequestered.

Precombustion capture is used along with the Integrated Gasification Combined Cycle (IGCC) in power plants [18] as schematically shown in Figure 1-4.

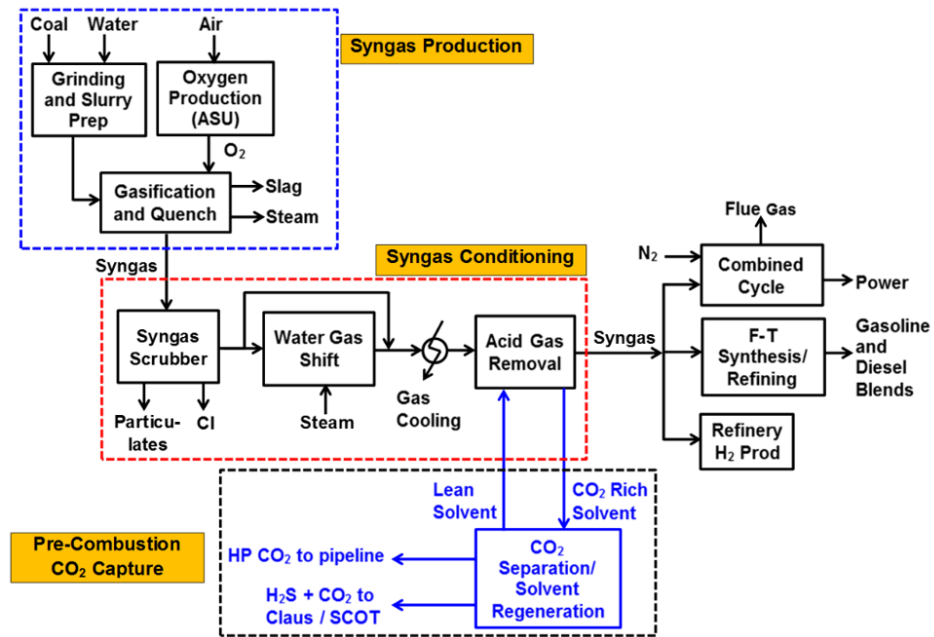
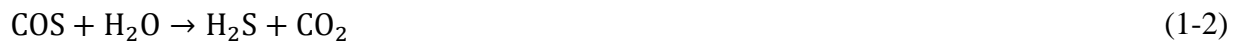


Figure 1-4: Precombustion CO₂ Capture Process [19]

In this process, an air separation unit (ASU) is used to separate O₂ from air. The oxygen along with water and pulverized coal (or coal/water slurry) are fed to a gasifier under controlled conditions to produce a syngas, consisting mainly of CO and H₂ [20]. The syngas is shifted in a water gas shift (WGS) reactor to increase its H₂ content, however, CO₂ is produced along with the H₂ [21]. Also, if carbonyl sulfide (COS) is present, it will be hydrolyzed to produce H₂S and CO₂ [22]. The WGS and COS hydrolysis reactions are given in Equations (1-1) and (1-2), respectively.



Since the WGS reactor is located upstream of the acid gas removal (AGR) facility, H₂S can be absorbed along with CO₂ in AGR units, whereas the shifted gas, consisting mainly of H₂ and CO [21], is sent to turbines.

Postcombustion capture refers to CO₂ capture from flue gas after the fossil fuel has undergone combustion in a boiler [23] as schematically shown in Figure 1-5. In Power generation unit, air and pulverized coal are conveyed to the boiler where combustion takes place at 1600 ~ 1800 °C. The generated steam from the boiler then goes to turbines to generate electricity. Due to the high temperature, N₂ can form nitrogen oxides (NO_x) which can be removed using selective catalytic reduction (SCR) [24]. It should be mentioned that it would be financially feasible for the existing power plants to make some retrofitting to allow for postcombustion of CO₂ capture [25].

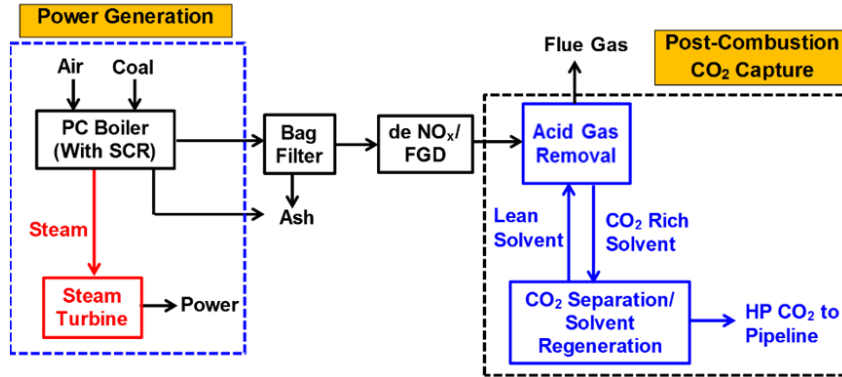


Figure 1-5: Postcombustion CO₂ Capture from Flue Gas [19]

A typical untreated flue gas composition from burning a low-sulfur eastern bituminous coal in a power plant is shown in Table 1-1 [26]. This flue gas needs further preconditioning, including, desulfurization, dehydration and deoxygenation, to prevent degradation of the chemical absorbents used for CO₂ capture.

Table 1-1: A Typical Flue gas Composition [26]

Species	Mole Fraction
H ₂ O	5~7%
O ₂	3~4%
CO ₂	15~16%
Total Hg	1 ppb
CO	20 ppm
Hydrocarbons	10 ppm
HCl	100 ppm
SO ₂	800 ppm
SO ₃	10 ppm
NO _x	500 ppm
N ₂	balance

CO₂ sequestration refers to safe, predictable, reliable, measurable, and verifiable CO₂ storage process [14]. Various sequestration strategies have been proposed, such as injection into geological formations (deep saline aquifers, depleted oil or gas reservoirs and deep coal seams), storage in deep oceans, in addition to CO₂ reduction via chemical or biological processes. CO₂ injection for enhanced oil recovery (EOR) has been widely accepted as an effective technique for oil production for over 40 years [27]. The economic benefits due to the oil produced are attractive and can offset the cost of CO₂ injection [28]. The fact is using CO₂ in EOR is not a typical sequestration option, since CO₂ has to come back to the surface during the EOR process and any CO₂ lost in the formation due to viscous fingering has to be made up. Reservoirs deeper than 6,000 ft (1,829 m) or having a water-drive are preferable for the EOR process using CO₂ [29]. Furthermore, the bottom of the ocean could be a potential place for CO₂ storage in the form of ice-like CO₂ hydrates. This is because the CO₂ density becomes greater than that of seawater at a depth > 3,000 m allowing liquid CO₂ to form a pool [30]. If temperature and pressure conditions are favorable, (i.e., high pressure and low temperature), a hydrate film at the interface between seawater and liquid CO₂ pool will form caging CO₂ [31]. This study is mainly focusing on CO₂ capture.

CO₂ can also be utilized as dry ice or as a food-grade in gaseous beverages or to produce high-value chemicals, such as sodium, ammonium or calcium carbonates or bicarbonates, which can be used or sold to offset some of the cost associated with the CO₂ capture process.

1.1 CO₂ Capture Methods

CO₂ capture includes 5 different methods: physical methods; chemical methods; solid sorbents; membranes; and cryogenics [32, 33]. Solid sorbents, membranes and cryogenics are not the subjects of this study and therefore they will not be here discussed. Only physical and chemical methods are briefly detailed.

1.1.1 Physical Methods

Dedicated mainly for precombustion applications, these methods employ physical solvents to selectively capture CO₂ from shifted syngas streams without any chemical reactions. The physical solvents have to be chemically and thermally stable and highly selective to CO₂. High CO₂ partial pressure and/or low temperature should increase the solubility of CO₂ in the solvents [34]. After CO₂ capture, the solvent is regenerated by pressure swing and/or temperature swing techniques to recover CO₂ and the regenerated clean solvent is recycled back into the process. Several physical solvents have been investigated as discussed in the following.

In 2008, Heintz et al. [35] investigated CO₂ absorption by three perfluorinated physical solvents, including PP10, PP11 and PP25 under high-pressures and temperatures. Under 6-30 bar pressure and 300-500 K temperature, the CO₂ solubility in PP25 was reported to be greater than those in PP10 and PP11. They concluded that PP25 is thermally and chemically stable to be a viable physical solvent for CO₂ capture from fuel gas streams, however, PP25 must be recovered entirely due to its significant solvent loss under high temperatures.

In 2009, Heintz et al. [36] measured the solubility and volumetric liquid-side mass transfer coefficient for CO₂ and H₂S in an ionic liquid (IL), TEGO IL K5, under pressure up to 30 bar and

temperature up to 500 K. They concluded that this solvent was chemically and physically stable and was more selective to H₂S than CO₂.

In 2013, Götz et al. [37] used an IL [EMIM][Tf] for CO₂ capture from biogas and concluded that CO₂ had high solubility in this IL and the ease of its regeneration led to a significant reduction of the electric power consumption in the CO₂ capture process.

In 2013, Basha et al. [38] used experimental data available in the literature for the IL [HMIM][Tf₂N] in Aspen Plus for CO₂ capture from a typical shifted gas steam at 30 bars and temperature ranging from 300 to 500 K in packed-bed absorbers. They used four adiabatic absorbers (2.4 m ID, 30 m high) packed with 0.025 m plastic Pall Rings and reported that 95.12 mol % of CO₂ was absorbed, while only 1.63 mol % of H₂ was lost in the exit stream and concluded that this IL had a strong potential for CO₂ capture.

In 2014, Basha et al. [39] used Aspen Plus for CO₂ capture from a simulated syngas for 400-MW using two ILs in adiabatic packed-beds. In their approach, the experimental data by Heintz et al. [36] on the solubilities of CO₂, H₂, N₂ and H₂S in two ILs, TEGO IL K5 and TEGO IL P51P, at pressures up to 30 bars and temperatures from 300 to 500 K were used in the Peng-Robinson (P-R) Equation-of-state (EOS) with Boston-Mathias α function and standard mixing rules to obtain the binary interaction parameters (δ_{ij} and L_{ij}) between the gas components and the solvent. Their capture process consisted of four identical adiabatic packed-bed absorbers (4.5 m ID, 27 m height, packed with 0.0254 m plastic Pall Rings). They reported CO₂ capture efficiency of 91.28% and 90.59% by the TEGO IL K5 and TEGO IL P51P, respectively.

In 2015, using Aspen Plus, Park et al. [40] compared 3 different physical solvents, including Selexol, Rectisol and Purisol for CO₂ capture using three different absorbers. For Selexol and Purisol, the operating temperature was -10 °C and pressure was 37 bars; and for Rectisol, the

operating temperature was $-20\text{ }^{\circ}\text{C}$ and pressure was 37 bars. The inside diameter (ID) of the absorbers were 1.87 m, 3 m and 2.8 m for Selexol, Rectisol and Purisol, respectively. The absorbers were packed with 75 mm IMTP random packing to a height of 75 m for the three solvents. They found that to achieve 90% CO_2 capture efficiency, a height of 25 m was required for Selexol, while a height of 28 m was required for Rectisol and Purisol. They also calculated the electric energy consumption, hydrogen loss and exhausted solvent flow rate, and found that Selexol was the most efficient solvent among the three solvents used in terms of the electric and thermal energy consumption.

In 2018, Taheri et al. [41] measured CO_2 solubilities in an IL [AMIM][Tf₂N], methanol and a mixture of IL-methanol at different temperatures (313.2, 333.2 and 353.2 K) and pressures up to 65 bar. The binary interaction parameters of UNIFAC-Lei model were introduced by correlating the experimental data. Their result showed that the IL and IL-methanol mixture were more efficient than the methanol alone in CO_2 capture at 243.2 K.

1.1.2 Chemical Methods

Dedicated mainly for postcombustion applications, chemical methods rely on direct reactions between CO_2 and a reactive absorbent often in a packed-bed followed by solvent regeneration, as shown schematically in Figure 1-6 [42]. The flue gas enters the packed-bed from the bottom, while a chemical absorbent enters from the top of the absorber. The absorber contains solid packings to increase the mass transfer between CO_2 and the absorbent. The absorber can be operated in a co-current or a countercurrent mode. The CO_2 -rich solvent is then sent to a regenerator where it is heated to release most of the CO_2 absorbed and the CO_2 -lean solvent is then recycled back into the absorber.

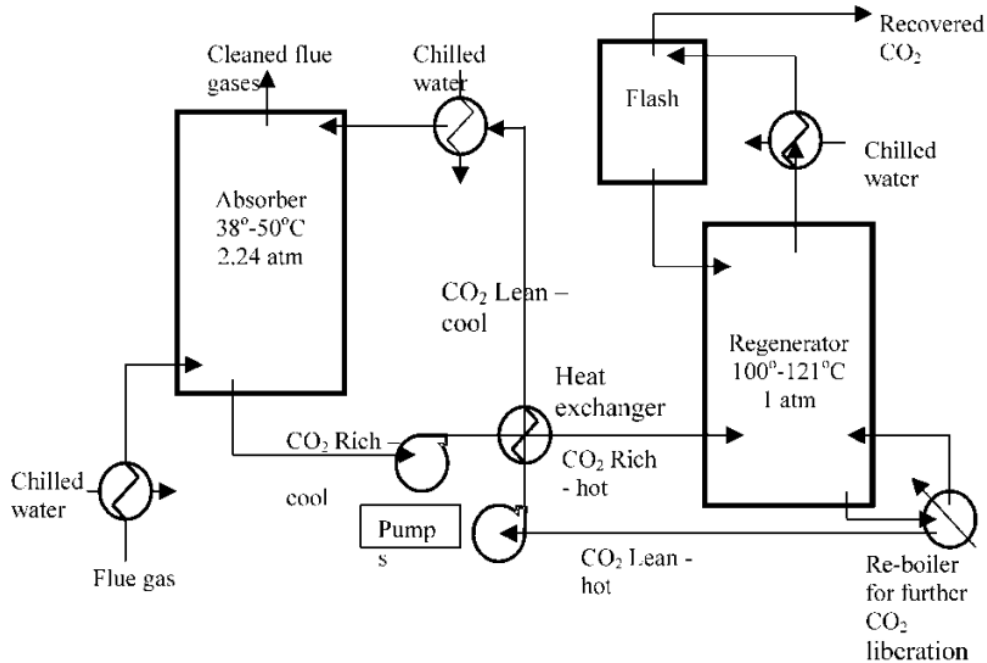


Figure 1-6: A Schematic of a Typical Chemical Absorption Process [42]

The widely used chemical absorbents for CO₂ capture are aqueous ammonia solutions, potassium carbonate solutions, and amines [43]. The Aqua-Ammonia process uses aqueous ammonium hydroxide to capture CO₂ from the postcombustion flue gas. The advantages of this process reside in the fact that ammonia does not cause equipment corrosion and does not suffer from degradation due to the presence of SO_x and O₂ in the flue gas [44]. In addition, the major products of this process are useful fertilizers, including ammonium sulfate and ammonium nitrate [43]. The drawback of this process, however, is ammonia's volatility, leading to its loss in the treated flue gas streams [45, 46]. In 2009, Kozak et al. [47] proposed a chilled ammonia process and constructed a field pilot-plant to capture 15,000 ton of CO₂ per year. The plant included absorber vessels, pressure vessels, circulation pumps, regenerator feed pumps, heat exchangers,

chillers, process instruments and control valves, Programmable Logic Controller (PLC) for process control, and a gas sampling system.

The Benfield process [48], employing potassium carbonate (K_2CO_3) as a solvent, was used to capture CO_2 from flue gas. The overall reaction between CO_2 and potassium carbonate is shown in the following equation (1-3) [49, 50].



In 2008, Ahmadi et al. [51] developed a model following the procedure by Aboudheir et al. [52] to model CO_2 capture from a simulated flue gas using a potassium-based solvent in a packed-bed absorber operating under a high pressure of 20.4 atm. The solvent contained 3.09 mol% K_2CO_3 , 2.85 mol% $KHCO_3$, 91.28 mol% water, 1.25 mol% KBO_2 and 0.28 mol% KVO_3 ; and the simulated flue gas consisted of 10.32 mol% CO_2 , 63 mol% N_2 , 15.09 mol% C_2H_4 , 6.27 mol% Ar and 3 mol% H_2O . The solvent and flue gas flow rates were 5,196.89 and 833.14 kmol/h, respectively. The temperature of the solvent and gas phases were 377.1 K and 321.2 K, respectively. The packed-bed dimensions were 1.219 m ID and 18.29 m height and it was packed with 50 mm steel Hy-pac. Under these conditions, the authors reported that the CO_2 capture efficiency reached 94.9% and their model was able to predict the experimental data with a good accuracy.

In 2009, Yi et al. [53] carried out experiments and modeled CO_2 capture by the Benfield solution in a rotating packed-bed. They reported a 10% deviation between their model predictions and the experimental data. They further used their model to study the effects of liquid flow rate, gas flow rate, rotating speed, temperature and end effects on the gas phase volumetric mass transfer coefficients.

In 2012, Mumford et al. [54] described the performance of a pilot-plant absorber for CO₂ capture using 30 wt% potassium carbonate (K₂CO₃) solution at a temperature of 240 °C and pressure of 1 kPag. The absorber dimensions were 1.5 m ID and 7 m height and it was packed with steel Sulzer nutter rings. Although only 20% ~ 25% of CO₂ from the flue gas were captured under these conditions, the authors claimed that valuable operating data were obtained, which enabled a process simulation using Aspen Plus and a direct comparison with actual pilot plant data. They reported that the Aspen Plus model predictions were within 5% of the pilot plant data and therefore they claimed their model can contribute to the development of the potassium carbonate process in large-scale CO₂ capture from postcombustion applications.

Alkanolamines and amino acids have also been used for CO₂ capture from postcombustion applications. Monoethanolamine (MEA) [43, 45, 55-60], 2-amino-2-methyl-1-propanol (AMP) [61-73] and sodium glycinate [74-82] are examples of such chemical absorbents.

Amino acids could form a zwitterion due to the presence of the basic amine group and the acidic carboxylic acid group in the same structure, as shown in Figure 1-7 (a). If an internal transfer of a hydrogen ion from the carboxylic acid group to the basic amine group, this will lead to an ion containing both negative and positive charges, as shown in Figure 1-7 (b). This is called a “zwitterion,” which is the form that amino acid exists even in a solid state. As a whole, a zwitterion is neutral, but it may contain separate groups which are positively or negatively charged.

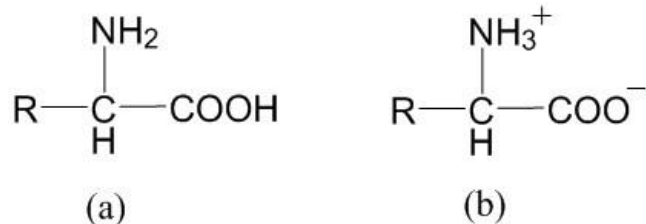
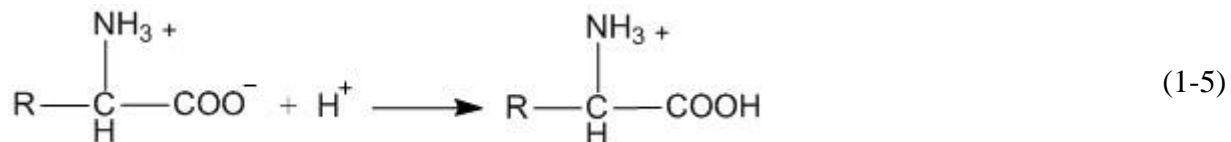
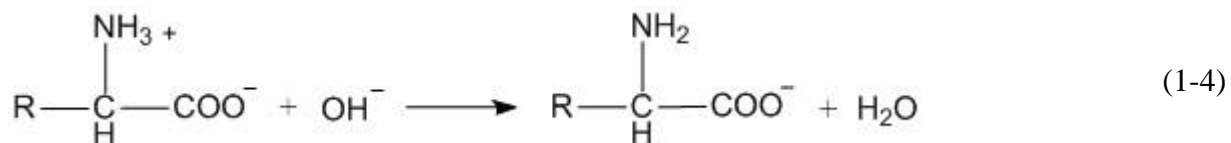
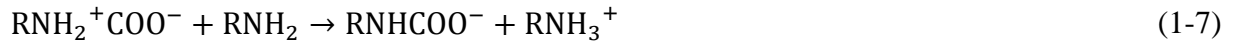


Figure 1-7: Amino Acid (a) and Zwitterion Structure (b)

For a zwitterion, if a hydroxide ion (OH^-) is added from NaOH , the hydrogen ion is removed from $-\text{NH}_3^+$ group as in Equation (1-4). On the other hand, if an acid ion (H^+) is added from HCl , the $-\text{COO}^-$ group of a zwitterion will pick up a hydrogen ion as in Equation (1-5).



In 1968, Caplow et al. [83] proposed a zwitterion formation mechanism for MEA, as shown in Equation (1-6). This mechanism was reintroduced by Danckwerts et al. [60, 64] in 1979 and was generally accepted. Equation (1-7) represents the base deprotonation of CO_2 -amine zwitterion [84-86]. Thus, the carbamate formation due to CO_2 reaction with MEA could be written as Equation (1-8). This carbamate is stable and cannot be hydrolyzed. Thus, the equilibrium CO_2 loading capacity of MEA is limited to 0.5 mol/mol.

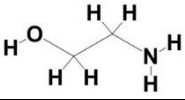
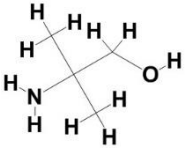
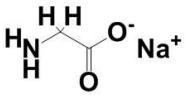


However, for hindered amine (e.g., AMP), the carbamate formed will undergo hydrolysis to produce amine and bicarbonate, as shown is Equation (1-9) [73, 87]. Hence, the integrated bicarbonate formation reaction between CO₂ and AMP solution is shown as Equation (1-10).



Since having similar functional group, sodium glycinate has a similar reaction mechanism as AMP [88]. A comparison between their absorption mechanisms is given in Table 1-2. According to the stoichiometry, the equilibrium CO₂ loading capacity of AMP and sodium glycinate is 1 mol/mol.

Table 1-2: Different Amines and Amino Acids for CO₂ Absorption

Chemical Absorbents	Structure	Chemical Reactions	References
MEA		$\text{CO}_2 + 2\text{RNH}_2 \rightarrow \text{RNHCOO}^- + \text{RNH}_3^+$	[59, 65, 89]
AMP		$\text{CO}_2 + \text{AMP} + \text{H}_2\text{O} \rightarrow \text{AMPH}^+ + \text{HCO}_3^-$	[64, 90]
Sodium Glycinate		$\text{CO}_2 + \text{R}'\text{NH}_2 + \text{H}_2\text{O} \rightarrow \text{R}'\text{NH}_3^+ + \text{HCO}_3^-$	[76, 91]

1.2 CO₂ Packed-Bed Absorbers

A packed-bed absorber frequently used in CO₂ capture processes is a hollow cylinder filled with either random or structured packing. Its purpose is to improve the contact between the gas and liquid phases in different processes, including absorption, stripping and distillation. A typical structure of a conventional packed-bed is shown in Figure 1-8.

The function of each part from top to the bottom is discussed in the following. (1) The demister pad, also called mist eliminator, is used to remove the entrained mist from the gas stream. (2) The liquid distributor serves to ensure an even distribution of the liquid in the packed-bed. If the liquid is unevenly distributed across the absorber area, the absorption efficiency will be low because the gas would select the least-resistance path to flow upward driving the liquid toward the wall.

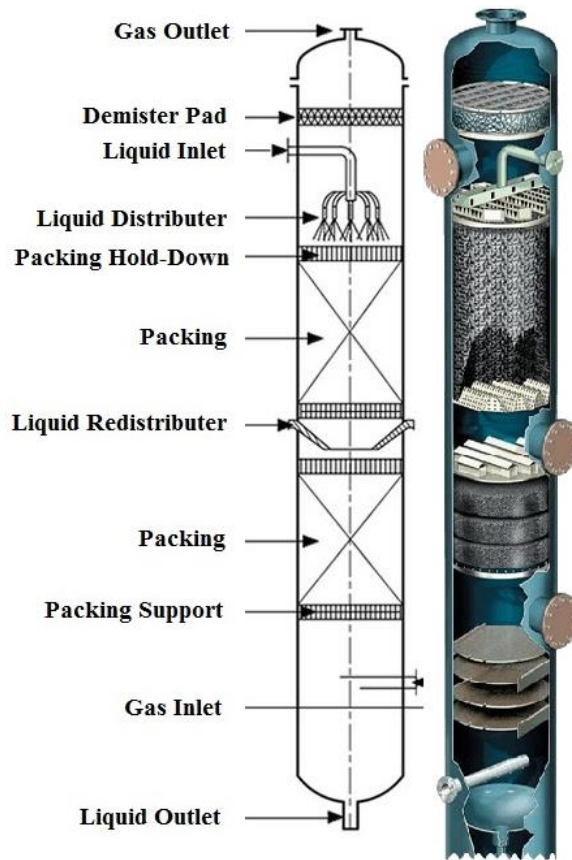


Figure 1-8: Packed Column Structure Arrangement [92]

(3) The packing hold-down is used to keep the packing from moving up due to the high gas throughput. (4) The packing is to enhance the gas-liquid interactions and maximize the mass and heat transfer. (5) The liquid redistributer is required in tall packed-beds to again maximize the gas-liquid interactions. (6) The packing support is used in the absorber to support the packing from falling or moving downward with the liquid. (7) The gas inlet is to make sure that the gas is well distributed at the bottom of the absorber and to eliminate gas channeling (8) the gas and liquid outlets are to ensure no gas nor liquid nor products would accumulate inside the absorber to maintain a continuous process.

Packed-bed absorbers are suited for CO₂ capture because their design parameters have been proven to be reliable, including low pressure drop, adequate heat and mass transfer coefficients and large gas-liquid as well as liquid-solid (wetted) interfacial areas [93]. Treybal [94] developed a computational method for a simple adiabatic three-components physical absorption in a packed-bed, accounting for simultaneous heat and mass transfer. Feintuch and Treybal [95] extended this method to multicomponent systems. Astarita [96] and Danckwerts et al. [97] proposed a design technique for gas-liquid chemical reaction in adiabatic packed-beds. Based on Danckwerts' and Treybal's work, Pandya [98] introduced a modeling procedure considering heat of absorption, solvent evaporation, chemical reaction in the liquid-phase along with mass and heat transfer in the gas and liquid phases. In 1988, Sanyal et al. [99] modeled the Benfield process using similar approach and reached a good agreement between the field data and simulation results.

In 1989, Tontiwachwuthikul et al. [100] built an experimental set-up, schematically shown in Figure 1-9, for measuring CO₂ absorption using NaOH as a chemical absorbent. In 1992, Tontiwachwuthikul et al. [93] conducted experiments for CO₂ absorption from CO₂-air mixture by AMP, NaOH and MEA solutions, using a packed-bed with 0.1 m ID and 7.2 m height containing 12.7 mm ceramic Berl Saddle packing. The packed-bed consisted of six sections (each 1.2 m) and due to liquid redistribution between the sections, the effective packed height in each section was 1.1 m, leading to a total of 6.6 m packing height. The flow rates of the absorbent aqueous solutions and CO₂-air mixture were measured using rotameters and the inlet gas and liquid temperatures were fixed at 15 °C using a constant temperature bath. An infrared gas analyzer was employed to measure the gas-phase composition. The authors reported the liquid temperature, CO₂ loading and CO₂ mole fraction in the gas-phase at each section. They also modeled their

experimental results with MEA based on the procedure by Pandya [98] and reported that their model predictions were in agreement with the experiment results.

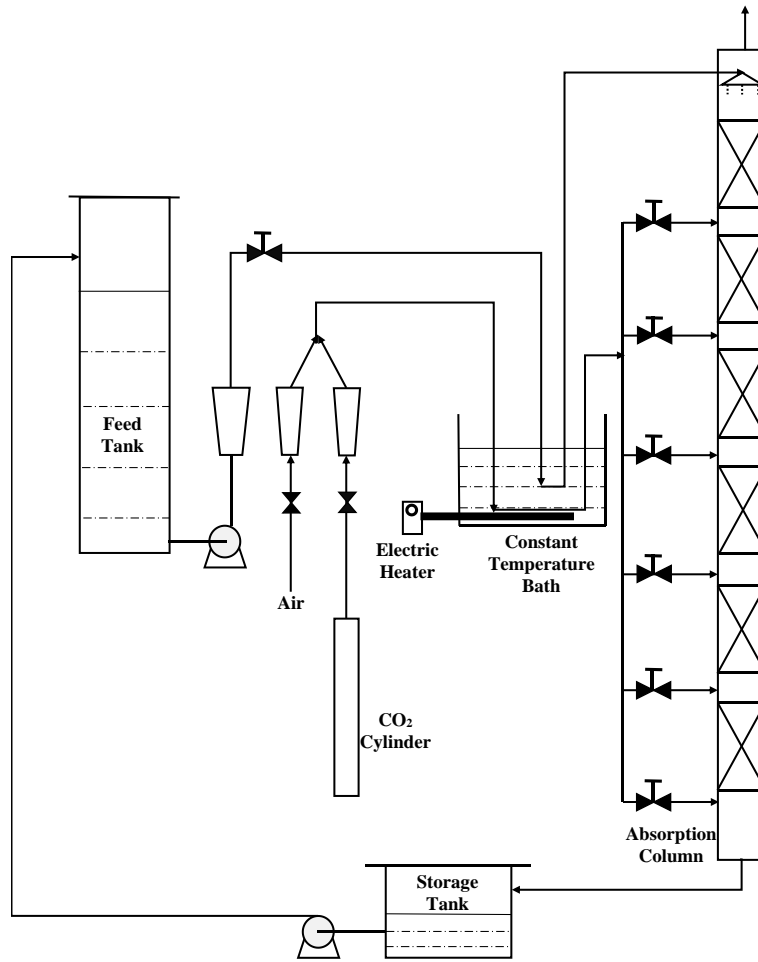


Figure 1-9: Experimental set-up for CO₂ Chemical Absorption by Tontiwachwuthikul et al. [100]

In 2006, Gabrielsen et al. [101] adopted the approach by Pandya [98] for modeling CO₂ capture from CO₂-air mixture using AMP solutions. Three sets of modeling predictions were found to be in agreement with the experimental results given by Tontiwachwuthikul et al. [93]. In 2006,

Aboudheir et al. [52] modeled CO₂ absorption from a mixture with air in AMP solutions using an absorber containing random packing (12.7 mm ceramic Berl Saddle) and structured packing (EX-type laboratory); and reported a good agreement between their model predictions and the experimental results.

1.3 Gas-liquid Mass Transfer in Packed-Beds

The two-film theory was used to describe gas absorption into liquid absorbents whether in physical or chemical methods as shown in Figure 1-10. The absorption takes place as follows:

Step 1: Transport of gas species through gas-bulk to the gas-film (δ_G);

Step 2: Transport of gas species through the gas-film to gas-liquid interface;

Step 3: Transport of the gas species from the gas-liquid interface through the liquid-film (δ_L), where physical absorption or chemical reaction would take place in the liquid film;

Step 4: Transport of the gas species from the liquid-film to the liquid-bulk; and

Step 5: Transport of the products or the gas species in the reverse directions from the liquid-bulk all the way to the gas-bulk.

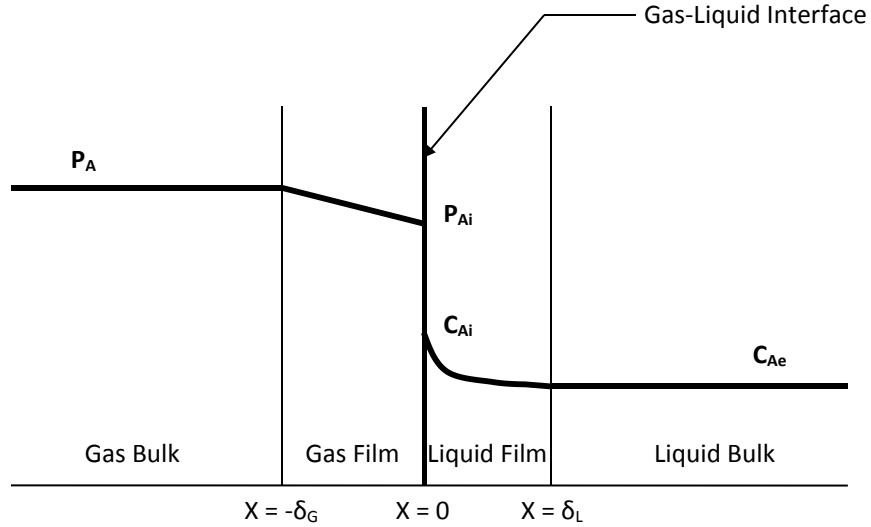


Figure 1-10: A Schematic of Two-Film Theory Schematic Plot

According to this two-film theory, the gas-side mass transfer coefficients, $k_G = D_G/\delta_G$, and the liquid-side mass transfer coefficient, $k_L = D_L/\delta_L$, where D_G and D_L are the diffusivities of the gaseous species in the gas and liquid films, respectively. Also, the mass transfer flux of component A in the gas-film, Equation (1-11) and in the liquid-film, Equation (1-12) are equal.

$$N_A = k_{G,A}(P_A - P_{Ai}) \quad (1-11)$$

$$N_A = Ek_{L,A}(C_{Ai} - C_{Ae}) \quad (1-12)$$

Where E is the enhancement factor due to the chemical reaction. Henry's law, Equation (1-13), is applicable at the interface:

$$H_e = \frac{P_{Ai}}{C_{Ai}} \quad (1-13)$$

The partial pressure of gas (A) at the gas-liquid interface could be calculated using Equation (1-14), obtained by coupling Equations (1-11) through (1-13).

$$P_{Ai} = \frac{P_A + \left(\frac{Ek_{L,A}}{k_{G,A}}\right)C_{Ae}}{1 + \frac{Ek_{L,A}}{k_{G,A}He}} \quad (1-14)$$

Where C_{Ae} is the concentration of CO_2 in liquid at equilibrium, which is assumed to be 0 for an instantaneous second order irreversible reaction. Wellek et al. [102] expressed E in rigorous chemical reaction calculations using Equation (1-15).

$$E = 1 + \frac{1}{\left[\left(\frac{1}{E_i - 1}\right)^{1.35} + \left(\frac{1}{E_1 - 1}\right)^{1.35}\right]^{1/1.35}} \quad (1-15)$$

The instantaneous enhancement factor (E_i), the Hatta number (Ha), and first-order enhancement factor E_1 are calculated using Equations (1-16), (1-17) and (1-18), respectively.

$$E_i = 1 + \left(\frac{C_{R,L}D_R}{bD_{A,L}C_{Ai}}\right) \quad (1-16)$$

$$Ha = \frac{\sqrt{D_{A,L}k_2C_{R,L}}}{k_L} \quad (1-17)$$

$$E_1 = \frac{Ha}{\tanh(Ha)} \quad (1-18)$$

If $Ha > 2$, the reaction is fast, and $E = Ha$.

The mass transfer coefficients of the gaseous species in the gas and liquid sides could be predicted using several correlations available in the literature [103-114]. Table 1-3 lists several correlations to predict the mass transfer coefficients in two-phase flow inside countercurrent packed-beds. Also, Table 1-4 lists different packings frequently used in gas absorbers.

Table 1-3: Correlations for Predicting Mass Transfer Coefficients in Countercurrent Packed-beds

References	Packing	System	Correlation
Sherwood and Holloway [103]	Raschig rings	CO ₂ /Water	$k_L a_w = 550 \left(\frac{\mu_L D_L}{\rho_L} \right)^{0.5} \left(\frac{u_L}{\mu_L} \right)^{0.54}$
Van Krevelen and Hoftijzer [104]		CO ₂ /MEA CO ₂ /DEA	$\frac{k_L \left(\frac{\mu^2}{\rho^2 g} \right)^{1/3}}{D} = 0.015 \left(\frac{L}{a_w \mu} \right)^{2/3} \left(\frac{\mu_L}{\rho D_L} \right)^{1/3}$
Onda et al. [105]	Raschig rings Berl Saddle Sphere Rod	CO ₂ /water CO ₂ /CCl ₄ CO ₂ /CH ₃ OH	$k_L \left(\frac{\rho_L}{\mu_L g} \right)^{1/3} = 0.0051 \left(\frac{\rho_L u_L}{a_w \mu_L} \right)^{2/3} \left(\frac{\mu_L}{\rho_L D_L} \right)^{-1/2} (ad_p)^{0.4}$ $a_w = a \left\{ 1 - \exp \left[-1.45 \left(\frac{\sigma_c}{\sigma_L} \right)^{0.75} Re_L^{0.1} Fr_L^{-0.05} We_L^{0.2} \right] \right\}$ σ_c = critical surface tension of the packing $Re_L = \frac{\rho_L u_L}{a \mu_L}$, $Fr_L = \frac{u_L^2 a}{g}$, $We_L = \frac{\rho_L u_L^2}{a \sigma_L}$
Mohunta et al. [106]	Raschig rings		$k_L a_w = 25 \times 10^{-4} \left(\frac{g \rho_L}{a \mu_L} \right)^{0.66} \left(\frac{g^2 \rho_L}{\mu_L} \right)^{1/9} \left(\frac{\mu_L u_L^3 a^3}{g^2 \rho_L} \right)^{0.25} \left(\frac{\mu_L}{\rho_L D_L} \right)^{-0.5}$
Akita and Yoshida [107]	Berl saddles	Water/O ₂ Glycerol solution/O ₂ 30 vol% glycol solution/O ₂ Methanol/O ₂ 0.15M Na ₂ SO ₃ solution/O ₂	$k_L a_w = 0.6 D_L^{0.5} u_L^{-0.12} \left(\frac{\sigma_L}{\rho_L} \right)^{-0.62} D_c^{0.17} g^{0.93} \epsilon_G^{1.1}$ $\frac{\epsilon_G}{(1 - \epsilon_G)^4} = 0.2 \left(\frac{g d_c^2 \rho_L}{\sigma_L} \right)^{1/8} \left(\frac{g d_c^3}{u_L^2} \right)^{1/12} \left(\frac{u_G}{\sqrt{g d_c}} \right)$ ϵ_G is gas hold up
Billet and Schultes [108]	Raschig ring Ralu flow Pall ring Ralu ring NOR PAC ring Hiflow ring Glitsch ring Glitsch CMR ring TOP Pak ring	CO ₂ /methanol CO ₂ /buffer solution 1 CO ₂ /buffer solution 2 solution CO ₂ -water/air CO ₂ -air/water O ₂ -water/air Chlorine-air/water	$k_L = C_L 12^{1/6} \left(\frac{u_L}{\beta_L} \right)^{1/2} \left(\frac{D_L}{d_h} \right)^{1/2}$ $\frac{a_w}{a} = 1.5 (ad_h)^{-0.5} \left(\frac{u_L d_h}{v_L} \right)^{-0.2} \left(\frac{u_L^2 \rho_L d_h}{\sigma_L} \right)^{0.75} \left(\frac{u_L^2}{g d_h} \right)^{-0.45}$ $k_G = \frac{C_G}{RT} \frac{D_G}{(\epsilon - \beta_L)^{1/2}} \left(\frac{a}{d_h} \right)^{1/2} \left(\frac{u_G}{av_G} \right)^{3/4} \left(\frac{v_G}{D_G} \right)^{1/3}$ C_L and C_G are characteristic parameter of packings d_h is hydraulic diameter of packing, available in Equation (3-112)

Table 1-3 (continued)

References	Packing	System	Correlation
Longo and Gasparella [109]	Pall rings	H ₂ O/LiCl H ₂ O/LiBr H ₂ O/KCOOH	$k_L = 25.1 \left(\frac{D_L}{d_p} \right) \left(\frac{d_p L'}{\mu_L} \right)^{0.45} Sc_L^{0.5}$ $Sc_L = \frac{\mu_L}{\rho_L D}$ $k_G = 1.195 \left[\frac{G'}{\mu_G} / (1 + \beta_L - \varepsilon) \right]^{-0.36} Sc_G^{-0.667}$ $Sc_G = \frac{\mu_G}{\rho_G D_G}$ <p>L' = Superficial liquid mass velocity G' = Superficial gas mass velocity</p>
Hanley et al. [110]	Pall Rings	Air/Isopar	$k_L = \frac{15D_L}{d_{eq}} (Re_L)^{0.5} Sc_L^{0.5}$ $k_G = \frac{0.075D_G}{D_c RT} (Re_G)^{0.5} Sc_G^{0.5}$ <p>d_{eq} is the equivalent particle diameter of the packing</p>
Brunazzi and Paglianti [111]	Mellapak Y BX	CO ₂ -water/air Gensorb 300/air Gensorb 1843/air	$\frac{4k_L \delta}{D_L} = A \frac{Gz^B}{Ka^C}$ $Ka = \frac{\sigma^3 \rho_L}{\mu_L^4 g}; \quad Gz = Re_L Sc_L \frac{\delta}{H}$ $\delta = \left(\frac{3\mu_L}{\rho_L g \sin(\alpha)} \frac{u_L}{\beta_L \sin(\alpha)} \right)^{0.5}$ $U_{L,eff} = \frac{u_L}{\beta_L \sin(\alpha)}$ $U_{G,eff} = \frac{u_G}{(\varepsilon - \beta_L) \sin(\varphi)}$ <p>α is 60° for Mellapak and 69° for BX packing φ is 45° for Mellapak and 60° for BX packing</p> $Sh_G = 0.054 \left[\frac{(U_{G,eff} + U_{L,eff}) \rho_G d_h}{\mu_G} \right]^{0.8} Sc_G^{0.33}$ $d_h = \frac{4\varepsilon}{a}, \quad k_G = \frac{Sh_G D_G}{d_h RT}$ <p>H = height of absorber A, B, C are characteristic constants for packings</p>

Table 1-3 (continued)

References	Packing	System	Correlation
Raynal et al. [112]	Mellapak	CO ₂ /NaOH	$k_L = \sqrt{\frac{4 D_{CO_2} U_{Leff}}{\pi S}}$ $U_{Leff} = \frac{u_L}{\beta_L}$ <p>S is characteristic packing dimension, m</p>
Haroun et al. [113]	Structured packing		$\frac{k_L e}{D_L} = 0.65 \left(\frac{e}{x}\right)^{0.5} Re_L^{0.5} Sc_L^{0.5}$ <p>e is average value of film thickness, m x is total contact length between gas and liquid phases, m</p>
Hanley and Chen [114]	Pall rings IMTP HY-PAK Flexipac Mellapak		$k_L = A_L Re_L Sc_L^{1/3} \left(\frac{D_L}{d_h}\right)$ $k_G = \frac{A_G}{RT} Re_G Sc_G^{1/3} \left(\frac{D_G}{d_h}\right)$ $d_h = \frac{4\varepsilon}{a}$ <p>A_L is characteristic constant for packing, 1 for metal IMTP and 0.33 for sheet metal structured packing A_G is characteristic constant for packing, 0.00473 for metal IMTP and 0.0084 for sheet metal structured packing</p>

Table 1-4: Packing Used in Gas Absorbers [115]

Packing	Materials	Nominal Size, in	Void Fraction, ϵ	Specific Area, ft^{-1}	Packing factor, F_p, ft^{-1}
Raschig rings	Ceramic	0.5	0.64	111	580
		1.0	0.74	58	179
		1.5	0.73	37	95
		2.0	0.74	28	65
Berl Saddle	Ceramic	0.5	0.62	142	240
		1.0	0.68	76	110
		2.0		32	45
Pall rings	Ceramic	1.0	0.94	63	56
		1.5	0.95	39	40
		2.0	0.96	31	27
Metal Intalox (IMTP)	Metal	1.0	0.97	70	41
		2.0	0.98	30	18
Hy-Pac	Metal	1.0	0.96	54	45
		2.0	0.97	29	26
Mellapak 250Y	Metal		0.95	76	20
Mellapak 500Y				152	34
Flexipac 2	Metal		0.93	68	22
Flexipac 4			0.98		6
Norton Intolax 2T	Metal		0.97	65	17
Norton Intolax 3T			0.97	54	13

1.4 Flooding in Countercurrent Packed-Bed Absorbers

In countercurrent two-phase flow in packed-beds, if the velocity of the gas flowing upward is high enough, the liquid flowing downward would be restricted, which is known as flooding. Therefore, when designing an industrial two-phase counter-current flow packed-bed, it is important to delineate the flooding conditions. In a packed-bed containing certain type and size of packing and at a given liquid flow rate, there is an upper limit of the gas velocity, known as flooding velocity ($U_{G,F}$) [115]. Similarly, at a given gas flow rate, there is a definite liquid velocity above which the column will be flooded [116]. Piché et al. [117] summarized several correlations

available in the literature for flooding predictions in countercurrent packed-beds, and several correlations are listed Table 1-5. If the flow pattern is close to flooding point, adjusting either the liquid or gas flow rate is an option to avoid flow instability in the packed-bed.

Table 1-5: Flooding Correlations in Countercurrent Packed-bed Absorbers [117]

References	Packing	System	Correlation	Constraints
Leva [118]	Ceramic Intolax Saddles Ceramic Raschig Rings Metal Raschig Rings Metal Pall Rings Metal Pall Rings	4% solution of NaOH/air + CO2 Water/air CaCl2 solution/air Methanol/ethanol	$\log[f(\mu_L)] = 0.1839 \log(\mu_L) - 0.011 \text{ if } d_p > 1 \text{ in}$ <p style="text-align: center;">Else</p> $\log[f(\mu_L)] = 0.0591 \cdot \log^3(\mu_L) + 0.0226 \cdot \log^2(\mu_L) + 0.1701 \cdot \log(\mu_L) - 0.0135$ $f(\rho_L) = 1.5052 \cdot \ln\left(\frac{\rho_w}{\rho_L}\right) + 1.1883$ $X = \frac{U_L}{U_{G,Fl}} \cdot \sqrt{\frac{\rho_L}{\rho_G}}$ $Y = 0.016 \left(\frac{\rho_G U_G^2}{g}\right) F_p \cdot f(\mu_L) \cdot f(\rho_L)$ $\log(Y_o) = -0.29 \log^2(X) - 1.075 \log(X) - 1.636$ <p>(Y_o represents the flooding line) (F_p is packing factor)</p>	$0.01 < X < 10$ $700 < \rho_L < 1400$ [kg/m ³] $0.2 \leq \mu_L \leq 20$ [cp] All English Units except for viscosity
Kister and Gill [119]			$Y = A \log^2(X) + B \log(X) + C$ $X = \frac{U_L}{U_{G,Fl}} \cdot \sqrt{\frac{\rho_L}{\rho_G}}$ $Y = \sqrt{U_{G,Fl}^2 \cdot \left(\frac{\rho_G}{\rho_L - \rho_G}\right) \left(\frac{\mu_L}{\rho_L}\right)^{0.1} Q}$ $A = 0.0665 \cdot \ln(\Delta P_{Fl}) - 0.1106 \quad 0.5 \leq \Delta P_{Fl} \leq 5.0$ $B = -0.252 \cdot \ln(\Delta P_{Fl}) - 0.8918 \quad 0.5 \leq \Delta P_{Fl} \leq 1.0$ $C = -0.8900 \quad 1.0 \leq \Delta P_{Fl} \leq 5.0$ $C = 0.1221 \cdot \ln(\Delta P_{Fl}) + 0.714 \quad 0.5 \leq \Delta P_{Fl} \leq 5.0$ $\Delta P_{Fl} = 0.115(Q)^{0.7}$	Q is packing factor $10 \leq Q \leq 100$ [ft ⁻¹] $0.005 \leq X \leq 1$
Kuzniewskalach [120]	Intalox et al. 94 packing types	Benzene/toluene Propanol/acetic acid Methanol/methyl acetate Methanol/acetic acid Ethanol/water Methanol/ethanol CO ₂ /H ₂ O Air dehumidification by H ₂ SO ₄ CO ₂ /4% NaOH	$U_{G,Fl} = A \cdot \varepsilon \cdot \left(\frac{a_T}{\varepsilon^3}\right)^B$ $A = (1608932 \cdot U_L^3 - 7846.1 \cdot U_L^2 + 237.3 \cdot U_L) \frac{(\rho_{air} \rho_L)^{0.5}}{(\rho_G \rho_w)}$ $+ 15.2) \frac{(\sigma_L)^{0.25} (\mu_L)^{0.02}}{(\sigma_w)^{0.25} (\mu_w)^{0.02}}$ $B = (-144.6 \cdot U_L^2 - 9.5 \cdot U_L - 0.273) \frac{(\rho_w \mu_L)^{0.02}}{(\rho_L \mu_w)} \frac{(\sigma_L)^{0.15} (\mu_G)^{0.1}}{(\sigma_w)^{0.15} (\mu_{air})^{0.1}}$	$700 < \rho_L < 1830$ $0.4 < \rho_G < 3.3$ [kg/m ³]

Table 1-5 (continued)

References	Packing	System	Correlation	Constraints
		Air dehumidification by H ₂ SO ₄ CO ₂ /4% NaOH Air dehumidification by ethylene glycol Air purification by machine oil, propylene carbonate and silicon oil		
Billet and Schultes [121]	Pall ring Ralu flow Ralu ring Nor PAC ring Hiflow ring Glitsch ring Glitsch CMR ring TOP-Pak ring Raschig ring VSP ring VSP ring Envi Pac ring Bialecki ring Raflux Berl saddle Mellapak Gempak Impulse packing		$U_{G,FI} = \frac{(\varepsilon - h_{T,FI})^{1.5}}{\varepsilon^{0.5}} \cdot \sqrt{\frac{2g}{\psi_L}} \cdot \sqrt{\frac{h_{T,FI}}{a_T}} \cdot \sqrt{\frac{\rho_L}{\rho_G}}$ $3h_{T,FI}^4 - \varepsilon h_{T,FI}^3 = \frac{6 a^2 \mu_L \varepsilon u_L}{g \rho_L}$ $\frac{1}{\psi_L} = \frac{C_F^2}{g} \left[\frac{U_L}{U_{G,FI}} \sqrt{\frac{\rho_L}{\rho_G}} \left(\frac{\mu_L}{\mu_G} \right)^{0.2} \right]^{2N_{FI}}$ <p>if $\frac{U_L}{U_{G,FI}} \cdot \sqrt{\frac{\rho_L}{\rho_G}} \leq 0.4$, $C_F = C_{FI}$, $N_{FI} = -0.194$</p> <p>if $\frac{U_L}{U_{G,FI}} \cdot \sqrt{\frac{\rho_L}{\rho_G}} \leq 0.4$, $C_F = 0.6244 \cdot C_{FI} \left(\frac{\mu_L}{\mu_G} \right)^{0.1028}$</p> $N_F = -0.708$	<p>C_{FI} is Packing Constant in reference</p> <p>758 < ρ_L < 1237</p> <p>0.07 < ρ_G < 4.93 [kg/m³]</p> <p>0.3 ≤ ν_L ≤ 1.66</p> <p>2.2 ≤ ν_g ≤ 126</p> <p>ν is kinetic viscosity [10⁻⁶m²/s]</p> <p>17.2 ≤ σ_L ≤ 74</p> <p>σ is surface tension [10⁻³kg/s²]</p>

In order to characterize flooding in packed-beds, Leva [118] modified the Generalized Pressure Drop Correlation (GPDC) proposed in 1953 as shown in Figure 1-11. In order to use this figure, knowing the gas and liquid superficial velocities and the corresponding gas and liquid densities, the value of X can be calculated using Equation (1-19). Also, knowing the liquid density and viscosity as well as the gas superficial gas velocity and density, in addition to the packing factor, a value of Y can be calculated using Equation (1-20). The point (X, Y) is then plotted on Figure 1-11. If the point lies within the figure, no flooding would occur, otherwise alterations of the liquid and/or gas flow rates are required to avoid flooding.

$$X = \frac{u_L}{u_G} \cdot \sqrt{\frac{\rho_L}{\rho_G}} \quad (1-19)$$

$$Y = 0.016 \frac{\rho_G U_G^2}{g} F_p \cdot f(\mu_L) \cdot f(\rho_L) \quad (1-20)$$

Where $f(\mu)$ and $f(\rho_L)$ are given in Table 1-5.

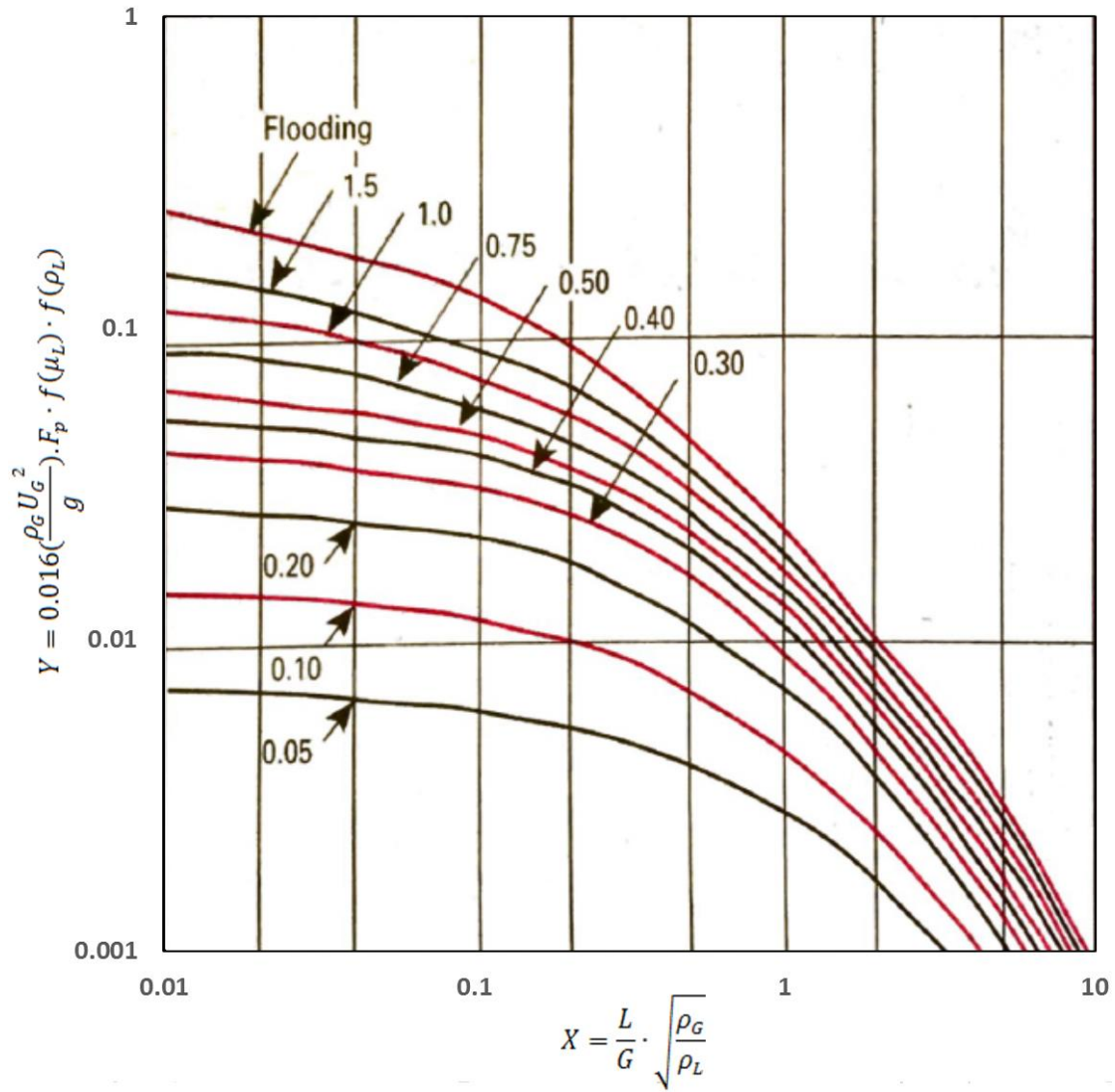


Figure 1-11: Leva's Pressure Drop Correlation [118]

1.5 Pressure Drop and Liquid Holdup

Pressure drop and liquid holdup are important parameters in packed-bed design. Systematic evaluations of different correlations available in the literature led to the recommendation of the correlations by Leva [118] and by Billet and Schultes [108, 121-123] to predict the pressure drop associated with two-phase flow in packed-beds [124].

To use Figure 1-11 by Leva [118] to obtain the two-phase pressure drop, testing for flooding should be conducted first as mentioned above, then the location of point (X, Y) on the figure would allow the interpolation of the pressure drop in the packed-bed under the prevailing conditions. The pressure drop in this figure is expressed in inches of water/ft of packing height.

In 1999, Billet and Schultes [108] correlated the pressure drop and liquid holdup based on over 3,500 measured data points, more than 50 test systems and over 70 types of random or structured packing and proposed Equation (1-21) to calculate the pressure drop.

$$\frac{\Delta P_0}{H} = \psi_L \frac{a}{(\varepsilon - \beta_L)^3} \frac{F_G^2}{2} \left(\frac{1}{K}\right) \quad (1-21)$$

$$\frac{1}{K} = 1 + \left(\frac{2}{3}\right) \left(\frac{1}{1 - \varepsilon}\right) \frac{d_p}{D_C} \quad (1-22)$$

$$Re_G = \frac{U_G d_p}{(1 - \varepsilon) \nu_G} K \quad (1-23)$$

$$\psi_L = C_{p,0} \left(\frac{64}{Re_G} + \frac{1.8}{Re_G^{0.08}} \right) \left(\frac{\varepsilon - \beta_L}{\varepsilon} \right)^{1.5} \left(\frac{a}{a_h} \right)^{0.2} \exp \left(\frac{13300}{a^{1.5}} \sqrt{\frac{u_L^2 a}{g}} \right) \quad (1-24)$$

$$F_G = U_G \sqrt{\rho_G} \quad (1-25)$$

$$d_p = \frac{6(1 - \varepsilon)}{a} \quad (1-26)$$

Where D_C is the ID of the absorber; and $C_{p,0}$ is a characteristic constant of the packing as given in Table 1-6.

It should be mentioned that Equation (1-21) is only valid under the following constraints:

$$361 \leq \text{liquid density} \leq 1,115 \text{ kg/m}^3$$

$$0.61 \leq \text{liquid velocity} \leq 60.1 \text{ m/h}$$

$$0.06 \leq \text{gas density} \leq 28 \text{ kg/m}^3$$

$$0.21 \leq F_G = \text{gas capacity factor} \leq 5.09 \text{ Pa}^{0.5}$$

$$1.4\text{e-}7 \leq \text{liquid kinematic viscosity} \leq 9.9\text{e-}5 \text{ m}^2/\text{s}$$

$$1.4\text{e-}7 \leq \text{gas kinematic viscosity} \leq 1.06\text{e-}4 \text{ m}^2/\text{s}$$

Table 1-6: Values of Characteristic Parameters of Packings for Billet and Schulte's Equation [108]

Packing	Materials	Nominal Size, mm	Void Fraction, ϵ	Specific Area, m^{-1}	C_h	$C_{p,0}$
Raschig Rings	Ceramic	25	0.68	190	0.577	1.329
		50	0.83	95		
Berl Saddle	Ceramic	13	0.65	545	0.833	
		25	0.68	260	0.62	
Pall rings	Plastic	25	0.887	225	0.528	0.865
		35	0.906	151.1	0.718	0.927
		50	0.919	111.1	0.593	0.698
VSP Ring	Metal	25	0.975	199.6	1.369	0.782
		50	0.98	104.6	1.135	0.773
Mellapak 250Y	Metal		0.97	250	0.554	0.292

Stichlmair et al. [125] developed pressure drop correlations in packed beds for both structured and dumped packings, including ceramic Berl Saddle and Mellapak.

$$\frac{\Delta P_0}{H} = \frac{3}{4} f_0' [(1 - \varepsilon')/\varepsilon'^{4.65}] \rho_G U_G^2 / d_p' \quad (1-27)$$

$$f_0 = \frac{C_1}{Re_G} + \frac{C_2}{Re_G^{1/2}} + C_3 \quad (1-28)$$

$$Re_G = \frac{U_G d_p \rho_G}{\mu_G} \quad (1-29)$$

$$\beta_L = 0.555 (U_L^2 \frac{a}{g \varepsilon^{4.65}})^{1/3} \quad (1-30)$$

$$\varepsilon' = \varepsilon - \beta_L \quad (1-31)$$

$$c = -\left(\frac{C_1}{Re_G} + \frac{C_2}{2Re_G^{1/2}}\right) \frac{1}{f_0} \quad (1-32)$$

$$d_p' = d_p [(1 - \varepsilon')/(1 - \varepsilon)]^{1/3} \quad (1-33)$$

$$f_0' = f_0 [(1 - \varepsilon')/(1 - \varepsilon)]^{c/3} \quad (1-34)$$

Where C_1 , C_2 and C_2 are characteristic parameters of packings available in Table 1-7.

Table 1-7: Values of Characteristic Parameters of Packings for Stichlmair's Equation [125]

Packing	Materials	Size, mm	Void Fraction, ε	Specific Area, m^{-1}	C_1	C_2	C_3
Raschig Rings	Ceramic	10	0.655	472	48	8	2
		15	0.676	314	48	10	2.3
		30	0.775	137	48	8	2
		35	0.773	126	48	8	2.15
Berl Saddle	Ceramic	15	0.561	300	32	6	0.9
		35	0.75	133	33	14	1
Pall Rings	Ceramic	25	0.94	215	0.05	1	3
		35	0.95	130	0.1	0.1	2.1
Mellapak 250Y	Metal		0.96	250	5	3	0.45

Billet and Schultes [108] also recommended Equation (1-35) for calculating the liquid holdup in two-phase flow. The liquid Reynolds number and Froude number are calculated using Equations (1-36) and (1-37) respectively.

$$\beta_L = \left(12 \cdot \frac{Fr_L}{Re_L} \right)^{1/3} \left(\frac{a_h}{a} \right)^{2/3} \quad (1-35)$$

$$Re_L = \frac{u_L \rho_L}{a \mu_L} \quad (1-36)$$

$$Fr_L = \frac{u_L^2 a}{g} \quad (1-37)$$

If $Re_L < 5$

$$\frac{a_h}{a} = C_h Re_L^{0.15} Fr_L^{0.1} \quad (1-38)$$

If $Re_L \geq 5$

$$\frac{a_h}{a} = 0.85 C_h Re_L^{0.25} Fr_L^{0.1} \quad (1-39)$$

Where C_h is characteristic constant of the packing as given in Table 1-6.

It should be noted that Equation (1-35) is only valid under the following constraints:

$$800 \leq \text{liquid density} \leq 1,810 \text{ kg/m}^3$$

$$7.4e-7 \leq \text{liquid kinematic viscosity} \leq 1.42e-4 \text{ m}^2/\text{s}$$

$$20.8 \leq \text{liquid surface tension} \leq 86.3 \text{ mN/m}$$

$$1.33 \leq \text{liquid velocity} \leq 82.8 \text{ m/h}$$

$$0.1 \leq F_G = \text{gas capacity factor} \leq 2.78 \text{ Pa}^{0.5}$$

2.0 Objective

As can be concluded from the previous section, in 1992, Tontiwachwuthikul et al. [93] conducted experiments for CO₂ capture from a CO₂-air gaseous mixture by AMP aqueous solutions using packed-bed absorber with internal liquid redistribution. The absorber had a 0.1 m ID and contains six packed sections with random packing (13 mm ceramic Berl Saddle) to an effective height of 6.6 m. These authors presented experimental data for liquid-phase temperature, CO₂ loading (moles of CO₂/moles of AMP) and CO₂ mole fraction in the gas-phase at different packing heights of the absorber, however, they did not model these results. Only in 2006, Gabrielsen et al. [101] modeled three runs (T25, T26 and T28) of the experimental data by Tontiwachwuthikul et al. [93] using Pandya's approach [98] and reported that their model predictions were in agreement with the experimental data of these runs. Similarly in 2006, Aboudheir et al. [52] modeled one run (T29) of the experimental data by Tontiwachwuthikul et al. [93] using Pandya's approach [98] and reported good agreement between their model predictions and the experimental data of this run. They also used their model to predict the behavior of the same absorber when the original random packing (12.7 mm ceramic Berl Saddle) was replaced by an EX-type laboratory structured packing.

It should be mentioned, however, that even though the model based on Pandya's approach [98] was used by the above authors for CO₂ absorption from CO₂-air mixture using AMP aqueous solutions, many equation parameters were not given, and the significant experimental errors in the CO₂ material balance calculations reported by Tontiwachwuthikul et al. [93] made the task of replicating their model predictions more difficult than expected.

Therefore, objectives of this study are:

1. To develop a mathematical model for CO₂ capture from CO₂-air gaseous mixture using AMP aqueous solutions as a chemical absorbent in an adiabatic small-scale (0.1 m ID) packed-bed absorber;
2. To validate the model predictions against the adequate experimental data (with accurate CO₂ material balance) reported by Tontiwachwuthikul et al. [93];
3. To use the validated model to predict the performance of a small-scale (0.1 m ID) absorber for CO₂ capture from a CO₂-air mixture using SG aqueous solutions;
4. To use the validated model to conduct a parametric study to optimize the behavior of a large-scale absorber (1.5 m ID) for CO₂ capture from a CO₂-N₂ gaseous mixture using AMP and SG aqueous solutions as chemical solvents.

In order to achieve these objectives, the following tasks are proposed:

- Task 1: Develop a mathematical model based on Pandya's approach [98] for CO₂ capture from a CO₂-air gaseous mixture using AMP aqueous solutions in a small-scale (0.1 m ID) countercurrent adiabatic packed-bed absorber in MATLAB 2017b.
- Task 2: Conduct extensive literature search to obtain and correlate the missing equation parameters used in the model for the CO₂-air mixture and the AMP aqueous solutions.
- Task 3: Validate the MATLAB model predictions against the adequate experimental data (with accurate CO₂ material balance) reported by Tontiwachwuthikul et al. [93].
- Task 4: Conduct extensive literature search to obtain and correlate the missing equation parameters used in the model for SG aqueous solutions.

Task 5: Use the validated model to predict the behavior of a small-scale (0.1 m ID) adiabatic countercurrent packed-bed absorber for CO₂ capture from a CO₂-air gaseous mixture using SG aqueous solutions.

Task 6: Use the validated model to conduct a parametric study to optimize the behavior of a countercurrent adiabatic large-scale (1.5 m ID) packed-bed absorber for CO₂ capture from a CO₂-N₂ gaseous mixtures using AMP and SG solutions. The effects of system pressure, liquid temperature, superficial gas velocity, superficial liquid velocity, CO₂ mole fraction in the inlet feed gas, and packing type on the model predictions were investigated.

3.0 Model Development for CO₂ Absorption in an Adiabatic Packed-Bed

The modeling approach by Pandya [98] includes five components: (1) a solute reactive gas (A), an inert carrier gas (B), a volatile solvent component (S), a non-volatile reactant (R) and a non-volatile product (P). The model equations for material and heat balances are written for a differential element (dz) of the packed-bed as shown in Figure 3-1. The model assumptions and equations are discussed in following.

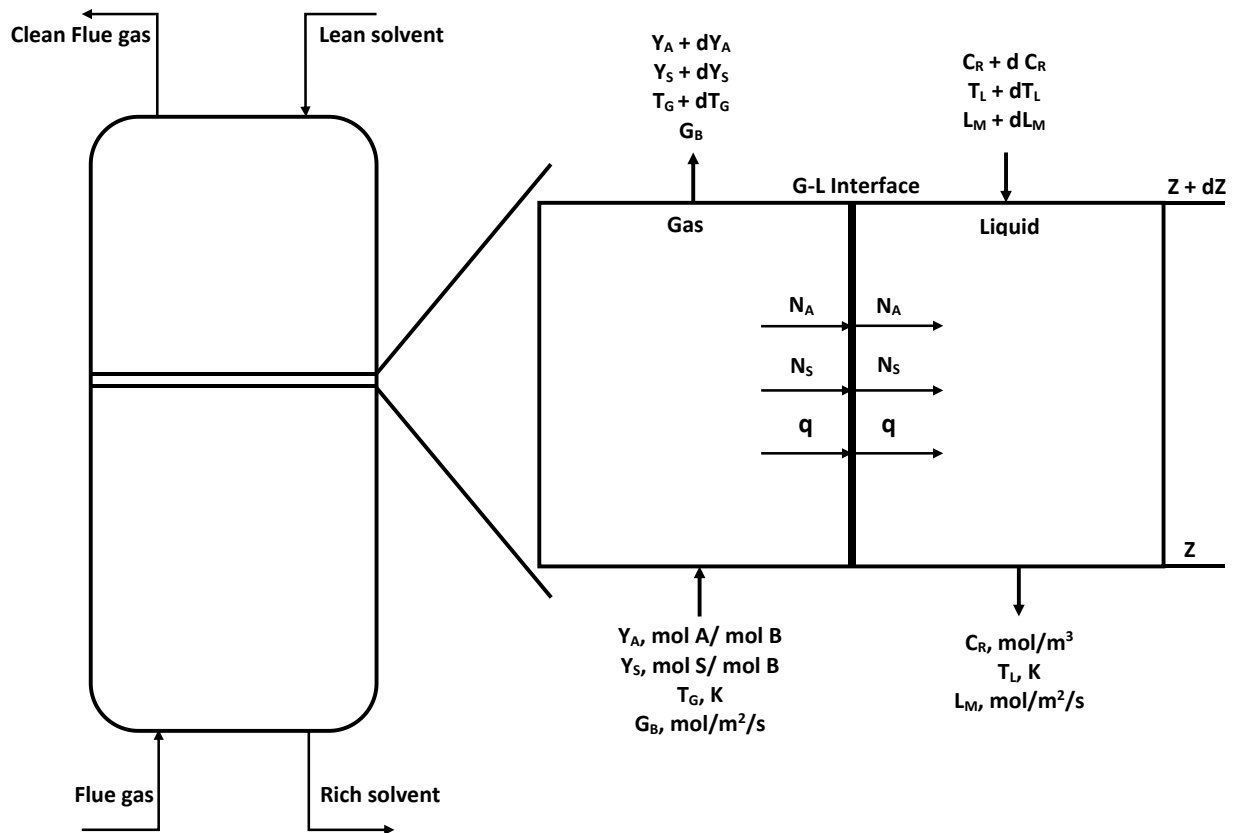


Figure 3-1: Schematic of the packed-bed absorber

3.1 Model Assumptions

1. The packed-bed is adiabatic. This assumption is acceptable because the heat loss due to heat transfer to the surroundings is generally small in industrial absorbers [94].
2. The carrier gas (B) is inert and does not react with any other component in the mixture.
3. The liquid-phase density is homogenous.
4. The liquid-side mass transfer resistance for the volatile solvent (S) is negligible.
5. The liquid-phase heat transfer resistance is negligible, which means that the interface temperature is the same as that of the bulk liquid.
6. The gas-liquid interfacial surface area is the same for heat and mass transfer. This assumption is valid when the packing is wet.
7. The reaction is so fast that it takes place in the liquid-film.
8. The equilibrium concentration of the dissolved gas (A) in the liquid-bulk is negligible. This assumption is true for an instantaneous second order irreversible reaction [98].

3.2 Model Equations

The material and heat balances in the control volume depicted in Figure 3-2 are required for modeling this adiabatic absorber. These balances allow calculating the molar ratio gradients, and the gas-phase as well as the liquid-phase temperatures.

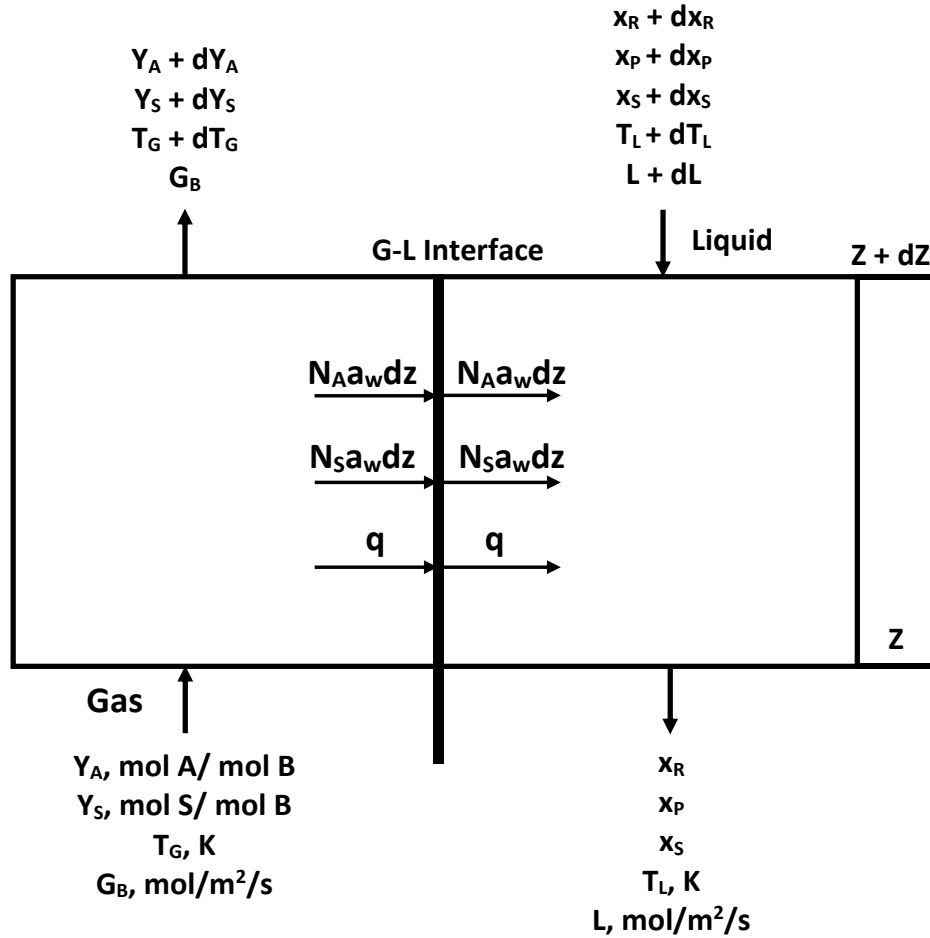


Figure 3-2: Schematic Plot of Control Volume

3.2.1 Material Balance

According to the reaction mechanism discussed in Table 1-2, one mole acid gas (A) reacts with one mole reactant (R) and one mole H₂O (S) to produce one mole of bicarbonate (P).



According to the stoichiometry of Equation (3-1), the following relationships could be developed:

$$\frac{N_A a_w dz}{1} = \frac{L}{\rho_m} \frac{dn_R}{1} = \frac{L}{\rho_m} \frac{dn_P}{-1} \quad (3-2)$$

$$\frac{N_S a_w dz}{1} = \frac{L}{\rho_m} \frac{dn_S}{-1} \quad (3-3)$$

$$dn_R = \frac{\rho_m}{L} N_A a_w dz \quad (3-4)$$

$$dn_P = -\frac{\rho_m}{L} N_A a_w dz \quad (3-5)$$

$$dn_S = -\frac{\rho_m}{L} N_S a_w dz \quad (3-6)$$

3.2.1.1 Material Balance in the Gas-Side

Considering the gas-side control volume shown in Figure 3-3, a steady-state material balance equations (no amass accumulation) in the differential element (dZ) for the gas-phase can be represented by Equations (3-7) through Equation (3-9).

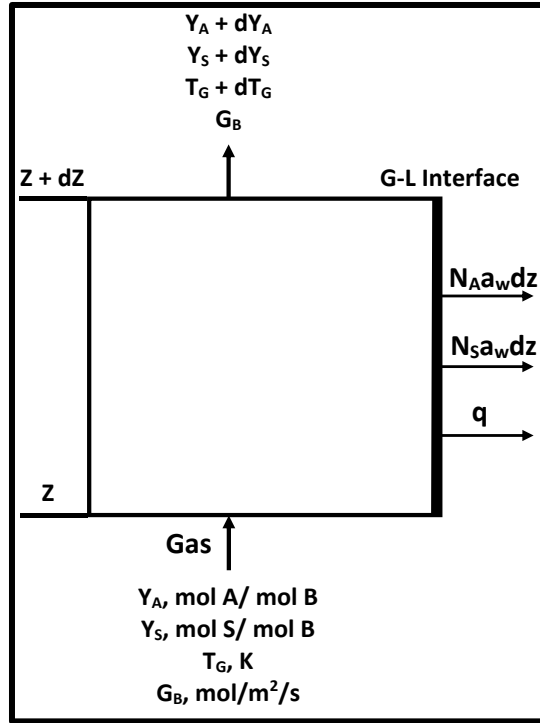


Figure 3-3: Gas-Side Control Volume

$$\text{Rate of gas mass in} = \text{Rate of gas mass out} \quad (3-7)$$

$$\text{Rate of gas mass in} = G \quad (3-8)$$

$$\text{Rate of gas mass out} = (G + dG) + (N_A a_w dz + N_S a_w dz) \quad (3-9)$$

Combining Equations (3-8) and (3-9) leads to Equation (3-10).

$$-dG = N_A a_w dz + N_S a_w dz \quad (3-10)$$

Since the gas-phase consists of component (A), (B) and (S), the total gas flow rate is expressed as a function of the inert gas (B) flow rate and molar ratios as presented in Equation (3-11).

$$G = G_B(1 + Y_A + Y_S) \quad (3-11)$$

Differentiating both sides of Equation (3-11) leads to Equation (3-12).

$$-dG = -G_B dY_A - G_B dY_S \quad (3-12)$$

Comparing Equation (3-10) and (3-12) gives Equation (3-13):

$$N_A a_w dZ = -G_B dY_A \quad (3-13)$$

$$N_S a_w dZ = -G_B dY_S$$

According to the two-film theory depicted in Figure 1-10, the mass transfer of components A and S can be written as:

$$N_A a_w dZ = k_{G,A} P (y_A - y_{Ai}) a_w dZ \quad (3-14)$$

$$N_S a_w dZ = k_{G,S} P (y_S - y_{Si}) a_w dZ \quad (3-15)$$

Coupling Equations (3-13), (3-14) and (3-15) yields:

$$-G_B dY_A = k_{G,A} a_w P (y_A - y_{Ai}) dZ \quad (3-16)$$

$$-G_B dY_S = k_{G,S} a_w P (y_S - y_{Si}) dZ \quad (3-17)$$

Thus, the molar ratio gradients for component A and S in the gas-phase can be written as follows:

$$\frac{dY_A}{dZ} = -\frac{k_{G,A} a_w P (y_A - y_{Ai})}{G_B} \quad (3-18)$$

$$\frac{dY_S}{dZ} = - \frac{k_{G,S} a_w P (y_S - y_{Si})}{G_B} \quad (3-19)$$

3.2.1.2 Material Balance in the Liquid-Side

Considering the liquid-side control volume shown in Figure 3-4, a steady-state material balance equations in the differential element (dZ) for the liquid-phase are described by Equations (3-20) through (3-22).

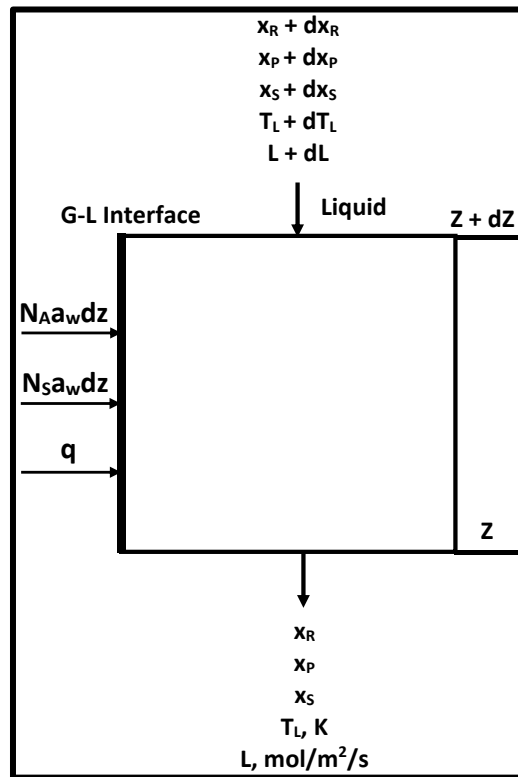


Figure 3-4: Liquid Side Control Volume

$$\text{Rate of liquid mass in} = \text{Rate of liquid mass out} \quad (3-20)$$

$$\text{Rate of liquid mass in} = (L + dL) + (N_A a_w dZ + N_S a_w dZ) \quad (3-21)$$

$$\text{Rate of liquid mass out} = L \quad (3-22)$$

Combining Equations (3-21) and (3-22) leads to Equation (3-23).

$$dL = - (N_A a_w dZ + N_S a_w dZ) \quad (3-23)$$

Combining with Equation (3-13) gives:

$$\frac{dL}{dZ} = G_B \left(\frac{dY_A}{dZ} + \frac{dY_S}{dZ} \right) \quad (3-24)$$

The liquid-phase consists of three components (R), (P) and (S). The material balance for R can be expressed by Equations (3-25) through (3-28). It should be emphasized that the stoichiometry of the chemical reaction is considered through the Equation (3-1) where the stoichiometric coefficient (γ) is 1.

$$\text{Rate of (R) mass in} - \text{Rate of mass consumed} = \text{Rate of (R) mass out} \quad (3-25)$$

$$\text{Rate of liquid mass in} = (L + dL)(x_R + dx_R) \quad (3-26)$$

$$\text{Rate of liquid mass consumed} = \gamma N_A a_w dZ \quad (3-27)$$

$$\text{Rate of liquid mass out} = L x_R \quad (3-28)$$

Neglecting $dL \cdot dx_R$ and combining Equations (3-26) through (3-28) gives:

$$d(Lx_R) = \gamma N_A a_w dZ \quad (3-29)$$

Similarly, the mole fraction gradient of the product (P) could be derived:

$$\text{Rate of (P) mass in} + \text{Rate of (P) produced} = \text{Rate of (P) mass out} \quad (3-30)$$

$$\text{Rate of liquid mass in} = (L + dL)(x_P + dx_P) \quad (3-31)$$

$$\text{Rate of (P) mass produced} = N_A a_w dZ \quad (3-32)$$

$$\text{Rate of liquid mass out} = Lx_P \quad (3-33)$$

$$d(Lx_P) = - N_A a_w dZ \quad (3-34)$$

Similarly, mole fraction gradient of the water (S) could be derived:

$$\text{Rate of (S) mass in} = \text{Rate of (S) mass out} \quad (3-35)$$

$$\text{Rate of liquid mass in} = (L + dL)(x_S + dx_S) + N_S a_w dZ \quad (3-36)$$

$$\text{Rate of liquid mass out} = Lx_S \quad (3-37)$$

$$d(Lx_S) = - N_S a_w dZ \quad (3-38)$$

3.2.2 Energy Balance

3.2.2.1 Energy Balance in the Gas-Side

Considering the gas-side control volume shown in Figure 3-3, the balance of the gas-phase enthalpy (H) per mole of component (B) can be written as follows:

$$\begin{aligned} \text{Rate of enthalpy in} - \text{Rate enthalpy out} & \\ & = \text{Rate of enthalpy transfer from gas to liquid} \end{aligned} \quad (3-39)$$

$$\text{Rate of enthalpy in} = G_B H \quad (3-40)$$

$$\begin{aligned} \text{Rate of enthalpy out} & \\ & = G_B(H + dH) + N_A a_w [(C_{PA}(T_G - T_o) + H_A^{\text{gas}}(T_o, P))] dz \\ & \quad + N_S a_w [(C_{PS}(T_G - T_o) + H_S^{\text{gas}}(T_o, P))] dz \end{aligned} \quad (3-41)$$

$$\text{Rate of enthalpy transfer from the gas to the liquid} = h_G(T_G - T_L) a_w dz \quad (3-42)$$

Plugging Equations (3-40) (3-41) and (3-42) into Equation (3-39) gives Equation (3-43):

$$\begin{aligned} -G_B dH - N_A a_w dz [(C_{PA}(T_G - T_o) + H_A^{\text{gas}}(T_o, P))] \\ - N_S a_w dz [(C_{PS}(T_G - T_o) + H_S^{\text{gas}}(T_o, P))] = h_G(T_G - T_L) a_w dz \end{aligned} \quad (3-43)$$

According to Equation (3-13), Equation (3-43) could be written as:

$$\begin{aligned} -G_B dH + G_B dY_A [(C_{PA}(T_G - T_o) + H_A^{\text{gas}}(T_o, P))] \\ + G_B dY_S [(C_{PS}(T_G - T_o) + H_S^{\text{gas}}(T_o, P))] = h_G(T_G - T_L) a_w dz \end{aligned} \quad (3-44)$$

The enthalpy of a gas mixture (H) is expressed in Equation (3-45) and the derivative of enthalpy (dH) is shown in Equation (3-46).

$$H = [(C_{PB}(T_G - T_o) + H_B^{gas}(T_o, P))] + Y_A [(C_{PA}(T_G - T_o) + H_A^{gas}(T_o, P))] + Y_S [(C_{PS}(T_G - T_o) + H_S^{gas}(T_o, P))] \quad (3-45)$$

$$dH = C_{PB}dT_G + Y_A C_{PA}dT_G + G_B Y_S C_{PS}dT_G + [(C_{PA}(T_G - T_o) + H_A^{gas}(T_o, P))]dY_A + [(C_{PS}(T_G - T_o) + H_S^{gas}(T_o, P))]dY_S \quad (3-46)$$

Substituting Equation (3-46) into Equation (3-43) and simplifying it gives:

$$-G_B(C_{P,B} + Y_A C_{P,A} + Y_S C_{P,S})dT_G = h_G a_w (T_G - T_L)dz \quad (3-47)$$

3.2.2.2 Energy Balance in the Liquid-Side

Considering the liquid-side control volume shown in Figure 3-4, the balance of the liquid-phase enthalpy (H_L) can be written as follows:

$$\begin{aligned} \text{Rate of enthalpy in} - \text{Rate enthalpy out} \\ = \text{Rate of enthalpy transfer from Liquid to gas} \end{aligned} \quad (3-48)$$

$$\begin{aligned} \text{Rate of enthalpy in} \\ = (L + dL)(H_L + dH_L) + N_A a_w [(C_{PA}(T_G - T_o) + H_A^{gas}(T_o, P))]dz \\ + N_S a_w [(C_{PS}(T_G - T_o) + H_S^{gas}(T_o, P))]dz \end{aligned} \quad (3-49)$$

$$\text{Rate of enthalpy out} = LH_L \quad (3-50)$$

$$\text{Rate of enthalpy transfer from liquid to gas} = -h_G(T_G - T_L)a_w dz \quad (3-51)$$

Plugging Equations (3-49), (3-50) and (3-51) into Equation (3-48) leads to Equation (3-52):

$$\begin{aligned} LdH_L + H_L dL + dLdH_L + N_A a_w [(C_{PA}(T_G - T_o) + H_A^{gas}(T_o, P))]dz \\ + N_S a_w [(C_{PS}(T_G - T_o) + H_S^{gas}(T_o, P))]dz = -h_G(T_G - T_L)a_w dz \end{aligned} \quad (3-52)$$

Since dL is negligible and $dL.dH_L$ is infinitesimal in Equation (3-13), Equation (3-53) can be obtained:

$$\begin{aligned} LdH_L - G_B dY_A [C_{PA}(T_G - T_0) + H_A^{gas}(T_0, P)] - G_B dY_S [C_{PS}(T_G - T_0) + H_S^{gas}(T_0, P)] \\ = -h_G(T_G - T_L)a_w dz \end{aligned} \quad (3-53)$$

On account of dilute solution where large amount of the volatile solvent (H_2O) exists, the molar density of the liquid is constant. The enthalpy of the solution can be as Equation (3-54).

$$H_L = \frac{1}{\rho_m} \sum_i n_i H_i^{aq}(T_L) = \frac{1}{\rho_m} \sum_i n_i \left[H_i^{aq}(T_0, P) + \int_{T_0}^{T_L} C_{P,i} dT \right] \quad (3-54)$$

Where i represents (A), (R), (P) and (S); ρ_m is molar density of solution, mol/m^3 ; n_i is molar concentration of species i , mol/m^3 . Liquid enthalpy derivative (dH_L) is represented by Equation (3-55).

$$\begin{aligned} dH_L &= \frac{1}{\rho_m} d \left\{ \sum_i n_i \left[H_i^{aq}(T_0, P) + \int_{T_0}^{T_L} C_{P,i} dT \right] \right\} \\ &= \frac{1}{\rho_m} \left\{ \sum_i [H_i^{aq}(T_0, P)] dn_i + \sum_i d \left[\int_{T_0}^{T_L} n_i C_{P,i} dT \right] \right\} \end{aligned} \quad (3-55)$$

$C_{P,i}$ is assumed to be an average heat capacity of species i between temperature T_0 and T_L , which is a reasonable assumption hence the heat capacity of the main component (H_2O) is not very sensitive to temperature. Therefore,

$$\begin{aligned}
dH_L &= \frac{1}{\rho_m} \left\{ \sum_i [H_i^{aq}(T_0, P)] dn_i + \sum_i d[n_i C_{P,i}(T_L - T_0)] \right\} \\
&= \frac{1}{\rho_m} \sum_i [H_i^{aq}(T_0, P)] dn_i + \frac{1}{\rho_m} \sum_i n_i C_{P,i} dT_L \\
&= \frac{1}{\rho_m} \sum_i [H_i^{aq}(T_0, P)] dn_i + C_L dT_L
\end{aligned} \tag{3-56}$$

Expanding Equation (3-56) for all species i and rearranging leads to:

$$\begin{aligned}
dH_L &= \frac{1}{\rho_m} [H_A^{aq}(T_0, P) dn_A + H_R^{aq}(T_0, P) dn_R + H_P^{aq}(T_0, P) dn_P + H_S^{aq}(T_0, P) dn_S] \\
&\quad + C_L dT_L
\end{aligned} \tag{3-57}$$

In this Equation, dn_A is negligible because (A) is the reactant, its molar concentration in the liquid (n_A) is small for an irreversible reaction. Therefore,

$$\begin{aligned}
dH_L &= \frac{1}{\rho_m} \left[H_R^{aq}(T_0, P) N_A a_w dz \frac{\rho_m}{L} - H_P^{aq}(T_0, P) N_A a_w dz \frac{\rho_m}{L} \right. \\
&\quad \left. - H_S^{aq}(T_0, P) N_S a_w dz \frac{\rho_m}{L} \right] + C_L dT_L \\
&= \frac{1}{L} [H_R^{aq}(T_0, P) N_A a_w dz - H_P^{aq}(T_0, P) N_A a_w dz - H_S^{aq}(T_0, P) N_S a_w dz] \\
&\quad + C_L dT_L
\end{aligned} \tag{3-58}$$

Using Equation (3-13), Equation (3-58) could be rewritten as:

$$dH_L = \frac{1}{L} [-H_R^{aq}(T_0, P) G_B dY_A + H_P^{aq}(T_0, P) G_B dY_A + H_S^{aq}(T_0, P) G_B dY_S] + C_L dT_L \tag{3-59}$$

Plugging Equation (3-59) into Equation (3-53) results in:

$$\begin{aligned}
 LC_L dT_L - H_R^{aq}(T_0, P)G_B dY_A + H_P^{aq}(T_0, P)G_B dY_A + H_S^{aq}(T_0, P)G_B dY_S \\
 - G_B dY_A [C_{PA}(T_G - T_0) + H_A^{gas}(T_0, P)] \\
 - G_B dY_S [C_{PS}(T_G - T_0) + H_S^{gas}(T_0, P)] = -h_G(T_G - T_L)a_w dz
 \end{aligned} \tag{3-60}$$

Rearranging the above Equation gives:

$$\begin{aligned}
 LC_L dT_L - G_B dY_A [H_A^{gas}(T_0, P) + H_R^{aq}(T_0, P) - H_P^{aq}(T_0, P)] \\
 - G_B dY_S [H_S^{gas}(T_0, P) - H_S^{aq}(T_0, P)] - G_B dY_A C_{PA}(T_G - T_0) \\
 - G_B dY_S C_{PS}(T_G - T_0) = -h_G(T_G - T_L)a_w dz
 \end{aligned} \tag{3-61}$$

Where the term $(-H_A^{gas}(T_0, P) - H_R^{aq}(T_0, P) + H_P^{aq}(T_0, P))$ is the heat of reaction (ΔH_R); and the term $(H_S^{gas}(T_0, P) - H_S^{aq}(T_0, P))$ is the latent heat of vaporization (ΔH_{LV}). Thus,

$$\begin{aligned}
 LC_L dT_L = G_B dY_A [C_{PA}(T_G - T_0) - \Delta H_R] + G_B dY_S [C_{PS}(T_G - T_0) + \Delta H_{LV}] \\
 - h_G(T_G - T_L)a_w dz
 \end{aligned} \tag{3-62}$$

Based on Equation (3-47) derived from the gas-phase heat balance, Equation (3-54) could be further expanded as:

$$\begin{aligned}
 LC_L dT_L = G_B dY_A [C_{PA}(T_G - T_0) - \Delta H_R] + G_B dY_S [C_{PS}(T_G - T_0) + \Delta H_{LV}] \\
 + G_B (C_{P,B} + Y_A C_{P,A} + Y_S C_{P,S}) dT_G
 \end{aligned} \tag{3-63}$$

Simplifying Equations (3-47) and (3-63), a temperature gradient in each differential element for gas-phase and liquid-phase is given in Equations (3-64) and (3-65).

$$\frac{dT_G}{dz} = \frac{-h_G a_w (T_G - T_L)}{G_B (C_{P,B} + Y_A C_{P,A} + Y_S C_{P,S})} \quad (3-64)$$

$$\begin{aligned} \frac{dT_L}{dz} = \frac{1}{LC_{PL}} \left\{ -h_G a_w (T_G - T_L) + G_B [C_{P,S} (T_G - T_o) + \Delta H_{LV}] \frac{dY_S}{dz} \right. \\ \left. + G_B [C_{P,A} (T_G - T_o) - \Delta H_r] \frac{dY_A}{dz} \right\} \end{aligned} \quad (3-65)$$

Where h_G is the overall heat transfer coefficient between the gas and liquid, ΔH_{LV} is the latent heat of vaporization and ΔH_r is the heat of absorption.

3.2.3 Solution Method

Since the enhancement factor (E) is a function of C_{Ai} which is implicit, as described in Equations (1-13) through (1-18), a trial and error method is needed to obtain (C_{Ai}) as well as the partial pressure at the interface (P_{Ai}). Details of the trial and error method are shown in Figure 3-5.

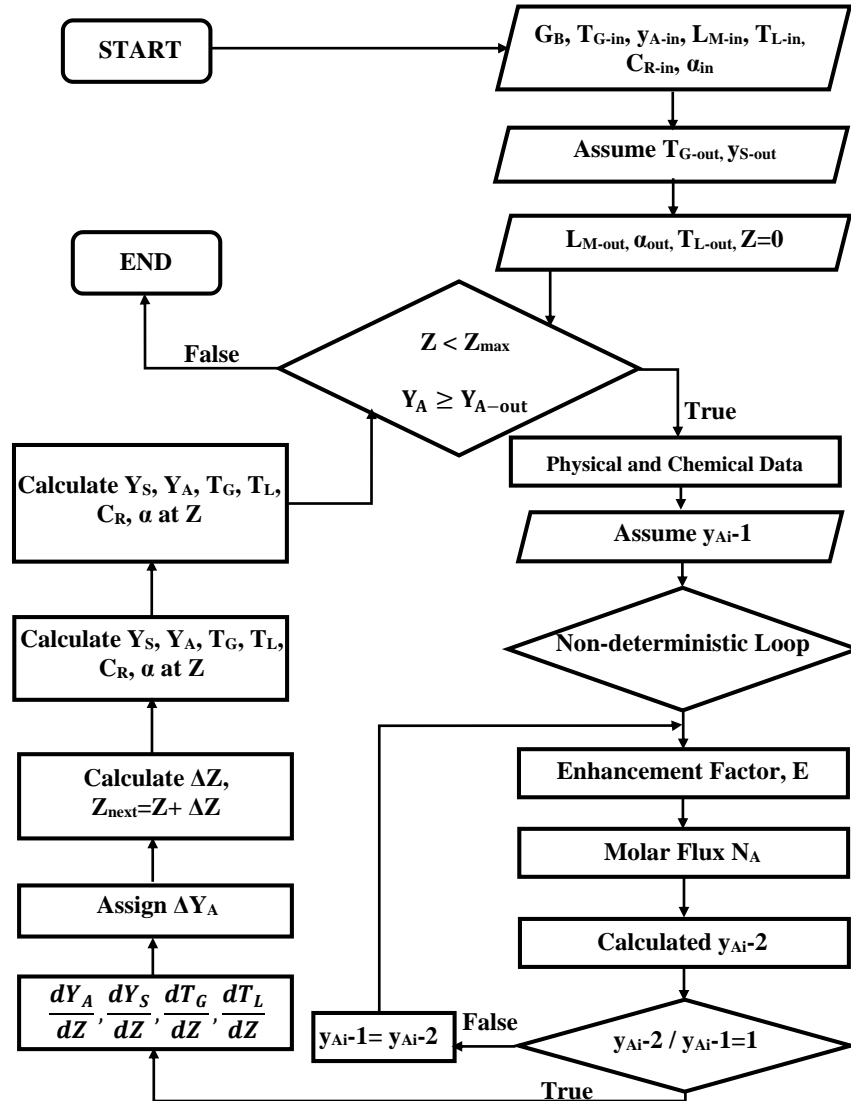


Figure 3-5: Algorithm for Gas Absorption in Packed-bed Absorber [98]

The iteration method is detailed in the following:

Assume the mole fraction of component A at the interface (y_{Ai-1}). According to Dalton's Law of partial pressures, P_{Ai} can be calculated and used in Equation (1-14) to obtain the concentration at the interface (C_{Ai}). The enhancement factor (E) is calculated using Equation (1-15). The mass transfer flux N_A is calculated from Equation (1-11). The partial pressure of A is

obtained from Equation (1-12). The mole fraction of A at the interface (y_{Ai-2}) is then calculated to compare with the assumption (y_{Ai-1}). A deterministic loop is then used to compare the values. If $y_{Ai-1} \neq y_{Ai-2}$, assign y_{Ai-2} to y_{Ai-1} and repeat the above calculations. The correct y_{Ai} is obtained when the deterministic expression turns to be true ($y_{Ai-1} = y_{Ai-2}$). It should be mentioned that in order to calculate the y_{Ai} during the trial and error, the initial assumption should be reasonable. For instance, if a negative value is assigned to y_{Ai} , the calculations will stop and show errors or give an unrealistic value. The assumed y_{Ai} is suggested to be about 30% of y_A . Since component A mole fraction has to be determined individually for each differential element, the assumed $y_{Ai,z+1}$ could be the true $y_{Ai,z}$ of the previous step.

3.3 Model Equation Parameters

The preceding section indicated that in order to solve the model equations of the combined material and energy balances, the following equation parameters are needed:

physico-chemical properties of the gas and liquid mixtures, gas/gas diffusivities, gas/liquid diffusivities, liquid/liquid diffusivity, Henry's law constant, latent heat of vaporization, heat of reaction or absorption, viscosity of the gas mixture, heat capacity of the gas mixture, thermal conductivity of the gas mixture, diffusivity of gas mixture, reaction rate constants, gas-phase heat transfer coefficient, AMP and SG aqueous solutions density, viscosity, surface tension and heat capacity. Details of calculating these equation parameters are given in the following section.

3.3.1 Gas Mixture Density

The cubic Peng-Robinson (P-R) Equation of State (EOS) [126] was used to calculate the gas density which is a function of pressure, temperature and gas composition. The P-R EOS can be written as:

$$P = \frac{RT}{v - b} - \frac{a}{v^2 + 2vb - b^2} \quad (3-66)$$

$$k = 0.37464 + 1.5422\omega - 0.26992\omega^2 \quad (3-67)$$

$$a(T) = 0.45724 \left(\frac{R^2 T_c^2}{P_c} \right) \left\{ 1 + k \left[1 - \left(\frac{T}{T_c} \right)^{0.5} \right] \right\}^2 \quad (3-68)$$

$$b = 0.07780 \frac{RT_c}{P_c} \quad (3-69)$$

Where ω is acentric factor, T_c is critical temperature and P_c is critical pressure. The values of these parameters for the selected gases used in this study (CO_2 , H_2O and N_2) are given in Table 3-1. In Equation (3-66), a and b are the attraction parameter and van der Waals co-volume, respectively. In order to use the P-R EOS for multicomponent system, the following mixing rules are used:

$$a_m = \sum_i^n \sum_j^n x_i x_j a_{ij} \quad (3-70)$$

$$b_m = \sum_i^n x_i b_i \quad (3-71)$$

$$a_{ij} = (a_{ii} a_{jj})^{0.5} (1 - k_{ij}) \quad (3-72)$$

Where a_m and b_m are the attraction parameter and van der Waals co-volume for the mixture, respectively, x_i is the mole fraction of species i , n is the number of species in the mixture, and k_{ij} is the binary interaction parameters between the i^{th} and j^{th} components. It is assumed that $k_{ij} = k_{ji}$ and $k_{ii} = k_{jj} = 0$.

Table 3-1: Critical Temperature, Critical Pressure and Acentric Factor for the Gases Used [127]

Elements	Tc (K)	Pc (bar)	ω
H ₂ O	647.3	221.2	0.344
N ₂	126.2	33.9	0.039
CO ₂	304.1	73.8	0.225

By solving equation (3-66), the gas mixture molar volume (v) at specific temperature and pressure is obtained. The gas mixture density can then be calculated using equation (3-73).

$$\rho = \frac{AMW}{v} \quad (3-73)$$

Where AMW is the apparent molecular weight of the gas mixture = $\sum y_i M_i$

3.3.2 Gas Mixture Viscosity

Herning and Zipperer [128] proposed Equation (3-74) to calculate the viscosity of a gas mixture, which was validated by Davidson [129] where a 1.5% average deviation was reported.

$$\mu_{\text{mix}} = \frac{\sum(\mu_i x_i \sqrt{M_i})}{\sum(x_i \sqrt{M_i})} \quad (3-74)$$

Davidson [129] suggested that this equation is not applicable for mixtures containing significant hydrogen content.

Also, Buddenberg and Wilke [130] suggested Equation (3-75) to calculate the viscosity of a gas mixture within 2.57% deviation:

$$\mu_{\text{mix}} = \sum_{i=1}^n \frac{\mu_i}{1 + \frac{1.385\mu_i}{x_i \rho_i} \sum_{\substack{j=1 \\ j \neq i}}^n \frac{x_j}{D_{ij}}} \quad (3-75)$$

Where ρ is the density (g/m^3); μ is the viscosity (cP); D is the diffusivity (cm^2/s); x is the mole fraction.

3.3.3 Gas Mixture Thermal Conductivity

The thermal conductivity of the gas mixture is required to estimate the gas-side heat transfer coefficient. Lindsay and Bromley [131] proposed a generalized correlation for the thermal conductivity, Equation (3-76), which is similar to that of the viscosity, Equation (3-75) derived by Buddenberg and Wilke [130]:

$$\lambda_{\text{mix}} = \sum_{i=1}^n \left(\frac{\lambda_i}{\frac{1}{x_i} \sum_{j=1}^n A_{ij} x_j} \right) \quad (3-76)$$

Where A_{ij} can be calculated using Equation (3-77):

$$A_{ij} = \frac{1}{4} \left\{ 1 + \left[\frac{\mu_i}{\mu_j} \left(\frac{M_j}{M_i} \right)^{3/4} \frac{(1 + \frac{S_i}{T})}{(1 + \frac{S_j}{T})} \right]^{1/2} \right\}^2 \frac{(1 + \frac{S_{ij}}{T})}{(1 + \frac{S_i}{T})} \quad (3-77)$$

Where μ_i/μ_j could be evaluated from Eucken Equation (3-78) [132] if the viscosity data are not available.

$$\frac{\mu_i}{\mu_j} = \frac{\lambda_i(C_{pj} + 1.25 R/M_j)}{\lambda_j(C_{pi} + 1.25 R/M_i)} \quad (3-78)$$

R is the universal gas constant.

S is the Sutherland constants taken as a function of the boiling point in Kelvin which is available in Table 3-2:

$$S = 1.5T_B \quad (3-79)$$

Table 3-2: Typical Gases Boiling Point

Elements	T_B (K)
N ₂	77.35
CO ₂	194.65
Air	78.8
H ₂ O	373.15
O ₂	90.15

If both molecules are nonpolar, S_{ij} is the geometric mean of Sutherland constant of each component:

$$S_{ij} = \sqrt{S_i S_j} \quad (3-80)$$

If one of components is polar, another coefficient, Equation (3-81) is required:

$$S_{ij} = 0.733 \sqrt{S_i S_j} \quad (3-81)$$

3.3.4 Gas/Gas Diffusivity

The gas/gas diffusivity is needed for calculating the gas-side mass transfer coefficient in gas mixtures. The gas composition includes the reactive component A, the volatile liquid component S and the inert gas component B. In order to obtain the mass transfer coefficient of a single gas component into the gaseous mixture, the binary gas diffusion coefficients should be determined. These binary gas diffusion coefficients include D_{AB} , D_{AS} and D_{BS} . Fuller et al. [133] proposed a method to predict the binary gas-phase diffusion coefficients as summarized in Equation (3-82), (3-83) and (3-84).

$$D_{AB} = D_{BA} = \frac{1 \times 10^{-3} T^{1.75} (1/M_A + 1/M_B)^{1/2}}{P \left[(\sum_A v_i)^{1/3} + (\sum_B v_i)^{1/3} \right]^2} \quad (3-82)$$

$$D_{AS} = D_{SA} = \frac{1 \times 10^{-3} T^{1.75} (1/M_A + 1/M_S)^{1/2}}{P \left[(\sum_A v_i)^{1/3} + (\sum_S v_i)^{1/3} \right]^2} \quad (3-83)$$

$$D_{BS} = D_{SB} = \frac{1 \times 10^{-3} T^{1.75} (1/M_S + 1/M_B)^{1/2}}{P \left[(\sum_S v_i)^{1/3} + (\sum_B v_i)^{1/3} \right]^2} \quad (3-84)$$

$\sum_A v_i$ is the summation of the diffusion volume of each atom of the component A molecules. Similarly, the diffusion volumes for components B and S can be calculated. Fuller et al. [133] gave several diffusion volumes of typical molecules as listed in Table 3-3. As for the diffusion volumes of alkanes, ethane (C₂H₆) for instance, the summation of diffusion volumes of all atoms is needed. In this case, two carbon atoms and six hydrogen atoms lead to a diffusion volume of 44.88.

Table 3-3: Atomic Diffusion Volume and Diffusion Volume of Typical Molecules [133]

Atom	Atomic Diffusion Volume	Substance	Diffusion volume of Molecules
C	16.5	CO ₂	26.9
H	1.98	N ₂	17.9
O	5.48	O ₂	16.6
N	5.69	H ₂ O	12.7
Cl	19.5	Air	20.1
S	17.0	He	2.88
Aromatic rings	-20.2	H ₂	7.07

Also, for multicomponent gas mixture, Fairbanks and Wilke [134] suggested using Equation (3-85) for calculating the diffusivity of a single component A in the gas mixture. Equations (3-86) and (3-87) are also similar for component B and S, respectively.

$$D_{Am} = \frac{1 - y_A}{\frac{y_B}{D_{AB}} + \frac{y_S}{D_{AS}}} \quad (3-85)$$

$$D_{Bm} = \frac{1 - y_B}{\frac{y_A}{D_{BA}} + \frac{y_S}{D_{BS}}} \quad (3-86)$$

$$D_{Sm} = \frac{1 - y_S}{\frac{y_B}{D_{SB}} + \frac{y_A}{D_{SA}}} \quad (3-87)$$

Where y_A , y_B , y_S are the mole fractions of components A, B, S; and D_{Am} , D_{Bm} , D_{Sm} are effective diffusivity of component A, B, S in the gas mixture, respectively.

3.3.5 Gas/Liquid Diffusivity

The Gas/liquid diffusivity refers to CO₂ diffusivity in AMP or SG aqueous solutions. Since CO₂ reacts with both solvents, direct measurement of the diffusivity is not feasible. Laddha et al. [135], proposed to use N₂O (with a molecular weight of 44 and electronic structure similar to CO₂) to measure its diffusivity in AMP and SG because N₂O will not react with them. CO₂ and N₂O are used to measure the diffusivity in water due to the absence of chemical reactions. Once these three diffusivities are determined, the diffusivity of CO₂ in AMP or SG can be calculated according to Equation (3-88).

$$\frac{D_{\text{CO}_2,\text{L}}}{D_{\text{N}_2\text{O},\text{L}}} = \frac{D_{\text{CO}_2,\text{water}}}{D_{\text{N}_2\text{O},\text{water}}} \quad (3-88)$$

For AMP solutions, Saha et al. [136] used N₂O analogy to estimate the diffusivity of CO₂ in AMP aqueous solution. It should be mentioned that the gas diffusivity is a function of temperature and solvent concentrations. Saha et al. [136] presented some diffusivity experimental data in AMP at several temperatures and concentrations, however, no correlation was provided.

In this study, for the sake of implementing accurate diffusivity value into our MATLAB model, Polymath 6.10 was used to regress the calculated CO₂ diffusivities in AMP as a function of temperature and AMP concentration as given in Equation (3-89) with a coefficient of determination R² of 0.994. These data are presented in Figure 3-6.

$$D_{\text{CO}_2,\text{AMP}} = \left[-3.79 + 1.936 \times \exp\left(\frac{-160.33}{-445.48 + T}\right) \right] \times \left[1 - 0.19167 \times \frac{C_{\text{AMP}}}{1000} - 0.01471 \times \left(\frac{C_{\text{AMP}}}{1000}\right)^2 \right] \times 10^{-9} \quad (3-89)$$

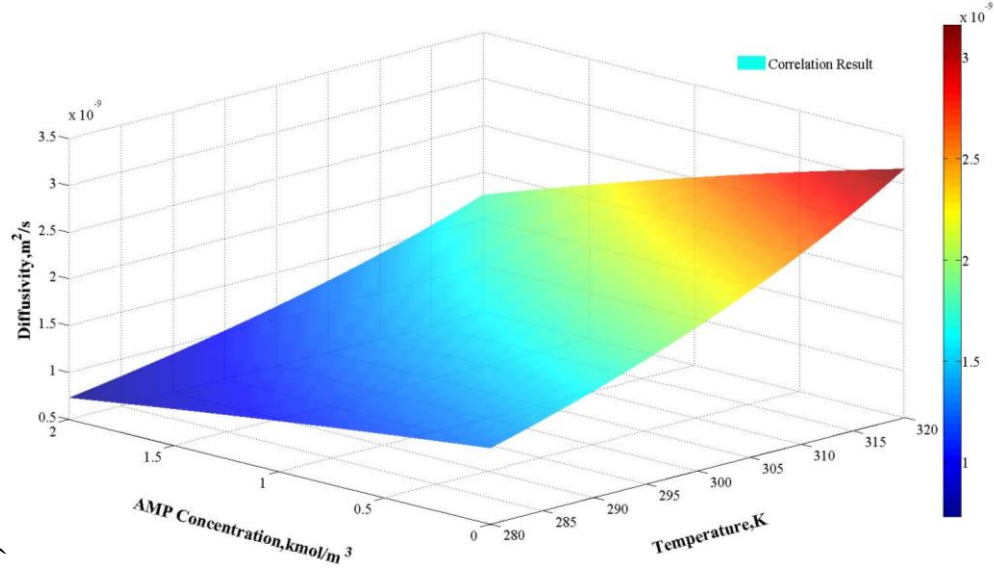


Figure 3-6: Correlated CO₂ Diffusivity as a Function of Temperature and AMP Concentration

3.3.6 Henry's Law Constant

The Henry's Law constant relates the concentration of species A in the liquid-phase to its partial pressure in the gas-phase under equilibrium conditions. Again, since CO₂ reacts with AMP, Henry's Law constant cannot be directly measured. Based on the N₂O analogy proposed by Laddha et al. [135], the Henry's law constant of CO₂ in AMP can be calculated according to Equation (3-90).

$$\frac{He_{CO_2,L}}{He_{N_2O,L}} = \frac{He_{CO_2,water}}{He_{N_2O,water}} \quad (3-90)$$

For AMP solution, Saha et al. [136] used N₂O to estimate Henry's Law Constant (He). For CO₂ in AMP solutions at different temperature and concentrations. The estimated He data were given, however, no correlation was provided.

In this study, Polymath 6.10 was used to develop a correlation for CO₂ Henry's law constant (He) in AMP using Equation (3-91) with a coefficient of determination R² of 0.994. The correlated He values for CO₂ in AMP as a function of temperature and AMP concentration are illustrated in Figure 3-7.

$$\begin{aligned}
 He_{\text{CO}_2, \text{AMP}} = & \left[643.6 + 5.197 \times 10^6 \times \exp\left(\frac{-2047.492}{-32.61 + T}\right) \right] \\
 & \times \left[1 + 0.0932515 \times \frac{C_{\text{AMP}}}{1000} + 0.0014758 \times \left(\frac{C_{\text{AMP}}}{1000}\right)^2 \right]
 \end{aligned}
 \tag{3-91}$$

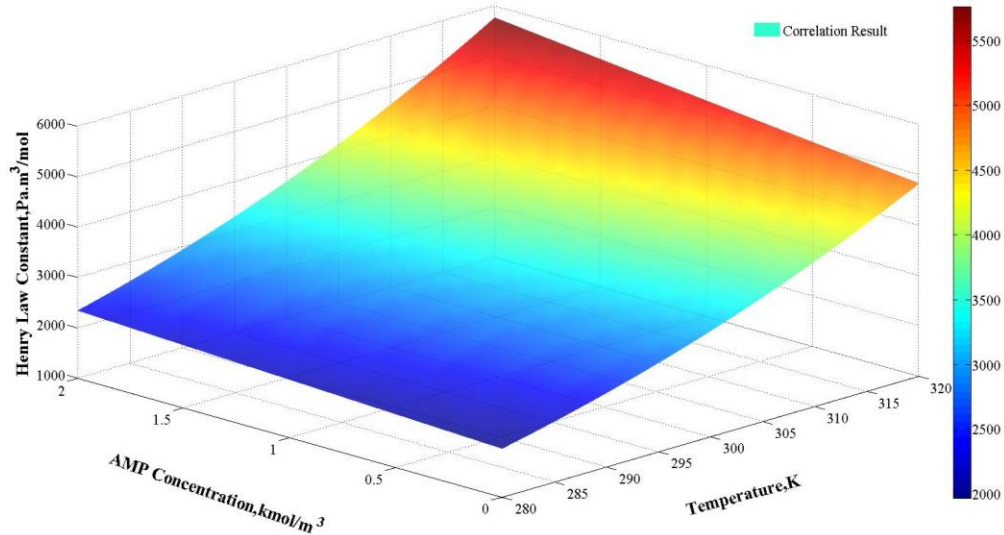


Figure 3-7: Correlated CO₂ Henry's Law Constant as a Function of Temperature and AMP Concentration

3.3.7 Liquid/Liquid Diffusivity

Liquid/liquid diffusivity is required for calculating the instantaneous Enhancement factor Equation (1-16). The diffusivity of AMP and SG solutions (R) in water (S) can be determined using Equation (3-92) developed by Wilke and Chang [137].

$$D_{R-S} = 7.4 \times 10^{-12} \frac{T(x \cdot M_s)^{1/2}}{\mu_s V_R^{0.6}} \quad (3-92)$$

Where M_s is molecular weight of the volatile solvent (S) in g/mol; V_R is molar volume of the reactant (R) at normal boiling point in cm^3/mol ; μ_s is viscosity of solvent cP; T is temperature in K; D_{R-S} is liquid/liquid diffusivity in m^2/s ; x is the association parameter, which is given in Table 3-4.

Table 3-4: Association Parameters of Different Solvents

Solvent	Association Parameter (x)
Water	2.6
Methyl Alcohol	1.9
Ethyl Alcohol	1.5
Benzene	1
Ether	1
Heptane	1

3.3.8 Heat of Absorption

The liquid-phase temperature in packed-beds is affected by the gas (A) reaction with the chemical absorbent (AMP of SG). Gabrielsen [138] introduced a model using the combined Henry's law and chemical equilibrium constant for CO₂ in AMP, (K_{CO_2}).

In this study, the values of K_{CO_2} were correlated as a function of temperature and CO₂ loading in AMP using Equation (3-93). The heat of absorption can then be calculated using the Gibbs-Helmholtz, Equation (3-94). Coupling these two equations, led to Equation (3-95), which can predict the heat of absorption as a function of temperature and CO₂ loading in AMP (α).

$$\ln(K_{CO_2}) = 37.3 - \frac{8,161}{T} + 23,826 \frac{\alpha}{T^2} \quad (3-93)$$

$$\frac{d(\ln(K_{CO_2}))}{d\left(\frac{1}{T}\right)} = \frac{-\Delta H_{CO_2}}{R} \quad (3-94)$$

$$\Delta H_{CO_2,AMP} = R\left(-8,161 + 47,652 \frac{\alpha}{T}\right) \quad (3-95)$$

Where $\Delta H_{CO_2,AMP}$ is heat of absorption J/(mol CO₂ in AMP).

For 30 wt% SG, the partial equilibrium pressures of CO₂ at a loading from 0.17 to 0.65 and temperature from 303.15 K to 323.15 K were measured by Song [75]. In this study, Equation (3-96) was developed using Polymath 6.10 to correlate these data with a coefficient of determination $R^2 = 0.92$. Similarly, for 20 wt% SG, Equation (3-97) was developed using Polymath 6.10 to correlate the CO₂ partial pressure data measured by Song [75] with a coefficient of determination $R^2 = 0.92$.

$$\ln(P_{\text{CO}_2}) = 21.52 - \frac{8,483}{T} + 1,636,000 \frac{\alpha}{T^2} \quad (3-96)$$

$$\ln(P_{\text{CO}_2}) = 15.64 - \frac{7080.35}{T} + 1,320,000 \frac{\alpha}{T^2} \quad (3-97)$$

Song [139] provided a method for calculating approximate values of the heat of absorption using the Gibbs-Helmholtz Equation (3-98).

$$\frac{d(\ln(P_{\text{CO}_2}))}{d\left(\frac{1}{T}\right)} = -\frac{\Delta H_{\text{CO}_2}}{R} \quad (3-98)$$

Therefore, for 30 wt% and 20 wt% SG solutions, the heat of reaction correlation are shown in Equation (3-99) and (3-100) respectively.

$$\Delta H_{\text{CO}_2, \text{SG}} = R\left(-8,483 + 3,272,000 \frac{\alpha}{T}\right) \quad (3-99)$$

$$\Delta H_{\text{CO}_2, \text{SG}} = R\left(-7080.35 + 2,642,000 \frac{\alpha}{T}\right) \quad (3-100)$$

Where $\Delta H_{\text{CO}_2, \text{SG}}$ is heat of absorption in J/(mol CO₂ in SG).

3.3.9 Water Vapor Pressure

Alduchov and Eskridge [140] proposed a correlation, Equation (3-101), for water vapor pressure as a function of temperature:

$$P_{\text{vap}} = 610.94 \exp\left(\frac{17.625(T - 273.15)}{T - 30.11}\right) \quad (3-101)$$

3.3.10 Latent Heat of Water Vaporization

The values of the water latent heat of vaporization (ΔH_{LV}) at temperature from 0.01 to about 220 °C are available in the Engineering Toolbox [141]. In this study, based on these values, a correlation, Equation (3-102), is developed with a coefficient of determination $R^2 = 0.999$.

$$\Delta H_{LV} = -3.068 \times 10^{-4}T^3 + 0.27778T^2 - 126.7T + 65197 \quad (3-102)$$

3.3.11 Reaction Mechanism

AMP (2-amino-2-methyl-1-propanol) is considered as an important hindered amine in sour gas treatment. The reaction mechanism of CO₂ with AMP is shown in following equations:



As can be seen, one mole of CO₂ reacts with two moles of AMP to produce one mole of carbamate. However, due to the instability of the carbamate produced, it instantly undergoes hydrolysis forming bicarbonate and releasing free amine to react again with CO₂. Hence the CO₂ loading maximum capacity of hindered amine is 1 mol of CO₂ per 1 mol amine according to stoichiometry in Equation (3-105) [87].

The carbamate formation, Equation (3-103), is applicable for primary (MEA) and secondary (DEA) amines. On the other hand, the carbamate hydrolysis, Equation (3-104), is only

applicable for tertiary amine (MDEA) or hindered amine (AMP). Thus, the comprehensive chemical expression for CO₂ reaction with AMP can be expressed by Equation (3-105), which is similar to that of CO₂ reaction with MDEA [142].

Similarly, CO₂ reacts with SG as with AMP [143]. The pseudo-first order reaction is shown below:



Thus, the stoichiometric coefficient (γ) for CO₂ reaction with SG is also 1.

3.3.12 Reaction Rate Constant

Saha et al. [64] reported that the reaction between CO₂ and AMP is first order with respect to CO₂ and first order with respect to AMP, which means the overall reaction is a second order ($k_{2,\text{CO}_2\text{-AMP}}$). They correlated the data using Equation (3-107).

$$\ln(k_{2,\text{CO}_2\text{-AMP}}) = 23.69 - \frac{5,176.49}{T} \quad (3-107)$$

Lee et al. [144] reported that the reaction between CO₂ and SG is first order with respect to CO₂ and first order with respect to SG, which means the overall reaction is a second order ($k_{2,\text{CO}_2\text{-SG}}$). They correlated the data using Equation (3-108).

$$k_{2,\text{CO}_2\text{-SG}} = 1.95 \times 10^{13} \exp\left(\frac{-7,670}{T}\right) \quad (3-108)$$

In Equations (3-107) and (3-108), k_2 is reaction rate constant expressed in $\text{m}^3/\text{kmol}/\text{s}$ and T is temperature in K.

Figure 3-8 shows an Arrhenius plot for CO_2 reactions with AMP and SG; and as can be seen in this figure, at the same temperature, CO_2 reaction rate constant with MP is always greater than that of SG.

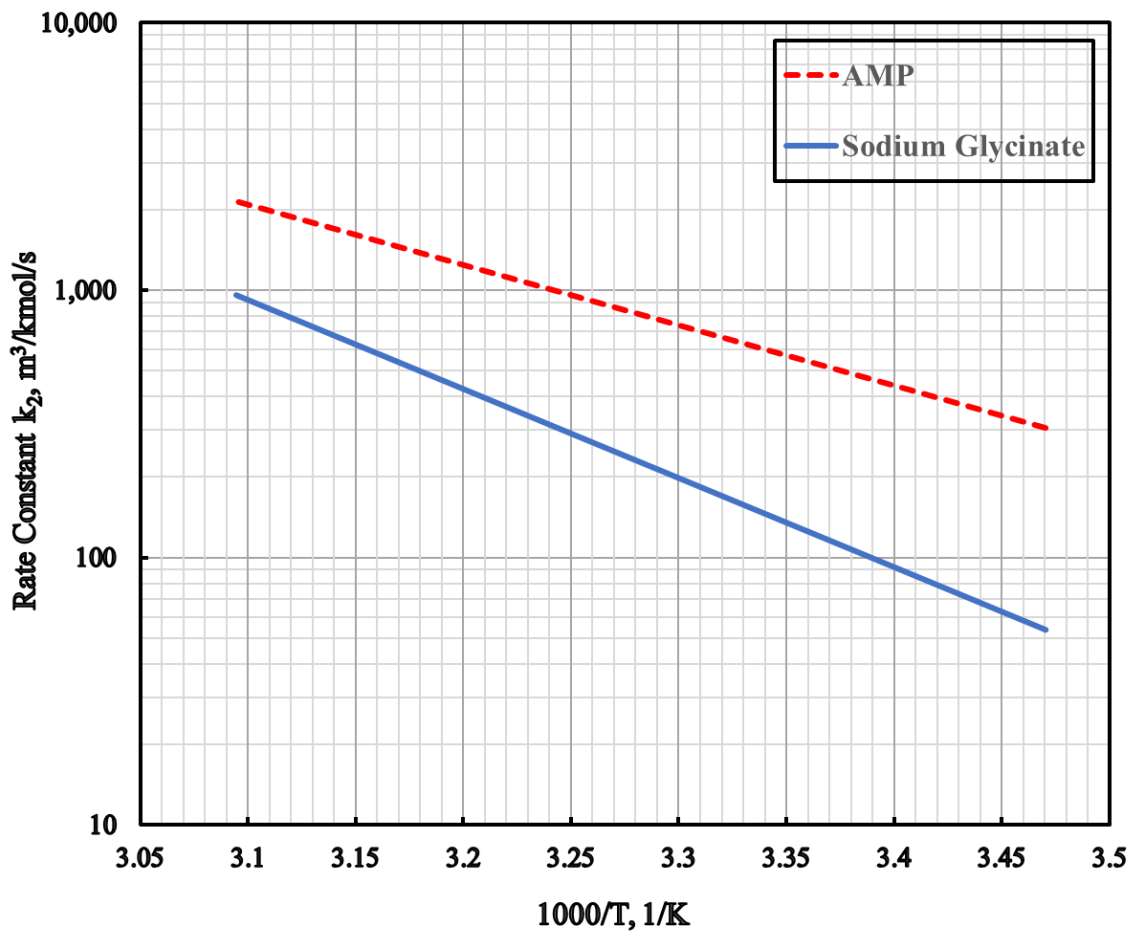


Figure 3-8: Comparison Between the Reaction Rate Constant (k_2) for AMP and SG [144, 145]

3.3.13 Mass Transfer Coefficients

In 1999, Billet and Schultes [108] updated their correlation for mass transfer coefficients with small deviation from experimental results based on one of the largest experimental database in the world at that time. They suggested the following equations to predict the specific gas-liquid interfacial area as well as the volumetric gas-side and liquid-side mass transfer coefficients:

$$\frac{a_w}{a} = 1.5(ad_h)^{-0.5} \left(\frac{u_L d_h}{v_L} \right)^{-0.2} \left(\frac{u_L^2 \rho_L d_h}{\sigma_L} \right)^{0.75} \left(\frac{u_L^2}{g d_h} \right)^{-0.45} \quad (3-109)$$

$$k_L = C_L 12^{\frac{1}{6}} \left(\frac{u_L}{\beta_L} \right)^{1/2} \left(\frac{D_L}{d_h} \right)^{1/2} \quad (3-110)$$

$$k_G = \frac{C_G}{RT} \frac{D_G}{(\varepsilon - \beta_L)^{1/2}} \left(\frac{a^{1/2}}{d_h^{1/2}} \right) \left(\frac{u_G}{av_G} \right)^{3/4} \left(\frac{v_G}{D_G} \right)^{1/3} \quad (3-111)$$

Where a_w is the specific wetted area; a is the specific packing area; ε is the bed porosity; C_L , C_G are the characteristic parameters of different packings; D_G and D_L is the gas and liquid diffusivities, d_h is hydraulic diameter of the packing which is defined by Equation (3-112); and β_L is liquid hold up which could be determined using Equation (1-35).

$$d_h = 4 \left(\frac{\varepsilon}{a} \right) \quad (3-112)$$

The characteristic parameters of different packings, including, C_G and C_L , are listed in Table 3-5. It is obvious that different packings lead to different wetted area and different mass transfer coefficients giving rise to different absorption pattern and CO₂ absorption efficiency.

Table 3-5: Characteristics of Different Packings

Packing	Nominal Size, mm	Void Fraction, ϵ	Specific Area, m^{-1}	C_L	C_G
Ceramic Berl Saddle	13	0.65	545	1.364	0.232
Ceramic Berl Saddle	25	0.68	260	1.246	0.387
Metal Pall Rings	25	0.954	223.5	1.44	0.336
Raschig Rings	50	0.83	95	1.416	0.21
Impulse Packing	100	0.838	91.4	1.317	0.327

3.3.14 Heat Transfer Coefficients

The heat transfer coefficient plays significant role in affecting the gas-phase and liquid-phase temperatures in the absorber. In order to estimate the gas-side heat transfer coefficient, Chilton and Colburn analogy [146] can be used as suggested in the literature [147]. In this analogy, the gas mass transfer related dimensionless numbers, Stanton number (St) and Schmidt number (Sc) are used to calculate the Chilton-Colburn factor for mass transfer (j_D). The definitions for these dimensionless number are given below:

$$St = \frac{k}{u} \quad (3-113)$$

$$Sc = \frac{\mu}{\rho D} \quad (3-114)$$

$$j_D = St \cdot Sc^{2/3} \quad (3-115)$$

Where k is gas-side mass transfer coefficients; D is gas diffusivity; u is the gas superficial velocity; and ρ_G is the gas density.

Also, the gas-side heat transfer related dimensionless numbers, including Stanton number for heat transfer (St_H), Prandtl number (Pr) are used to calculate the Chilton-Colburn factor for heat transfer (j_H). The definitions for these dimensionless number are given below:

$$St_H = \frac{h}{\rho C_p u} \quad (3-116)$$

$$Pr = \frac{C_p \mu}{\lambda} \quad (3-117)$$

$$j_H = St_H \cdot Pr^{2/3} \quad (3-118)$$

Where h is heat transfer coefficient, $W/m^2/K$; C_p is heat capacity, $J/kg.K$; μ is viscosity, $Pa \cdot s$; and λ is thermal conductivity, $W/m.K$.

To apply this analogy, the Chilton-Colburn factor for mass transfer and heat transfer should be equated as in Equation (3-119).

$$j_D = j_H \quad (3-119)$$

Substituting Equations (3-115) and (3-118) into Equation (3-119) gives:

$$St \cdot Sc^{2/3} = St_H \cdot Pr^{2/3} \quad (3-120)$$

Plug Equations (3-113), (3-114), (3-116) and (3-117) into Equation (3-120) and rearrange to obtain the heat transfer coefficient.

$$h = k\rho C_p \left(\frac{\lambda}{\rho C_p D} \right)^{2/3} \quad (3-121)$$

It should be mentioned that all properties in the above equation are average properties for the gas mixture. These average properties were approximately obtained using the mole fraction for each component in the mixture as shown in Equations (3-122) and (3-123).

$$\bar{D} = y_A D_{Am} + y_B D_{Bm} + y_S D_{Sm} \quad (3-122)$$

$$\bar{k} = y_A k_{Am} + y_B k_{Bm} + y_S k_{Sm} \quad (3-123)$$

For a large mass transfer flux, Pandya [98] recommended the following correlation:

$$h_G' a_w = \frac{-G_B \left(C_{PA} \frac{dY_A}{dZ} + C_{PS} \frac{dY_S}{dZ} \right)}{1 - \exp \left\{ G_B \left(C_{PA} \frac{dY_A}{dZ} + C_{PS} \frac{dY_S}{dZ} \right) / h_G a_w \right\}} \quad (3-124)$$

Where h_G is the original heat transfer coefficient and h_G' is the corrected heat transfer coefficient.

4.0 Validation of the Model Predictions Using the Data by Tontiwachwuthikul Et Al. [93] for AMP

4.1 Equation Parameters for CO₂-AMP System

In order to validate the model predictions with the experimental data by Tontiwachwuthikul et al. [93] using AMP under given boundary conditions, the following equation parameters are required to solve the combined material and energy balance equations outlined in Sections 3.2.1 and 3.2.2 .

4.1.1 Heat Capacity of the Gases Used

Aly and Lee [148] correlated the heat capacities as a function of temperature for over fifty different gaseous species. Equations (4-1), (4-3) and (4-2) represent their correlations for CO₂, N₂ and H₂O, respectively. Hilsenrath et al. [149] correlated the heat capacity of air as a function of temperature by Equation (4-4). Figure 4-1 shows the heat capacities for these four gases as a function of temperature.

$$C_{P,CO_2} = 4.184 \left\{ 7.54056 + 7.51625 \left[\frac{1442.7/T}{\sinh(1442.7/T)} \right]^2 + 5.38023 \left[\frac{647.502/T}{\cosh(647.502/T)} \right]^2 \right\} \quad (4-1)$$

$$C_{P,N_2} = 4.184 \left\{ 6.95808 + 2.03952 \left[\frac{1681.6/T}{\sinh(1681.6/T)} \right]^2 \right. \\ \left. + 0.506863 \left[\frac{5.05495/T}{\cosh(5.05495/T)} \right]^2 \right\} \quad (4-2)$$

$$C_{P,H_2O} = 4.184 \left\{ 7.97183 + 6.27078 \left[\frac{2572.63/T}{\sinh(2572.63/T)} \right]^2 \right. \\ \left. + 2.0501 \left[\frac{1156.72/T}{\cosh(1156.72)} \right]^2 \right\} \quad (4-3)$$

$$C_{P,Air} = 7 \times 10^{-12}T^4 - 3 \times 10^{-8}T^3 + 4 \times 10^{-5}T^2 - 0.0144T + 31.648 \quad (4-4)$$

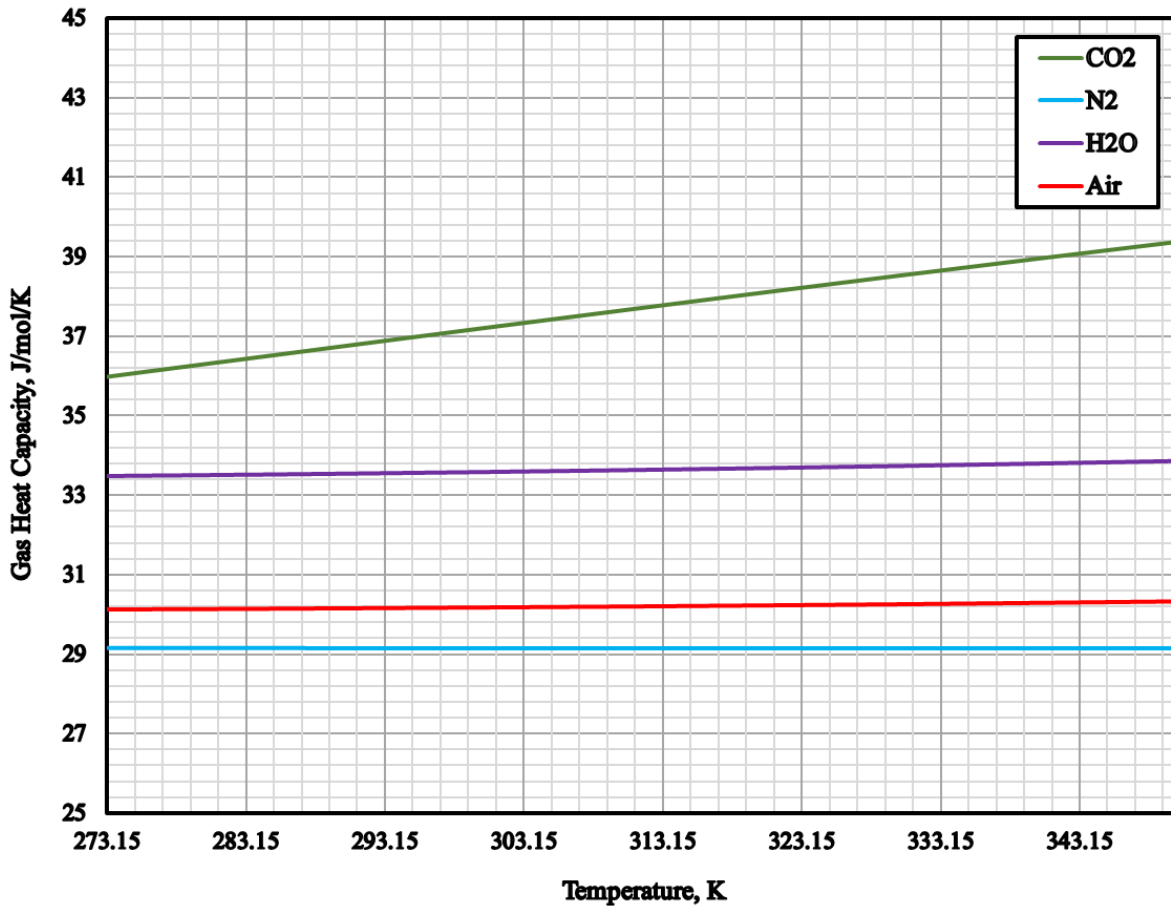


Figure 4-1: Heat Capacity of Gases as a Function of Temperature

4.1.2 Viscosity of the Gases Used

The NIST ThermoData Engine (TDE) [150] included viscosity correlations for the different gaseous species as a function of temperature. Equations (4-5) (4-7) and (4-6) represent the correlations for CO₂, N₂ and H₂O, respectively. The viscosity for air was derived from

Sutherland's formula [151] as given in Equation (4-8). Figure 4-2 shows predicted viscosities for these four gases as a function of temperature.

$$\begin{aligned} \mu_{\text{CO}_2} = & 3.322982 \times 10^{-15}T^3 - 1.882443 \times 10^{-11}T^2 + 5.84534 \times 10^{-8}T \\ & - 8.849986 \times 10^{-7} \end{aligned} \quad (4-5)$$

$$\begin{aligned} \mu_{\text{N}_2} = & 1.109011 \times 10^{-14}T^3 - 3.652352 \times 10^{-11}T^2 + 6.314212 \times 10^{-8}T \\ & + 1.897999 \times 10^{-6} \end{aligned} \quad (4-6)$$

$$\begin{aligned} \mu_{\text{H}_2\text{O}} = & 1.946393 \times 10^{-14}T^3 - 3.955387 \times 10^{-11}T^2 + 6.283711 \\ & \times 10^{-8}T - 6.607122 \times 10^{-6} \end{aligned} \quad (4-7)$$

$$\mu_{\text{Air}} = 1.827 \times 10^{-5} \left(\frac{410.85885}{0.999T + 120} \right) \left(\frac{1.8T}{524.07} \right)^{3/2} \quad (4-8)$$

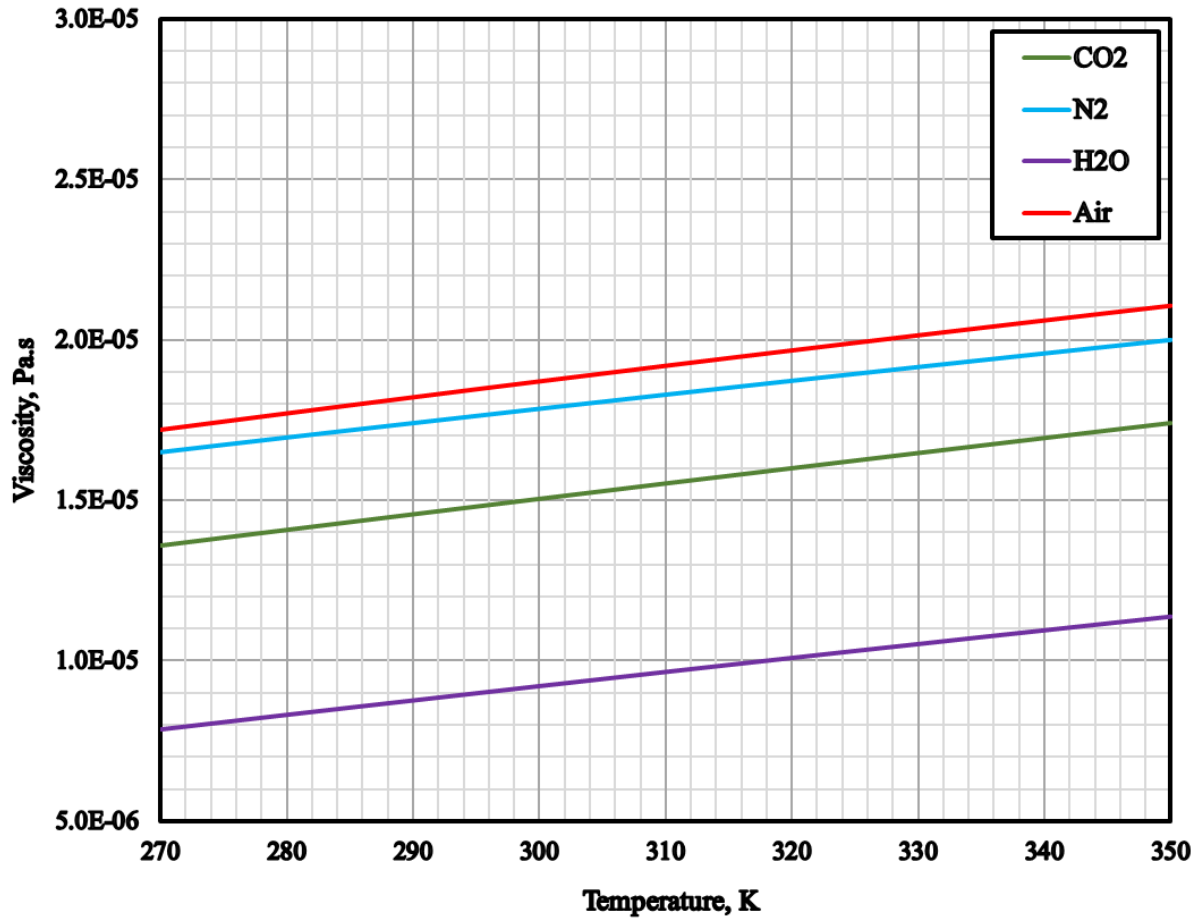


Figure 4-2: Viscosity of Gases as a Function of Temperature

4.1.3 Thermal Conductivity of the Gases Used

The NIST ThermoData Engine (TDE) [150] included thermal conductivity correlations for different gaseous species as a function of temperature. Equations (4-9) and (4-11) represent the thermal conductivities for CO₂ and H₂O, respectively. It should be mentioned that Equation (4-11)

is applicable at $T > 326$ K. At low temperature, the water vapor is extremely small and accordingly its thermal conductivity is negligible. The thermal conductivity of N_2 is reported by Nuttall and Ginnings [152] as Equation (4-10). The thermal conductivity of air is obtained from Reference [153] as Equation (4-12). Figure 4-3 shows the thermal conductivities for the four gases as a function of temperature.

$$\lambda_{CO_2} = -1.075683 \times 10^{-10}T^3 + 1.527046 \times 10^{-7}T^2 + 1.364015 \times 10^{-5}T + 0.001530777 \quad (4-9)$$

$$\lambda_{N_2} = 2.495 \times 10^{-2} + 6.366 \times 10^{-5}(T - 273.15) - 1.065 \times 10^{-8}(T - 273.15)^2 \quad (4-10)$$

$$\lambda_{H_2O} = 5.123663 \times 10^{-10}T^3 - 9.526834 \times 10^{-7}T^2 + 0.0006864713T - 0.132026 \quad (4-11)$$

$$\lambda_{Air} = 1.5207 \times 10^{-11}T^3 - 4.8574 \times 10^{-8}T^2 + 1.0184 \times 10^{-4}T - 3.9333 \times 10^{-4} \quad (4-12)$$

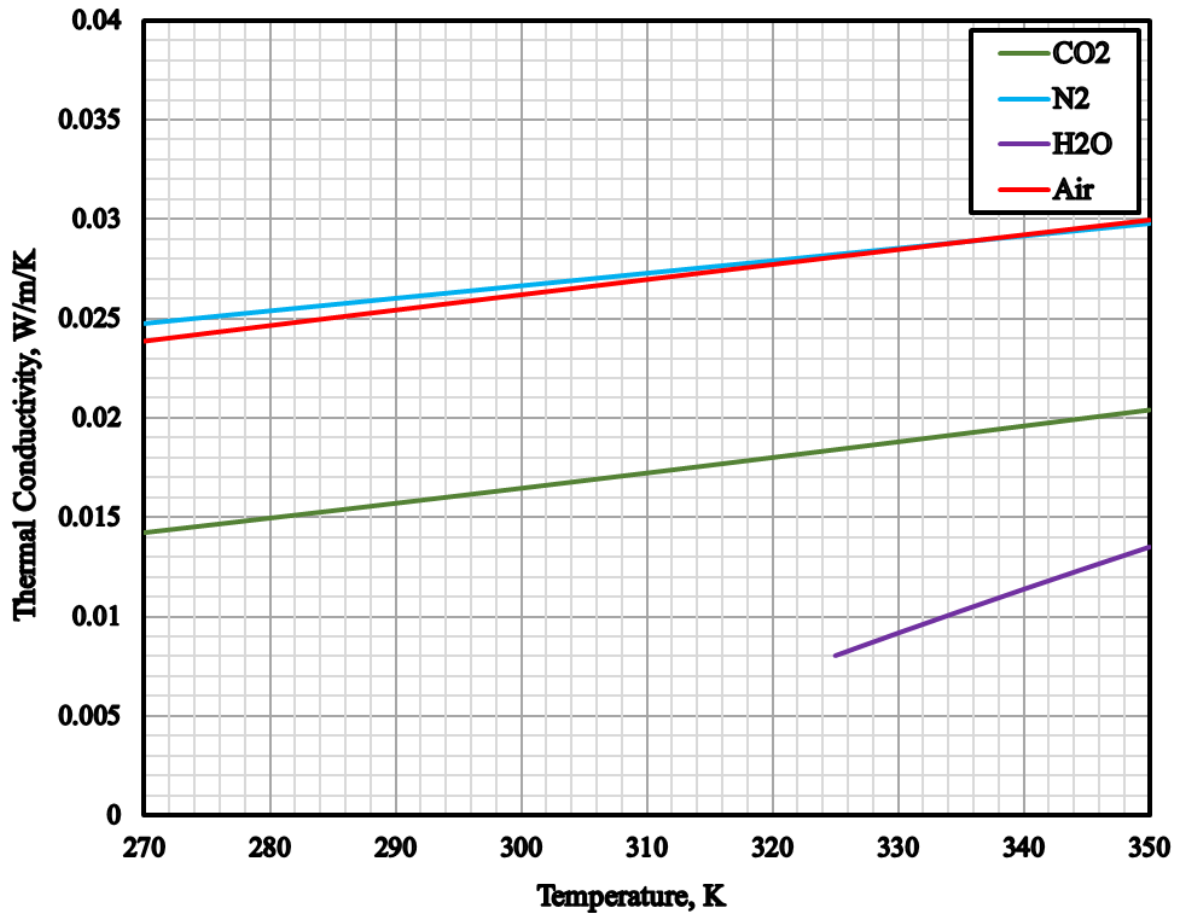


Figure 4-3: Thermal Conductivity of Gases as a Function of Temperature

4.1.4 Density of AMP Aqueous Solutions

The density of AMP aqueous solutions was measured by Henni et al. [154] at different mole fractions of AMP and temperature from 25 °C to 70 °C. In this study, Equation (4-13) is developed using Polymath 6.10 to predict the experimental data with a coefficient of determination

$R^2 = 0.993$. Figure 4-4 shows the density of AMP solution as a function of its mole fraction (X_2) at different temperatures.

$$\rho_{AMP-H_2O} = (1.15 - 0.062X_2 - 0.257X_2^2 + 0.4125X_2^3 - 0.182X_2^4) \times \left[888 - 0.52(T - 273.15) - 1.6 \frac{(T - 273.15)^2}{1000} \right] \quad (4-13)$$

Where, X_2 represents AMP mole fraction in solution.

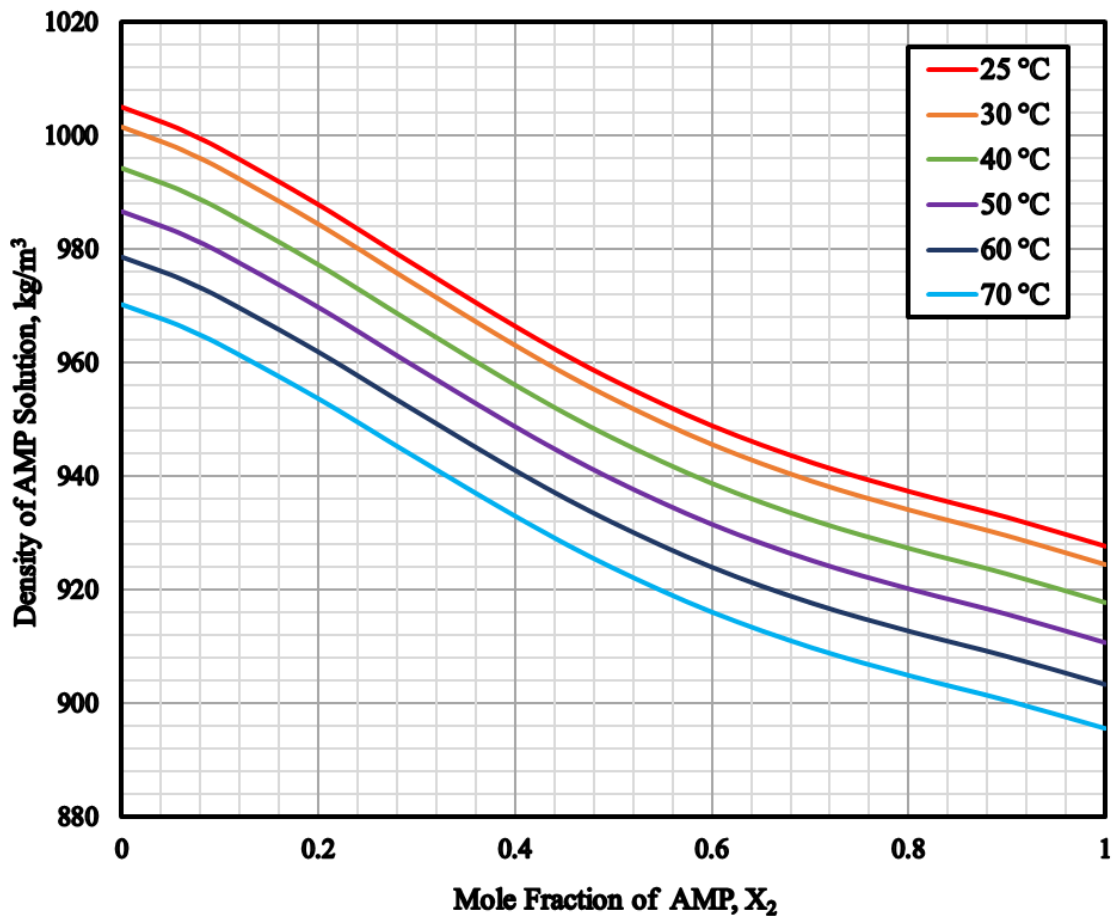


Figure 4-4: Density of AMP Aqueous Solutions as a Function of Their Mole Fractions at Different Temperatures

4.1.5 Viscosity of AMP Aqueous Solutions

The viscosity of AMP aqueous solutions was measured by Henni et al. [154] as a function of mole fraction of AMP at different temperatures from 25 °C to 70 °C. In this study, Equation (4-14) is developed using Polymath 6.10 to predict the data with a coefficient of determination R^2

= 0.987. Figure 4-5 shows the viscosity of AMP aqueous solutions as a function of its mole fraction (X_2) at different temperatures.

$$\mu_{\text{AMP-H}_2\text{O}} = \exp \left\{ \left(-0.23 + 10.68X_2 - 18.84X_2^2 + 17.765X_2^3 - 6.833X_2^4 \right) \left[2.86 - 39.72 \frac{T - 273.15}{1000} + 154.01 \left(\frac{T - 273.15}{1000} \right)^2 \right] \right\} \quad (4-14)$$

Where $\mu_{\text{AMP-H}_2\text{O}}$ is viscosity of AMP solution, mPa.s.

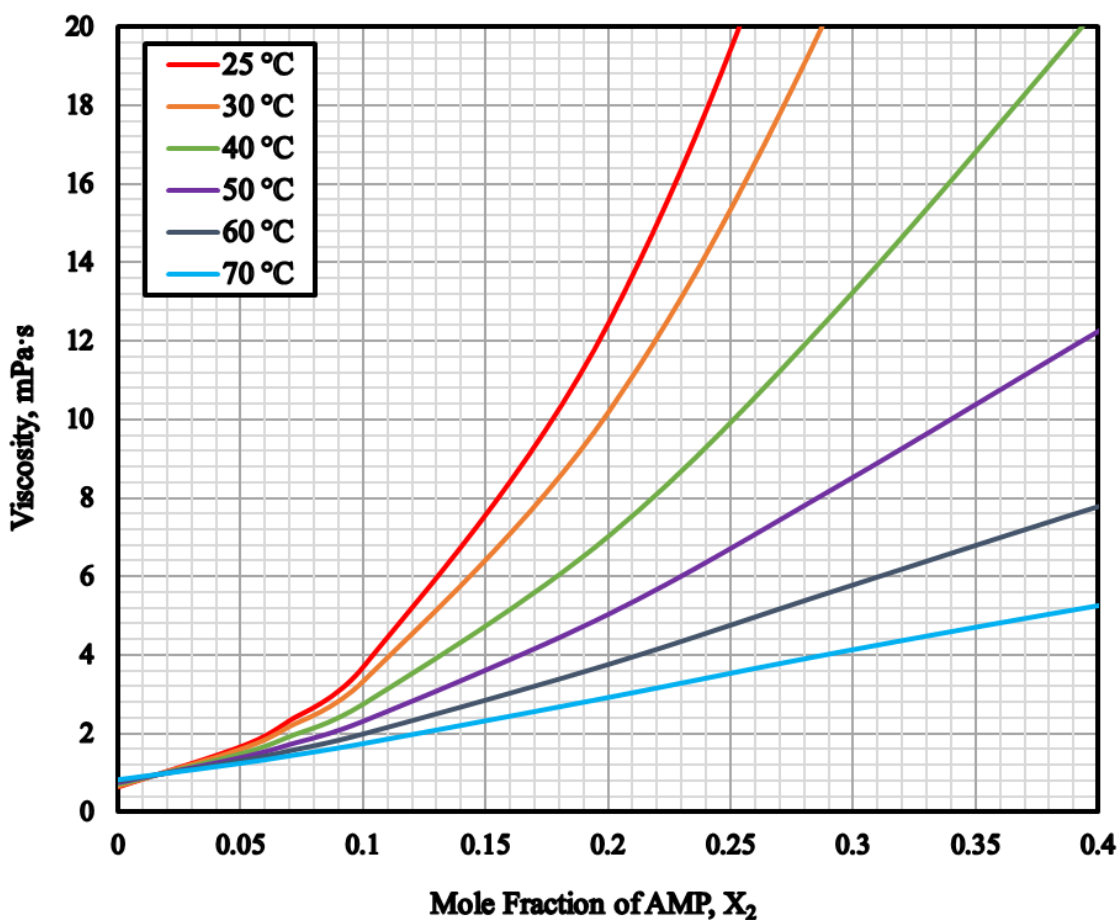


Figure 4-5: Viscosity of AMP Aqueous Solutions as a Function of Their Mole Fractions at Different Temperatures

4.1.6 Surface Tension of AMP Aqueous Solutions

The surface tension of AMP aqueous solutions was measured by Vazquez et al. [155] as a function of its mole fraction at temperatures from 25 °C to 50 °C. In this study, Equation (4-15) is developed using Polymath 6.10 to predict the data with a coefficient of determination $R^2 = 0.998$.

Figure 4-6 shows the surface tension of AMP aqueous solution as a function of its mole fraction (X_2) at different temperatures.

$$\begin{aligned} \sigma_{\text{AMP-H}_2\text{O}} = & \exp\{[1.17533 - 0.0489693\ln(X_2)] \\ & \times [2.979431 - 0.0023579(T - 273.15)]\} \end{aligned} \quad (4-15)$$

Where $\sigma_{\text{AMP-H}_2\text{O}}$ is surface tension of AMP solution, mN/m.

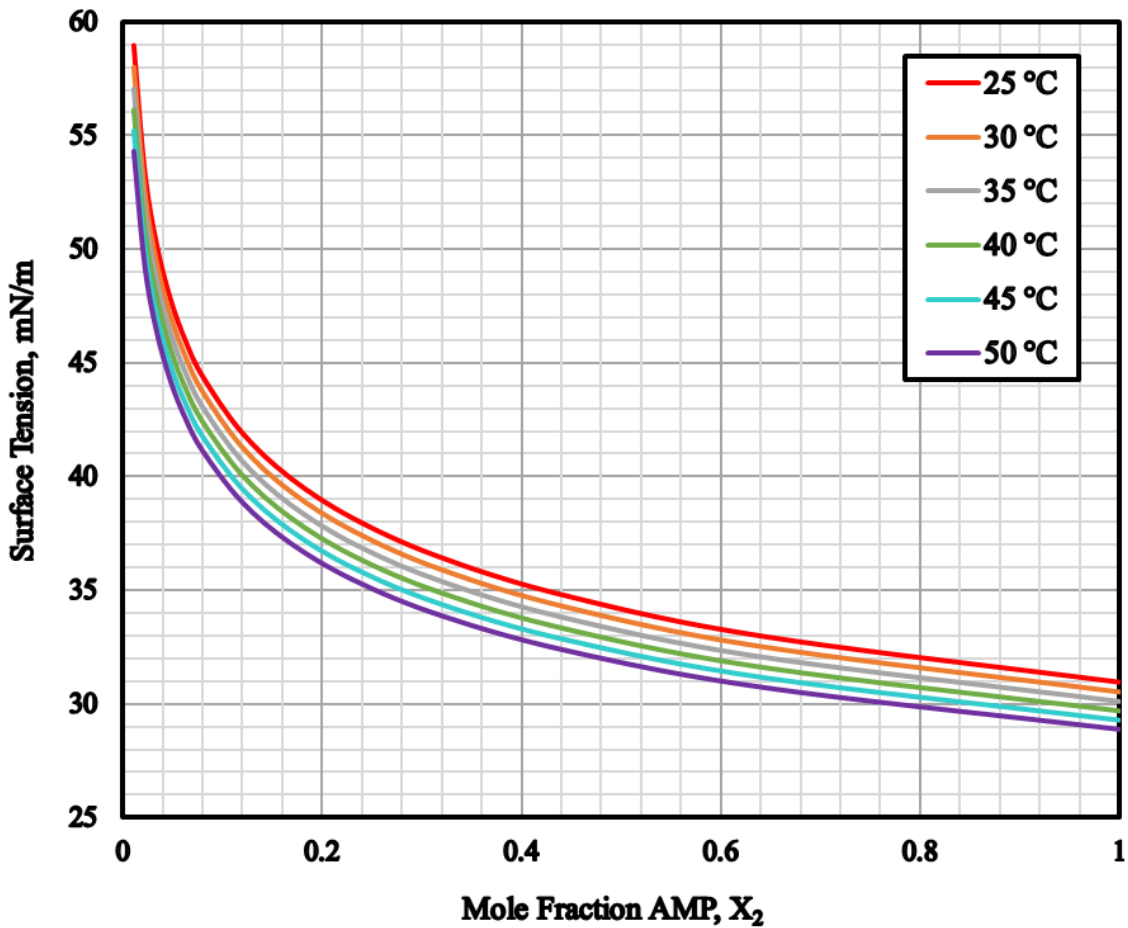


Figure 4-6: Surface Tension of AMP Aqueous Solutions as a Function of Their Mole Fractions at Different Temperatures

4.1.7 Heat Capacity of AMP Aqueous Solutions

The molar heat capacity of pure AMP by Chen and Li [156] was correlated as a function of temperature by Equation (4-17). The molar heat capacity of AMP aqueous solutions was also measured as a function by Chen and Li [156] as a function of its mole fraction at temperatures from 30 °C to 80 °C and they provided a correlation to predict their experimental data. Lide and

Kehiaian [157] proposed a method to calculate the heat capacity of a mixture using Equation (4-18). Also, in this study, the heat capacity for liquid H₂O as a function of temperature, available at NIST ThermoData Engine (TDE) [150] are correlated using Equation (4-16).

$$C_{P,H_2O} = \left[1000.182 / \left(1 - \frac{T}{647.1081} \right) + 53867.96 + 282.323T - 1.173532T^2 + 0.001503196T^3 \right] / 1000 \quad (4-16)$$

$$C_{P,AMP} = 85.68 + 0.513T \quad (4-17)$$

$$C_{P,AMP-H_2O} = C_{pExcess} + \sum_i x_i C_{P,i} \quad (4-18)$$

Where $C_{pExcess}$ is the excess molar heat capacity and $C_{p,i}$ represents the molar heat capacity of pure component.

For a binary system, Redlich and Kister [158] proposed Equation (4-19) to calculate the excess molar heat capacity.

$$C_{pExcess} = x_1 x_2 \sum_{i=1}^2 A_i (x_1 - x_2)^{i-1} \quad (4-19)$$

Where the temperature-dependent parameter A_i could be determined using Equations (4-20) and (4-21), developed specifically by Chen and Li [156] for AMP aqueous solutions.

$$A_1 = -170.32 + 0.6236T \quad (4-20)$$

$$A_2 = -52.19 + 0.1575T \quad (4-21)$$

Figure 4-7 shows the heat capacity of AMP aqueous solutions as a function of their mole fractions (X_2) at different temperatures.

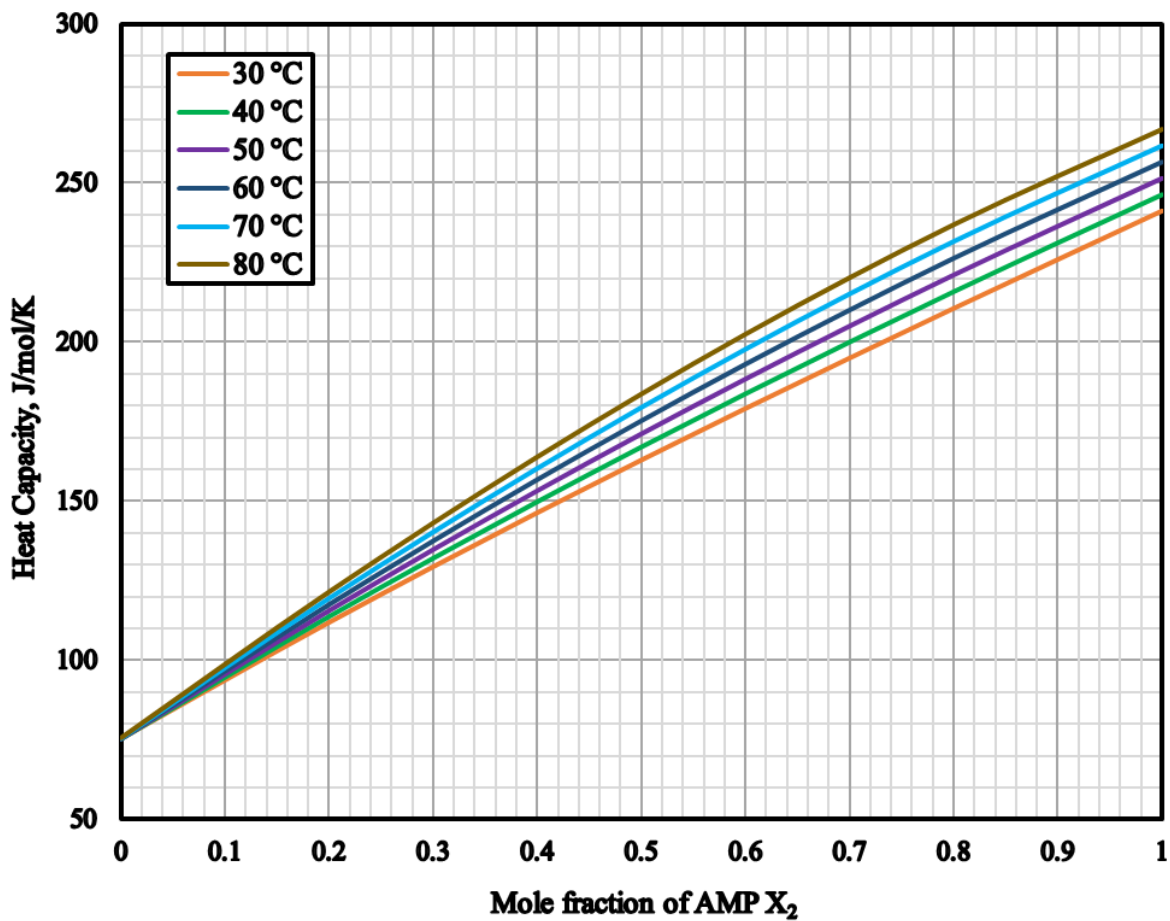


Figure 4-7: Heat Capacity of AMP Aqueous Solutions as a Function of Their Mole Fractions at Different Temperatures

4.2 Comparison Between Model Predictions and the Data by Tontiwachwuthikul Et Al.

[93]

All equation parameters correlated and plotted in the previous sections were inserted in the model equations, which were implemented in MATLAB 2017b to solve the equations under given boundary conditions. The experimental data by Tontiwachwuthikul et al. [93] for CO₂ absorption from a mixture with air in AMP in aqueous solutions using an adiabatic lab-scale packed-bed absorber were used to validate our model predictions. Tontiwachwuthikul et al. [93] conducted a total of 8 different runs for CO₂ absorption using AMP aqueous solutions in a small-scale (0.1 m ID) adiabatic absorber packed with a 12.7 mm ceramic Berl Saddles to a height of 6.55m). It should be mentioned that some runs were replicates, to ensure reproducibility, and other runs exhibit significant errors in the CO₂ material balance.

In this study, runs T24, T25, T26 and T28 were selected to validate our model predictions, which covers CO₂ loading from 0.22 to 0.371 mole CO₂/initial mole of AMP. It should be mentioned that the initial AMP concentration is 2 kmol/m³ in all runs. However, since the given initial loading of CO₂ in the solutions is different for these runs, the inlet AMP concentrations in Table 4-1 should be different. In addition, because the packing characteristics for 12.7 mm ceramic Berl Saddles are not available in the literature, a 13 mm ceramic Berl Saddles packing with the characteristics shown in Table 3-5 was used in our model.

Table 4-1: Inlet Stream Conditions Used in Our Model

Inlet Parameters	T24	T25	T26	T28
Gas Temperature, °C	15	15	15	15
CO ₂ Mole Fraction	0.1545	0.189	0.1865	0.1915
Inert Gas (Air) Flow Rate, mol/m ² /s	14.8	14.8	14.8	14.8
Packed height, m	4.35	6.55	6.55	6.55
Liquid Temperature, °C	15	15	15	15
Liquid Velocity, m/h	9.5	9.5	9.5	9.5
Inlet AMP Concentration, mol/m ³	1,706	1,696	1,956	1,258
Initial CO ₂ Loading, mol CO ₂ /mol AMP	0.147	0.152	0.022	0.371

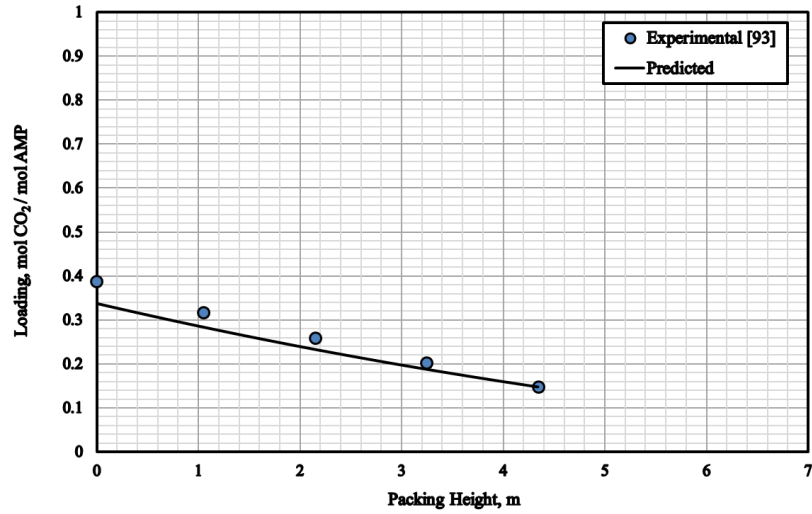
Figure 4-8 shows a comparison between the experimental loading (mole of CO₂/initial mole of AMP) for Runs T24, T25, T26 and T28. As can be observed in this figure, the predicted values are in a good agreement with the experimental data, particularly for T28. However, the deviation in T24 and T25 can be attributed to the experimental errors in the CO₂ material balance calculations in these runs.

Figure 4-9 shows a comparison between the experimental and predicted liquid temperature profiles for Runs T24, T25, T26 and T28 and a good agreement between the model predictions and the experimental data can be reported. The slight deviation between the experimental and predicted data for run T28 corroborate previous findings by Gabrielsen et al. [101]. It should be emphasized that the predicted temperature profiles fit experimental data better than the model by Gabrielsen et al [101], especially for run T25. Tontiwachwuthikul et al. [93] did not measure the gas temperature profile, however, the model predicted that the gas enters at the bottom of the bed at 15 °C and it exhibits a rise in a form of bulge once CO₂ reacts the AMP. The gas then continues

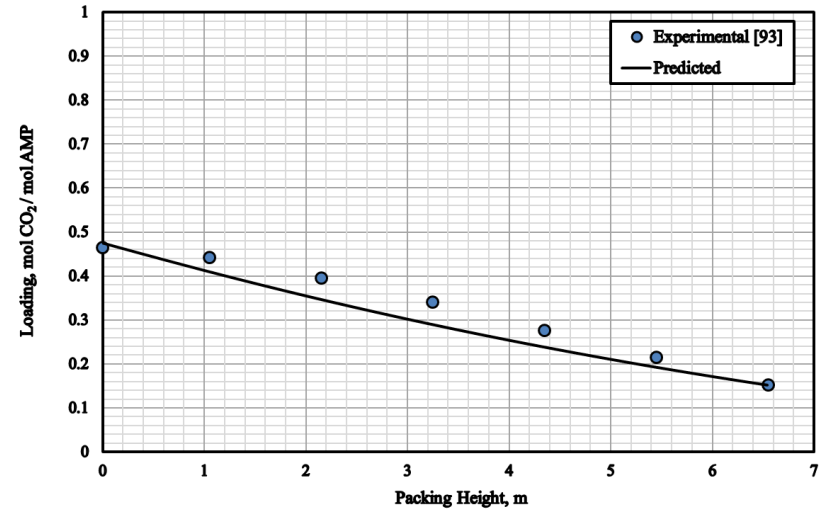
to react and exchange heat with the liquid to ultimately exit at the top of the absorber at about 15°C which is the liquid inlet temperature.

Figure 4-11 shows the mole fraction profiles of the CO₂ for Runs T24, T25, T26 and T28 and a slight maximum deviation (+ 11%) can be calculated between the experimental data and predicted values. However, to our surprise the deviation appears to be larger for run (T28), since the experimental errors of CO₂ mole fraction were minimum. This slight deviation could be related to the difference between the packing size since Tontiwachwuthikul et al. [93] used 12.7 mm in their studies where 13 mm packing was used in our model.

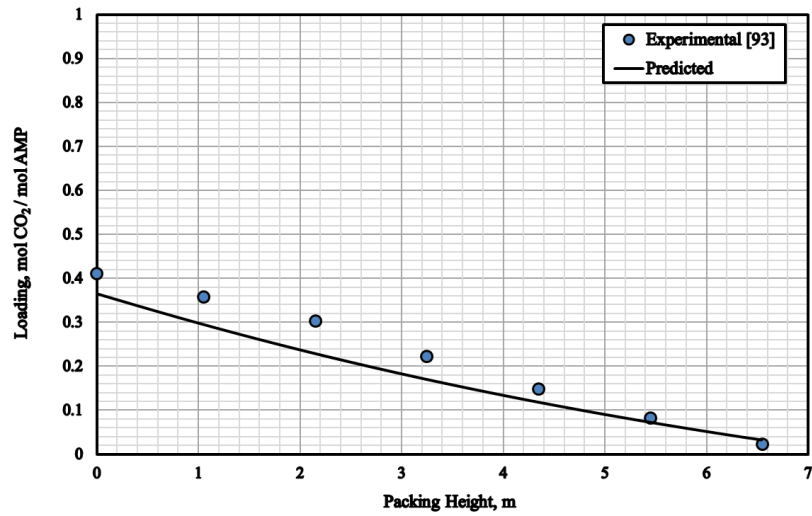
Figure 4-12 shows the enhancement factor and Hatta number due to the chemical reaction between CO₂ and AMP; and as can be observed the enhancement factor value are between 4.85 and 5.3 for run T25, between 5.4 and 5.95 for run T26 and between 3.7 and 4.1 for run T28. In all runs, Hatta number (Ha) is > 2 and accordingly the reaction is fast. These findings are also in agreement with previous analysis of the same data by Gabrielsen et al. [101].



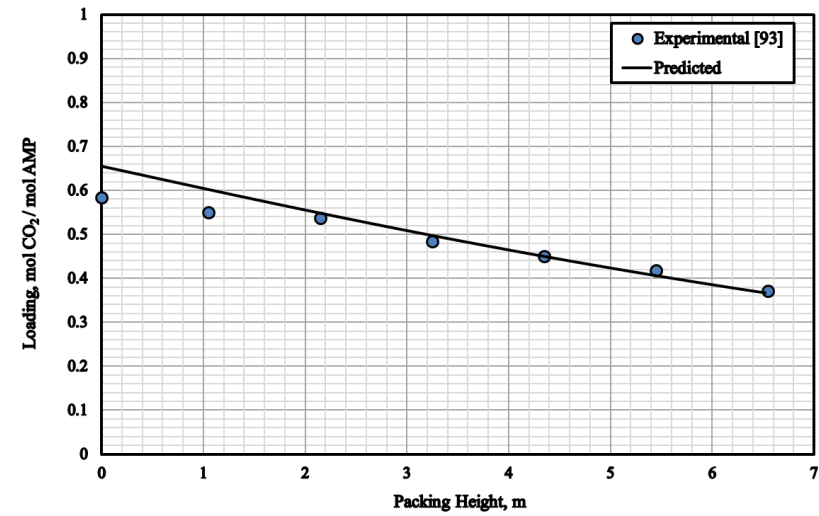
(a) Run T24



(b) Run T25

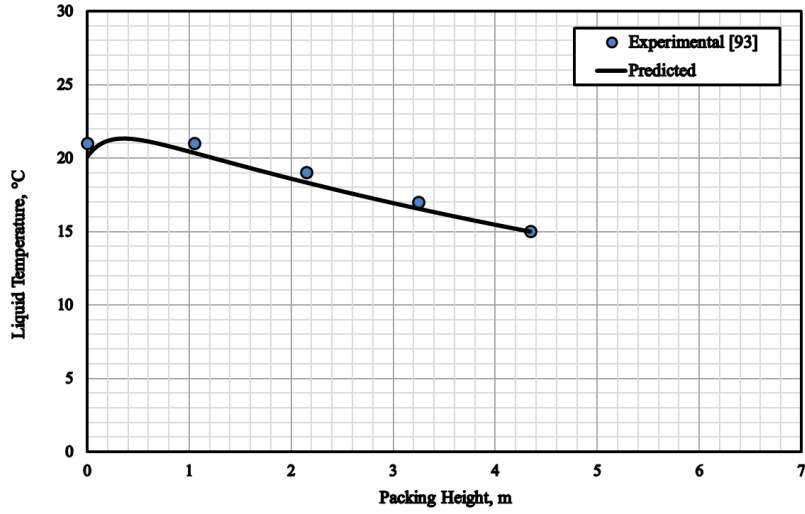


(c) Run T26

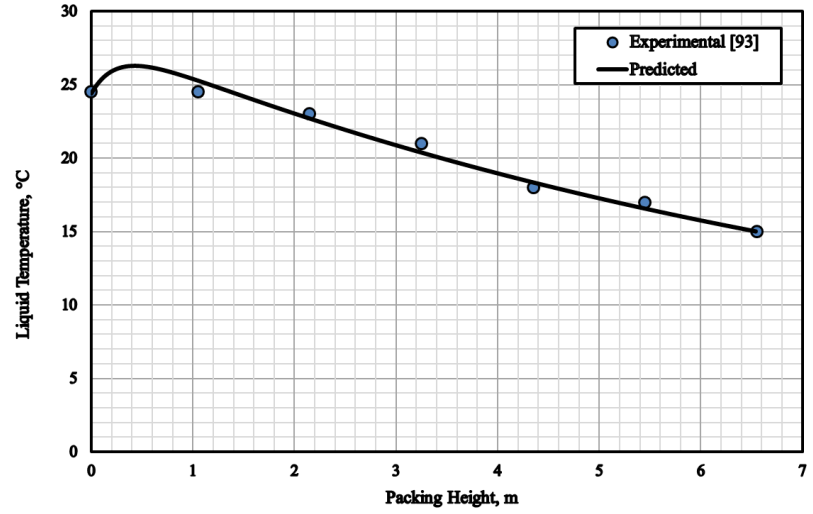


(d) Run T28

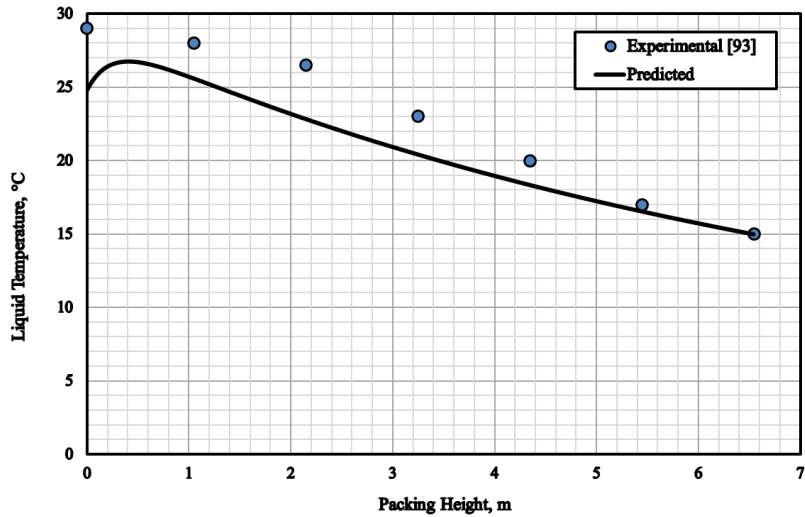
Figure 4-8: Comparison Between CO₂ Loading of Experimental Data [93] and Model Predictions



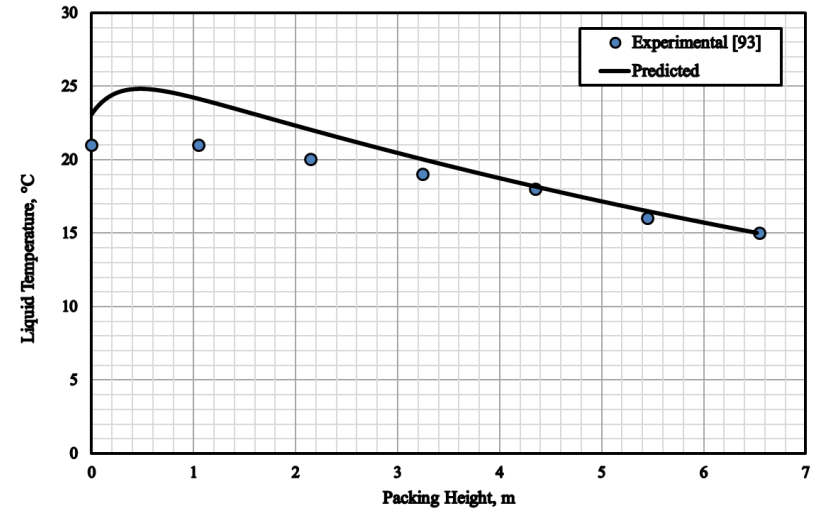
(a) Run T24



(b) Run T25

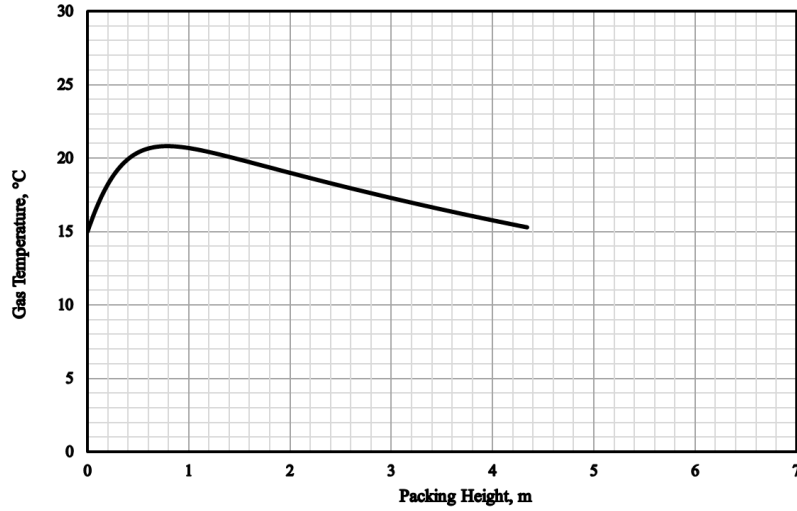


(c) Run T26

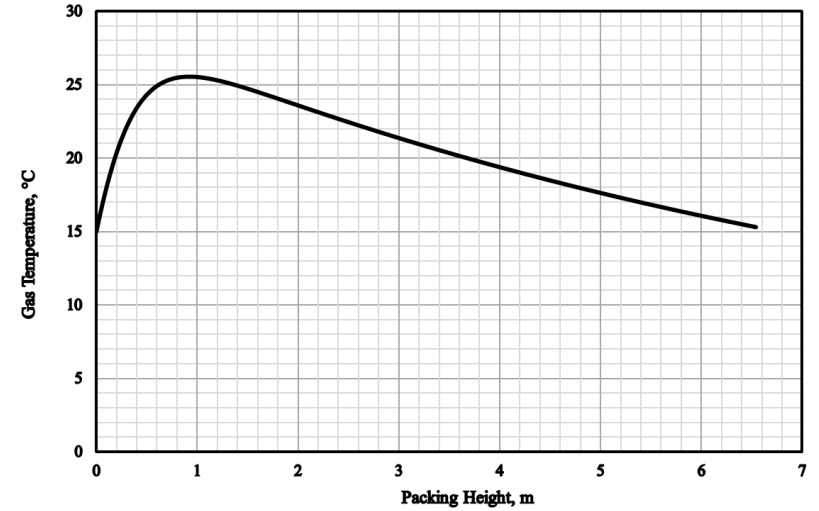


(d) Run T28

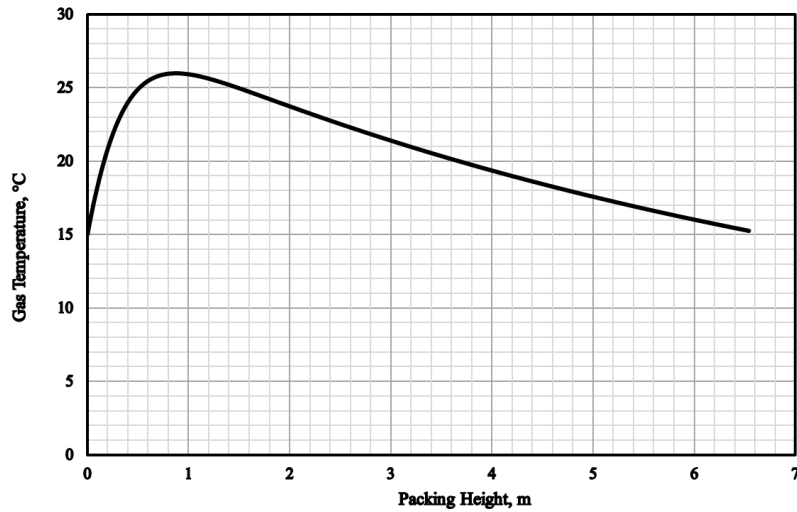
Figure 4-9: Comparison Between Liquid Temperature of Experimental Data [93] and Model Predictions



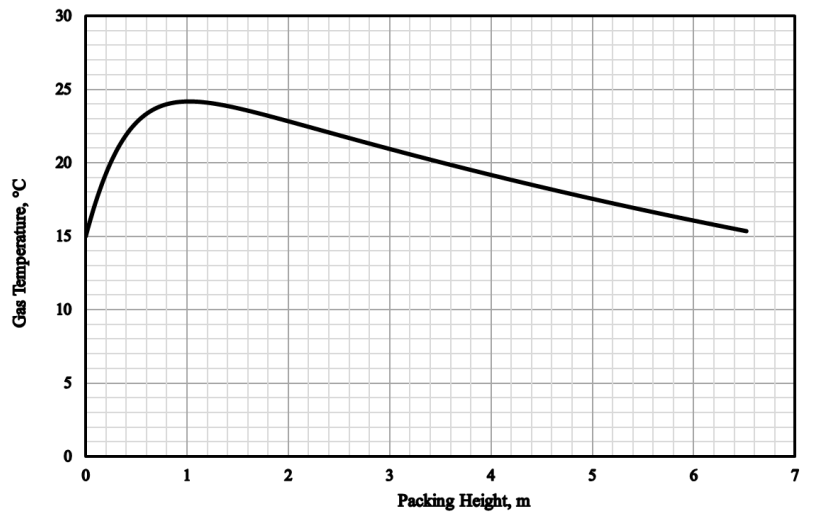
(a) Run T24



(b) Run T25

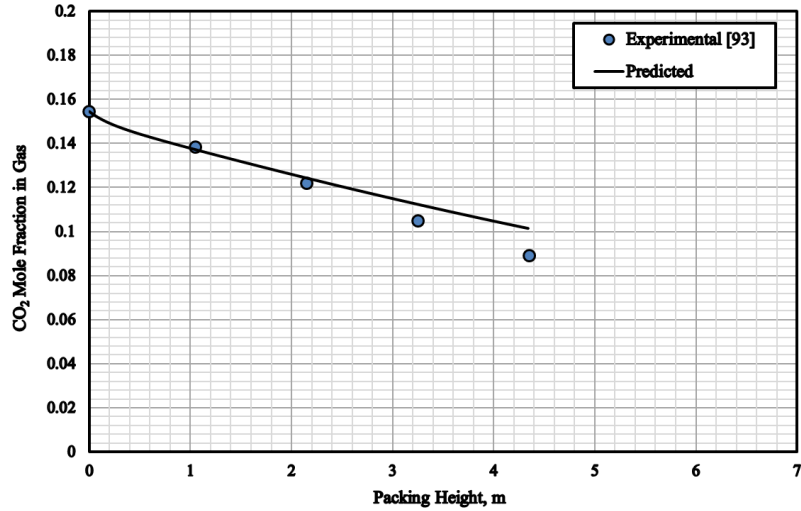


(c) Run T26

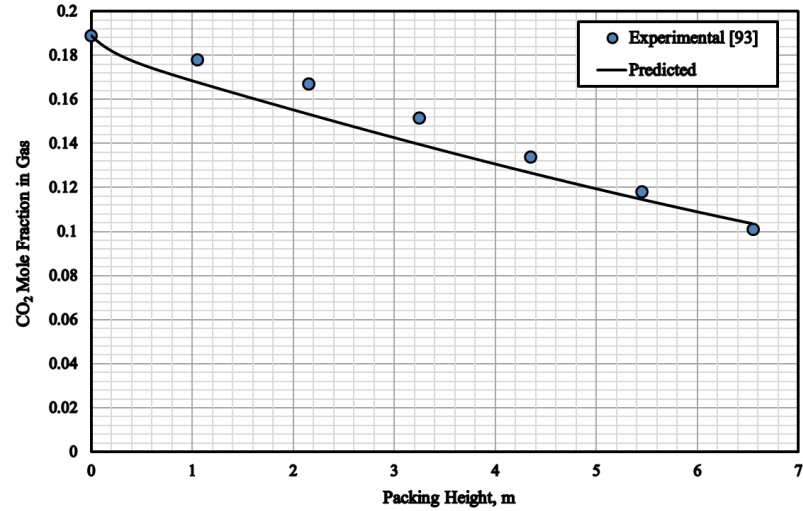


(d) Run T28

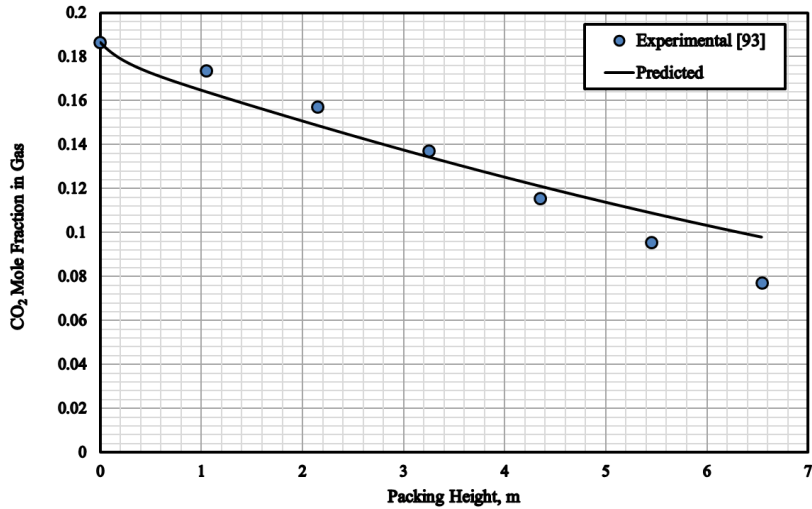
Figure 4-10: Model Predictions of Gas Temperature



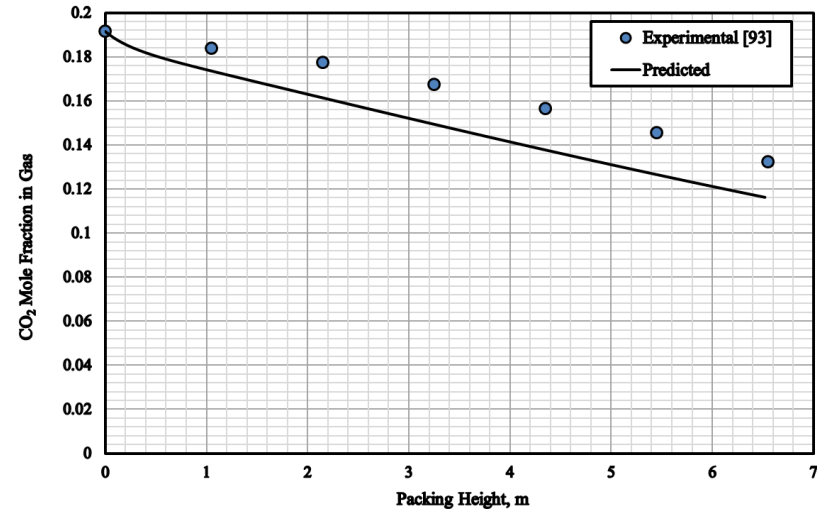
(a) Run T24



(b) Run T25

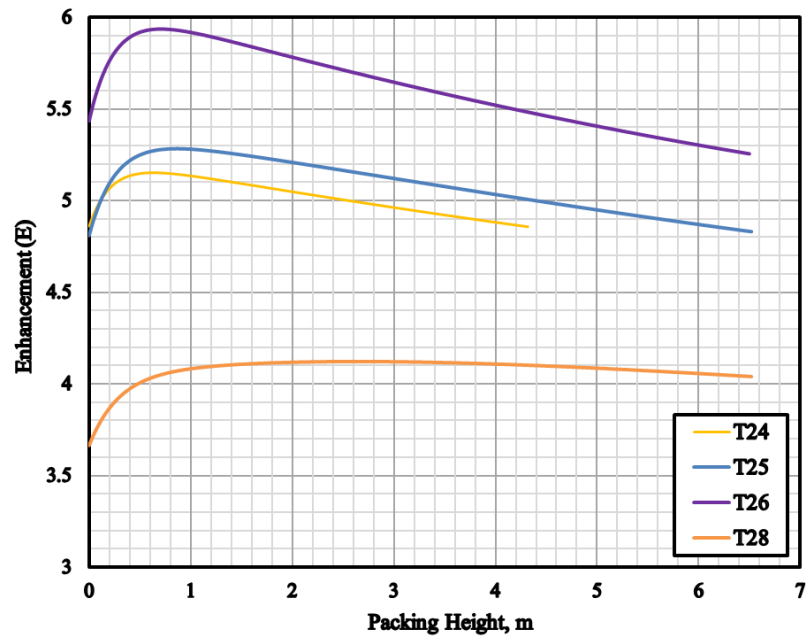


(c) Run T26

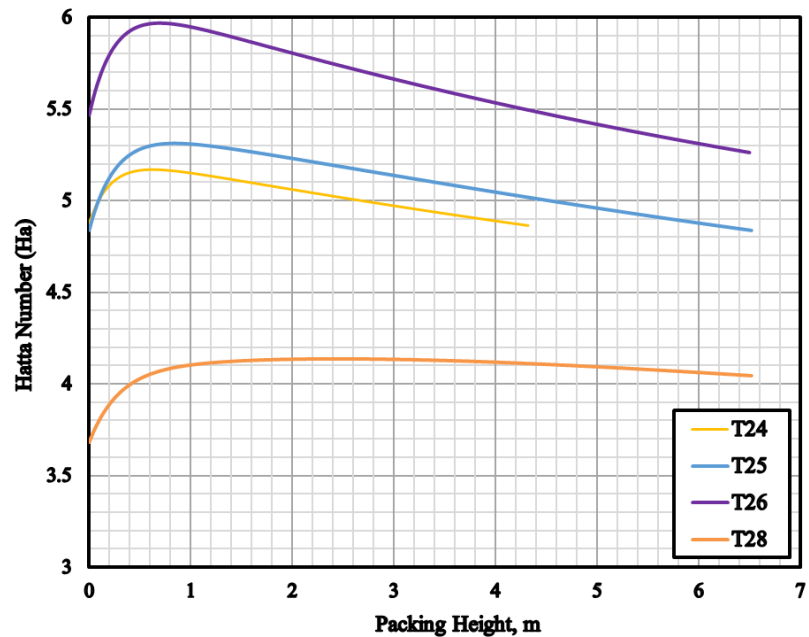


(d) Run T28

Figure 4-11: Comparison Between CO₂ Mole Fraction of Experimental Data [93] and Model Predictions



(a)



(b)

Figure 4-12: Predicted Enhancement Factor and Hatta Number Along the Absorber

4.3 Model Predictions of CO₂ Absorption from CO₂-Air Mixtures Using SG

The validated model was then used to predict the performance of a small-scale (0.1 m ID) packed-bed absorber for CO₂ capture from a CO₂/air gaseous mixture using SG aqueous solutions. The model predictions include CO₂ mole fraction, CO₂ loading, CO₂ capture efficiency, gas-phase temperature, liquid-phase temperature, bicarbonate production, etc.

4.3.1 Equation Parameters for CO₂-SG System

The equation parameters for CO₂-SG solutions used in the model are calculated in the following.

4.3.1.1 Diffusivity of CO₂ in SG Aqueous Solution

Lee et al. [159] calculated the CO₂ diffusivity in SG aqueous solutions based on N₂O approach since CO₂ will react with SG. In 2007, Lee et al. [144] reported some CO₂ Diffusivity data at different temperatures and concentrations of aqueous SG.

In this study, the calculated data for CO₂ diffusivity in SG by Lee et al. [144] were correlated as a function of temperature and SG mole fraction using Equation (4-22) with a coefficient of determination R^2 of 0.973 and the correlated data are presented in Figure 4-13.

$$D_{\text{CO}_2,\text{SG}} = \left[-11.72677 + 4.710358 \times \exp\left(\frac{-371.6519}{-645.3103 + T}\right) \right] \times \left[1 - 0.2537316 \times \frac{C_{\text{SG}}}{1000} + 0.0393937 \times \left(\frac{C_{\text{SG}}}{1000}\right)^2 \right] \times 10^{-9} \quad (4-22)$$

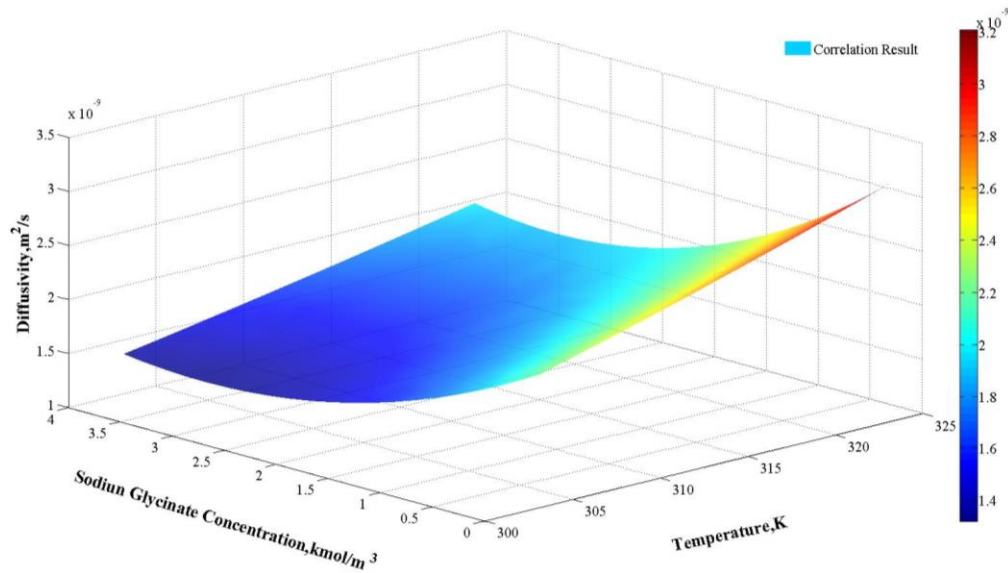


Figure 4-13: Correlated CO₂ Diffusivities in SG Aqueous Solutions

4.3.1.2 Henry's Law Constant of CO₂ in SG in Water Solution

Lee et al. [144, 159] reported CO₂ Henry's law constant (H_e) for CO₂ in SG solutions at different temperatures (303.15 K to 323.15 K) and SG concentrations.

In this study, the H_e values were correlated as a function of temperature and SG concentrations using Equation (4-23) with a coefficient of determination R^2 of 0.990 and the correlation is illustrated and given in Figure 4-14.

$$H_{e_{CO_2,SG}} = \left[1830.944 + 1.91 \times 10^7 \times \exp\left(\frac{-2129.477}{-78.36419 + T}\right) \right] \times \left[1 + 0.0537939 \times \frac{C_{SG}}{1000} - 0.0026344 \times \left(\frac{C_{SG}}{1000}\right)^2 \right] \quad (4-23)$$

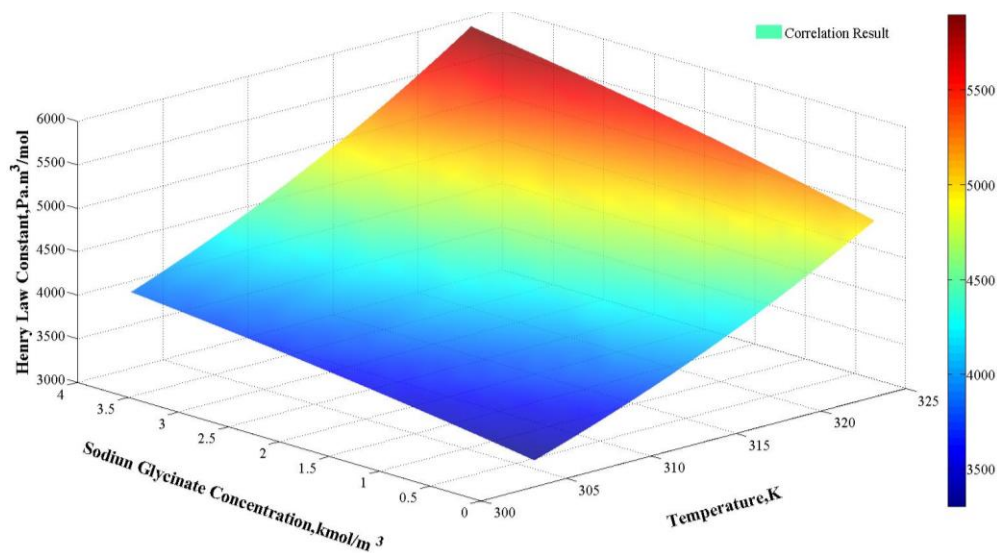


Figure 4-14: Correlated Henry's Law Constant for CO₂ in SG Aqueous Solutions

4.3.1.3 Density of SG Aqueous Solutions

The density of SG aqueous solutions was measured by Lee et [160] as a function of its weight percent at temperatures from 30 °C to 80 °C. The weight percent was converted to mole fraction based on the measured density value. In this study, Equation (4-24) is developed using Polymath 6.10 to predict the data with a coefficient of determination $R^2 = 0.999$ and the correlations are shown in Figure 4-15.

$$\begin{aligned} \rho_{\text{SG-H}_2\text{O}} = & (1.10499 + 3.273805X_2 - 20.18844X_2^2 + 70.23025X_2^3 \\ & - 54.81152X_2^4) \left[893.8859 - 0.1150903(T - 273.15) \right. \\ & \left. - 2.8016 \frac{(T - 273.15)^2}{1000} \right] \end{aligned} \quad (4-24)$$

Where, X_2 represents SG mole fraction in solution.

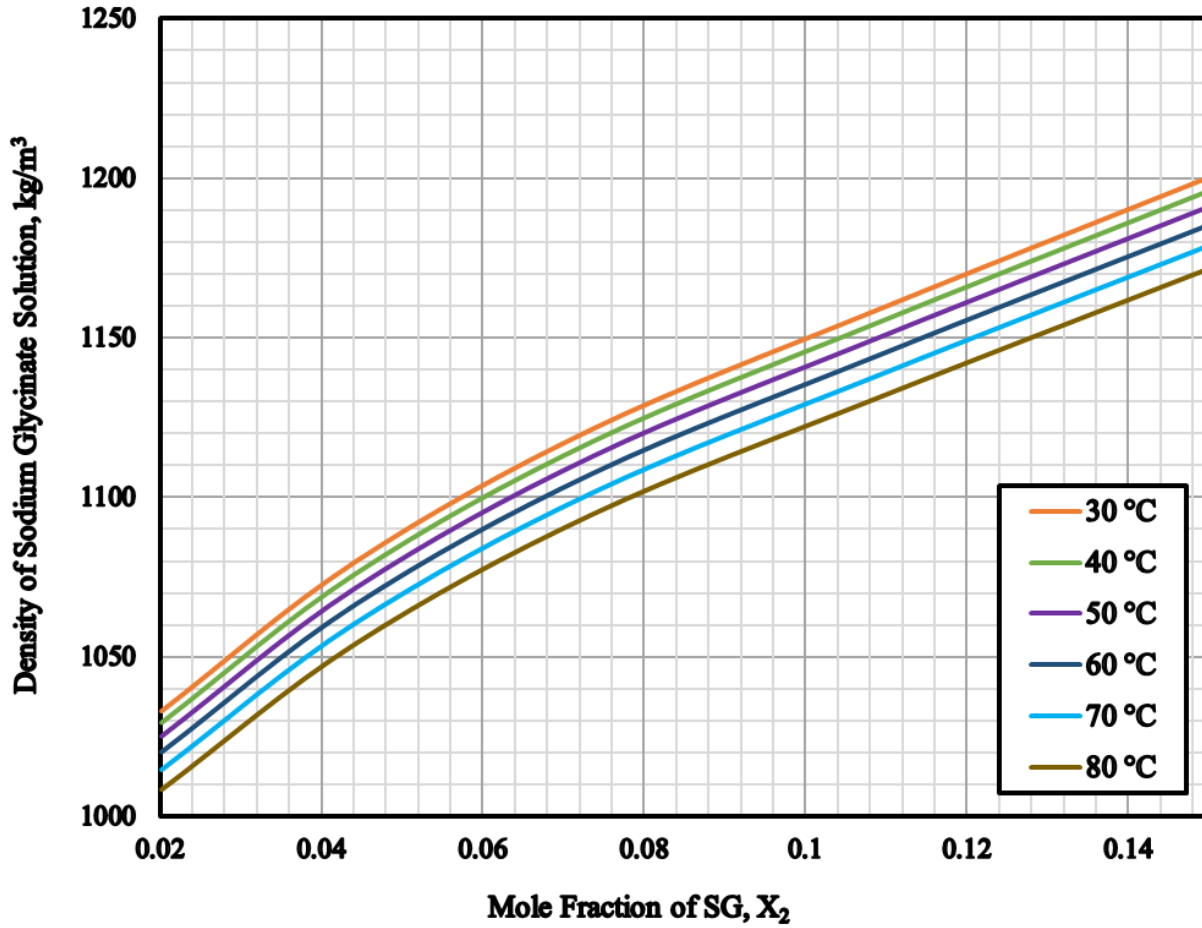


Figure 4-15: Density of SG Aqueous Solutions as a Function of Their Mole Fractions at Different Temperatures

4.3.1.4 Viscosity of SG Aqueous Solutions

The viscosity of SG aqueous solutions was measured by Lee et al. [160] as a function of its mole fraction at temperatures from 30 °C to 60 °C. In this study, Equation (4-25) is developed using Polymath 6.10 to predict the data with a coefficient of determination $R^2 = 0.982$ and the correlations are presented in Figure 4-16.

$$\mu_{\text{SG-H}_2\text{O}} = \exp \left\{ \left(0.1461444 + 2.213918X_2 + 5.934166X_2^2 + 645.4621X_2^3 - 2636.87X_2^4 \right) \left[2.143924 - 47.90743 \frac{T - 273.15}{1000} + 327.2387 \left(\frac{T - 273.15}{1000} \right)^2 \right] \right\} \quad (4-25)$$

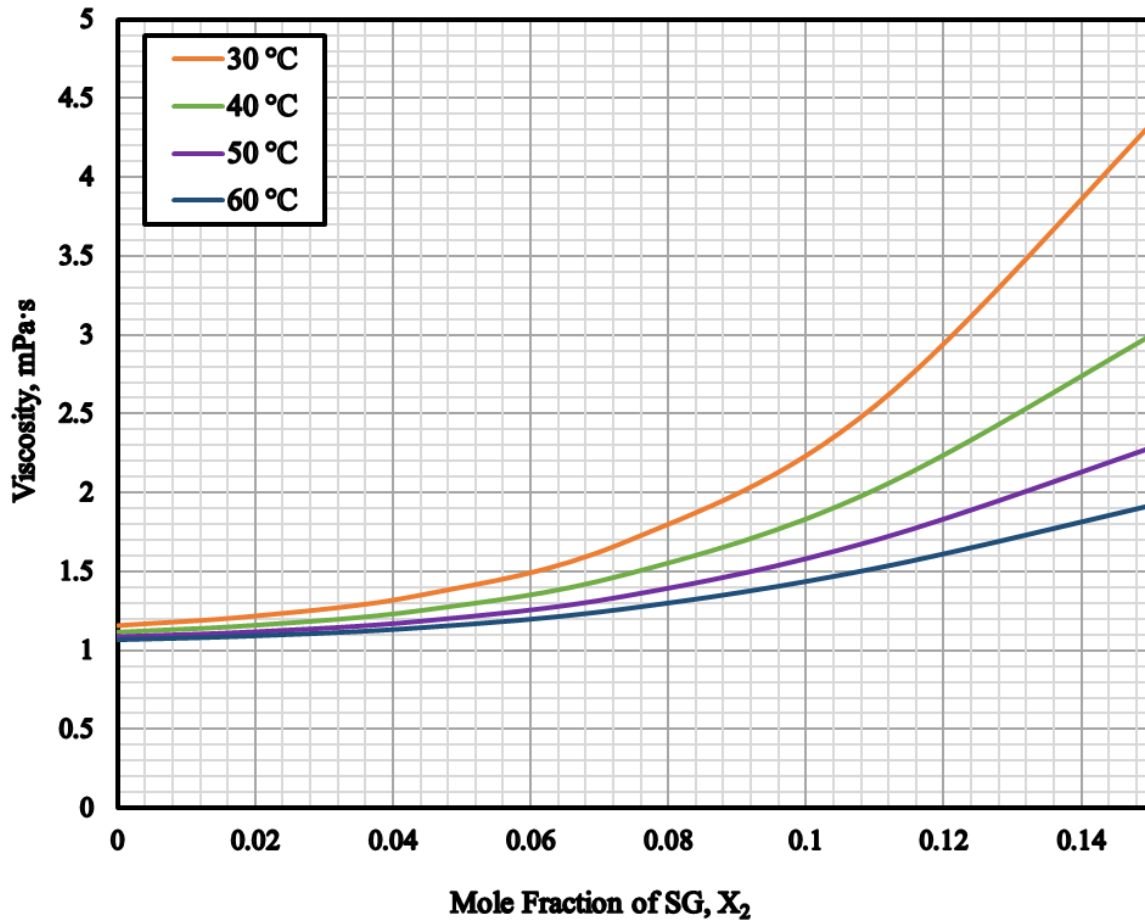


Figure 4-16: Viscosity of SG Aqueous Solutions as a Function of Their Mole Fractions at Different Temperatures

4.3.1.5 Surface Tension of SG Aqueous Solutions

The surface tension of SG aqueous solutions was measured by Lee et al. [160] as a function of its mole fraction at temperatures from 20 °C to 60 °C. In this study, Equation (4-26) is developed using Polymath 6.10 to predict the data with a coefficient of determination $R^2 = 0.994$ and the correlations are illustrated in Figure 4-17.

$$\begin{aligned} \sigma_{\text{SG-H}_2\text{O}} = & \exp\{[1.295026 + 0.1037197 \ln(X_2) + 0.0109542 \ln^2(X_2)] \\ & \times [3.641384 - 0.0079264(T - 273.15)]\} \end{aligned} \quad (4-26)$$

Where $\sigma_{\text{SG-H}_2\text{O}}$ is surface tension of SG solution, mN/m.

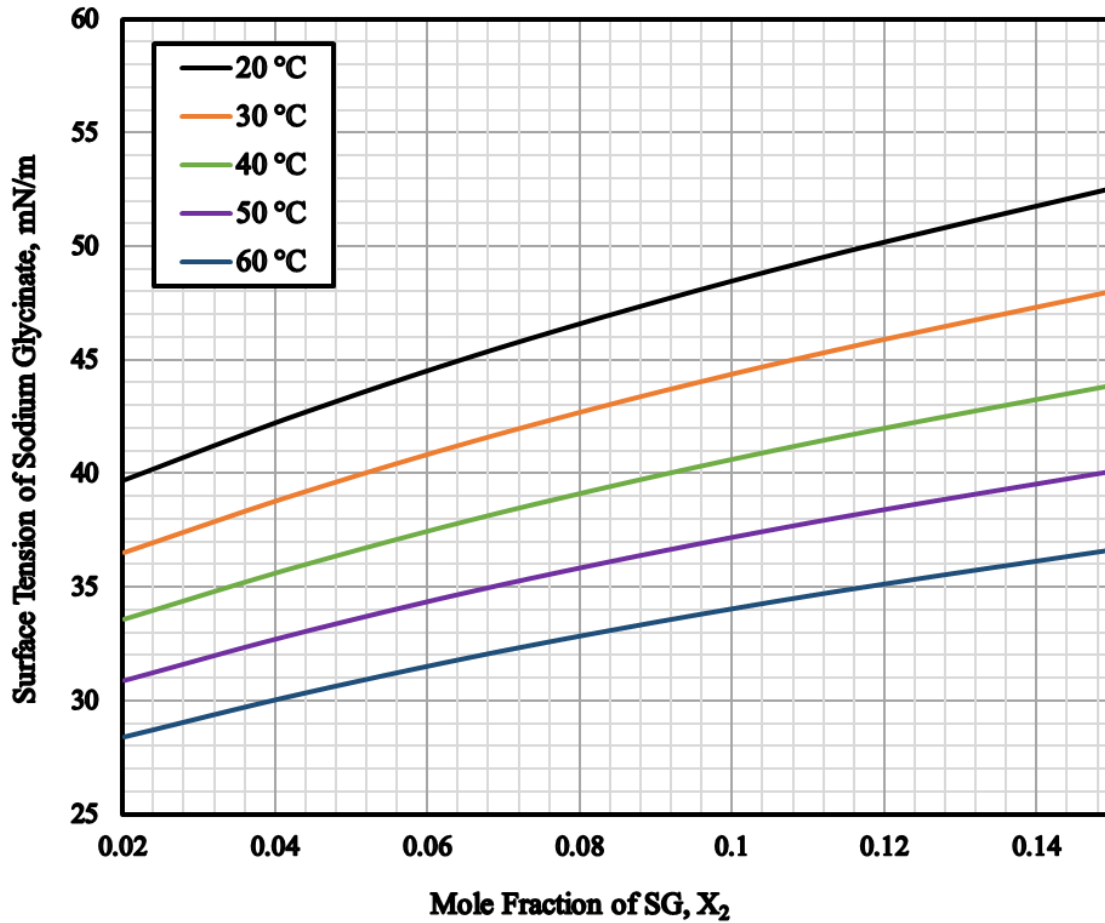


Figure 4-17: Surface Tension of SG Aqueous Solutions as a Function of Their Mole Fractions at Different Temperatures

4.3.1.6 Heat Capacity of SG Aqueous Solutions

According to Equation (4-18), the heat capacity of SG aqueous solutions depends on the heat capacity of pure components and the excess heat capacity. Due to the lack of literatures on the excess heat capacity of SG-H₂O system, its value was assumed negligible in the present calculations. This is a reasonable assumption since the excess heat capacity was negligible when

compared with pure component as can be seen in Chen and Li [156]. Thus, Equation (4-27) is used for estimating the heat capacity of SG/water system.

$$C_{P,SG-H_2O} = x_2 C_{P,SG} + (1 - x_2) C_{P,H_2O} \quad (4-27)$$

Song [79] proposed Equation (4-28) to calculate the heat capacity for 30 wt% SG aqueous solution.

$$C_{P,30wt\% SG-H_2O} = 75.51208 + 0.021598T \quad (4-28)$$

Considering the density and molecular weight, 30 wt% SG in water solution represents 7.3635 mol% of SG (x_2 is 0.073635). The heat capacity of water is given in Equation (4-16). Based on Equation (4-27), the heat capacity of pure SG could be predicted using Equation (4-29). The correlation is presented in Figure 4-18.

$$C_{P,SG} = 347.82 - 3.26T + 1.476 \times 10^{-2}T^2 - 1.891 \times 10^{-5}T^3 \quad (4-29)$$

$$- 12.59 / \left(1 - \frac{T}{647.1081}\right)$$

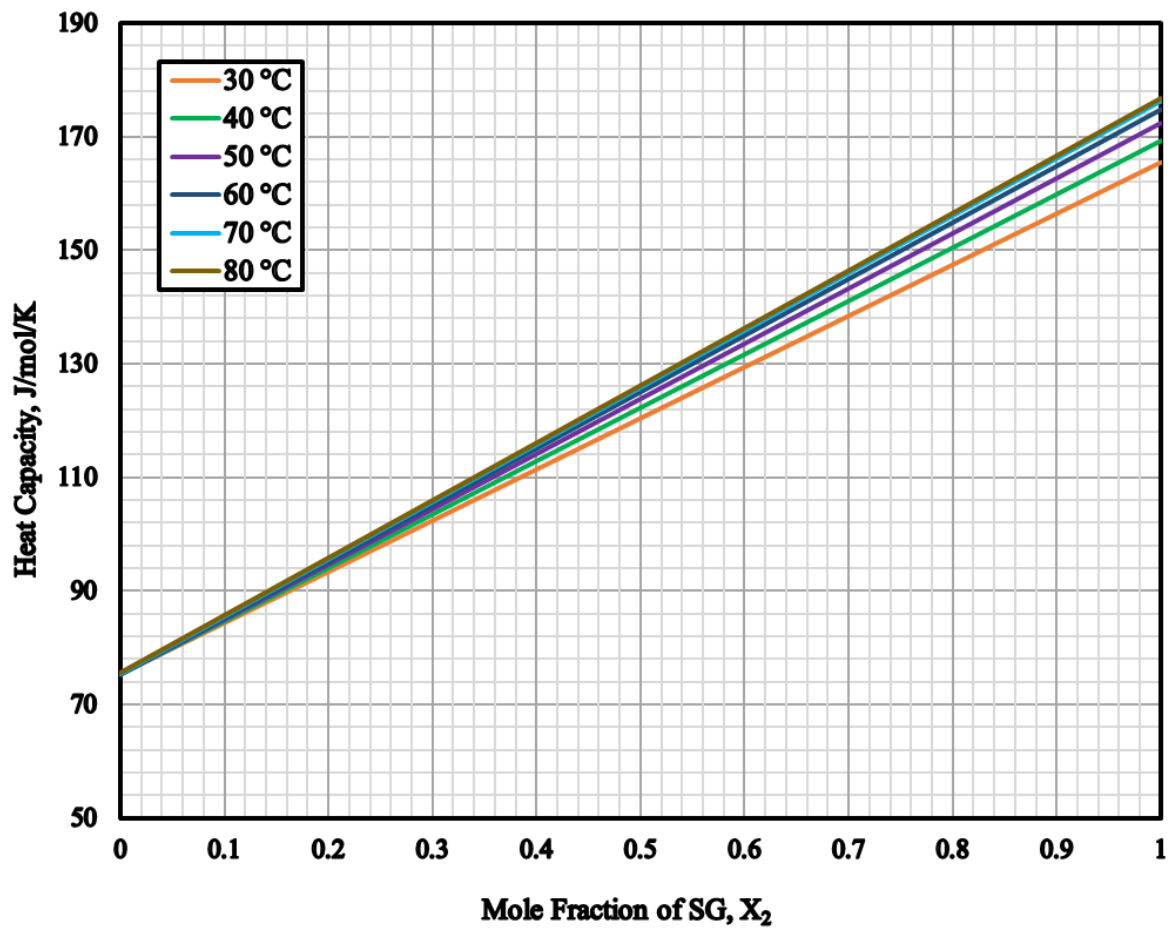


Figure 4-18: Heat Capacity of SG Aqueous Solutions as a Function of Their Mole Fractions at Different Temperatures

4.3.2 Model Predictions of CO₂ Absorption Using SG and Comparison with AMP

Following the estimation of the equation parameters, the validated model is used for CO₂-SG solutions under 4 different set of operating conditions (R-1, R-2, R-3 and R-4) with the inlet values given in Table 4-2, where a packing of 13 mm ceramic Berl Saddles was used in the model. These inlet conditions are almost identical to runs (T24, T25, T26 and T28) reported by Tontiwachwuthikul et al. [93] in an adiabatic absorber (0.1 m (ID), packed with a 12.7 mm ceramic Berl Saddles as listed in Table 4-2. Since the calculations for AMP were made with 13 mm ceramic Berl Saddles as mentioned in Section 4.2, a direct comparison between the validated model predictions using AMP and SG aqueous solutions for CO₂ absorption in this absorber can be made. It should be emphasized in their studies; the initial concentration of AMP is C_i mol/m³ and the given inlet loading at the top is α_i and accordingly the actual inlet AMP concentration (C_a) can be calculated as follows:

$$C_a = C_i(1 - \alpha_i) \quad (4-30)$$

Table 4-2: Inlet Stream Conditions Used in the Validated Model for CO₂-SG Solutions

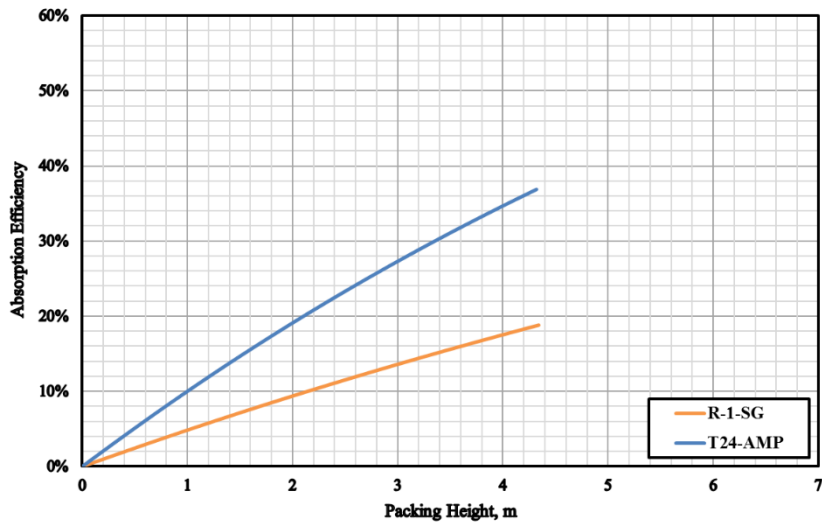
Inlet Variable	R-1 (SG) T24 (AMP)	R-2 (SG) T25 (AMP)	R-3 (SG) T26 (AMP)	R-4 (SG) T28 (AMP)
Gas Temperature, °C	15	15	15	15
CO ₂ Mole Fraction	0.1545	0.189	0.1865	0.1915
Inert Gas (Air) Flow Rate, mol/m ² /s	14.8	14.8	14.8	14.8
Packed height, m	4.35	6.55	6.55	6.55
Liquid Temperature, °C	15	15	15	15
Liquid Velocity, m/h	9.5	9.5	9.5	9.5
Initial AMP or SG Concentration, mol/m ³	2000	2000	2000	2000
Given Loading at the Top, mol CO ₂ /mol SG	0.147	0.152	0.022	0.371
Calculated Inlet AMP or SG Concentration, mol/m ³	1706	1696	1956	1258

Table 4-2 shows that the calculated inlet AMP or SG concentrations are different because the given loading is also different. The predicted values of the CO₂ loading are shown in Figure 4-21 and as can be observed, the CO₂ loading in AMP and SG increases from top to bottom and CO₂ loading in AMP is greater than that in SG under the conditions listed in Table 4-2. This can be related to the greater reaction rate constant (k_2) for AMP than that of SG.

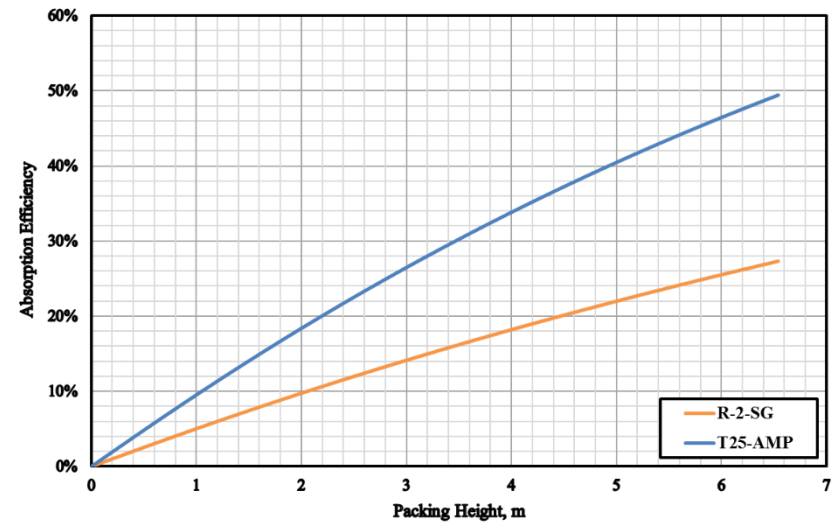
Figure 4-22 shows the greatest liquid temperature in Run R-3 corresponds to the highest inlet AMP or SG concentration, which generates the largest heat of reaction, however, due to the heat transfer between the gas and liquid as well as the latent heat of water vaporization, the liquid temperature decreases going down the adiabatic reactor. Likewise, as shown in Figure 4-23, the gas temperature is significantly affected by liquid temperature due to gas-liquid heat transfer in the adiabatic absorber and subsequently, the gas exits at 15 °C, which is the inlet liquid temperature for all cases investigated.

In Figure 4-20, the CO₂ mole fraction decreases with the reactor height for all runs and the decrease is sharper for AMP than for SG. This decrease is due to the reaction rate constant for AMP is greater than that of SG.

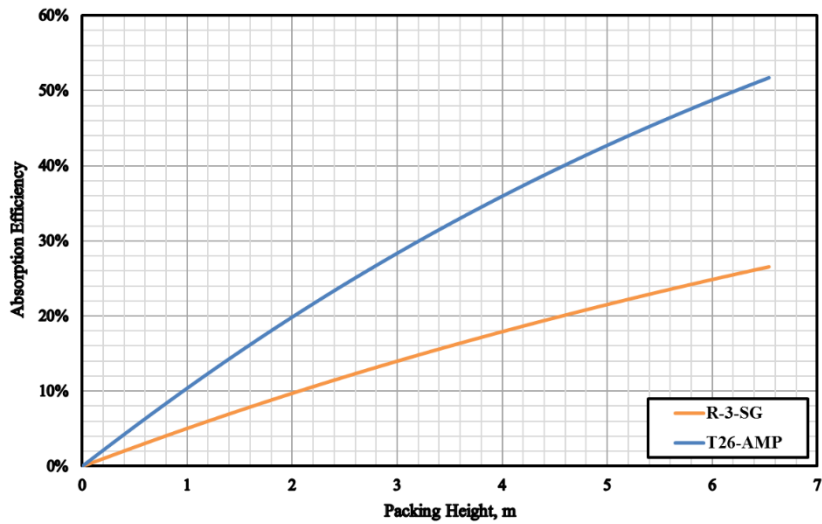
Figures 4-24 and 4-25 show the enhancement factor (E) and Hatta number (Ha) for AMP are greater than those of SG. Again, this behavior can be related to the fact that the reaction rate constant and CO₂ diffusivity in AMP is greater than that in SG.



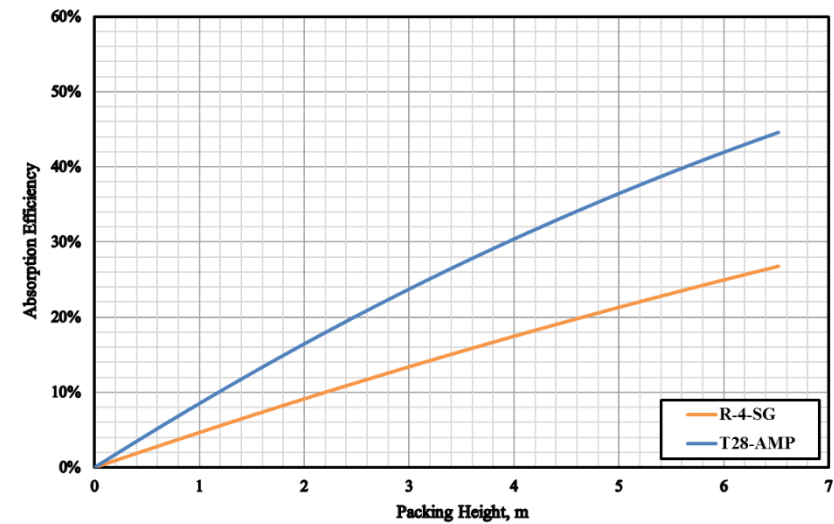
(a) R-1 and T24



(b) R-2 and T25

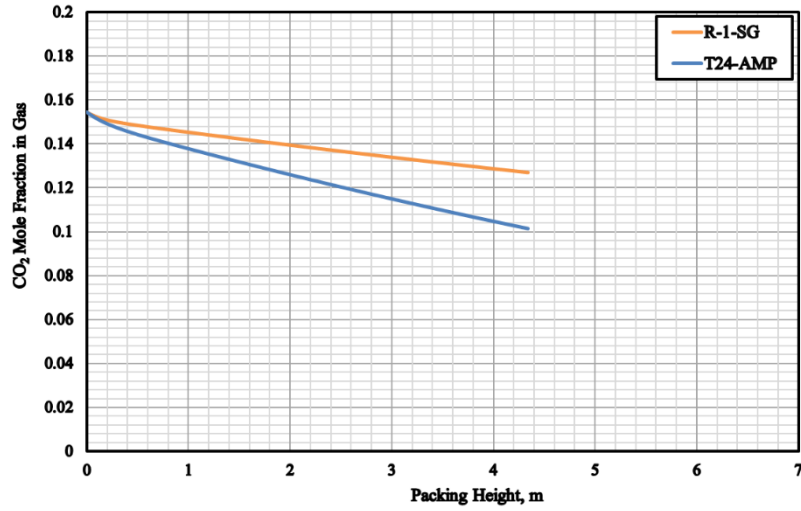


(c) R-3 and T26

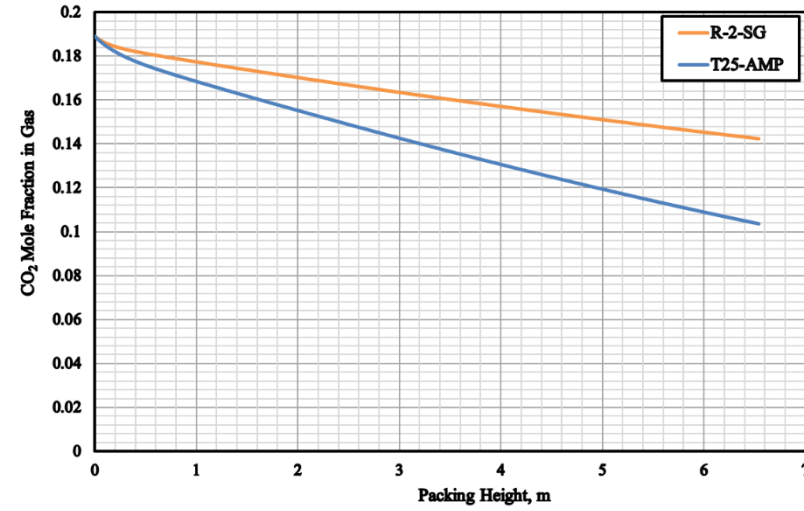


(d) R-4 and T28

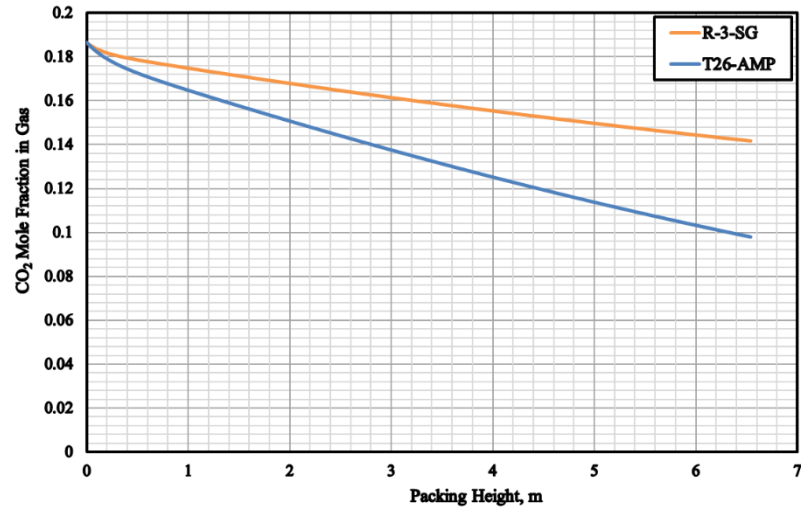
Figure 4-19: CO₂ Absorption Efficiency Using AMP and SG



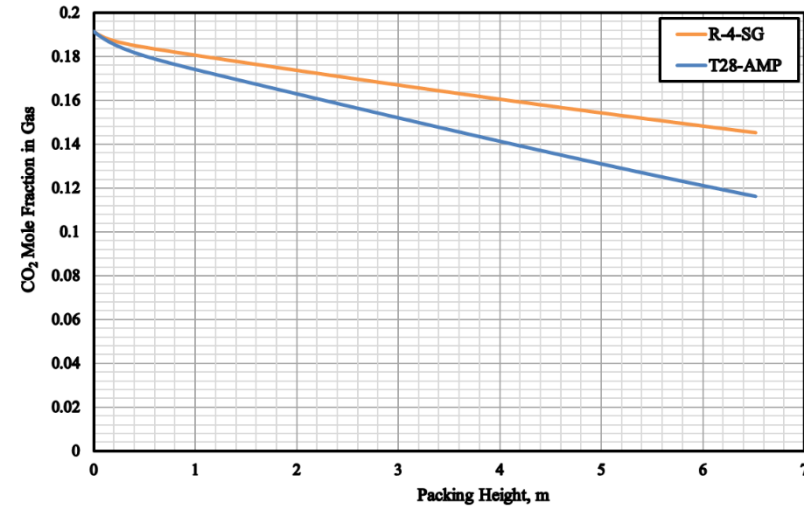
(a) R-1 and T24



(b) R-2 and T25

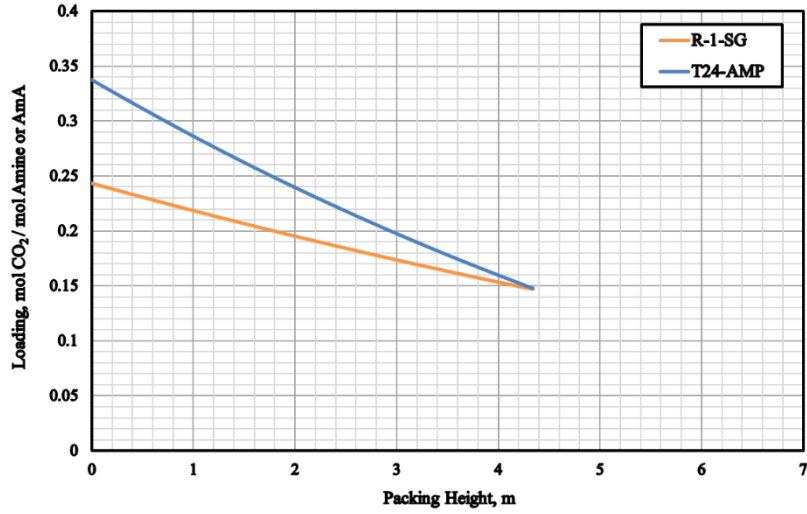


(c) R-3 and T26

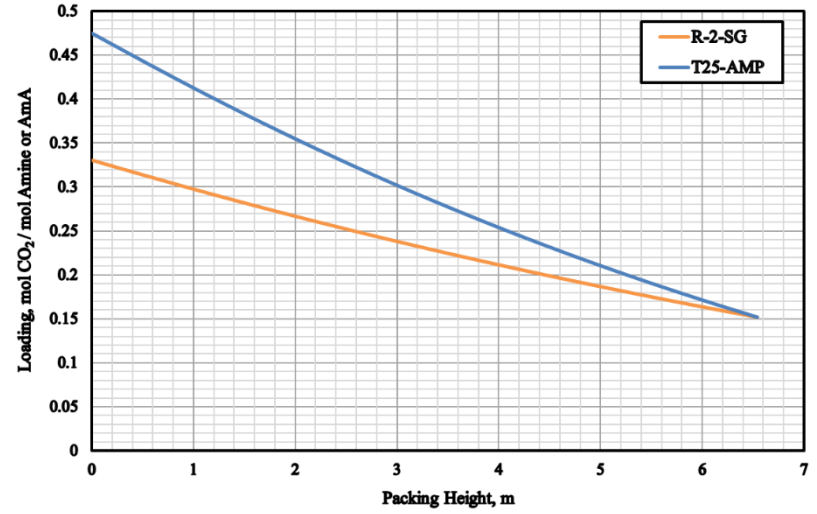


(d) R-4 and T28

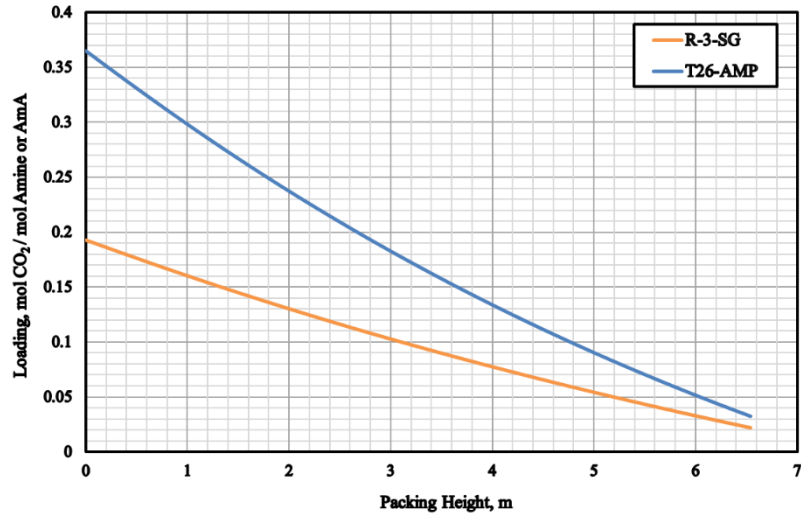
Figure 4-20: CO₂ Mole Fraction Profiles Using AMP and SG



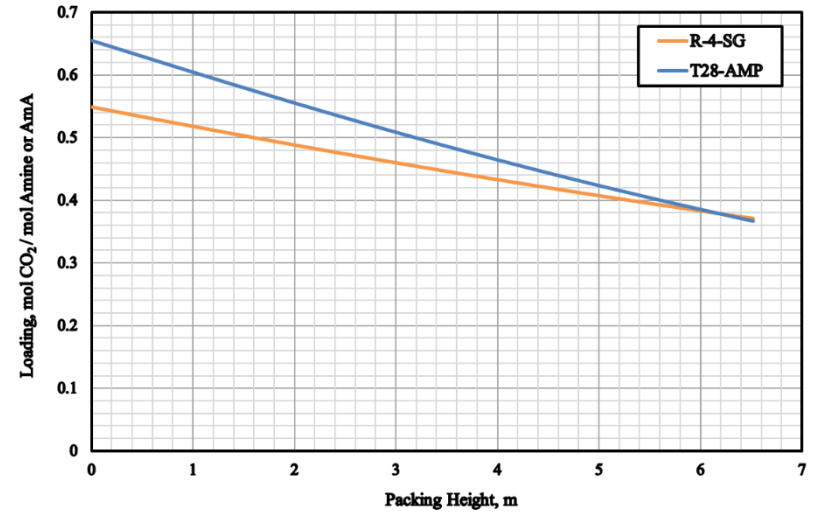
(a) R-1 and T24



(b) R-2 and T25

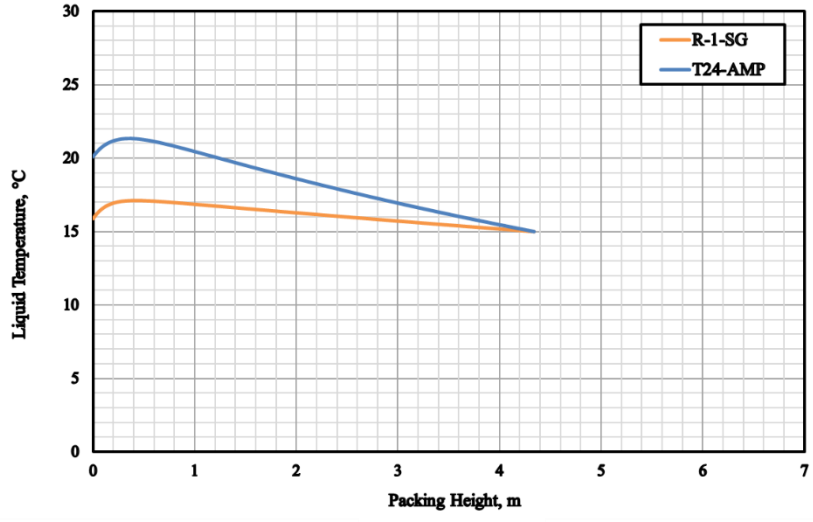


(c) R-3 and T26

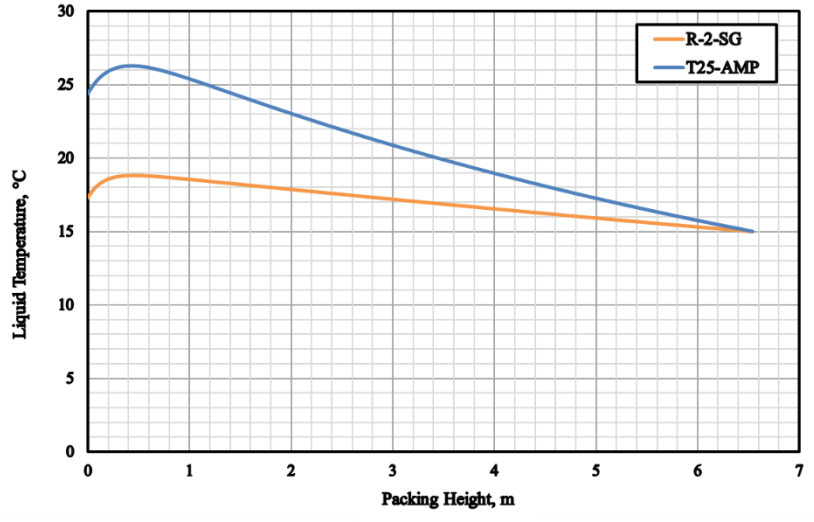


(d) R-4 and T28

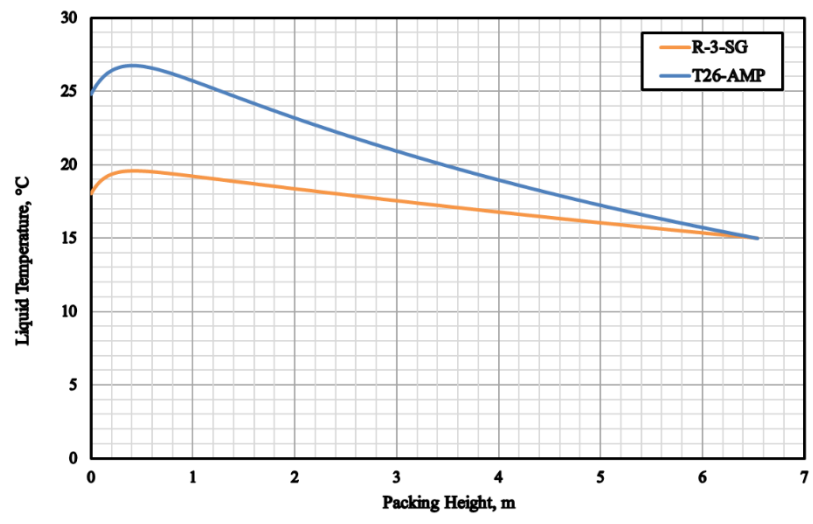
Figure 4-21: CO₂ Loading Profiles Using AMP and SG



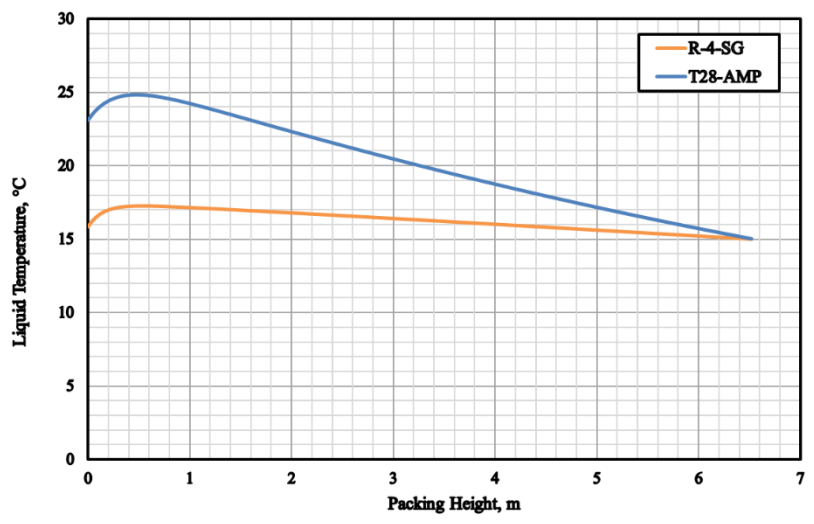
(a) R-1 and T24



(b) R-2 and T25

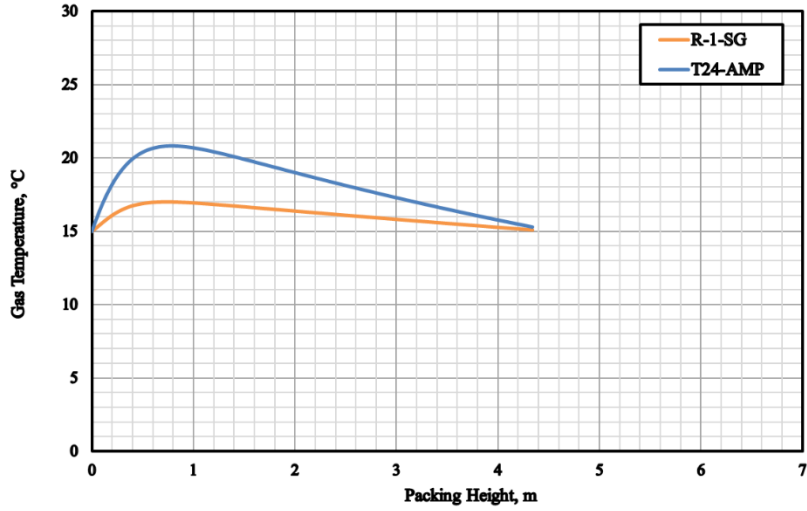


(c) R-3 and T26

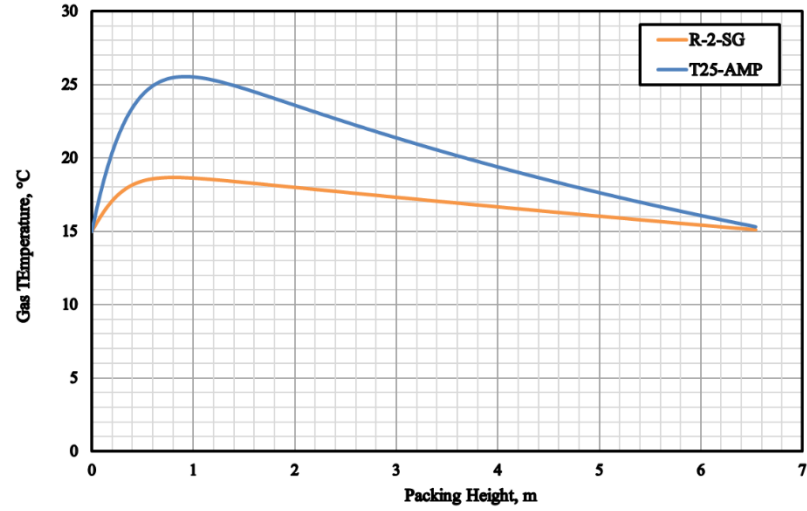


(d) R-4 and T28

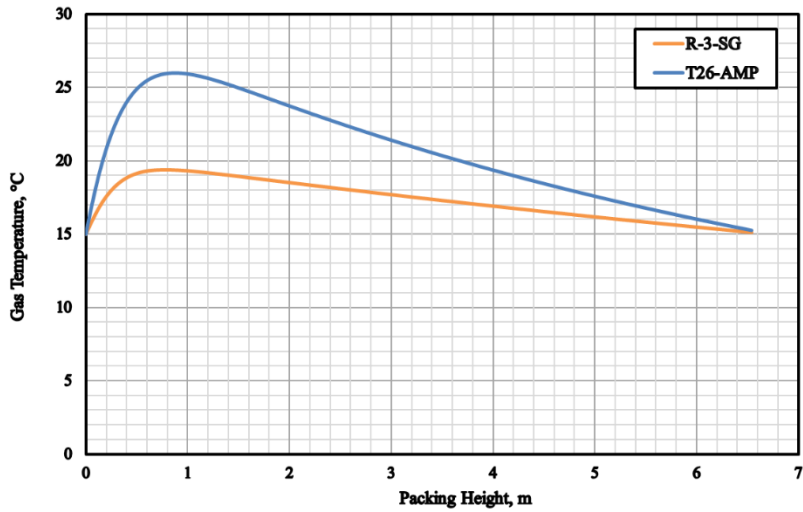
Figure 4-22: Liquid Temperature Profiles Using AMP and SG



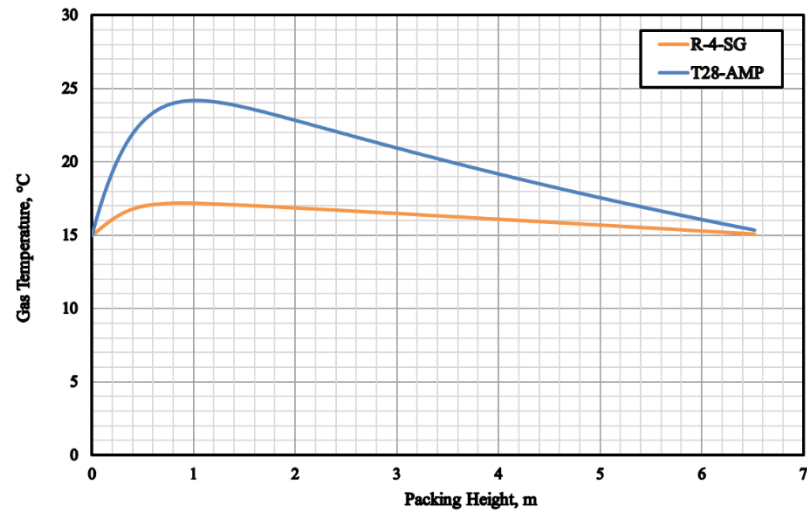
(a) R-1 and T24



(b) R-2 and T25

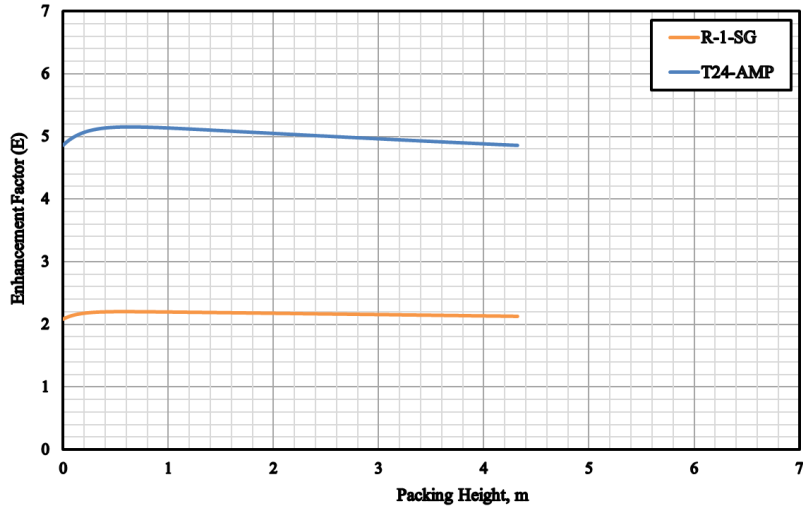


(c) R-3 and T26

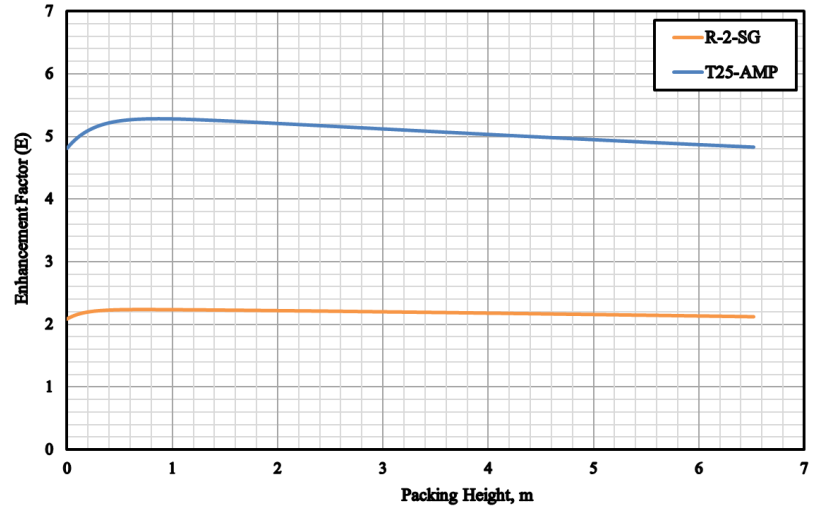


(d) R-4 and T28

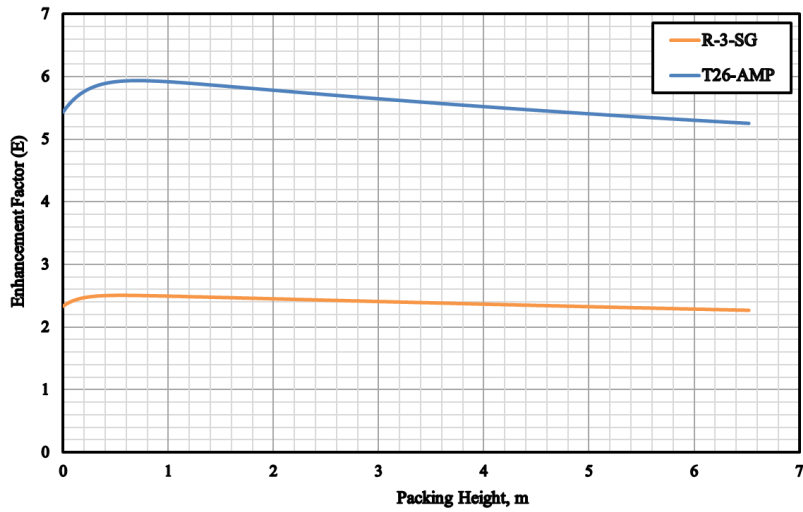
Figure 4-23: Gas Temperature Profiles using AMP and SG



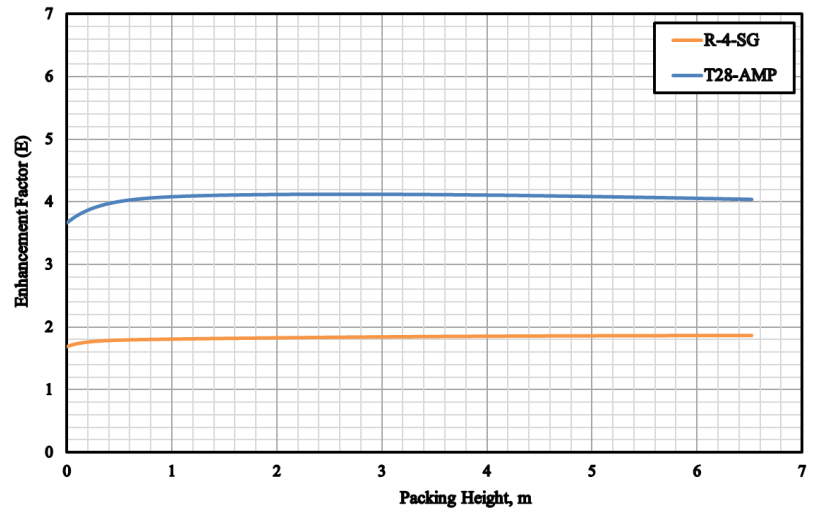
(a) R-1 and T24



(b) R-2 and T25

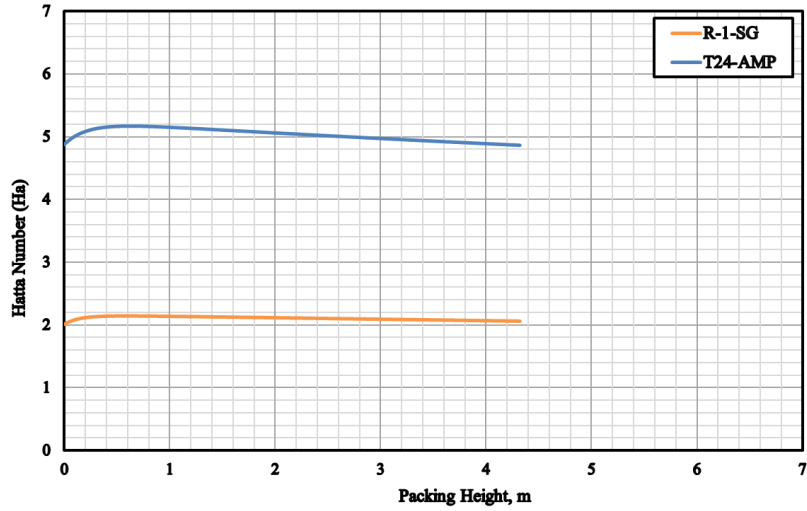


(c) R-3 and T26

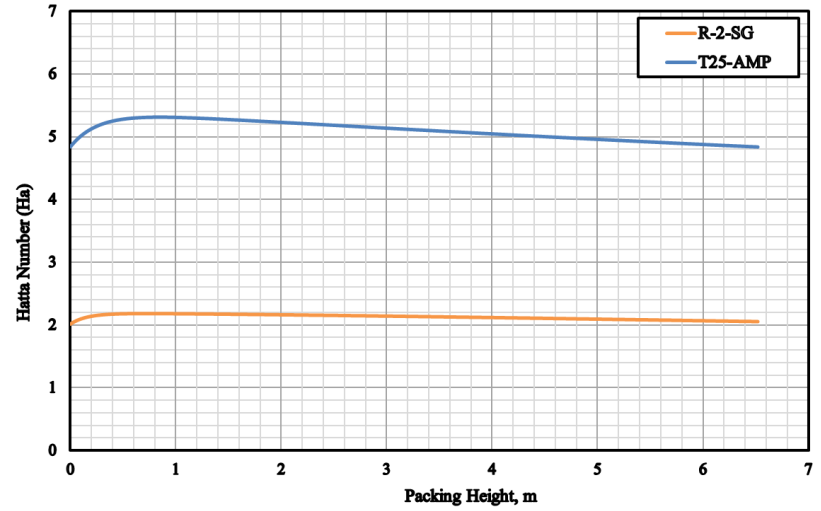


(d) R-4 and T28

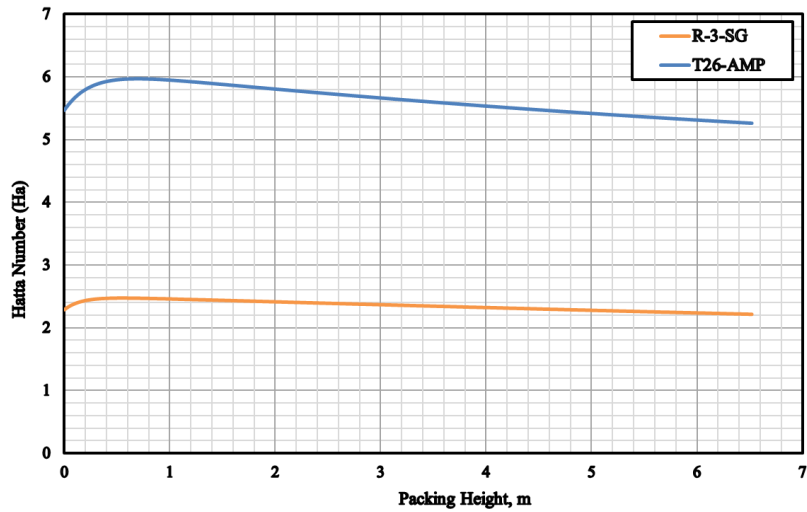
Figure 4-24: Enhancement Factor Profile Using AMP and SG



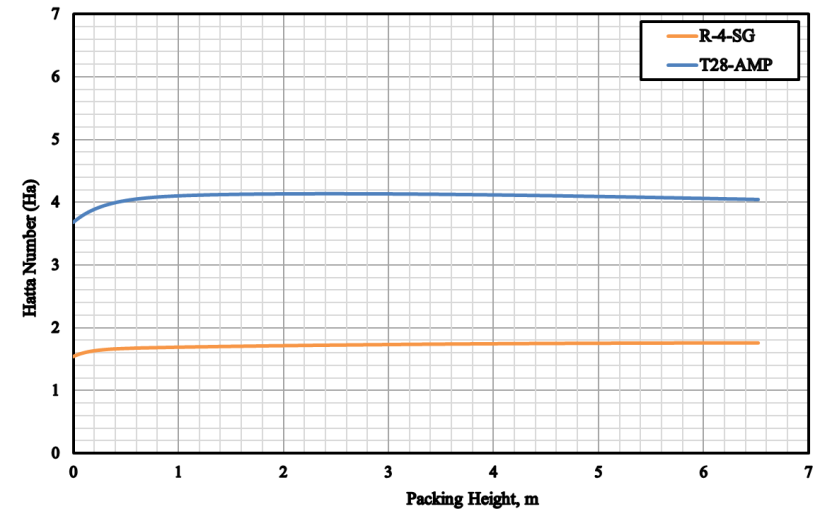
(a) R-1 and T24



(b) R-2 and T25



(c) R-3 and T26



(d) R-4 and T28

Figure 4-25: Hatta Number Profiles Using AMP and SG

5.0 Prediction of the Behavior of a Large-Scale Absorber

The validated model is used to conduct a parametric study to predict the behavior of a large-scale (1.5 m ID) adiabatic packed-bed absorber for CO₂ capture from CO₂-N₂ gaseous mixtures using AMP and SG aqueous solutions. The effects of system pressure, gas and liquid temperatures, superficial gas and liquid velocities, CO₂ partial pressure and packing type on the model predictions are investigated. The inlet variables used in this study for both absorbents are listed in Table 5-1. It should be noted that the inlet AMP concentration is kept at 2,000 mol/m³ whereas that of SG is kept at 3,500 mol/m³. This is because at similar concentrations of 2,000 mol/m³ SG led to substantially low CO₂ capture efficiency as previously shown in Figure 4-19 for the small-scale absorber. The model predictions include the profiles of CO₂ absorption efficiency, gas temperature, liquid temperature, CO₂ mole fraction, CO₂ loading (mole of CO₂/initial moles of reactant), bicarbonate production, mass transfer coefficient, Hatta number and enhancement factor at any given operating conditions.

Table 5-1: Inlet Stream Conditions Used in the Large-Scale Absorber

Inlet Variable	AMP	SG
Gas Temperature, °C	25	25
Superficial Gas Mass Velocity, kg/m ² /s	3.64	3.64
Liquid Temperature, °C	25	25
Superficial Liquid Velocity, m/s	0.2	0.2
Inlet AMP Concentration, mol/m ³	2000	3500
Pressure, bar	1	1
Column ID, m	1.5	1.5
Packing	Ceramic Berl Saddle 13mm	Ceramic Berl Saddle 13mm

5.1 Effect of System Pressure

The system pressure is varied from 1 bar to 10 bar according to Table 5-2.

Table 5-2: Effect of Pressure on the Absorber Performances

System Pressure, bar	1.0	2.5	5.0	7.5	10.0
Gas Temperature, °C	25				
Gas Density, kg/m ³	1.23	3.08	6.15	9.225	12.3
Superficial Gas Velocity, m/s	2.959	1.184	0.592	0.395	0.296
Superficial Gas Mass Velocity, kg/m ² .s	3.64				
Gas Volumetric Flow Rate, m ³ /s	5.226	2.092	1.046	0.697	0.523
Gas Volumetric Flow Rate at Standard Conditions, MMSCF/day (Ts = 60 °F and Ps = 14.696 psia)	15.7				
Liquid Temperature, °C	25				
Superficial Liquid Velocity, m/s	0.2				
Inlet AMP Concentration, mol/m ³	2000				
Packing Height for AMP to Achieve 90% CO ₂ Absorption Efficiency, m	18.34	7.22	3.62	2.42	1.84
Inlet SG Concentration, mol/m ³	3500				
Packing Height for SG to Achieve 90% CO ₂ Absorption Efficiency, m	19.34	7.72	3.86	2.58	1.94
Column ID, m	1.5				
Packing	Ceramic Berl Saddle 12.7 mm				

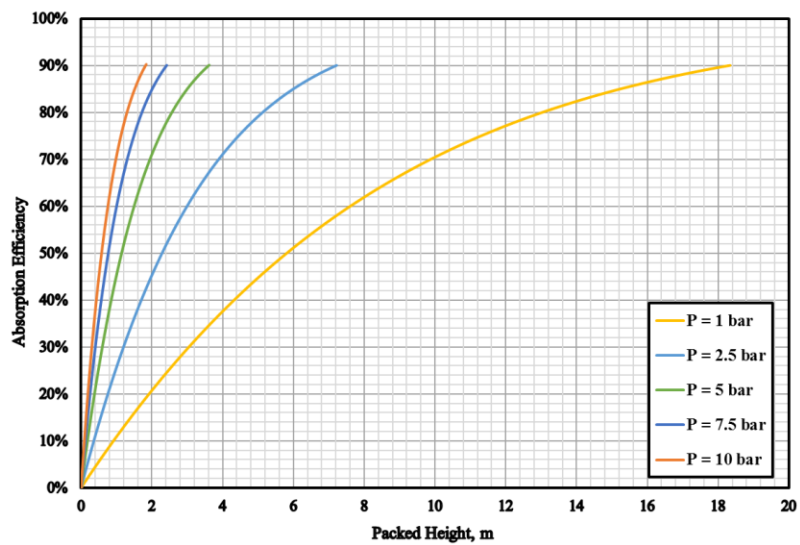
The overall CO₂ absorption efficiency is fixed at 90% by changing the packing height in the absorber. The model predictions of CO₂ absorption by AMP aqueous solutions are shown in Figures 5-1 and 5-2, and those by SG aqueous solutions are shown in Figures 5-3 and 5-4.

These figures indicate that increasing system pressure increases the CO₂ absorption efficiency for both AMP and SG, which is translated into a decrease of the packing height required to achieve the targeted 90% CO₂ absorption efficiency as shown in Table 5-2. This behavior can be related to the decrease of the superficial gas velocity and subsequently the increase of the

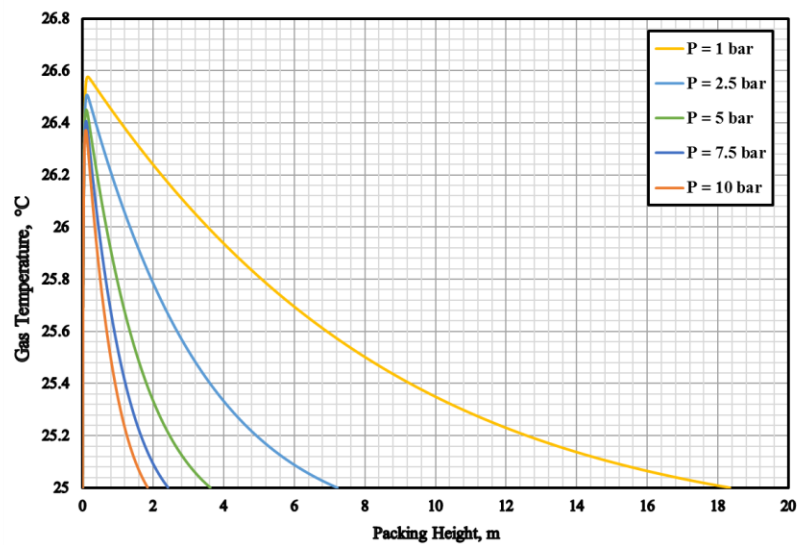
residence (contact) time with increasing pressure, allowing for more time for the gas-liquid reactions and mass transfer.

These figures also show that the gas and liquid temperature profiles along the absorber are similar, which can be attributed to the intimate heat transfer between the gas and liquid phases due to the adiabatic behavior of the absorber. Also, the liquid outlet temperatures appeared to be the same under all pressures investigated (1 - 10 bar) because the absorption efficiency and the inlet gas composition are fixed in the calculations.

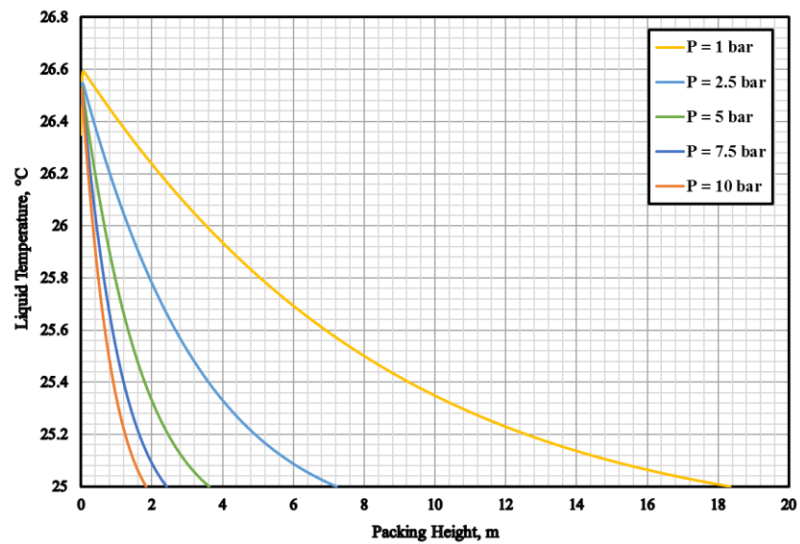
In general, the model predictions show that to achieve 90% CO₂ absorption efficiency, lower packing heights are needed using AMP when compared with those using SG under all pressures investigated. This behavior is due to the higher reaction rate constant (k_2) of AMP than that of SG under the same temperature as shown in Figure 3-8.



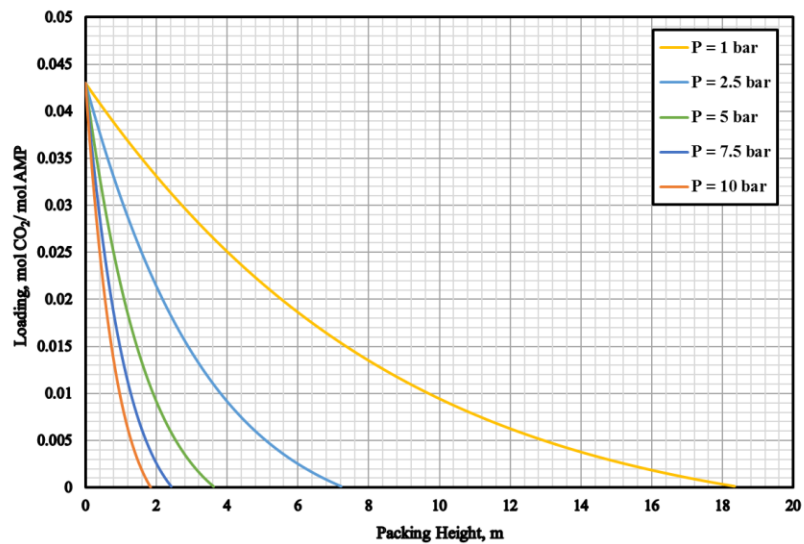
(A)



(B)



(C)



(D)

Figure 5-1: Effect of Pressure on CO₂ Absorption by AMP Aqueous Solutions (A, B, C, D)

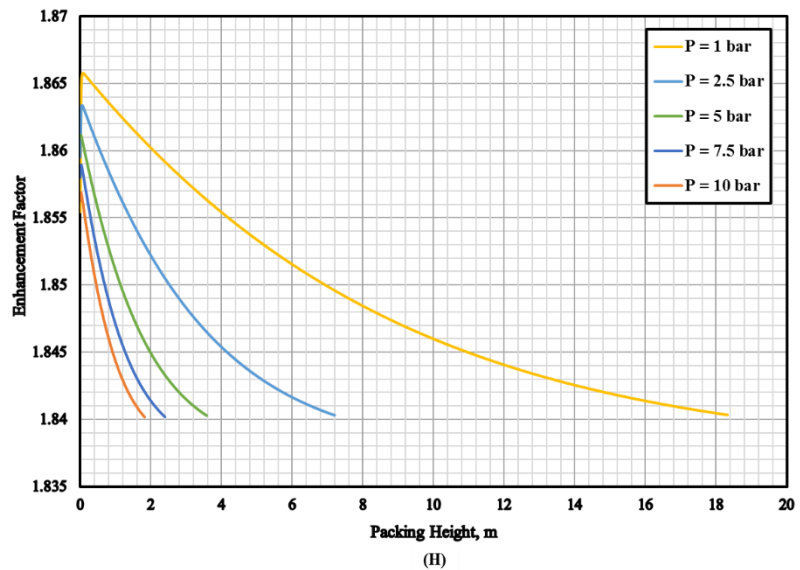
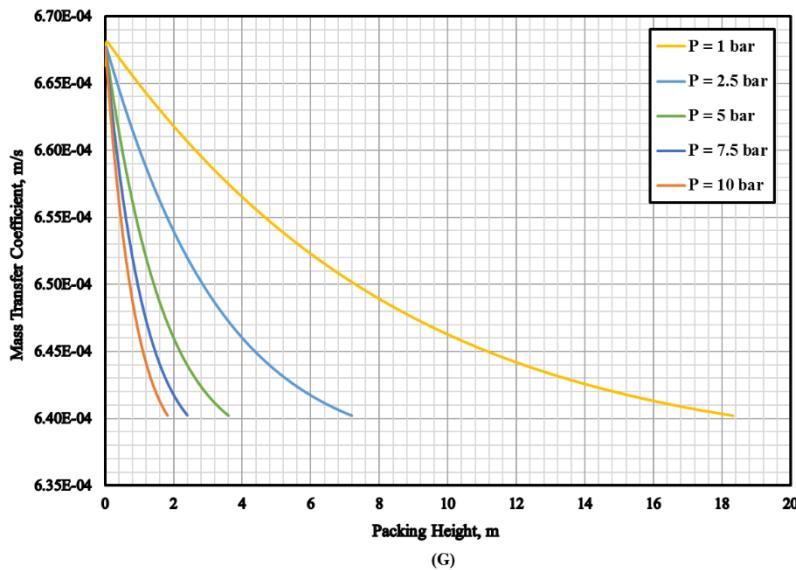
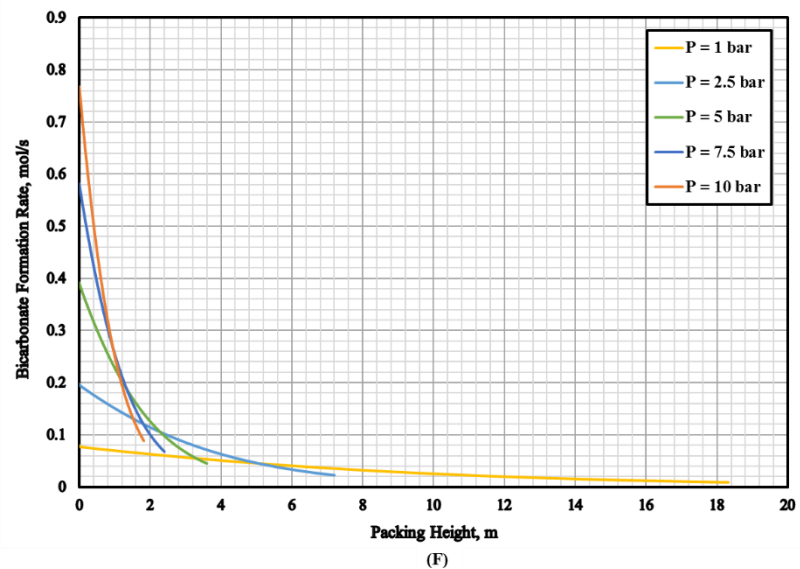
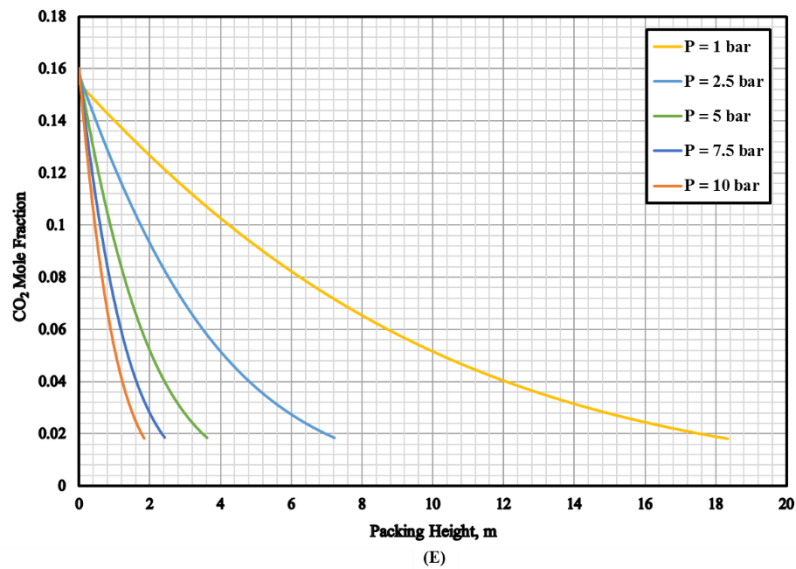
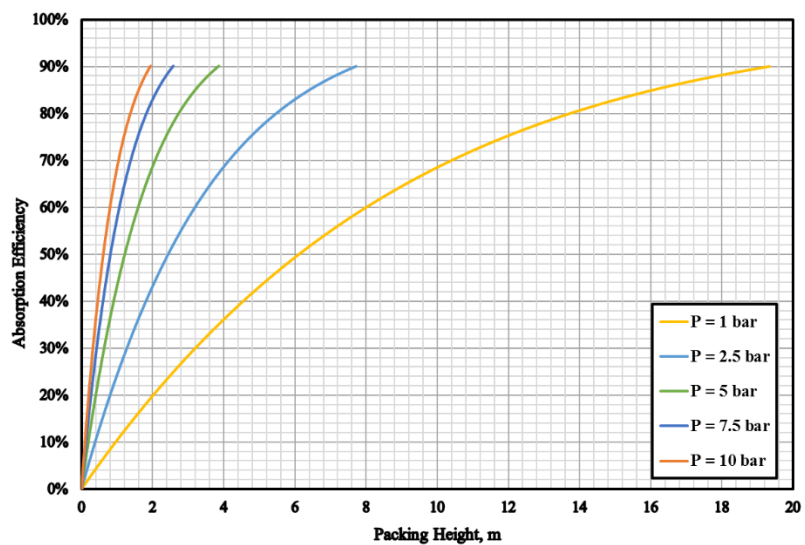
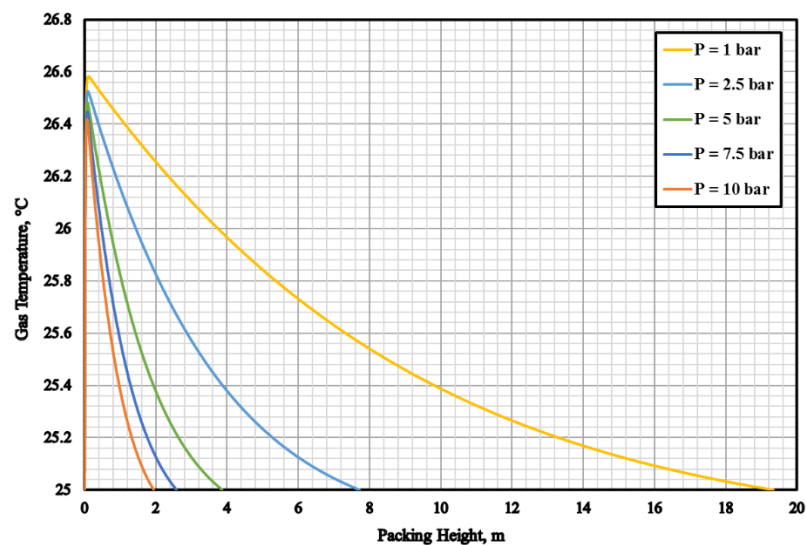


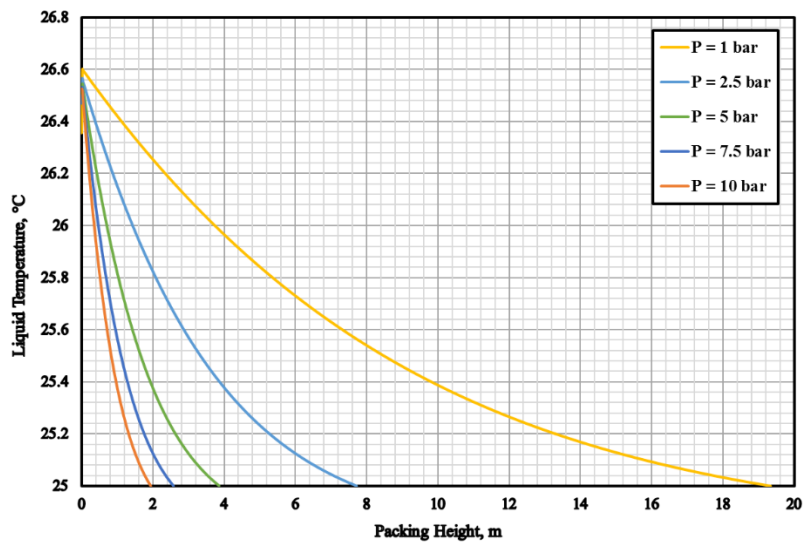
Figure 5-2: Effect of Pressure on CO₂ Absorption by AMP Aqueous Solutions (E, F, G, H)



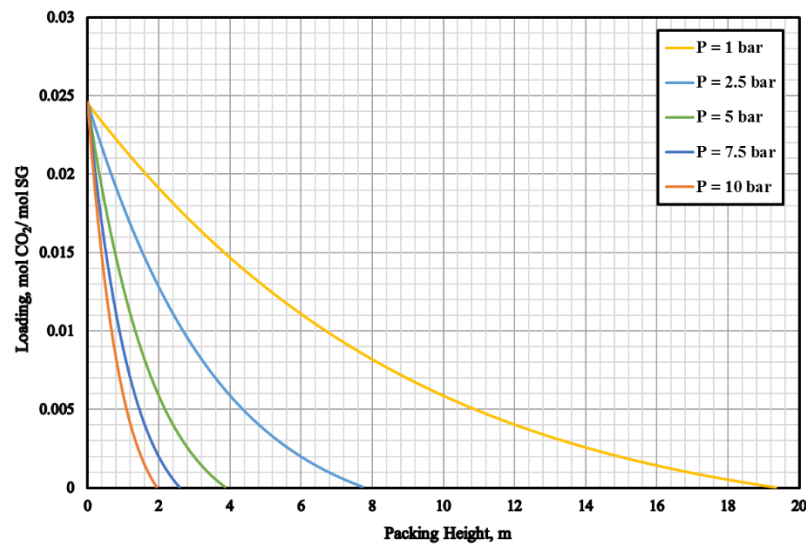
(A)



(B)



(C)



(D)

Figure 5-3: Effect of Pressure on CO₂ Absorption by SG Aqueous Solutions (A, B, C, D)

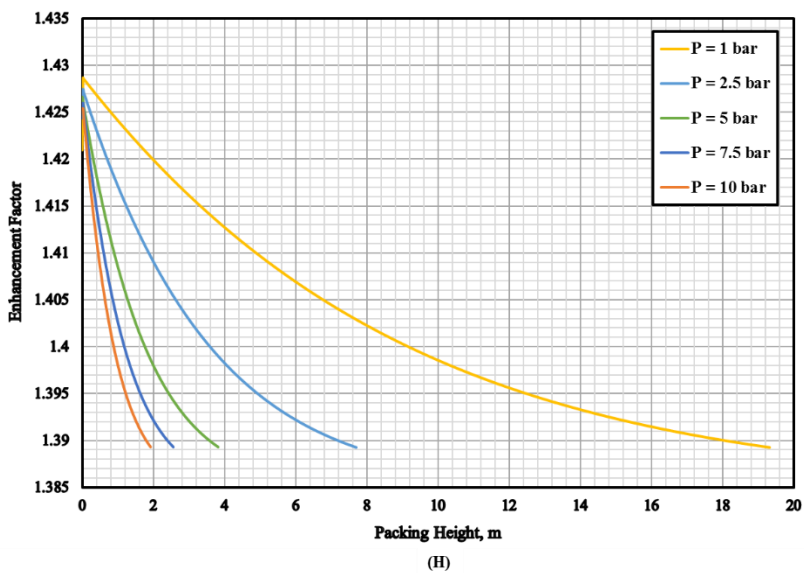
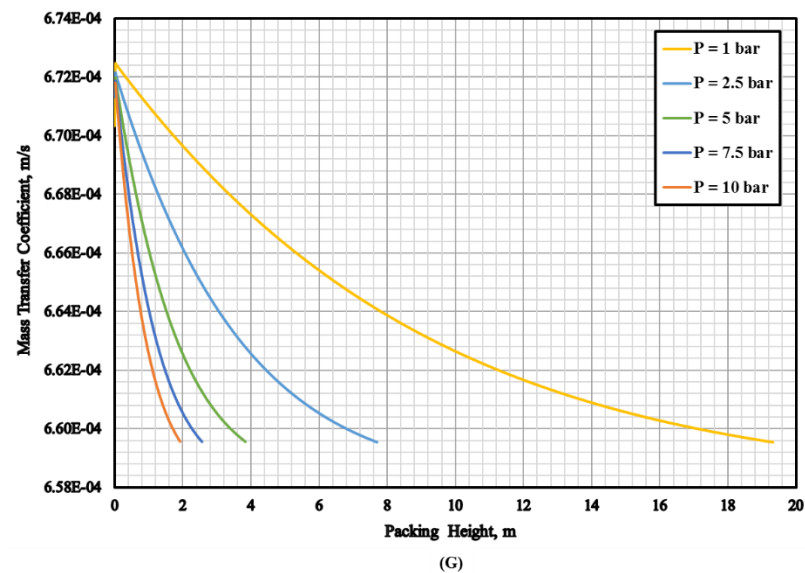
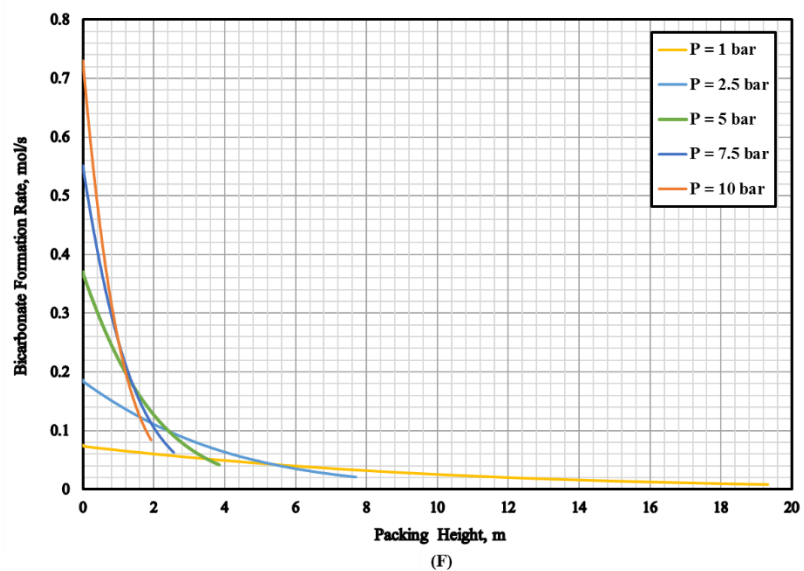
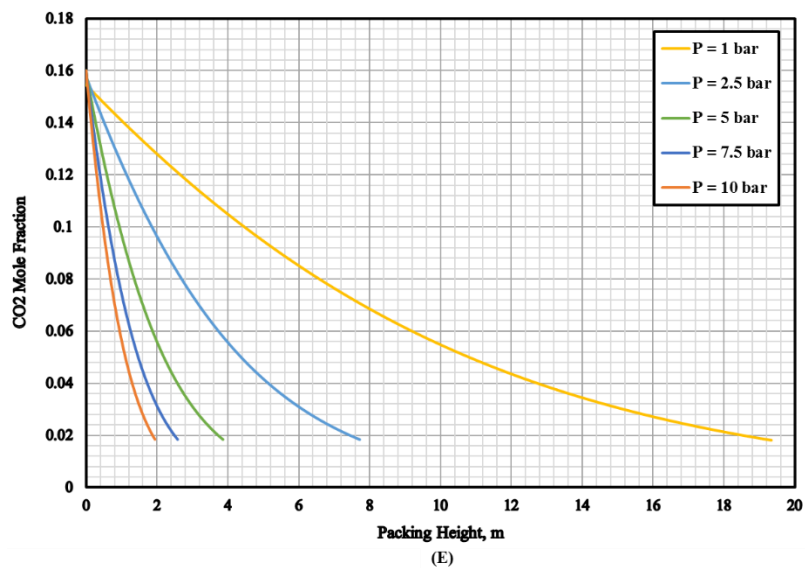


Figure 5-4: Effect of Pressure on CO₂ Absorption by SG Aqueous Solutions (E, F, G, H)

5.2 Effect of Liquid Temperature

The liquid temperature is varied from 10 to 30 °C according to Table 5-3.

Table 5-3: Effect of Liquid Temperature on the Absorber Performances

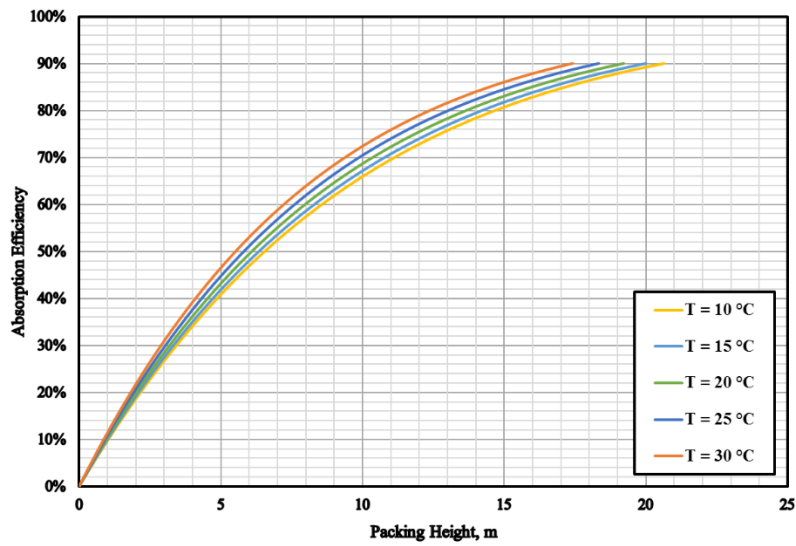
Liquid Temperature, °C	10	15	20	25	30
System Pressure, bar	1.0				
Gas Temperature, °C	25				
Gas Density, kg/m ³	1.23				
Superficial Gas Velocity, m/s	2.959				
Superficial Gas Mass Velocity, kg/m ² .s	3.64				
Gas Volumetric Flow Rate, m ³ /s	5.226				
Gas Volumetric Flow Rate at Standard Conditions, MMSCF/day	15.7				
Liquid Temperature, °C	25				
Superficial Liquid Velocity, m/s	0.2				
Inlet AMP Concentration, mol/m ³	2000				
Packing Height for AMP to Achieve 90% CO ₂ Absorption Efficiency, m	20.64	20.00	19.22	18.34	17.42
Inlet SG Concentration, mol/m ³	3500				
Packing Height for SG to Achieve 90% CO ₂ Absorption Efficiency, m	24.44	22.72	21.06	19.34	17.62
Column ID, m	1.5				
Packing	Ceramic Berl Saddle 13 mm				

The overall CO₂ absorption efficiency is fixed at 90% by changing the absorber packing height. The model predictions of CO₂ absorption using AMP aqueous solutions are shown in Figures 5-5 and 5-6; and those using SG aqueous solutions are presented in Figures 5-7 and 5-8.

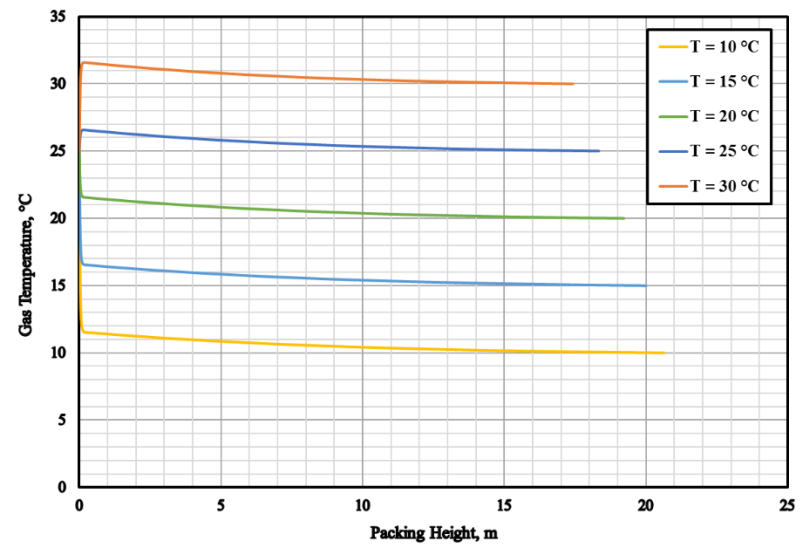
These figures indicate that increasing liquid temperature increases the CO₂ absorption efficiency or decreases the packing height required to achieve 90% CO₂ absorption efficiency. This behavior is different from CO₂ absorption in physical processes. High temperature decreases the solubility of CO₂ in the physical solvent, which eventually decreases the CO₂ absorption efficiency, even though the diffusivity of CO₂ increases with temperature leading to high mass transfer coefficients. In chemical processes using AMP and SG, however, increasing temperature increases the reaction rate constant (k_2) as shown in Figure 3-8, which increases Hatta number, Equation (1-17) as well as the enhancement factor (E) as given in Figures 5-6 (H) and 5-8 (H). Increasing temperatures also increases the diffusivity of CO₂ in both AMP and SG as can be seen in Figures 3-6 and 4-13, which leads to increasing the mass transfer coefficients according to the Billet and Schultes' correlation (3-110). Therefore, the CO₂ absorption efficiency significantly increases when increasing the liquid temperature in CO₂ chemical absorption processes.

These figures also show that the overall heat released and the difference between the inlet and outlet liquid temperatures are the same in the liquid temperature range 10 - 30 °C investigated since the CO₂ absorption efficiency is kept constant at 90%. It should be mentioned that when the inlet liquid temperature is smaller than the inlet gas temperature (25°C), the gas is cooled by the liquid.

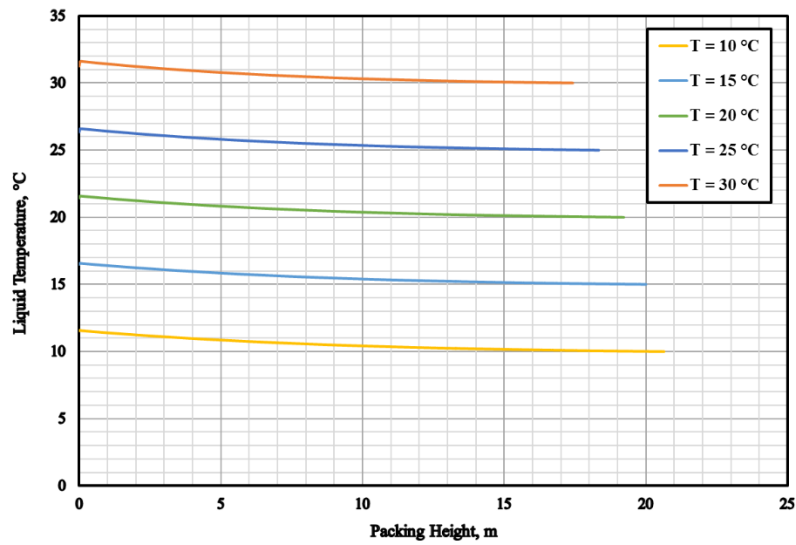
In general, under similar liquid temperatures, the CO₂ absorption in AMP is always greater than that in SG because it requires lower packing height than that for SG to achieve the targeted CO₂ absorption efficiency of 90%.



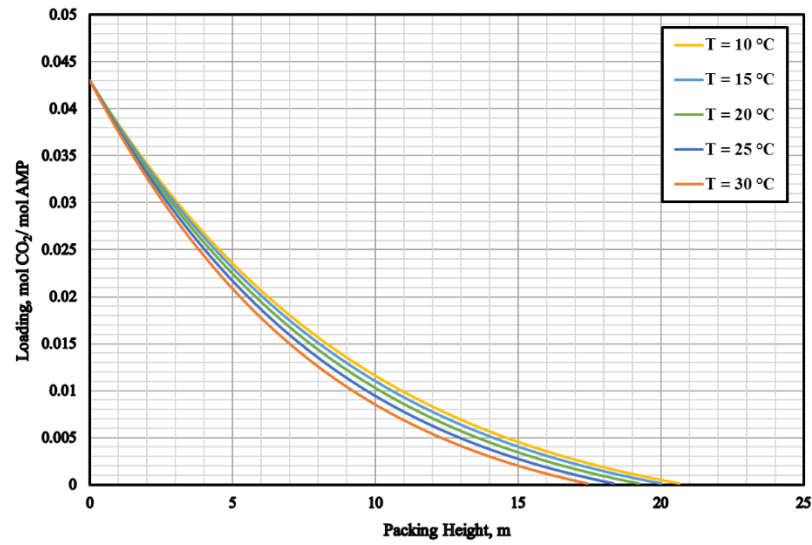
(A)



(B)



(C)



(D)

Figure 5-5: Effect of Liquid Temperature on CO₂ Absorption Using AMP Aqueous Solutions (A, B, C, D)

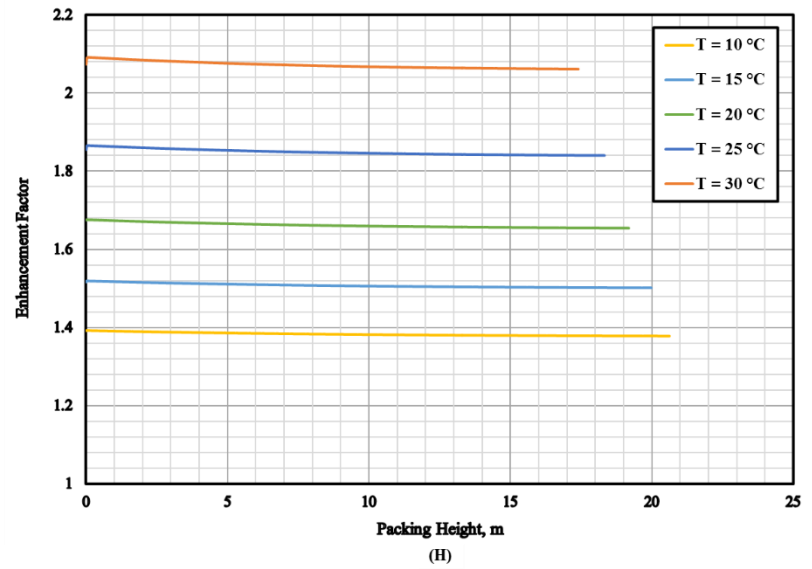
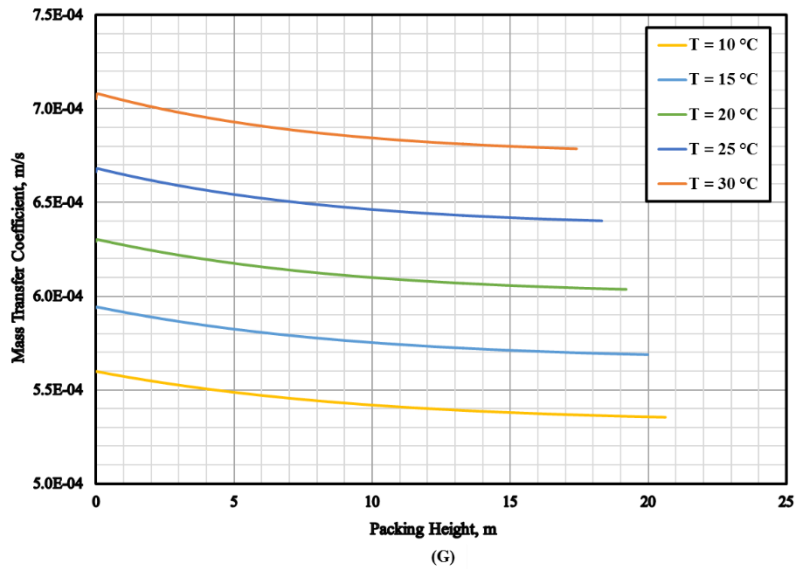
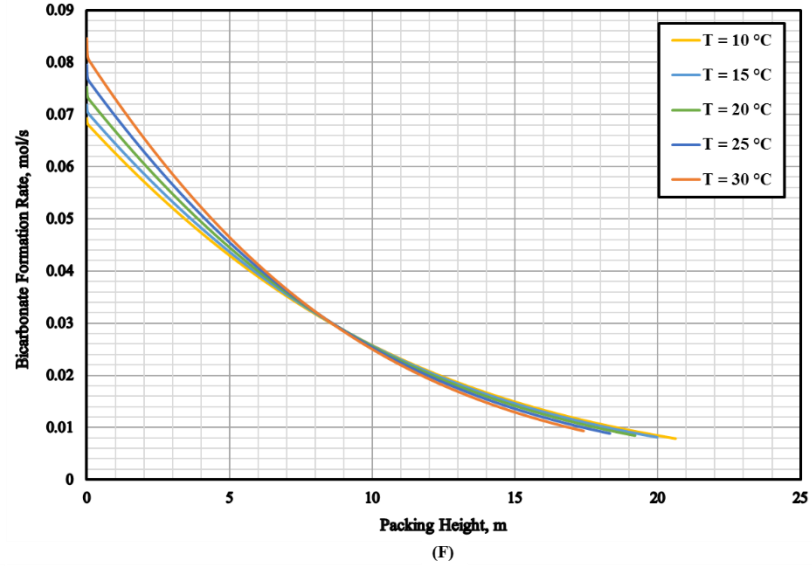
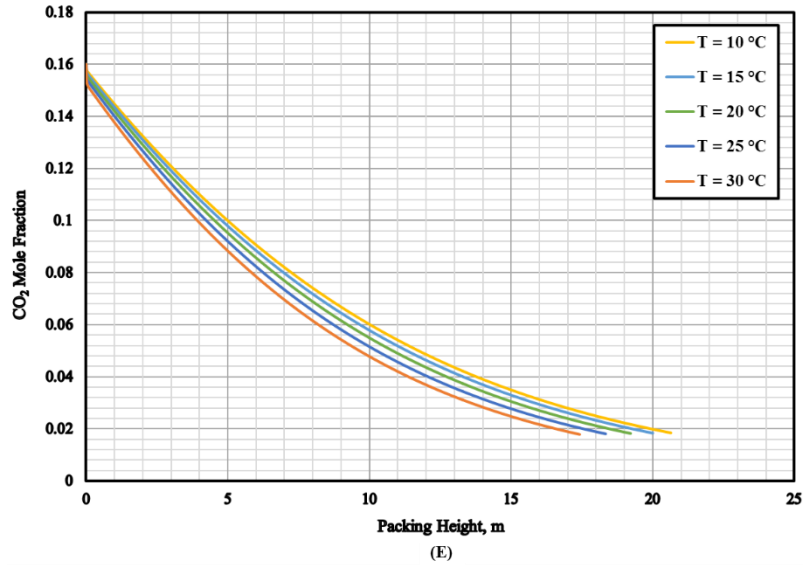
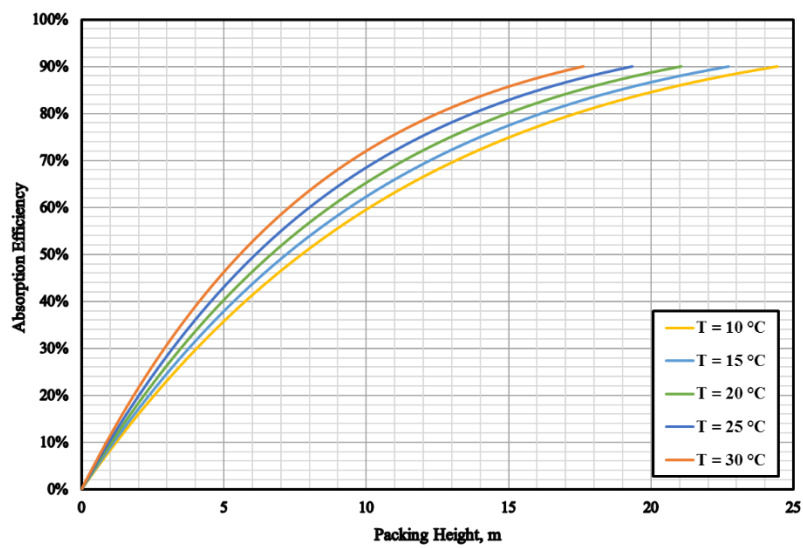
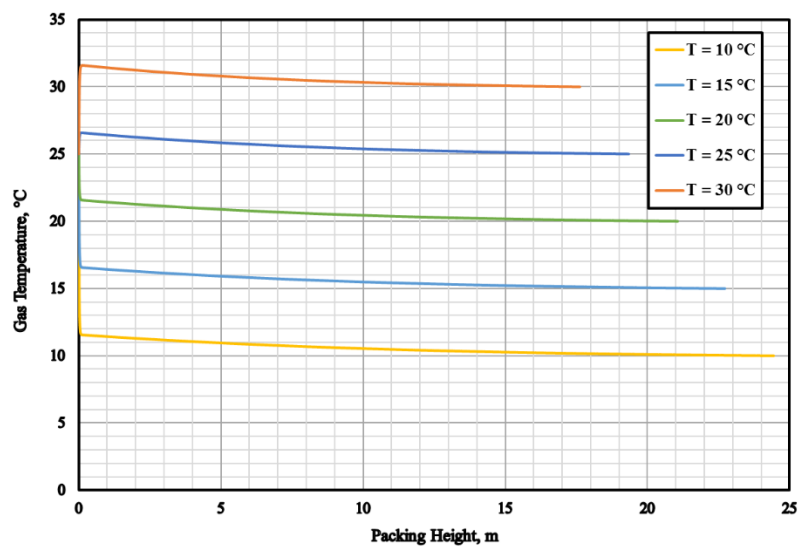


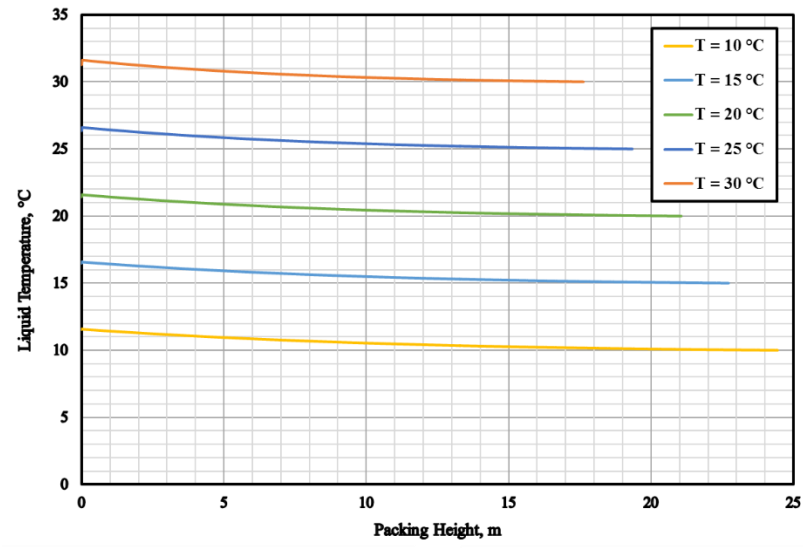
Figure 5-6: Effect of Liquid Temperature on CO₂ Absorption Using AMP Aqueous Solutions (E, F, G, H)



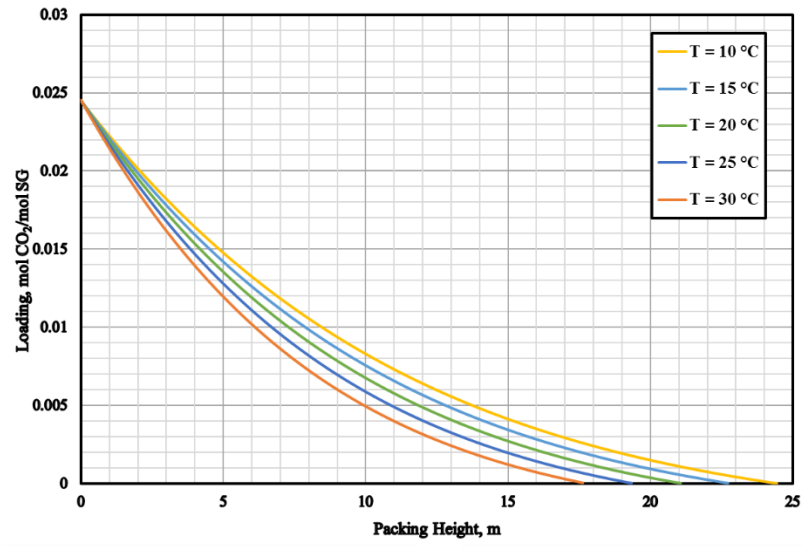
(A)



(B)



(C)



(D)

Figure 5-7: Effect of Liquid Temperature on CO₂ Absorption Using SG Aqueous Solution (A, B, C, D)

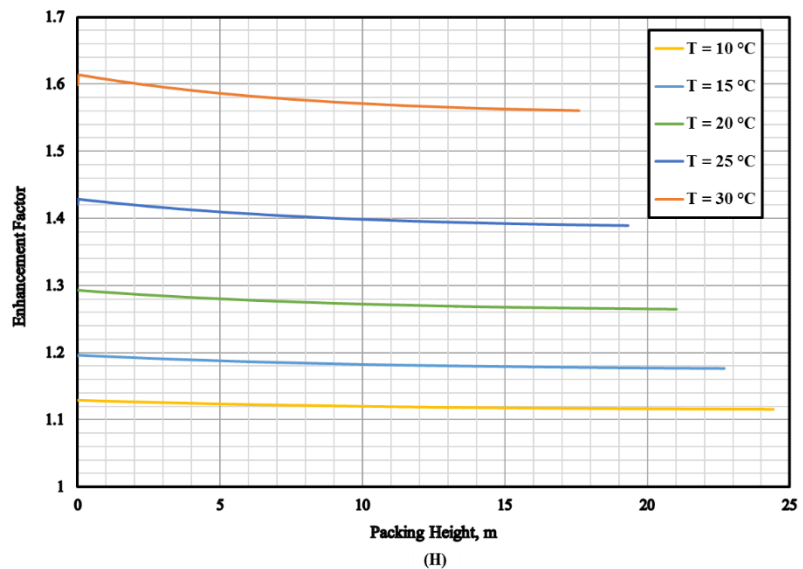
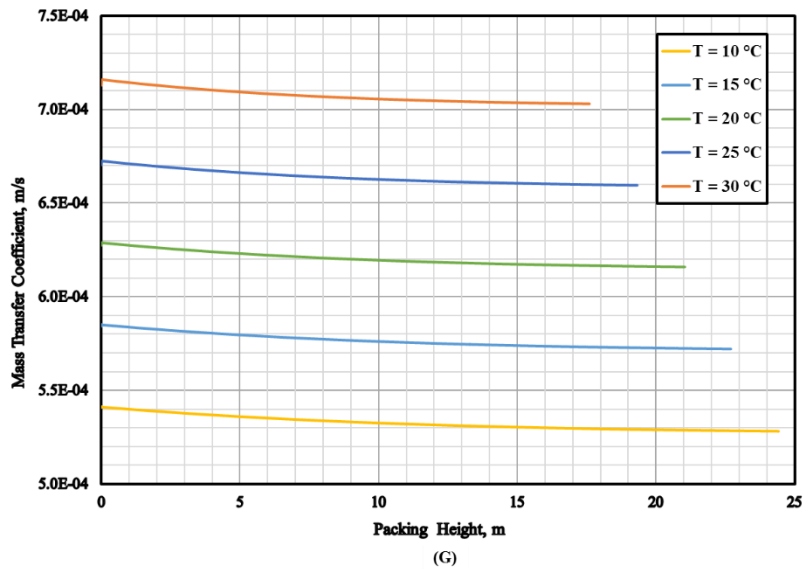
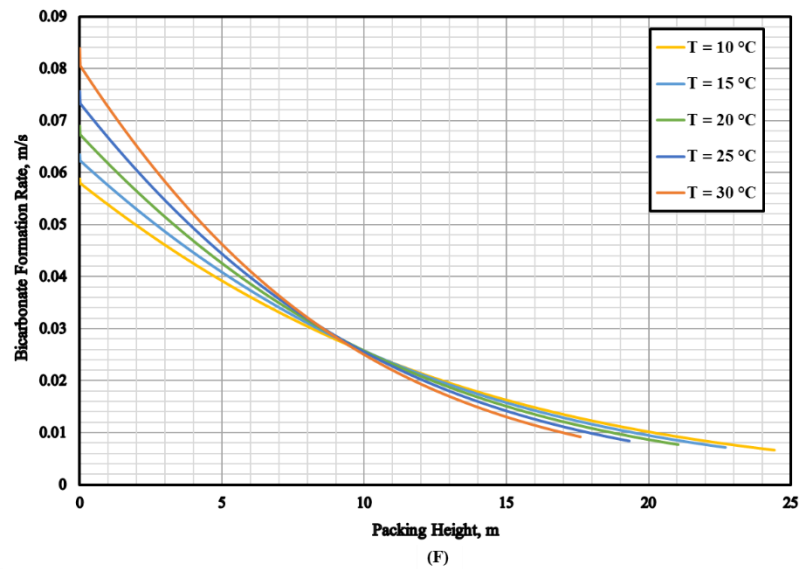
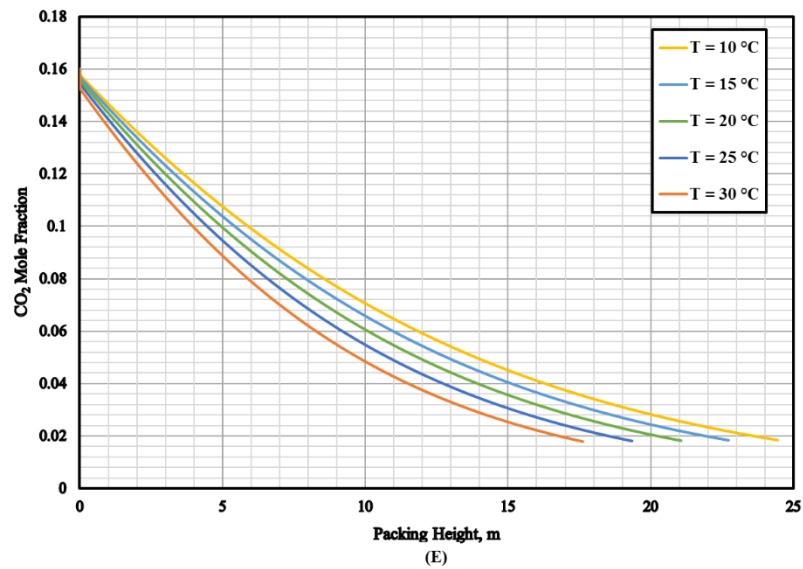


Figure 5-8: Effect of Liquid Temperature on CO₂ Absorption Using SG Aqueous Solutions (E, F, G, H)

5.3 Effect of Superficial Liquid Velocity

The superficial liquid velocity is varied from 0.02 to 0.30 m/s and the packing height is kept constant at 19.34 m according to Table 5-4.

Table 5-4: Effect of Superficial Liquid Velocity on the Absorber Performances

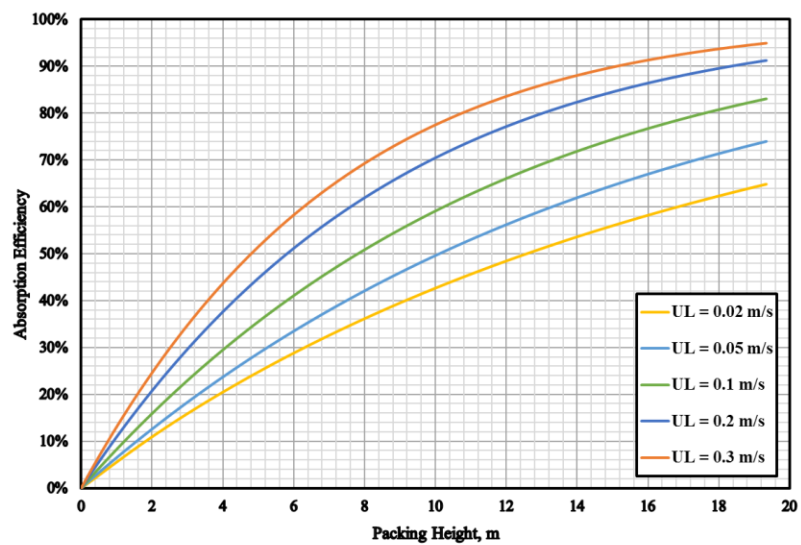
Superficial Liquid Velocity, m/s	0.02	0.05	0.10	0.20	0.30
System Pressure, bar	1.0				
Gas Temperature, °C	25				
Gas Density, kg/m ³	1.23				
Superficial Gas Velocity, m/s	2.959				
Superficial Gas Mass Velocity, kg/m ² .s	3.64				
Gas Volumetric Flow Rate, m ³ /s	5.226				
Gas Volumetric Flow Rate at Standard Conditions, MMSCF/day	15.7				
Packing Height, m	19.34				
Liquid Temperature, °C	25				
Inlet AMP Concentration, mol/m ³	2000				
CO ₂ Absorption Efficiency using AMP, %	64.85	73.98	83.07	91.26	94.94
Inlet SG Concentration, mol/m ³	3500				
CO ₂ Absorption Efficiency using SG, %	55.62	67.91	79.34	90.00	94.67
Column ID, m	1.5				
Packing	Ceramic Berl Saddle 13 mm				

The model predictions of CO₂ absorption by AMP aqueous solutions are shown in Figures 5-9 and 5-10; and those by SG aqueous solutions are shown in Figures 5-11 and 5-12.

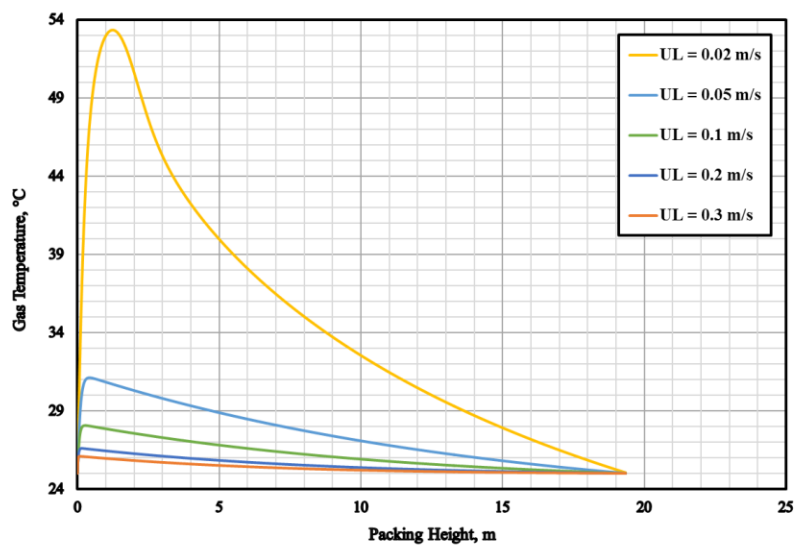
These figures show that increasing the liquid superficial velocity increases the CO₂ absorption efficiency. This behavior can be related to the increase of the liquid holdup and the specific wetted area of the packing (a_w) as well as the mass transfer coefficients (k_L) according to Billet and Schultes' correlation (3-110).

Increasing the superficial liquid velocity leads to decreasing the difference between the inlet and outlet temperatures in the gas and liquid phases because it allows for efficient removal of the heat of reaction from the adiabatic absorber.

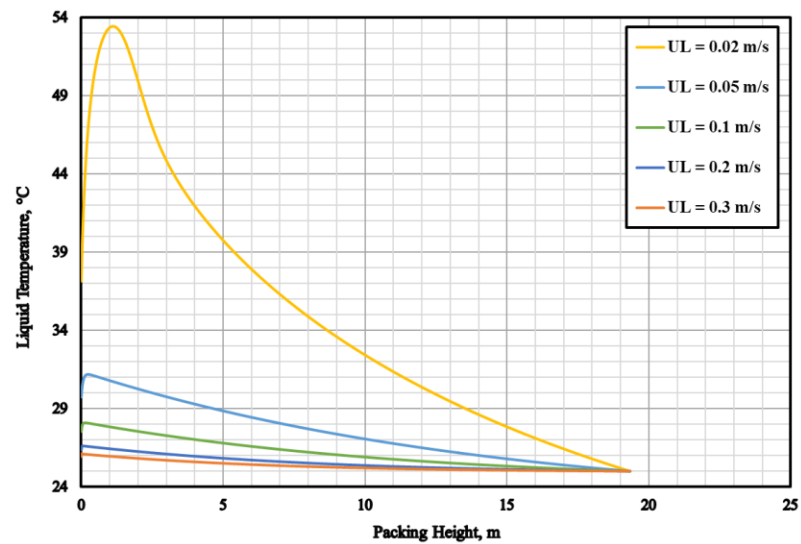
These figures also show that at low superficial liquid velocity, the CO₂ loading is high because the total number of moles of the AMP and SG are low since their inlet concentrations are constant. In addition, AMP appears to have greater CO₂ absorption efficiency than that of SG under similar superficial liquid velocities.



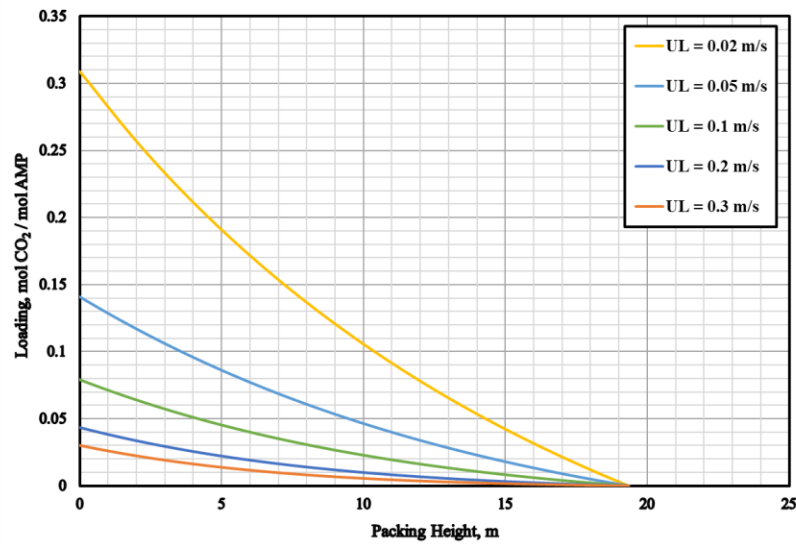
(A)



(B)



(C)



(D)

Figure 5-9: Effect of Liquid Velocity on CO₂ Absorption by AMP (A, B, C, D)

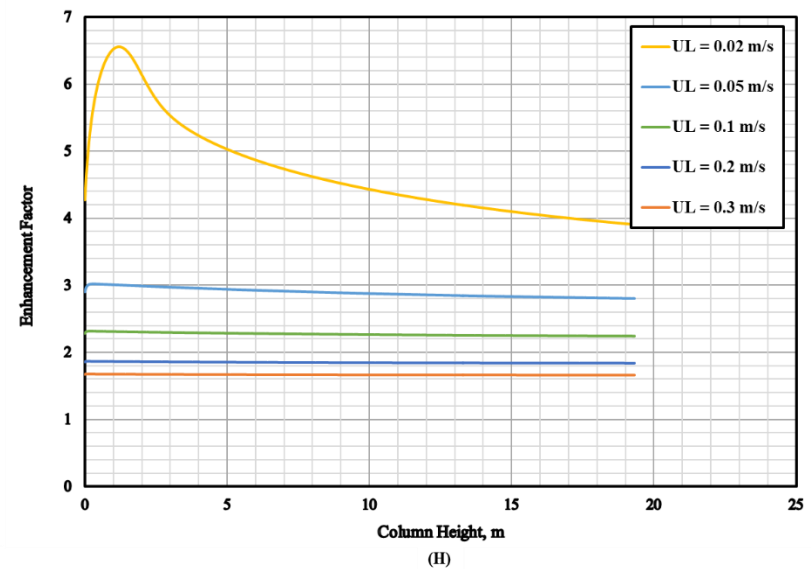
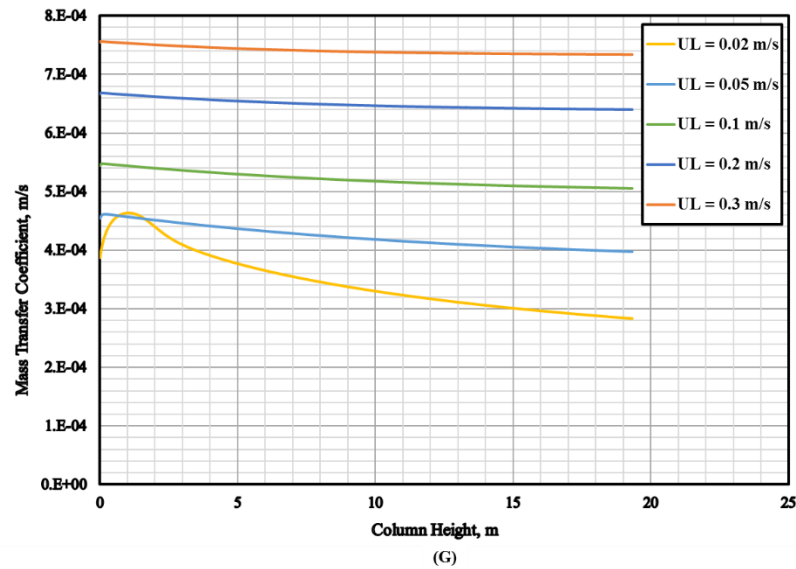
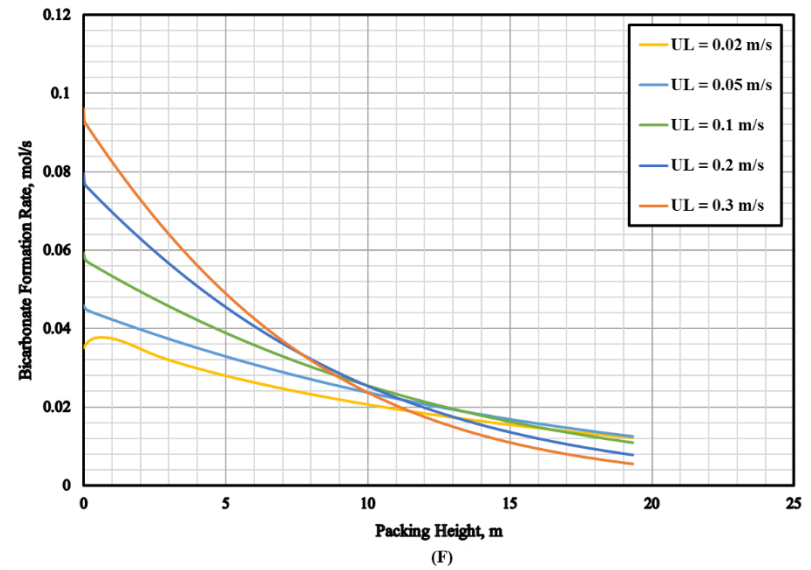
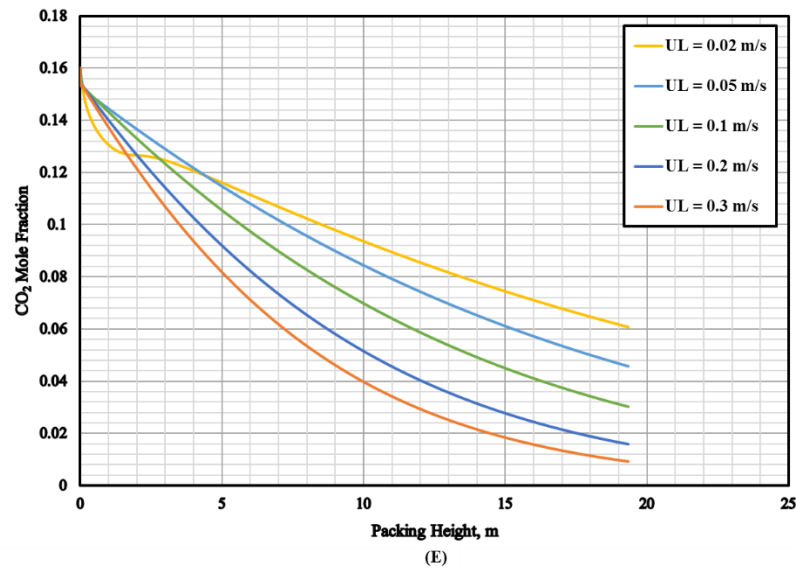
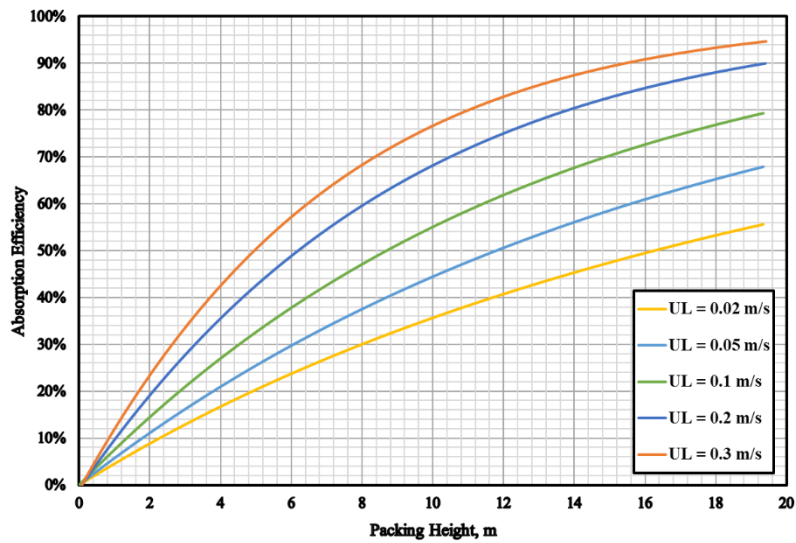
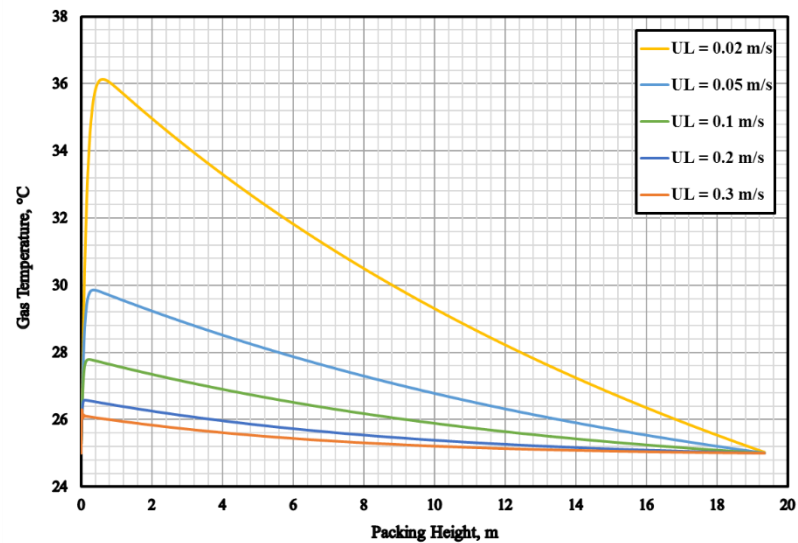


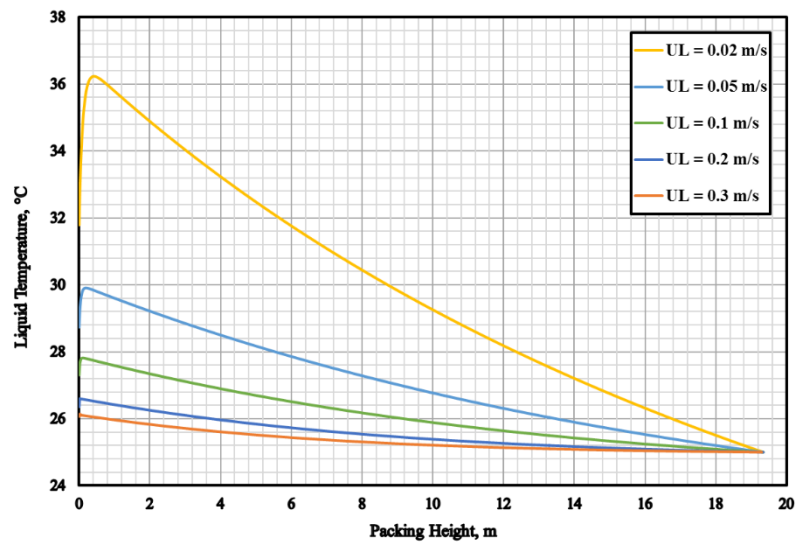
Figure 5-10: Effect of Liquid Velocity on CO₂ Absorption by AMP (E, F, G, H)



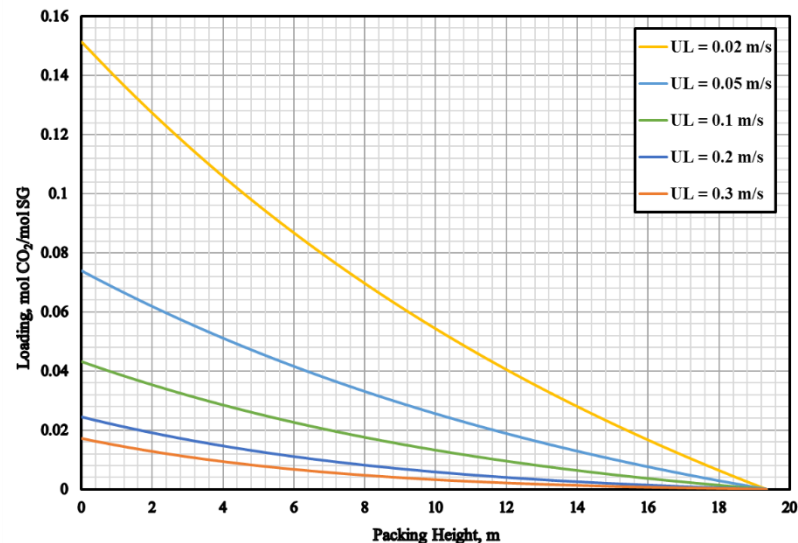
(A)



(B)



(C)



(D)

Figure 5-11: Effect of Liquid Velocity on CO₂ Absorption by SG (A, B, C, D)

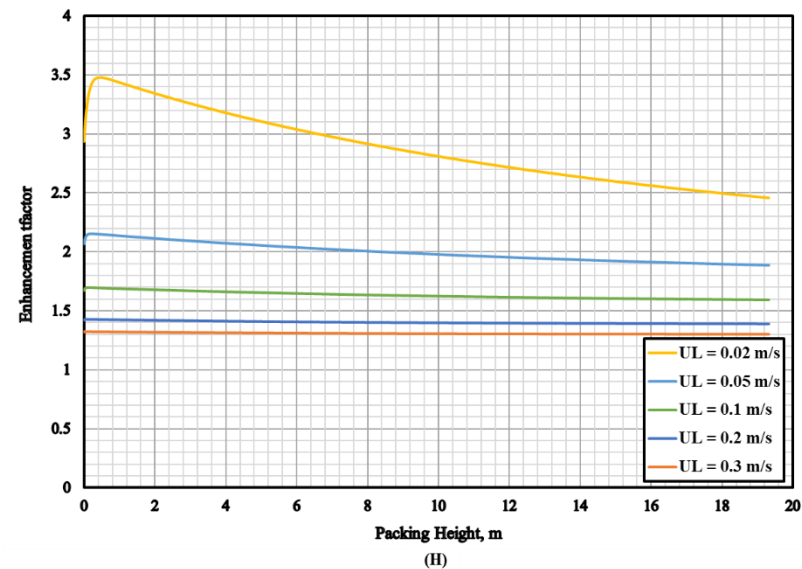
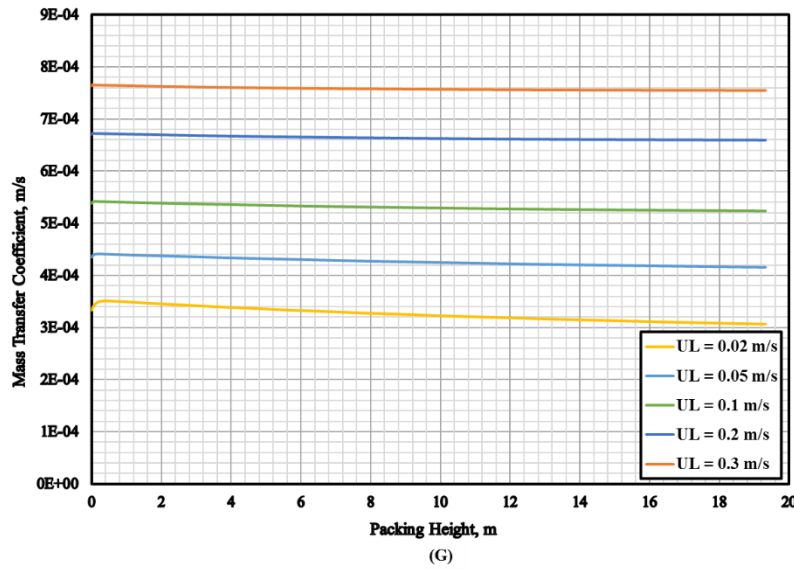
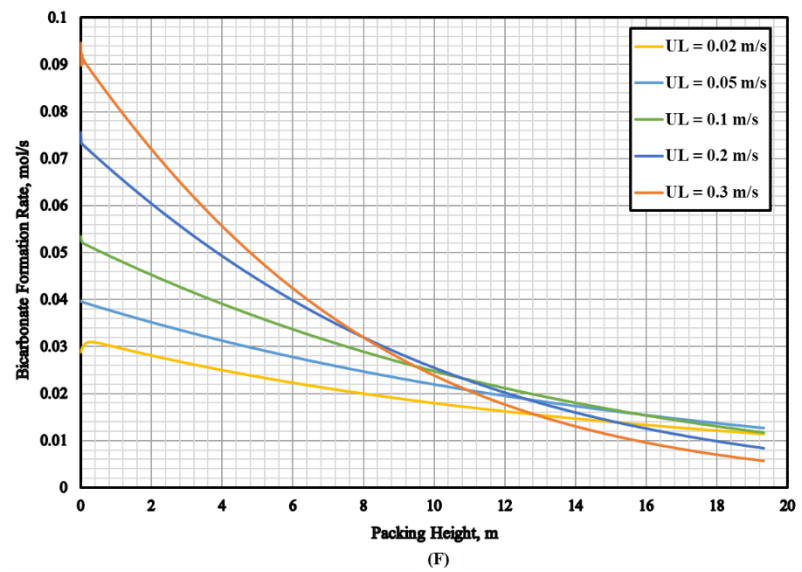
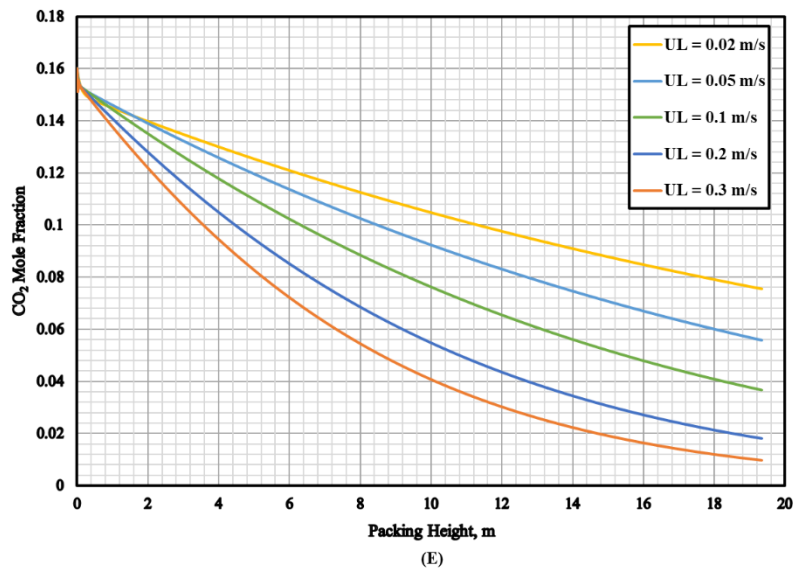


Figure 5-12: Effect of Liquid Velocity on CO₂ Absorption by SG (E, F, G, H)

5.4 Effect of CO₂ Mole Fraction in the Inlet Gas Feed

In postcombustion applications, the flue gas composition could vary depending on the coal quality as well as combustion conditions. In this parametric study, the CO₂ mole fraction in the flue gas is varied from 12% to 20% according to Table 5-5.

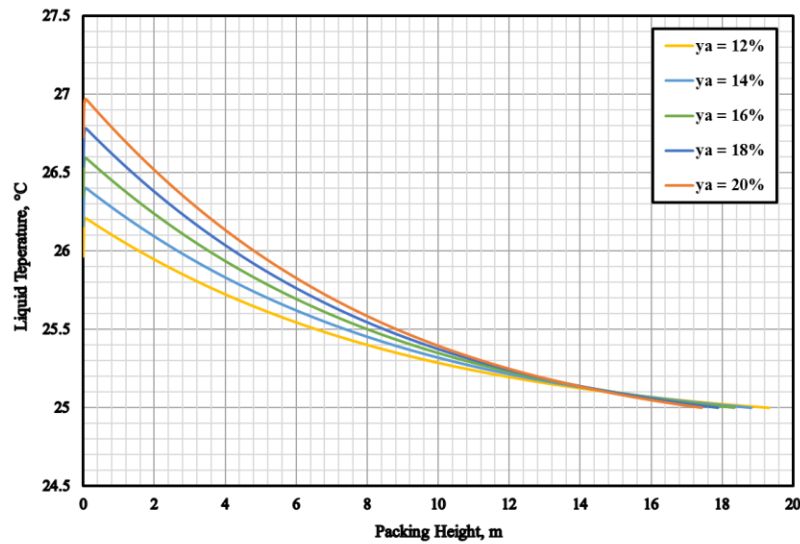
Table 5-5: Effect of CO₂ Mole Fraction on the Absorber Performances

CO ₂ mole Fraction, %	12%	14%	16%	18%	20%
Gas Temperature, °C	25				
Gas Density, kg/m ³	1.2067	1.2197	1.2308	1.2457	1.2587
Superficial Gas Velocity, m/s	3.016	2.984	2.957	2.922	2.892
Superficial Gas Mass Velocity, kg/m ² /s	3.64				
Gas Volumetric Flow Rate, m ³ /s	5.331	5.274	5.226	5.164	5.110
Gas Volumetric Flow Rate at Standard Condition, MMSCF/day	16.05	15.88	15.74	15.55	15.39
Liquid Temperature, °C	25				
Superficial Liquid Velocity, m/s	0.2				
Inlet AMP Concentration, mol/m ³	2000				
Packing Height for AMP to Achieve 90% CO ₂ Absorption Efficiency, m	19.32	18.82	18.34	17.88	17.42
Inlet SG Concentration, mol/m ³	3500				
Packing Height for SG to Achieve 90% CO ₂ Absorption Efficiency, m	20.32	19.84	19.34	18.88	18.4
Packed Column ID, m	1.5				
Packing	Ceramic Berl Saddle 13 mm				

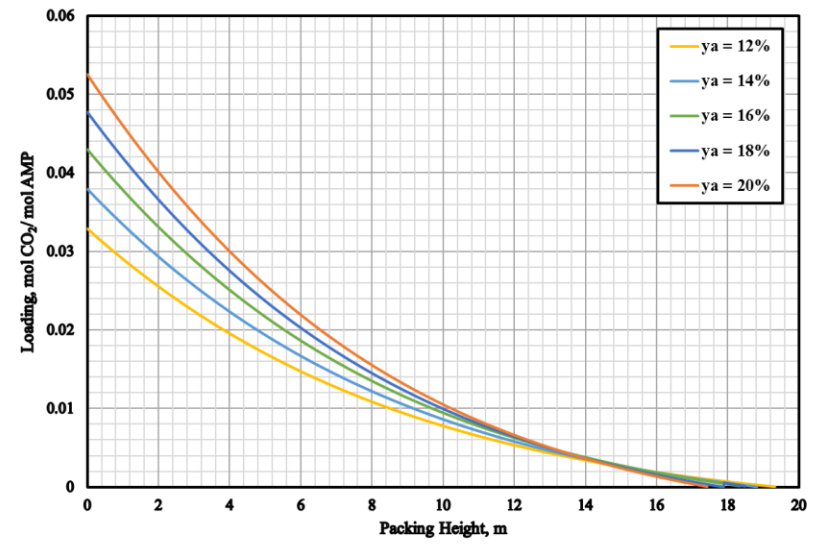
For AMP and SG aqueous solutions, the height of the packing is adjusted to reach 90% CO₂ absorption efficiency. The model predictions for AMP are shown in Figures 5-13 and 5-14 and those for SG are illustrated in Figures 5-15 and 5-16.

These figures indicate that increasing CO₂ mole fraction in the gas feed increases the CO₂ absorption efficiency. This behavior is because the mass transfer coefficient and enhancement factor increase with increasing the CO₂ mole fraction.

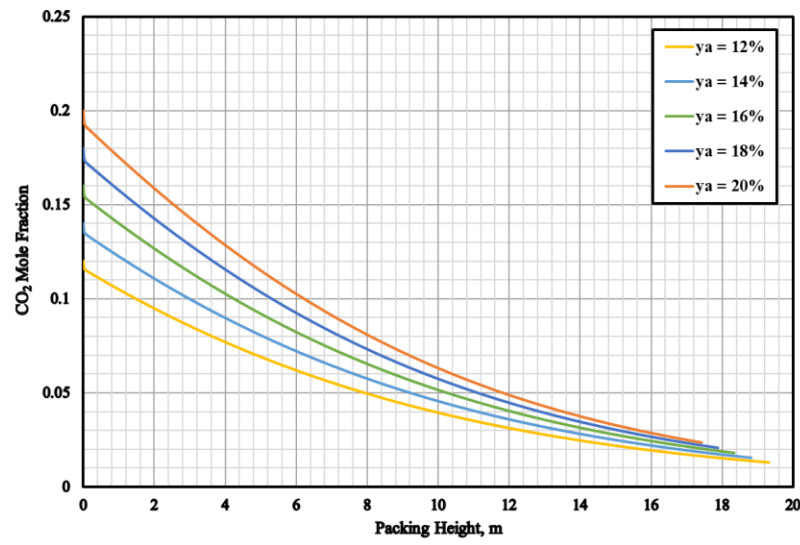
These figures also show that increasing the CO₂ mole fraction in the feed gas increases the outlet liquid temperature. This is due to the availability of more CO₂ to react with the solvent (AMP or SG), increasing the heat of reaction, which is essentially removed by the liquid phase. Moreover, high temperature leads to low liquid viscosity, high gas/liquid diffusivity as well as high reaction rate constant, which all increase the enhancement factor (E) and the mass transfer coefficients.



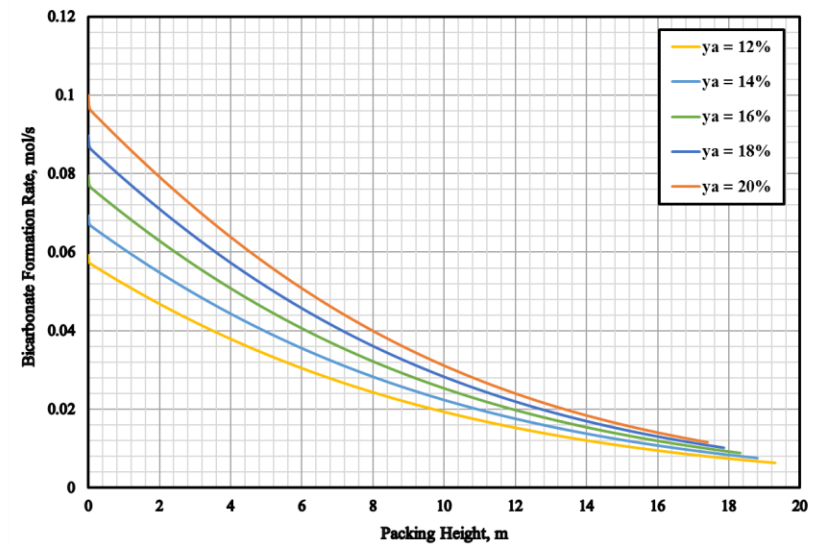
(C)



(D)



(E)



(F)

Figure 5-13: Effect of CO₂ Mole Fraction on Absorber Performance using AMP Aqueous Solutions (A, B, C, D)

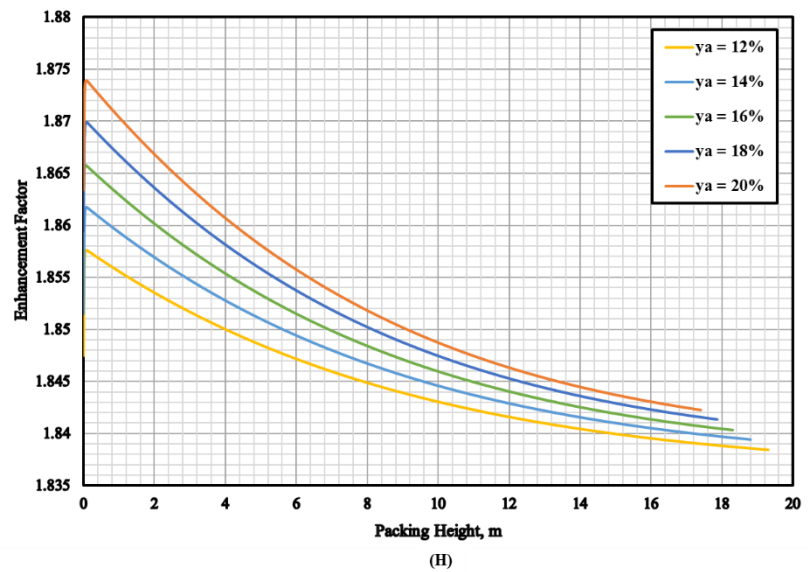
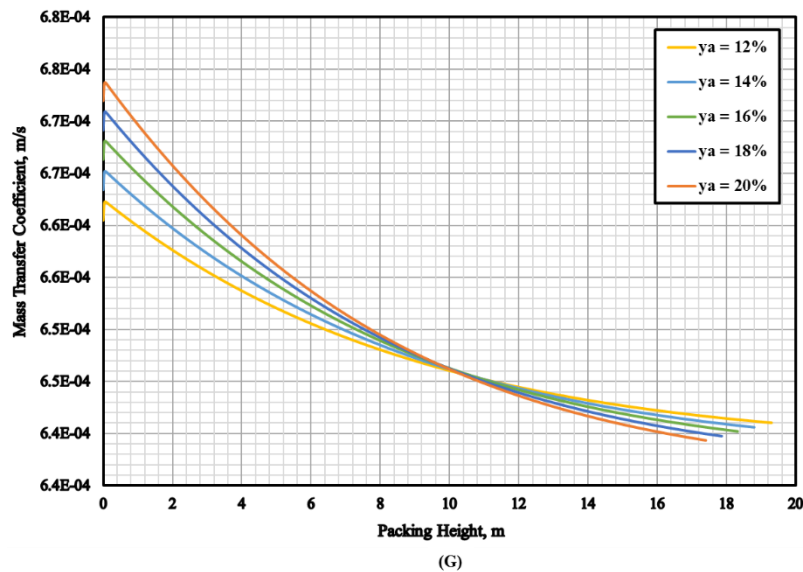
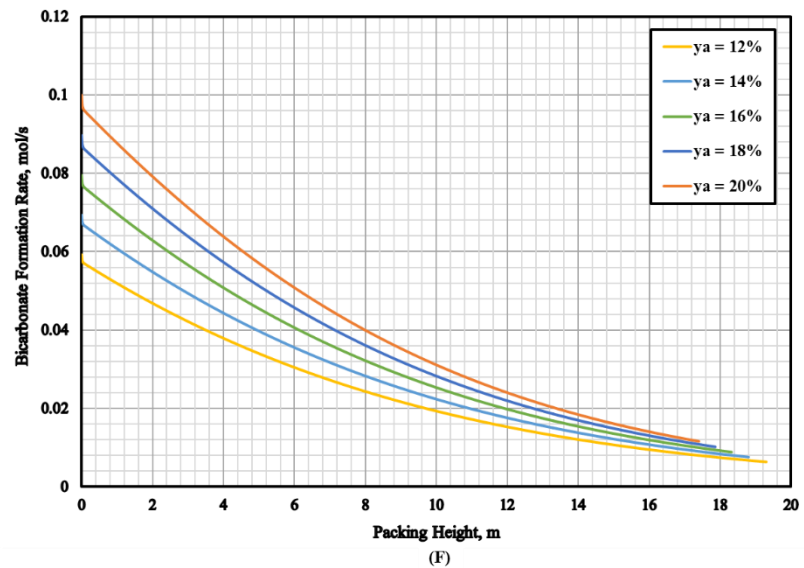
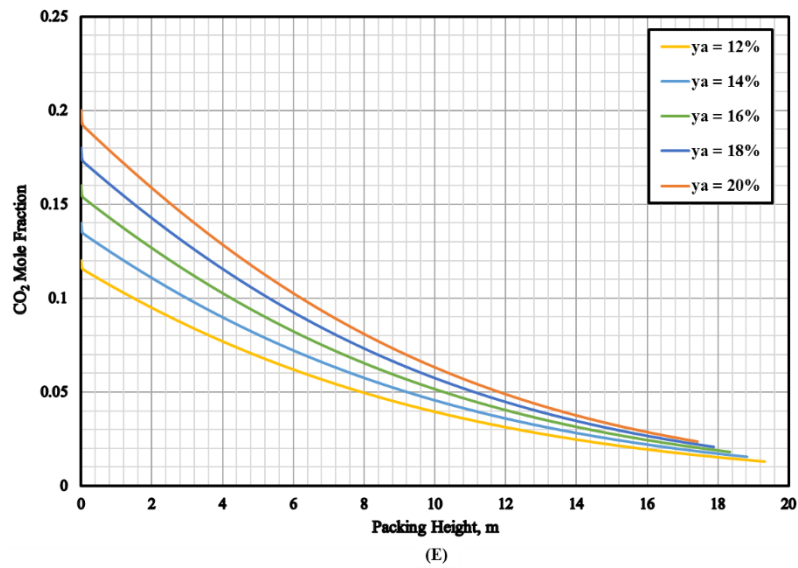
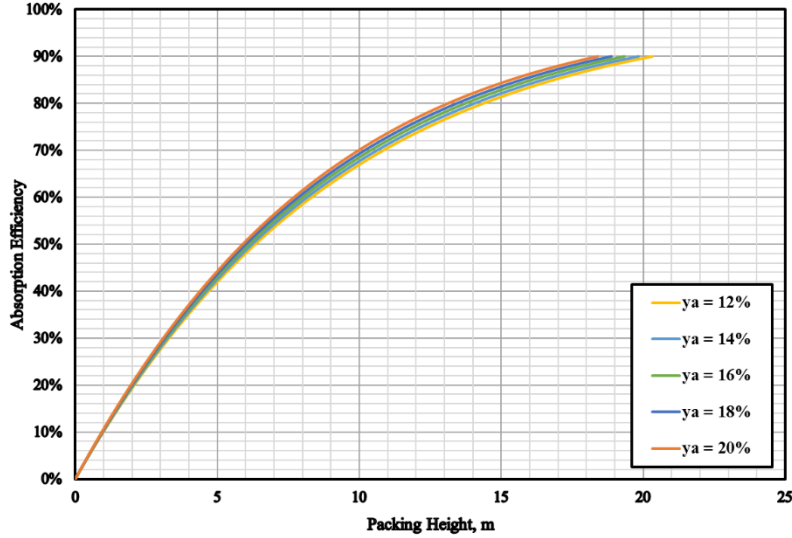
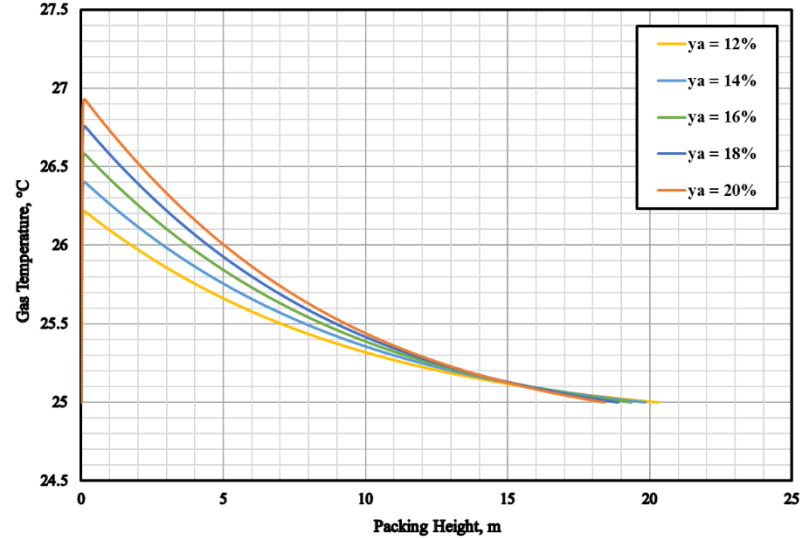


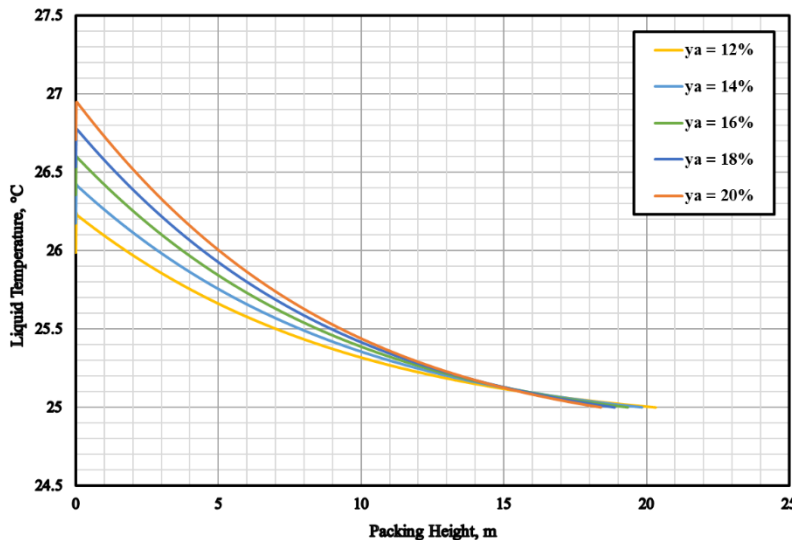
Figure 5-14: Effect of CO₂ Mole Fraction on Absorber Performance using AMP Aqueous Solutions (E, F, G, H)



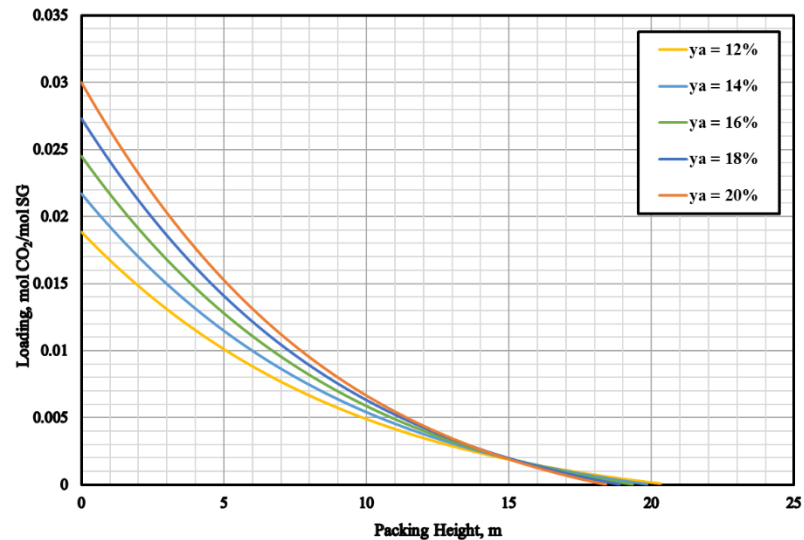
(A)



(B)



(C)



(D)

Figure 5-15: Effect of CO₂ Mole Fraction on Absorber Performance using SG Aqueous Solutions (A, B, C, D)

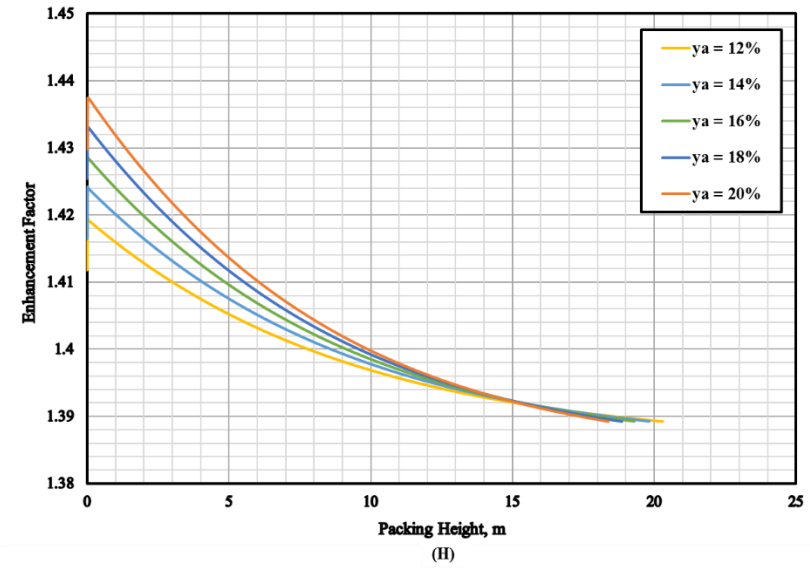
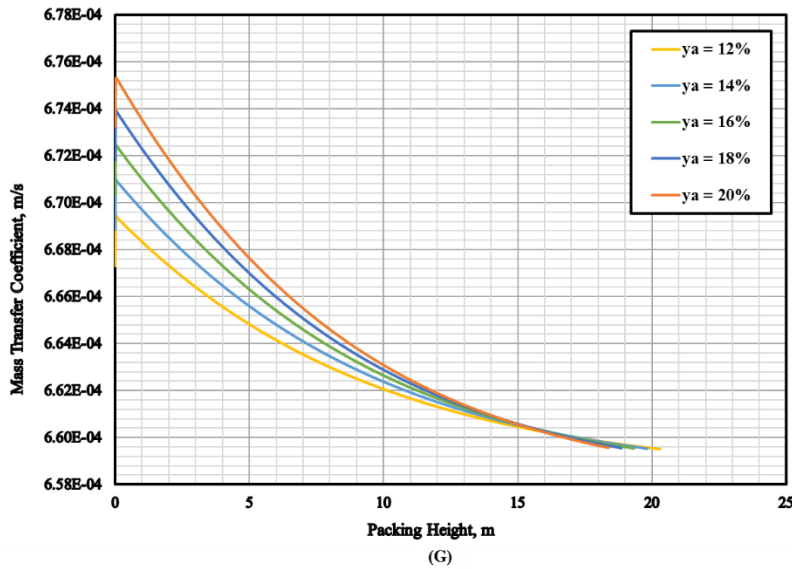
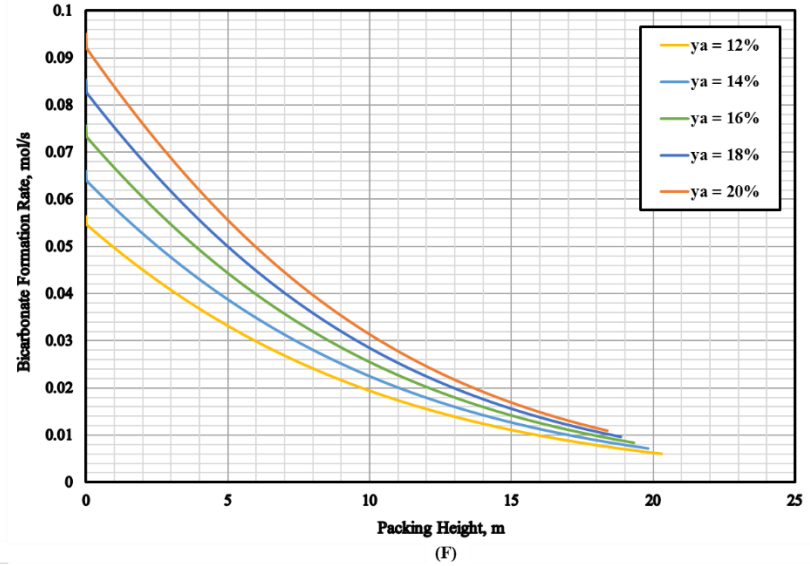
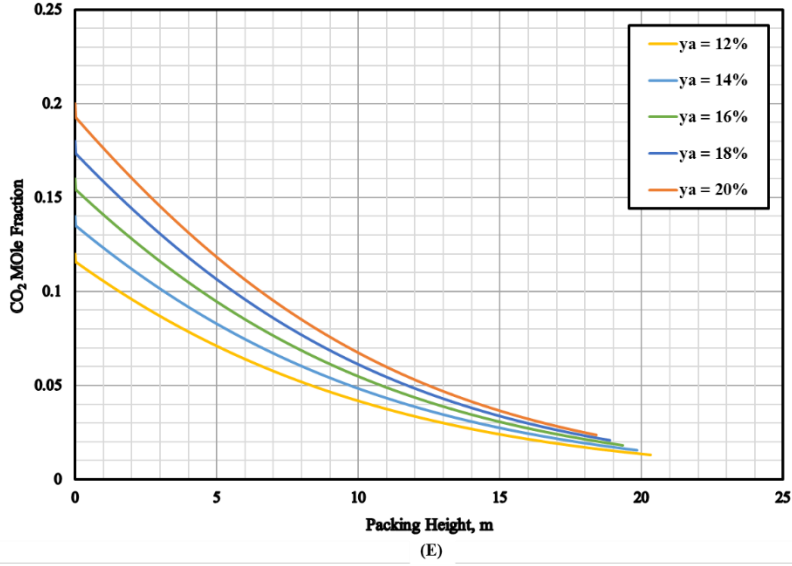


Figure 5-16: Effect of CO₂ Mole Fraction on Absorber Performance using SG Aqueous Solutions (E, F, G, H)

5.5 Effect of Packing Type

Five packings are used in this parametric study as listed in Table 5-6. All packings are random, except the Ceramic Impulse, which is a structured packing.

It should be noted that all packings used in this study are inert packing which means they do not take part in the chemical reaction between CO₂ and AMP or SG. Thus, the packing has essentially a hydrodynamic role, which affects the gas-liquid mass transfer coefficients and the specific wetted surface area. Therefore, at given operating conditions, different packings exhibit different pressure drops, liquid holdups, specific wetted areas and gas-liquid mass transfer coefficients. In this study, the packing height is adjusted to achieve 90% CO₂ absorption efficiency.

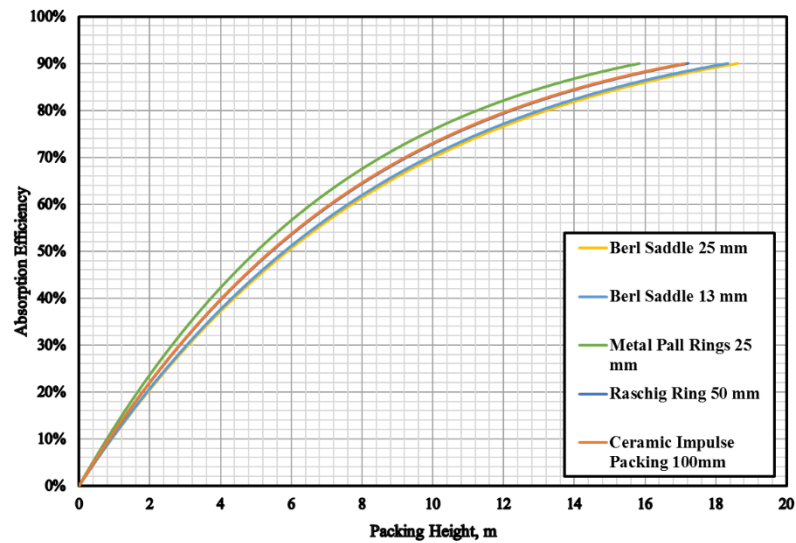
The model predictions are presented in Figures 5-17 and 5-18 for AMP and in Figures 5-19 and 5-20 for SG, respectively.

As can be observed in these figures, the metal Pall Ring 25 mm gives the greatest mass transfer coefficient whereas the ceramic Impulse structured packing gives the lowest mass transfer coefficients. This behavior is because Pall Ring 25 mm has the largest specific wetted area (606 m²/m³) when compared with those of the other packing used as shown in Table 5-6.

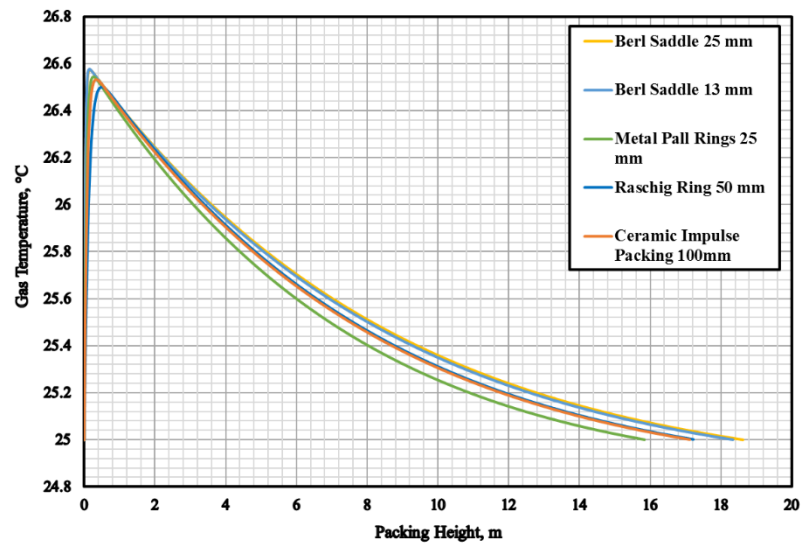
These Figures also show the outlet gas and liquid temperatures are similar at 90% CO₂ absorption efficiency for all the packings used since the amount of heat released due to the chemical reaction is the same at similar gas and liquid superficial velocities.

Table 5-6: Effect of Packing Type on the Absorber Performances

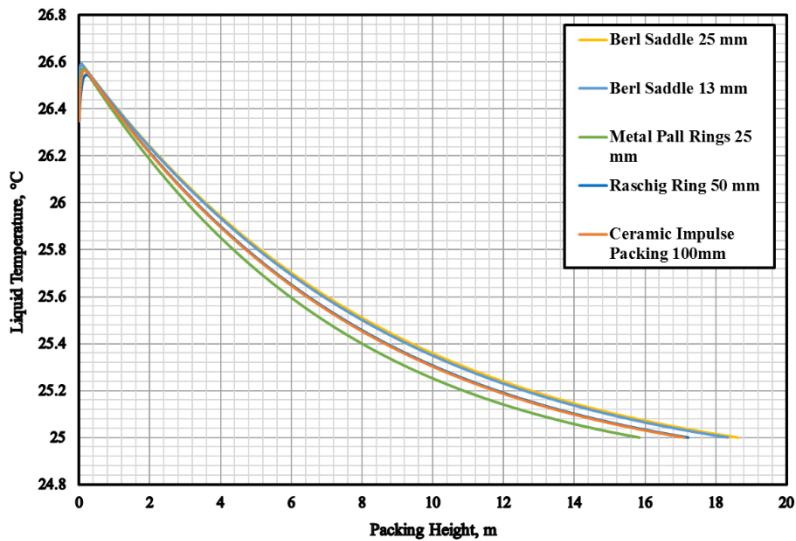
Packing	Ceramic Berl Saddle 13 mm	Ceramic Berl Saddle 25 mm	Metal Pall Ring 25 mm	Raschig Ring 50 mm	Ceramic Impulse 100 mm
Specific Surface Area (a), m ² /m ³	545	260	223.5	95	91.4
Porosity (Voidage), %	65	68	95.4	83	83.8
System Pressure, bar	1.0				
Gas Temperature, °C	25				
Superficial Gas Mass Velocity, kg/m ² /s	3.64				
Superficial Gas Velocity, m/s	2.957				
Gas Volumetric Flow Rate, m ³ /s	5.226				
Gas Standard Volumetric Flow Rate, MMSCF/day	15.7				
Liquid Temperature, °C	25				
Superficial Liquid Velocity, m/s	0.2				
Inlet AMP Concentration, mol/m ³	2000				
Packing Height for AMP to Achieve 90% CO ₂ Absorption Efficiency, m	18.34	18.62	15.84	17.22	17.12
Specific Wetted Surface Area for AMP (a _w), m ² /m ³	414	424	502	468	470
Inlet SG Concentration, mol/m ³	3500				
Packing Height for SG to Achieve 90% CO ₂ Absorption Efficiency, m	19.34	20.76	17.84	19.68	19.88
Specific Wetted Surface Area for SG (a _w), m ² /m ³	501	512	606	566	568
Column ID, m	1.5				



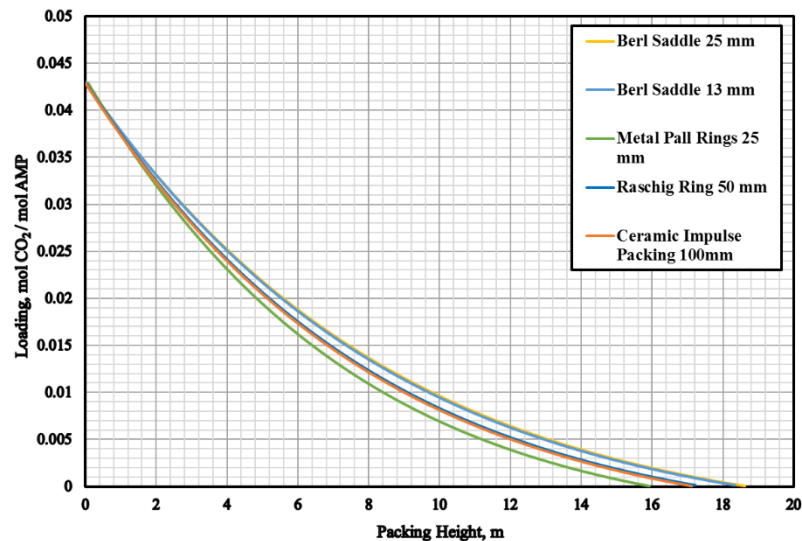
(A)



(B)

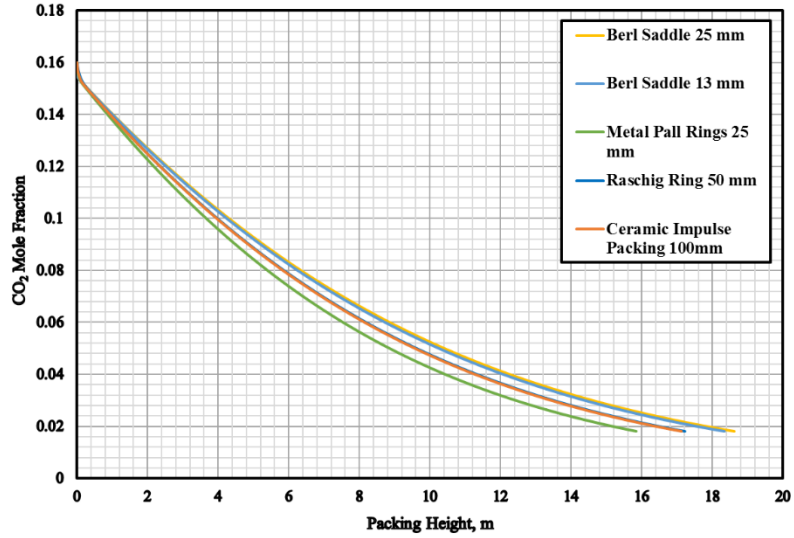


(C)

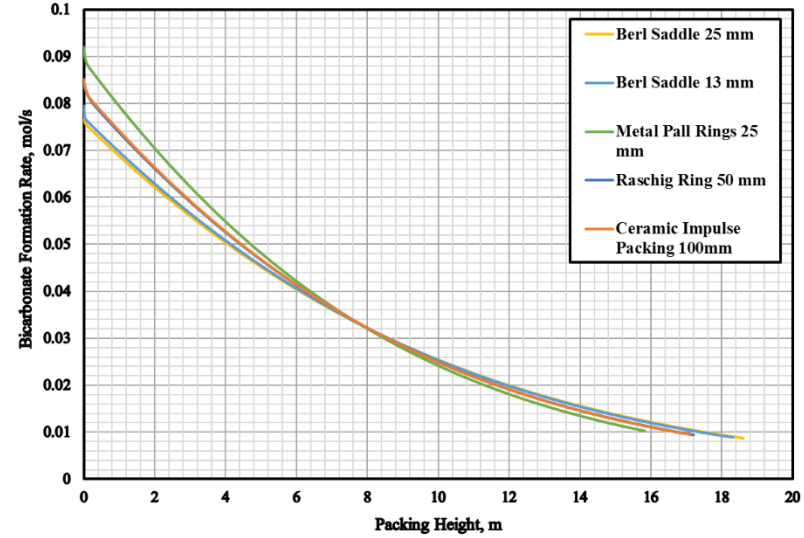


(D)

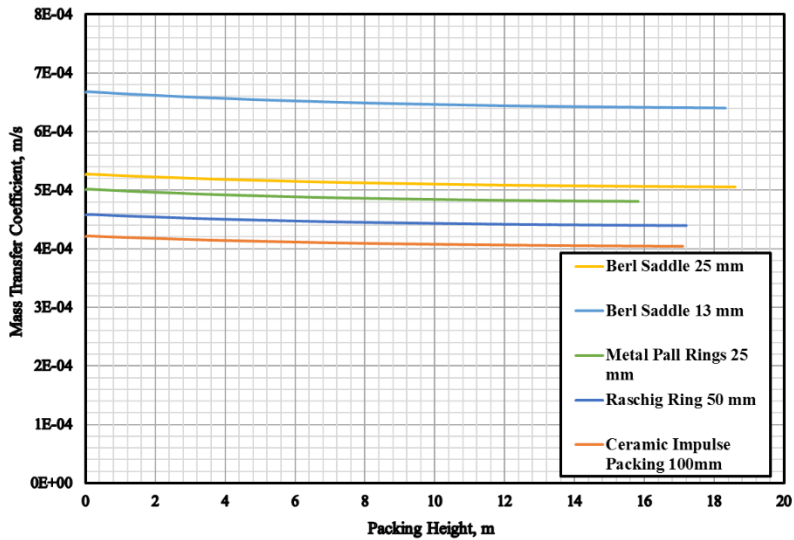
Figure 5-17: Effect of Packing Type on CO₂ Absorption Using AMP Aqueous Solutions (A, B, C, D)



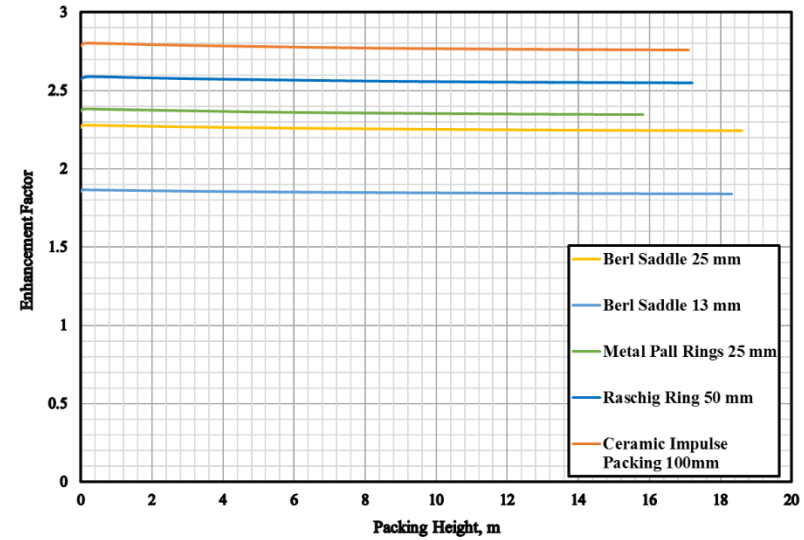
(E)



(F)

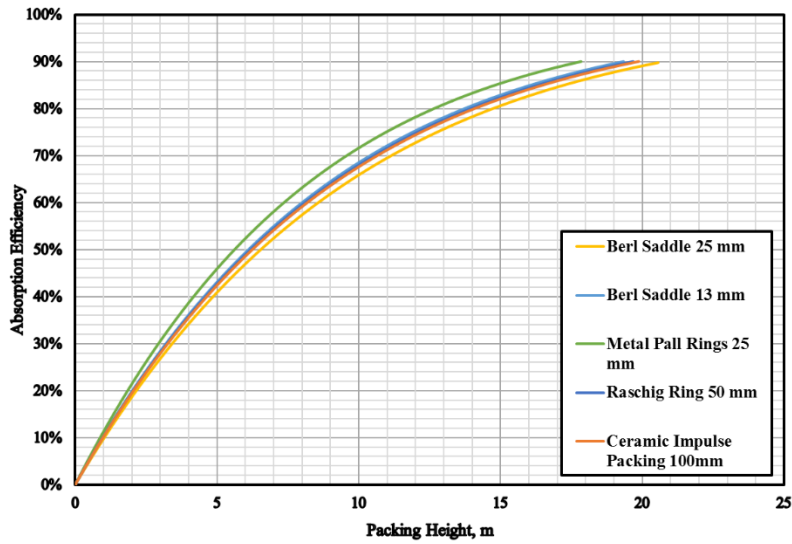


(G)

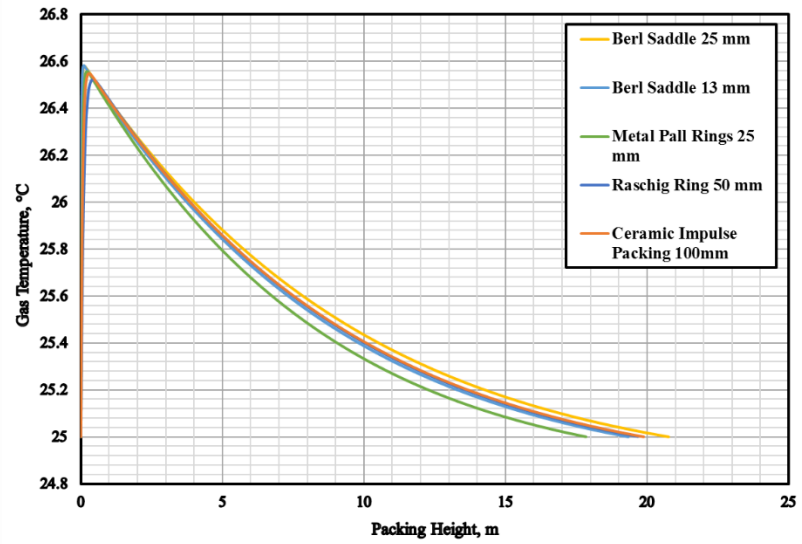


(H)

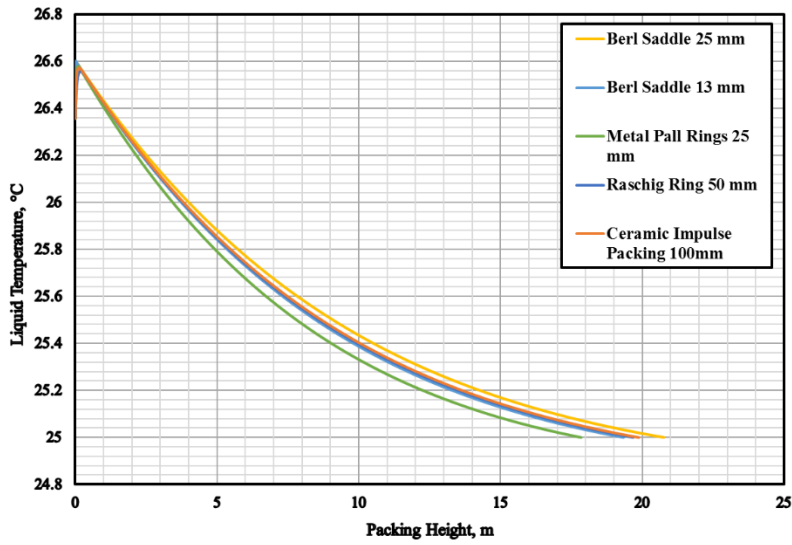
Figure 5-18: Effect of Packing Type on CO₂ Absorption Using AMP Aqueous Solutions (E, F, G, H)



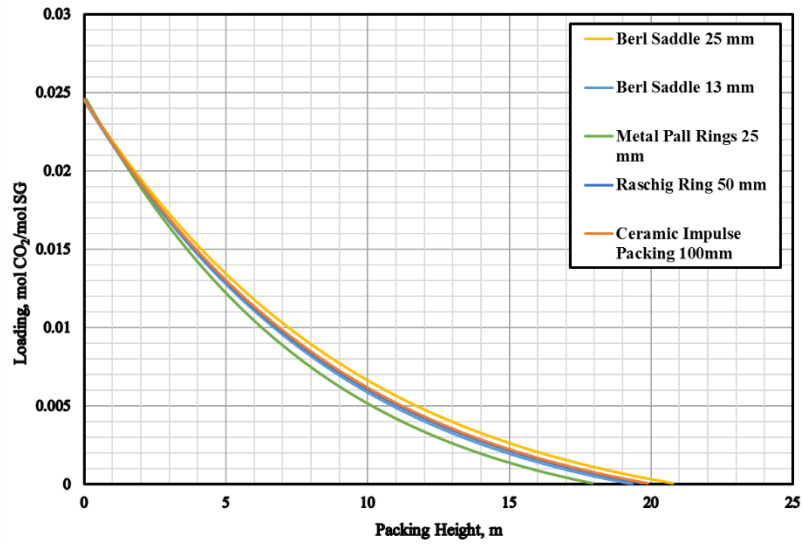
(A)



(B)



(C)



(D)

Figure 5-19: Effect of Packing Type on CO₂ Absorption Using SG Aqueous Solutions (A, B, C, D)

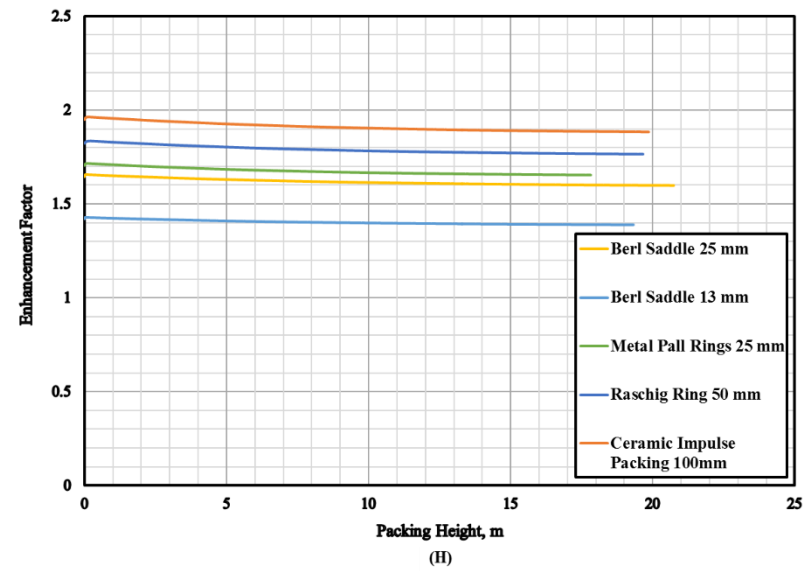
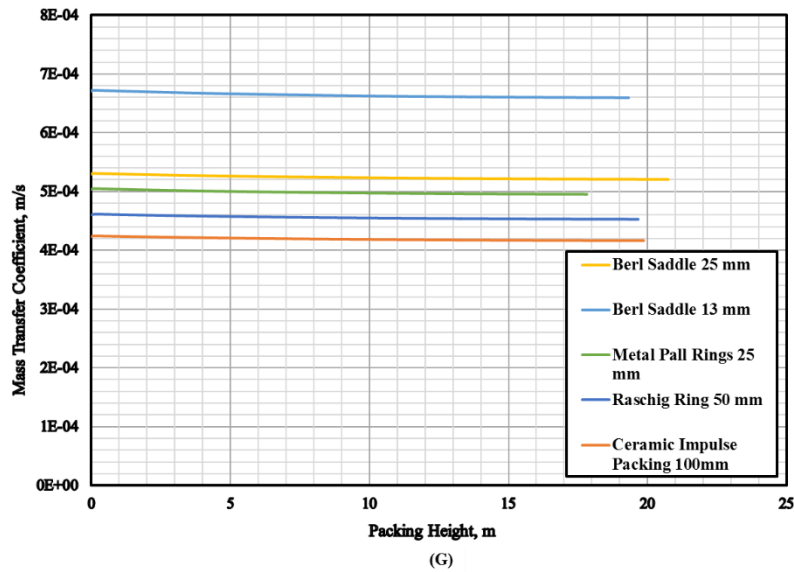
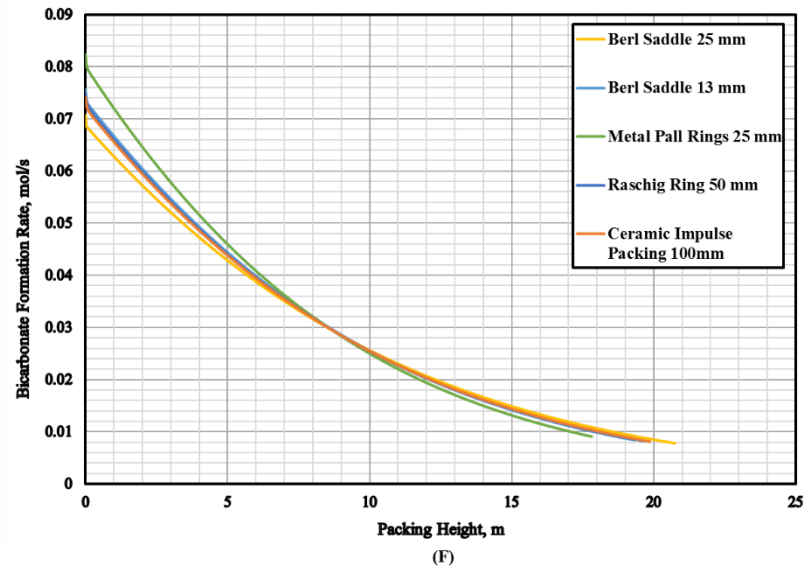
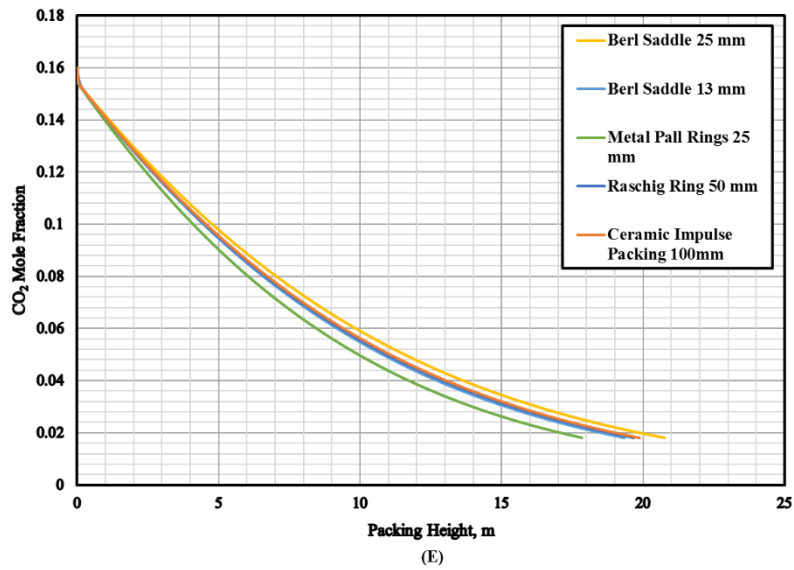


Figure 5-20: Effect of Packing Type on CO₂ Absorption Using SG Aqueous Solutions (E, F, G, H)

5.6 Comparison Between the Performance of AMP and SG Absorbents

A comparison between the predicted profiles for 2,000 mol/m³ AMP and 3,500 mol/m³ SG aqueous solutions is carried out under the inlet operating variables given in Table 5-7. The packing height of the absorber is also adjusted to achieve 90% CO₂ absorption efficiency.

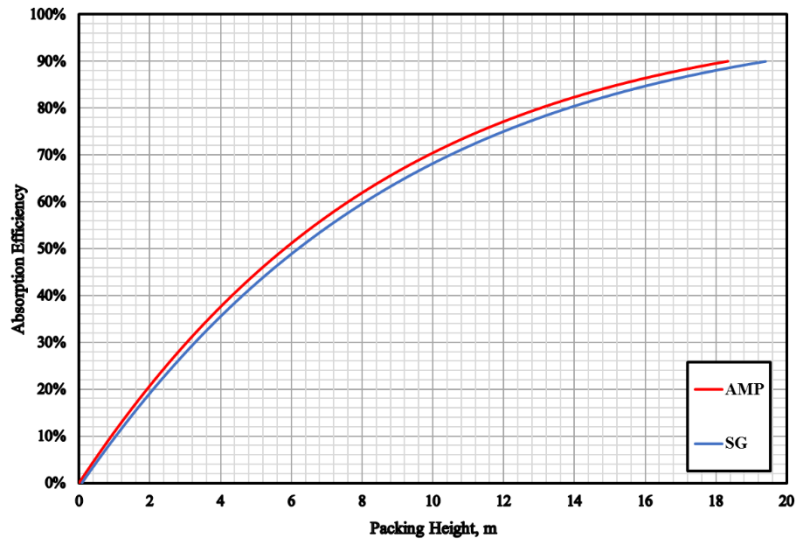
Table 5-7: Inlet Parameters for AMP and SG Aqueous Solution Used

Inlet Variables	AMP	SG
Superficial Gas Mass Velocity, kg/m ² /s	3.64	3.64
Gas Density, kg/m ³	1.23	1.23
Superficial Liquid Velocity, m/s	0.2	0.2
Absorbent Concentration, mol/m ³	2,000	3,500
Liquid Density, kg/m ³	1,001	1,223
Liquid Inlet Temperature, °C	25	25
Gas Inlet Temperature, °C	25	25

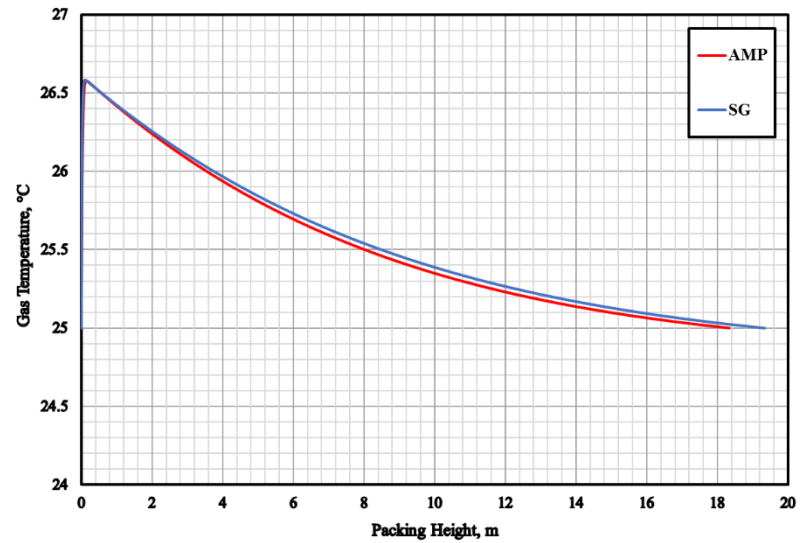
From the model predictions for AMP and SG shown in Figures 5-21 and 5-22, the following remarks can be made:

- (1) Lower packing height is required for 2M AMP than that for 3.5M SG to achieve 90% CO₂ absorption efficiency. This behavior is due to the greater reaction rate constant (k_2) of AMP when compared with that of SG, as illustrated previously in Figure 3-8 and again by the enhancement factor profile, Figure 5-22 (H).

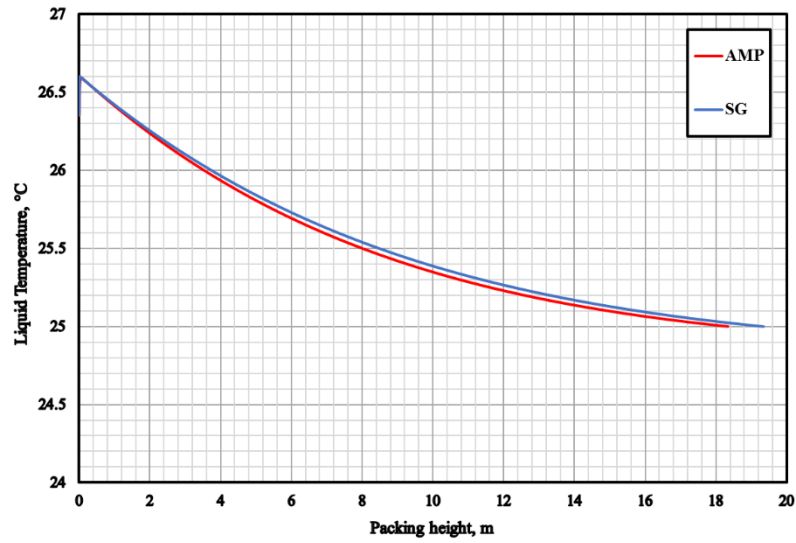
- (2) The liquid temperature profiles are similar for AMP and SG aqueous solution. This is because the heat released from the chemical reactions are similar between AMP and SG at low loading. For instance, at a loading of 0.02 and a temperature of 303.15 K the heat of reaction for AMP using Equation (3-95) is - 67,824 J/mole of CO₂ and that for SG using Equation (3-99) is - 68,733 J/mole of CO₂. These values are relatively close to each other. Moreover, heat capacity of AMP and SG dilute aqueous solution are similar.
- (3) The loading, defined as moles of CO₂ absorbed/initial mole of reactant, is greater for AMP than that of SG. This behavior can be related to the initial concentration difference, lower initial AMP concentration of 2,000 mole/m³ gives higher loading than SG with an initial concentration of 3500 mole/m³.



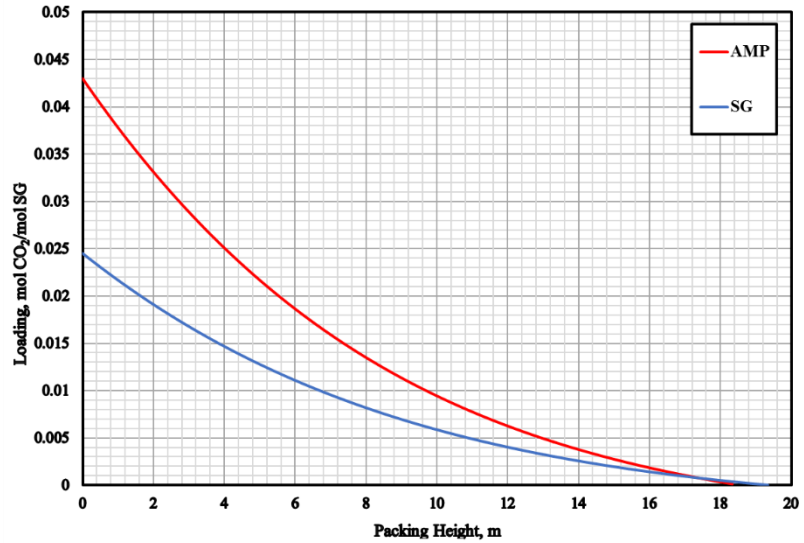
(A)



(B)



(C)



(D)

Figure 5-21: Comparison Between AMP and SG (A, B, C, D)

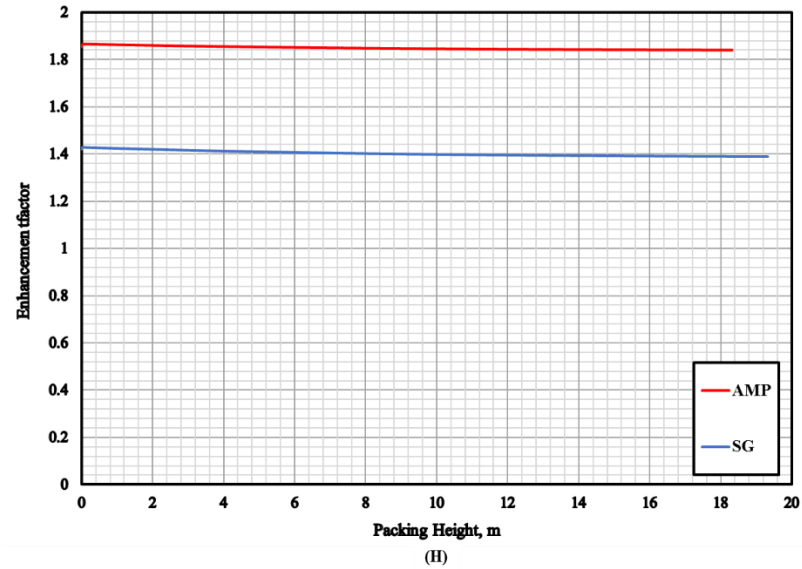
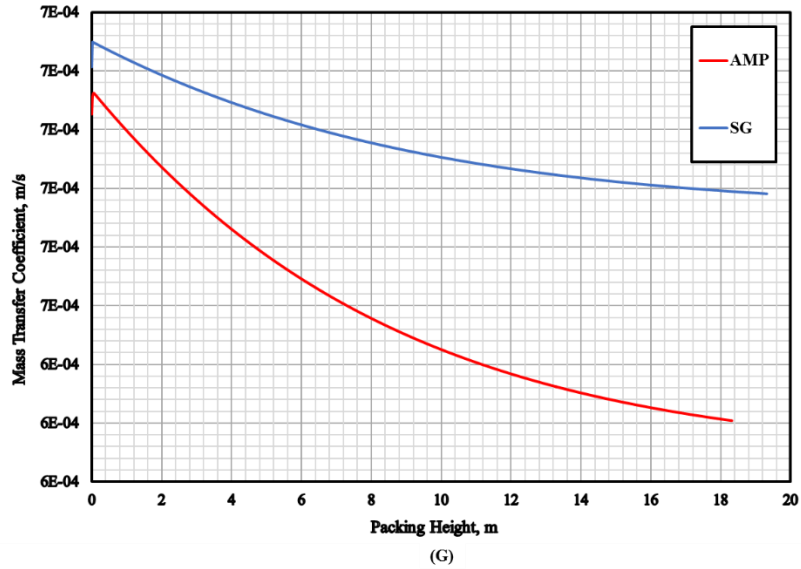
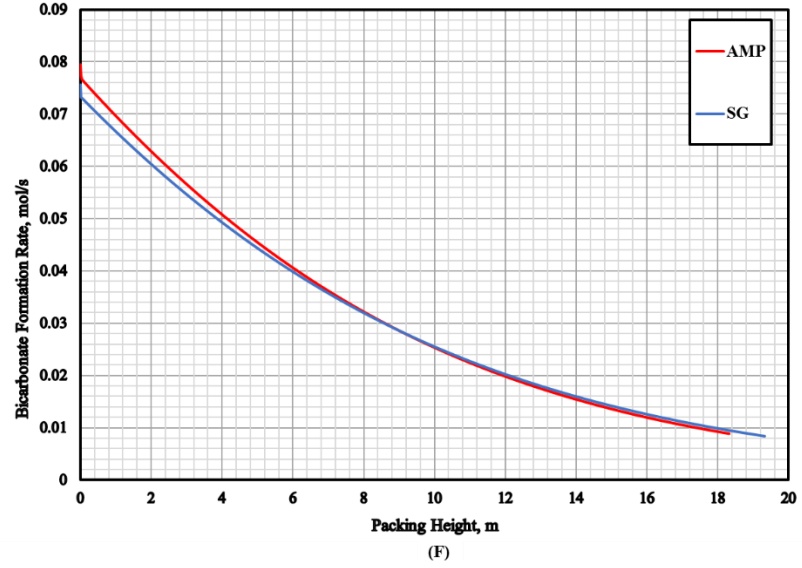
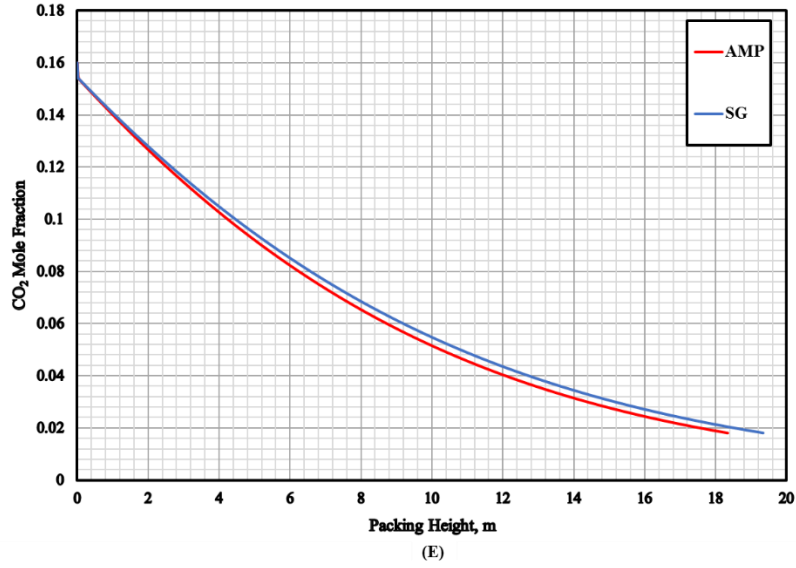


Figure 5-22: Comparison Between AMP and SG (E, F, G, H)

6.0 Concluding Remarks

1. A five-components mathematical model is developed to predict CO₂ absorption from a gaseous mixture by chemical absorbent in a countercurrent packed-bed adiabatic absorber. The five components are gaseous reactant (CO₂), inert carrier gas (air or nitrogen), liquid absorbent (AMP or SG), volatile solvent (water), and non-volatile product (bicarbonate). Material and energy balance equations are derived for the gas and liquid phases and implemented in MATLAB 2017b. An extensive literature survey is conducted to find, correlate and compile the required equation parameters, including physico-chemical and thermodynamic properties, reaction rate kinetics, gas-liquid mass transfer coefficients, and hydrodynamic as well as flooding criteria. The model solves the combined material and energy balances under different boundary conditions or packing types to predict the profiles along the absorber height of CO₂ absorption efficiency, CO₂ loading, CO₂ mole fraction, gas and liquid phase temperatures, in addition to the enhancement factor and Hatta number to assess the speed of the chemical reactions taking place.
2. The model predictions are validated using four different runs of the experimental data by Tontiwachwuthikul et al. [93] obtained in a small-scale absorber (0.1 m ID) for CO₂ absorption from a CO₂-Air mixture by AMP aqueous solution. The model reasonably predicts the experimental data for CO₂ loading and liquid temperature, however, the slight deviation of predicted CO₂ mole fraction profile could be attributed to experimental error in the CO₂ material balance calculations reported by Tontiwachwuthikul et al. [93].
3. The validated model is used to predict the performance of a similar small-scale (0.1 m ID) absorber for CO₂ capture from a CO₂-air mixture using sodium glycinate (SG) aqueous

solutions under identical inlet operating conditions. A direct comparison between CO₂ absorption by AMP and SG shows that AMP has better CO₂ absorption efficiency than that of SG due to former greater reaction rate constant (k_2) under similar temperature.

4. The validated model is used to conduct a parametric study to investigate the performance of a countercurrent adiabatic large-scale (1.5 m ID) packed-bed absorber for CO₂ capture from a CO₂/N₂ gaseous mixture using AMP and SG aqueous solutions. The system pressure, liquid temperature, superficial liquid velocity, CO₂ mole fraction and packing type are varied and the following remarks can be made:
 - a. Increasing system pressure decreases the superficial gas velocity and increases the CO₂ absorption efficiency in both solvents. This behavior is due to the increase of the gas-residence time in the absorber with increasing pressure. Compared with other parameters, system pressure appears to have the strongest effect on the CO₂ absorption efficiency.
 - b. Increasing liquid temperature increase, on one hand, the gas-liquid mass transfer by decreasing the liquid viscosity and increases the gas diffusivity and, on the other hand, increases the reaction rate constant (k_2). This combined effect of increasing liquid temperature contributes to increasing the CO₂ absorption efficiency.
 - c. Higher superficial liquid velocity yields higher absorption efficiency but lower CO₂ loading. This behavior is related to the increase of the liquid holdup, the specific wetted area, and the mass transfer coefficients (k_L). The low loading at high superficial liquid velocity is because of the large AMP and SG moles in the liquid phase at a fixed CO₂ inlet mole fraction in the gas phase.
 - d. When gas superficial mass velocity is fixed, increasing the CO₂ mole fractions in the feed gas increases the CO₂ absorption efficiency.

- e. The pressure appears to have the strongest effect on the CO₂ absorption efficiency than those of the other variables investigated.
- f. Consistent with small-scale absorber (0.1 m ID) at identical concentrations of 2,000 mol/m³, in the large-scale absorber (1.5 m ID), AMP at 2,000 mol/m³ has greater CO₂ absorption capacity than SG even at 3,500 mol/m³. Again, this can be related to the fact that the reaction rate constant (k_2) of AMP is greater than that of SG at similar temperature.
- g. Metal Pall Ring 25 mm is found to be the most efficient packing in CO₂ absorption due to its largest specific wetted area.

7.0 Future Work

1. Conduct experiments to measure the CO₂ absorption using SG aqueous solutions in a small-scale absorber to validate the model predictions.
2. Conduct experiments to measure the heat of absorption data to validate the estimations using Gibbs-Helmholtz Equation.
3. Measure the heat transfer coefficients using SG or develop a better model to calculate the average diffusivity and thermal conductivity in SG.
4. Improve the MATLAB model to allow for CO₂ absorption from a multicomponent gas mixture typical to a postcombustion flue gas, containing H₂O, O₂, HCl, NO_x, CO, and SO_x, etc.
5. Use Aspen Plus to compare with the MATLAB model predictions and eventually perform techno-economic analysis using SG.

Bibliography

- [1] T. F. Stocker *et al.*, "Climate change 2013: The physical science basis," ed: Cambridge University Press Cambridge, 2013.
- [2] M. Parry, M. L. Parry, O. Canziani, J. Palutikof, P. Van der Linden, and C. Hanson, *Climate change 2007-impacts, adaptation and vulnerability: Working group II contribution to the fourth assessment report of the IPCC*. Cambridge University Press, 2007.
- [3] J. Hansen, R. Ruedy, M. Sato, and K. Lo, "Global surface temperature change," *Reviews of Geophysics*, vol. 48, no. 4, 2010.
- [4] NOAA. (2016, 05/06). *National Centers for Environmental Information*.
- [5] J. Hansen, M. Sato, R. Ruedy, A. Lacis, and V. Oinas, "Global warming in the twenty-first century: An alternative scenario," *Proceedings of the National Academy of Sciences*, vol. 97, no. 18, pp. 9875-9880, 2000.
- [6] E. Ozdemir, K. Schroeder, and B. I. Morsi, "Global warming: Carbon dioxide sequestration in coal seams," *Proc. of Am. Chem. Soc*, vol. 42, pp. 310-317, 2002.
- [7] "contribution of working group III to fifth assessment report of the Intergovernmental panel on climate change," 2014.
- [8] A. Sieminski, "International energy outlook," *Energy Information Administration*, vol. 18, 2014.
- [9] J. Conti, P. Holtberg, J. Diefenderfer, A. LaRose, J. T. Turnure, and L. Westfall, "International energy outlook 2016 with projections to 2040," USDOE Energy Information Administration (EIA), Washington, DC (United States ...2016.
- [10] P. Freund, "Making deep reductions in CO₂ emissions from coal-fired power plant using capture and storage of CO₂," *Proceedings of the Institution of Mechanical Engineers, Part A: Journal of Power Energy*, vol. 217, no. 1, pp. 1-7, 2003.
- [11] I. e. agency, "CO₂ EMISSIONS FROM FUEL COMBUSTION: OVERVIEW," IEA statistics2017.
- [12] M. Meinshausen *et al.*, "Greenhouse-gas emission targets for limiting global warming to 2 C," *Nature*, vol. 458, no. 7242, p. 1158, 2009.
- [13] M. Tubman, Center for Climate and Energy Solutions: Washington, DC, USA, "President Obama's Climate Action Plan: Two Years Later," 2015.
- [14] D. Reichle, J. Houghton, B. Kane, and J. Ekmann, "Carbon sequestration research and development," Oak Ridge National Lab., TN (US); National Energy Technology Lab ...1999.

- [15] A. B. Rao and E. S. Rubin, "A technical, economic, and environmental assessment of amine-based CO₂ capture technology for power plant greenhouse gas control," *Environmental science technology*, vol. 36, no. 20, pp. 4467-4475, 2002.
- [16] E. S. Rubin, "CO₂ capture and transport," *Elements*, vol. 4, no. 5, pp. 311-317, 2008.
- [17] B. Metz, O. Davidson, H. de Coninck, M. Loos, and L. Mayer, "Intergovernmental Panel on Climate Change (IPCC) Special Report on Carbon Dioxide Capture and Storage," 2005.
- [18] "PRE-COMBUSTION CO₂ CAPTURE."
- [19] O. M. Basha, ed, 2019.
- [20] C. Kunze and H. Spliethoff, "Modelling of an IGCC plant with carbon capture for 2020," *Fuel processing technology*, vol. 91, no. 8, pp. 934-941, 2010.
- [21] T. Fout, "Cost and performance baseline for fossil energy plants volume 1: bituminous coal (IGCC) to electricity," *National Energy Technology Laboratory: Washington, DC, USA*, 2015.
- [22] R. P. Field and R. Brasington, "Baseline flowsheet model for IGCC with carbon capture," *Industrial Engineering Chemistry Research*, vol. 50, no. 19, pp. 11306-11312, 2011.
- [23] *POST-COMBUSTION CO₂ CAPTURE*. Available: <https://www.netl.doe.gov/coal/carbon-capture/post-combustion>
- [24] S. Wang *et al.*, "Mercury emission and speciation of coal-fired power plants in China," *Atmospheric Chemistry Physics*, vol. 10, no. 3, pp. 1183-1192, 2010.
- [25] M. Wang, A. Lawal, P. Stephenson, J. Sidders, and C. Ramshaw, "Post-combustion CO₂ capture with chemical absorption: a state-of-the-art review," *Chemical Engineering Research and Design*, vol. 89, no. 9, pp. 1609-1624, 2011.
- [26] E. J. Granite and H. W. Pennline, "Photochemical removal of mercury from flue gas," *Industrial & Engineering Chemistry Research*, vol. 41, no. 22, pp. 5470-5476, 2002.
- [27] F. Gozalpour, S. R. Ren, and B. Tohidi, "CO₂ Eor and Storage in Oil Reservoir," *Oil Gas Science Technology - Rev. IFP*, vol. 60, no. 3, pp. 537-546, 2005.
- [28] S. Bachu, J. C. Shaw, and R. M. Pearson, "Estimation of Oil Recovery and CO₂ Storage Capacity in CO₂ EOR Incorporating the Effect of Underlying Aquifers," presented at the SPE/DOE Symposium on Improved Oil Recovery, Tulsa, Oklahoma, 2004/1/1/, 2004. Available: <https://doi.org/10.2118/89340-MS>
- [29] M. H. Holtz, P. K. Nance, and R. J. Finley, "Reduction of Greenhouse Gas Emissions through CO₂ EOR in Texas," *Environmental Geosciences*, vol. 8, no. 3, pp. 187-199, 2001.
- [30] Q. Kang, I. N. Tsimpanogiannis, D. Zhang, and P. C. Lichtner, "Numerical modeling of pore-scale phenomena during CO₂ sequestration in oceanic sediments," *Fuel Processing Technology*, vol. 86, no. 14, pp. 1647-1665, 2005/10/01/ 2005.

- [31] P. Linga, R. Kumar, and P. Englezos, "The clathrate hydrate process for post and pre-combustion capture of carbon dioxide," *Journal of Hazardous Materials*, vol. 149, no. 3, pp. 625-629, 2007/11/19/ 2007.
- [32] J. Dymont and S. Watanasiri, "Acid gas cleaning using DEPG physical solvents: validation with experimental and plant data," *The USA: Aspen Technology Inc*, 2015.
- [33] A. J. Kidnay, W. R. Parrish, and D. G. McCartney, *Fundamentals of natural gas processing*. CRC press, 2011.
- [34] S. A. Ebenezer and J. Gudmunsson, "Removal of Carbon dioxide from natural gas for LPG production," *Semester project work*, 2005.
- [35] Y. J. Heintz, L. Sehabiague, B. I. Morsi, K. L. Jones, and H. W. Pennline, "Novel physical solvents for selective CO₂ capture from fuel gas streams at elevated pressures and temperatures," *Energy Fuels*, vol. 22, no. 6, pp. 3824-3837, 2008.
- [36] Y. J. Heintz, L. Sehabiague, B. I. Morsi, K. L. Jones, D. R. Luebke, and H. W. Pennline, "Hydrogen sulfide and carbon dioxide removal from dry fuel gas streams using an ionic liquid as a physical solvent," *Energy Fuels*, vol. 23, no. 10, pp. 4822-4830, 2009.
- [37] M. Götz, F. Ortloff, R. Reimert, O. Basha, B. I. Morsi, and T. Kolb, "Evaluation of organic and ionic liquids for three-phase methanation and biogas purification processes," *Energy Fuels*, vol. 27, no. 8, pp. 4705-4716, 2013.
- [38] O. M. Basha, M. J. Keller, D. R. Luebke, K. P. Resnik, and B. I. Morsi, "Development of a conceptual process for selective CO₂ capture from fuel gas streams using [hmim][Tf₂N] ionic liquid as a physical solvent," *Energy Fuels*, vol. 27, no. 7, pp. 3905-3917, 2013.
- [39] O. M. Basha, Y. J. Heintz, M. J. Keller, D. R. Luebke, K. P. Resnik, and B. I. Morsi, "Development of a conceptual process for selective capture of CO₂ from fuel gas streams using two TEGO ionic liquids as physical solvents," *Industrial Engineering Chemistry Research*, vol. 53, no. 8, pp. 3184-3195, 2014.
- [40] S. H. Park, S. J. Lee, J. W. Lee, S. N. Chun, and J. B. Lee, "The quantitative evaluation of two-stage pre-combustion CO₂ capture processes using the physical solvents with various design parameters," *Energy*, vol. 81, pp. 47-55, 2015.
- [41] M. Taheri, C. Dai, and Z. Lei, "CO₂ capture by methanol, ionic liquid, and their binary mixtures: Experiments, modeling, and process simulation," *AIChE Journal*, vol. 64, no. 6, pp. 2168-2180, 2018.
- [42] D. Aaron and C. Tsouris, "Separation of CO₂ from flue gas: a review," *Separation Science Technology*, vol. 40, no. 1-3, pp. 321-348, 2005.
- [43] Y. Peng, B. Zhao, and L. Li, "Advance in post-combustion CO₂ capture with alkaline solution: a brief review," *Energy Procedia*, vol. 14, pp. 1515-1522, 2012.
- [44] K. P. Resnik, J. T. Yeh, and H. W. Pennline, "Aqua ammonia process for simultaneous removal of CO₂, SO₂ and NO_x," *International journal of environmental technology management*, vol. 4, no. 1-2, pp. 89-104, 2004.

- [45] W. M. Budzianowski, "Mitigating NH₃ vaporization from an aqueous ammonia process for CO₂ capture," *International journal of chemical reactor engineering*, vol. 9, no. 1, 2011.
- [46] V. Darde, K. Thomsen, W. J. Van Well, and E. H. Stenby, "Chilled ammonia process for CO₂ capture," *Energy Procedia*, vol. 1, no. 1, pp. 1035-1042, 2009.
- [47] F. Kozak, A. Petig, E. Morris, R. Rhudy, and D. Thimsen, "Chilled ammonia process for CO₂ capture," *Energy Procedia*, vol. 1, no. 1, pp. 1419-1426, 2009.
- [48] H. Benson, J. Field, and R. Jameson, "CO₂/sub 2/absorption: employing hot potassium carbonate solutions," *Chem. Eng. Prog.*, vol. 50, no. 7, 1954.
- [49] D. W. Savage, G. Astarita, and S. Joshi, "Chemical absorption and desorption of carbon dioxide from hot carbonate solutions," *Chemical Engineering Science*, vol. 35, no. 7, pp. 1513-1522, 1980/01/01/ 1980.
- [50] A. H. G. Cents, D. W. F. Brilman, and G. F. Versteeg, "CO₂ absorption in carbonate/bicarbonate solutions: The Danckwerts-criterion revisited," *Chemical Engineering Science*, vol. 60, no. 21, pp. 5830-5835, 2005/11/01/ 2005.
- [51] M. Ahmadi, V. G. Gomes, and K. Ngian, "Advanced modelling in performance optimization for reactive separation in industrial CO₂ removal," *Separation and Purification Technology*, vol. 63, no. 1, pp. 107-115, 2008/10/01/ 2008.
- [52] A. Aboudheir, P. Tontiwachwuthikul, and R. Idem, "Rigorous model for predicting the behavior of CO₂ absorption into AMP in packed-bed absorption columns," *Industrial engineering chemistry research*, vol. 45, no. 8, pp. 2553-2557, 2006.
- [53] F. Yi, H.-K. Zou, G.-W. Chu, L. Shao, and J.-F. Chen, "Modeling and experimental studies on absorption of CO₂ by Benfield solution in rotating packed bed," *Chemical Engineering Journal*, vol. 145, no. 3, pp. 377-384, 2009/01/01/ 2009.
- [54] K. A. Mumford *et al.*, "Post-combustion capture of CO₂: results from the solvent absorption capture plant at Hazelwood power station using potassium carbonate solvent," *Energy fuels*, vol. 26, no. 1, pp. 138-146, 2011.
- [55] H. Rangwala, B. Morrell, A. Mather, and F. Otto, "Absorption of CO₂ into aqueous tertiary amine/MEA solutions," *The Canadian Journal of Chemical Engineering*, vol. 70, no. 3, pp. 482-490, 1992.
- [56] Y. E. Kim, J. A. Lim, S. K. Jeong, Y. I. Yoon, S. T. Bae, and S. C. Nam, "Comparison of carbon dioxide absorption in aqueous MEA, DEA, TEA, and AMP solutions," *Bulletin of the Korean Chemical Society*, vol. 34, no. 3, pp. 783-787, 2013.
- [57] H. R. Godini and D. Mowla, "Selectivity study of H₂S and CO₂ absorption from gaseous mixtures by MEA in packed beds," *Chemical engineering research and design*, vol. 86, no. 4, pp. 401-409, 2008.
- [58] A. Chakma, A. Mehrotra, and B. Nielsen, "Comparison of chemical solvents for mitigating CO₂ emissions from coal-fired power plants," *Heat Recovery Systems CHP*, vol. 15, no. 2, pp. 231-240, 1995.

- [59] G. Versteeg, L. Van Dijck, and W. P. M. van Swaaij, "On the kinetics between CO₂ and alkanolamines both in aqueous and non-aqueous solutions. An overview," *Chemical Engineering Communications*, vol. 144, no. 1, pp. 113-158, 1996.
- [60] P. Danckwerts, "The reaction of CO₂ with ethanolamines," *Chemical Engineering Science*, vol. 34, no. 4, pp. 443-446, 1979.
- [61] G. F. Versteeg and W. P. M. Van Swaaij, "Solubility and diffusivity of acid gases (carbon dioxide, nitrous oxide) in aqueous alkanolamine solutions," *Journal of Chemical & Engineering Data*, vol. 33, pp. 29-34, 1988.
- [62] S. Xu, F. D. Otto, and A. E. Mather, "Physical properties of aqueous AMP solutions," *Journal of Chemical and Engineering Data*, vol. 36, pp. 71-75, 1991.
- [63] A. K. Saha, S. S. Bandyopadhyay, and A. K. Biswas, "Solubility and diffusivity of nitrous oxide and carbon dioxide in aqueous solutions of 2-amino-2-methyl-1-propanol," *Journal of Chemical and Engineering Data*, vol. 38, pp. 78-82, 1993.
- [64] A. K. Saha, S. S. Bandyopadhyay, and A. K. Biswas, "Kinetics of absorption of CO₂ into aqueous solutions of 2-amino-2-methyl-1-propanol," *Chemical Engineering Science*, vol. 50, pp. 3587-3598, 1995.
- [65] A. Aroonwilas and P. Tontiwachwuthikul, "High-efficiency structured packing for CO₂ separation using 2-amino-2-methyl-1-propanol (AMP)," *Separation and purification technology*, vol. 12, pp. 67-79, 1997.
- [66] G. Vázquez, E. Alvarez, J. M. Navaza, R. Rendo, and E. Romero, "Surface tension of binary mixtures of water+ monoethanolamine and water+ 2-amino-2-methyl-1-propanol and tertiary mixtures of these amines with water from 25 C to 50 C," *Journal of Chemical & Engineering Data*, vol. 42, pp. 57-59, 1997.
- [67] Y.-J. Chen and M.-H. Li, "Heat Capacity of Aqueous Mixtures of Monoethanolamine with 2-Amino-2-methyl-1-propanol," *Journal of Chemical & Engineering Data*, vol. 46, pp. 102-106, 2001.
- [68] J.-J. Ko, T.-C. Tsai, C.-Y. Lin, H.-M. Wang, and M.-H. Li, "Diffusivity of nitrous oxide in aqueous alkanolamine solutions," *Journal of Chemical & Engineering Data*, vol. 46, pp. 160-165, 2001.
- [69] E. Álvarez, Á. Cancela, R. Maceiras, J. M. Navaza, and R. Táboas, "Surface tension of aqueous binary mixtures of 1-amino-2-propanol and 3-amino-1-propanol, and aqueous ternary mixtures of these amines with diethanolamine, triethanolamine, and 2-amino-2-methyl-1-propanol from (298.15 to 323.15) K," *Journal of Chemical & Engineering Data*, vol. 48, pp. 32-35, 2003.
- [70] A. Henni, J. J. Hromek, P. Tontiwachwuthikul, and A. Chakma, "Volumetric properties and viscosities for aqueous AMP solutions from 25 C to 70 C," *Journal of Chemical & Engineering Data*, vol. 48, pp. 551-556, 2003.
- [71] B. P. Mandal, M. Kundu, and S. S. Bandyopadhyay, "Physical solubility and diffusivity of N₂O and CO₂ into aqueous solutions of (2-amino-2-methyl-1-propanol+

- monoethanolamine) and (N-methyldiethanolamine+ monoethanolamine)," *Journal of Chemical & Engineering Data*, vol. 50, pp. 352-358, 2005.
- [72] H. Arcis, L. Rodier, and J.-Y. Coxam, "Enthalpy of solution of CO₂ in aqueous solutions of 2-amino-2-methyl-1-propanol," *The Journal of Chemical Thermodynamics*, vol. 39, pp. 878-887, 2007.
- [73] A. Chakraborty, G. Astarita, and K. Bischoff, "CO₂ absorption in aqueous solutions of hindered amines," *Chemical Engineering Science*, vol. 41, no. 4, pp. 997-1003, 1986.
- [74] S. Lee, H.-J. Song, S. Maken, H.-C. Shin, H.-C. Song, and J.-W. Park, "Physical solubility and diffusivity of N₂O and CO₂ in aqueous sodium glycinate solutions," *Journal of Chemical Engineering Data*, vol. 51, no. 2, pp. 504-509, 2006.
- [75] H.-J. Song, S. Lee, S. Maken, J.-J. Park, and J.-W. Park, "Solubilities of carbon dioxide in aqueous solutions of sodium glycinate," *Fluid Phase Equilibria*, vol. 246, no. 1-2, pp. 1-5, 2006.
- [76] S. Lee, H.-J. Song, S. Maken, and J.-W. Park, "Kinetics of CO₂ absorption in aqueous sodium glycinate solutions," *Industrial engineering chemistry research*, vol. 46, no. 5, pp. 1578-1583, 2007.
- [77] F. Harris, K. A. Kurnia, M. I. A. Mutalib, and M. Thanapalan, "Solubilities of carbon dioxide and densities of aqueous sodium glycinate solutions before and after CO₂ absorption," *Journal of Chemical Engineering Data*, vol. 54, no. 1, pp. 144-147, 2008.
- [78] S.-W. Park, Y.-S. Son, D.-W. Park, and K.-J. Oh, "Absorption of carbon dioxide into aqueous solution of sodium glycinate," *Separation Science Technology*, vol. 43, no. 11-12, pp. 3003-3019, 2008.
- [79] H.-J. Song *et al.*, "Simplified estimation of regeneration energy of 30 wt% sodium glycinate solution for carbon dioxide absorption," *Industrial Engineering Chemistry Research*, vol. 47, no. 24, pp. 9925-9930, 2008.
- [80] W. Zhao, Y. SHI, J.-w. WEI, and Q. YE, "Experimental study on CO₂ absorption and regeneration of aqueous sodium glycinate solutions," *Journal of Chemical Engineering of Chinese Universities*, vol. 22, pp. 690-695, 2008.
- [81] V. n. Salazar, Y. Sánchez-Vicente, C. Pando, J. A. Renuncio, and A. Cabañas, "Enthalpies of absorption of carbon dioxide in aqueous sodium glycinate solutions at temperatures of (313.15 and 323.15) K," *Journal of Chemical Engineering Data*, vol. 55, no. 3, pp. 1215-1218, 2009.
- [82] S. Mazinani, A. Samsami, A. Jahanmiri, and A. Sardarian, "Solubility (at low partial pressures), density, viscosity, and corrosion rate of carbon dioxide in blend solutions of monoethanolamine (MEA) and sodium glycinate (SG)," *Journal of Chemical Engineering Data*, vol. 56, no. 7, pp. 3163-3168, 2011.
- [83] M. Caplow, "Kinetics of carbamate formation and breakdown," *Journal of the American Chemical Society*, vol. 90, no. 24, pp. 6795-6803, 1968.

- [84] P. Blauwhoff, G. Versteeg, and W. P. M. Van Swaaij, "A study on the reaction between CO₂ and alkanolamines in aqueous solutions," *Chemical Engineering Science*, vol. 38, no. 9, pp. 1411-1429, 1983.
- [85] S. Laddha and P. Danckwerts, "Reaction of CO₂ with ethanolamines: kinetics from gas-absorption," *Chemical engineering science*, vol. 36, no. 3, pp. 479-482, 1981.
- [86] G. Versteeg and W. P. M. van Swaaij, "On the kinetics between CO₂ and alkanolamines both in aqueous and non-aqueous solutions—II. Tertiary amines," *Chemical engineering science*, vol. 43, no. 3, pp. 587-591, 1988.
- [87] G. Sartori and D. W. Savage, "Sterically hindered amines for carbon dioxide removal from gases," *Industrial Engineering Chemistry Fundamentals*, vol. 22, no. 2, pp. 239-249, 1983.
- [88] P. Kumar, J. Hogendoorn, G. Versteeg, and P. Feron, "Kinetics of the reaction of CO₂ with aqueous potassium salt of taurine and glycine," *AIChE Journal*, vol. 49, no. 1, pp. 203-213, 2003.
- [89] Available: <https://pubchem.ncbi.nlm.nih.gov/compound/700> (accessed on May 5, 2019)
- [90] Available: <https://pubchem.ncbi.nlm.nih.gov/compound/11807> (accessed on May 5, 2019)
- [91] Available: <https://pubchem.ncbi.nlm.nih.gov/compound/4684308> (accessed on May 5, 2019)
- [92] Available: <https://www.demisterpads.com/index.html>
- [93] P. Tontiwachwuthikul, A. Meisen, and C. J. Lim, "CO₂ absorption by NaOH, monoethanolamine and 2-amino-2-methyl-1-propanol solutions in a packed column," *Chemical Engineering Science*, vol. 47, no. 2, pp. 381-390, 1992.
- [94] R. E. Treybal, "Adiabatic gas absorption and stripping in packed towers," *Industrial Engineering Chemistry*, vol. 61, no. 7, pp. 36-41, 1969.
- [95] H. M. Feintuch and R. E. Treybal, "The design of adiabatic packed towers for gas absorption and stripping," *Industrial Engineering Chemistry Process Design Development*, vol. 17, no. 4, pp. 505-513, 1978.
- [96] G. Astarita, "Mass transfer with chemical reaction," 1967.
- [97] P. V. Danckwerts and A. Lannus, "Gas-liquid reactions," *Journal of The Electrochemical Society*, vol. 117, no. 10, pp. 369C-370C, 1970.
- [98] J. Pandya, "Adiabatic gas absorption and stripping with chemical reaction in packed towers," *Chemical Engineering Communications*, vol. 19, no. 4-6, pp. 343-361, 1983.
- [99] D. Sanyal, N. Vasishtha, and D. N. Saraf, "Modeling of carbon dioxide absorber using hot carbonate process," *Industrial engineering chemistry research*, vol. 27, no. 11, pp. 2149-2156, 1988.
- [100] P. Tontiwachwuthikul, A. Meisen, and C. J. Lim, "Novel pilot plant technique for sizing gas absorbers with chemical reactions," vol. 67, no. 4, pp. 602-607, 1989.

- [101] J. Gabrielsen, M. L. Michelsen, E. H. Stenby, and G. M. Kontogeorgis, "Modeling of CO₂ absorber using an AMP solution," *AIChE journal*, vol. 52, no. 10, pp. 3443-3451, 2006.
- [102] R. Wellek, R. Brunson, and F. Law, "Enhancement factors for gas-absorption with second-order irreversible chemical reaction," *The Canadian Journal of Chemical Engineering*, vol. 56, no. 2, pp. 181-186, 1978.
- [103] T. Sherwood and F. Holloway, "Performance of packed towers-liquid film data for several packings," *Trans Am. Inst. Chem. Engrs*, vol. 36, pp. 39-70, 1940.
- [104] D. Van Krevelen and P. Hoftijzer, "Kinetics of gas-liquid reactions part I. General theory," *Recueil des Travaux Chimiques des Pays-Bas*, vol. 67, no. 7, pp. 563-586, 1948.
- [105] K. Onda, H. Takeuchi, and Y. Okumoto, "Mass transfer coefficients between gas and liquid phases in packed columns," *Journal of chemical engineering of Japan*, vol. 1, no. 1, pp. 56-62, 1968.
- [106] D. Mohunta, A. Vaidyanathan, and G. Laddha, "Prediction of liquid phase mass transfer coefficients in columns packed with raschig rings," *Indian Chem. Eng.*, vol. 11, no. 3, pp. 73-9, 1969.
- [107] K. Akita and F. Yoshida, "Gas holdup and volumetric mass transfer coefficient in bubble columns. Effects of liquid properties," *Industrial Engineering Chemistry Process Design Development*, vol. 12, no. 1, pp. 76-80, 1973.
- [108] R. Billet and M. Schultes, "Prediction of mass transfer columns with dumped and arranged packings: updated summary of the calculation method of Billet and Schultes," *Chemical Engineering Research and Design*, vol. 77, no. 6, pp. 498-504, 1999.
- [109] G. A. Longo and A. Gasparella, "Experimental and theoretical analysis of heat and mass transfer in a packed column dehumidifier/regenerator with liquid desiccant," *International Journal of Heat and Mass Transfer*, vol. 48, no. 25, pp. 5240-5254, 2005/12/01/ 2005.
- [110] B. Hanley, B. Dunbobbin, and D. Bennett, "A unified model for countercurrent vapor/liquid packed columns. 2. Equations for the mass-transfer coefficients, mass-transfer area, the HETP, and the dynamic liquid holdup," *Industrial engineering chemistry research*, vol. 33, no. 5, pp. 1222-1230, 1994.
- [111] E. Brunazzi and A. Paglianti, "Liquid-Film Mass-Transfer Coefficient in a Column Equipped with Structured Packings," *Industrial & Engineering Chemistry Research*, vol. 36, no. 9, pp. 3792-3799, 1997/09/01 1997.
- [112] L. Raynal, J.-P. Ballaguet, and C. Barrere-Tricca, "Determination of mass transfer characteristics of co-current two-phase flow within structured packing," *Chemical Engineering Science*, vol. 59, no. 22, pp. 5395-5402, 2004/11/01/ 2004.
- [113] Y. Haroun, D. Legendre, and L. Raynal, "Direct numerical simulation of reactive absorption in gas-liquid flow on structured packing using interface capturing method," *Chemical Engineering Science*, vol. 65, no. 1, pp. 351-356, 2010/01/01/ 2010.
- [114] B. Hanley and C.-C. Chen, "New mass-transfer correlations for packed towers," vol. 58, no. 1, pp. 132-152, 2012.

- [115] C. J. Geankoplis, "Transport process and separation process principles," *New Jersey: Prentice-Hall*, 2003.
- [116] T. Sherwood, G. Shipley, and F. Holloway, "Flooding velocities in packed columns," *Industrial Engineering Chemistry*, vol. 30, no. 7, pp. 765-769, 1938.
- [117] S. Piché, F. Larachi, and B. P. A. Grandjean, "Flooding Capacity in Packed Towers: Database, Correlations, and Analysis," *Industrial & Engineering Chemistry Research*, vol. 40, no. 1, pp. 476-487, 2001/01/01 2001.
- [118] M. Leva, "Reconsider packed-tower pressure-drop correlations," *Chemical engineering progress*, vol. 88, no. 1, pp. 65-72, 1992.
- [119] H. Kister and D. Gill, "Predict flood point and pressure-drop for modern random packings," *Chemical Engineering Progress*, vol. 87, no. 2, pp. 32-42, 1991.
- [120] I. Kuźniewska-lach, "Estimation of phase velocities at flooding point in packed columns for any gas/liquid system," *The Canadian Journal of Chemical Engineering*, vol. 77, no. 3, pp. 439-446, 1999.
- [121] R. Billet and M. Schultes, "Fluid dynamics and mass transfer in the total capacity range of packed columns up to the flood point," *Chemical Engineering Technology: Industrial Chemistry-Plant Equipment-Process Engineering-Biotechnology*, vol. 18, no. 6, pp. 371-379, 1995.
- [122] R. Billet and M. Schultes, "A physical model for the prediction of liquid hold-up in two-phase countercurrent columns," *Chemical Engineering & Technology: Industrial Chemistry-Plant Equipment-Process Engineering-Biotechnology*, vol. 16, pp. 370-375, 1993.
- [123] R. Billet and M. Schultes, "Predicting mass transfer in packed columns," *Chemical Engineering Technology: Industrial Chemistry-Plant Equipment-Process Engineering-Biotechnology*, vol. 16, no. 1, pp. 1-9, 1993.
- [124] F. Heymes, P. Manno Demoustier, F. Charbit, J. Louis Fanlo, and P. Moulin, "Hydrodynamics and mass transfer in a packed column: Case of toluene absorption with a viscous absorbent," *Chemical Engineering Science*, vol. 61, no. 15, pp. 5094-5106, 2006/08/01/ 2006.
- [125] J. Stichlmair, J. Bravo, and J. Fair, "General model for prediction of pressure drop and capacity of countercurrent gas/liquid packed columns," *Gas SeparationPurification*, vol. 3, no. 1, pp. 19-28, 1989.
- [126] D.-Y. Peng and D. B. Robinson, "A new two-constant equation of state," *Industrial Engineering Chemistry Fundamentals*, vol. 15, no. 1, pp. 59-64, 1976.
- [127] R. C. Reid, J. M. Prausnitz, and B. E. Poling, "The properties of gases and liquids," 1987.
- [128] F. Herning and L. Zipperer, "Calculation of the viscosity of technical gas mixtures from the viscosity of the individual gases," *Gas u. Wasserfach*, vol. 79, p. 69, 1936.

- [129] T. A. Davidson, "Simple and accurate method for calculating viscosity of gaseous mixtures," 1993.
- [130] J. W. Buddenberg and C. R. Wilke, "Calculation of Gas Mixture Viscosities," *Industrial & Engineering Chemistry*, vol. 41, no. 7, pp. 1345-1347, 1949/07/01 1949.
- [131] A. L. Lindsay and L. A. Bromley, "Thermal Conductivity of Gas Mixtures," *Industrial & Engineering Chemistry*, vol. 42, no. 8, pp. 1508-1511, 1950/08/01 1950.
- [132] A. Eucken, "Über das Wärmeleitvermögen, die spezifische Wärme und die innere Reibung der Gase," *Phys. Z*, vol. 14, no. 8, pp. 324-332, 1913.
- [133] E. N. Fuller, P. D. Schettler, and J. C. Giddings, "New method for prediction of binary gas-phase diffusion coefficients," *Industrial Engineering Chemistry*, vol. 58, no. 5, pp. 18-27, 1966.
- [134] D. F. Fairbanks and C. R. Wilke, "Diffusion Coefficients in Multicomponent Gas Mixtures," *Industrial & Engineering Chemistry*, vol. 42, no. 3, pp. 471-475, 1950/03/01 1950.
- [135] S. Laddha, J. Diaz, and P. Danckwerts, "The N₂O analogy: the solubilities of CO₂ and N₂O in aqueous solutions of organic compounds," *Chemical Engineering Science*, vol. 36, no. 1, pp. 228-229, 1981.
- [136] A. K. Saha, S. S. Bandyopadhyay, and A. K. Biswas, "Solubility and diffusivity of nitrous oxide and carbon dioxide in aqueous solutions of 2-amino-2-methyl-1-propanol," *Journal of Chemical Engineering Data*, vol. 38, no. 1, pp. 78-82, 1993.
- [137] C. Wilke and P. Chang, "Correlation of diffusion coefficients in dilute solutions," *AIChE Journal*, vol. 1, no. 2, pp. 264-270, 1955.
- [138] J. Gabrielsen, M. L. Michelsen, E. H. Stenby, and G. M. Kontogeorgis, "A model for estimating CO₂ solubility in aqueous alkanolamines," *Industrial engineering chemistry research*, vol. 44, no. 9, pp. 3348-3354, 2005.
- [139] H.-J. Song *et al.*, "Simplified estimation of regeneration energy of 30 wt% sodium glycinate solution for carbon dioxide absorption," *Industrial & Engineering Chemistry Research*, vol. 47, pp. 9925-9930, 2008.
- [140] O. A. Alduchov and R. E. Eskridge, "Improved Magnus form approximation of saturation vapor pressure," *Journal of Applied Meteorology*, vol. 35, no. 4, pp. 601-609, 1996.
- [141] E. Toolbox. *Water-Heat of Vaaporization*. Available: https://www.engineeringtoolbox.com/water-properties-d_1573.html
- [142] A. K. Chakraborty, G. Astarita, and K. B. Bischoff, "CO₂ absorption in aqueous solutions of hindered amines," *Chemical Engineering Science*, vol. 41, no. 4, pp. 997-1003, 1986/01/01/ 1986.
- [143] S.-W. Park, Y.-S. Son, D.-W. Park, and K.-J. Oh, "Absorption of Carbon Dioxide into Aqueous Solution of Sodium Glycinate," *Separation Science and Technology*, vol. 43, no. 11-12, pp. 3003-3019, 2008/08/08 2008.

- [144] S. Lee, H.-J. Song, S. Maken, and J.-W. Park, "Kinetics of CO₂ Absorption in Aqueous Sodium Glycinate Solutions," *Industrial & Engineering Chemistry Research*, vol. 46, no. 5, pp. 1578-1583, 2007/02/01 2007.
- [145] A. K. Saha, S. S. Bandyopadhyay, and A. K. Biswas, "Kinetics of absorption of CO₂ into aqueous solutions of 2-amino-2-methyl-1-propanol," *Chemical Engineering Science*, vol. 50, no. 22, pp. 3587-3598, 1995.
- [146] T. H. Chilton and A. P. Colburn, "Mass Transfer (Absorption) Coefficients Prediction from Data on Heat Transfer and Fluid Friction," *Industrial & Engineering Chemistry*, vol. 26, no. 11, pp. 1183-1187, 1934/11/01 1934.
- [147] R. Taylor and R. Krishna, *Multicomponent mass transfer*. John Wiley & Sons, 1993.
- [148] F. A. Aly and L. L. Lee, "Self-consistent equations for calculating the ideal gas heat capacity, enthalpy, and entropy," *Fluid Phase Equilibria*, vol. 6, no. 3-4, pp. 169-179, 1981.
- [149] J. Hilsenrath *et al.*, "Tables of thermal properties of gases' NBS Circular 564," *National Bureau of Standards*, 1955.
- [150] (June, 2019). *NIST ThermoData Engine* Available: <https://trc.nist.gov/tde.html>
- [151] *Viscosity of Gases*. Available: <http://hyperphysics.phy-astr.gsu.edu/hbase/Kinetic/visgas.html>
- [152] R. Nuttall and D. Ginnings, "Thermal conductivity of nitrogen from 50 to 500 C and 1 to 100 atmospheres," *Journal of Research of the National Bureau of Standards*, vol. 58, no. 5, p. 271, 1957.
- [153] *Thermal Conductivity of Air*. Available: http://bouteloup.pierre.free.fr/lica/phythe/don/air/air_k_plot.pdf
- [154] A. Henni, J. J. Hromek, P. Tontiwachwuthikul, and A. Chakma, "Volumetric properties and viscosities for aqueous AMP solutions from 25 C to 70 C," *Journal of Chemical Engineering Data*, vol. 48, no. 3, pp. 551-556, 2003.
- [155] G. Vázquez, E. Alvarez, J. M. Navaza, R. Rendo, and E. Romero, "Surface tension of binary mixtures of water+ monoethanolamine and water+ 2-amino-2-methyl-1-propanol and tertiary mixtures of these amines with water from 25 C to 50 C," *Journal of Chemical Engineering Data*, vol. 42, no. 1, pp. 57-59, 1997.
- [156] Y.-J. Chen, M.-H. Li, and E. Data, "Heat Capacity of Aqueous Mixtures of Monoethanolamine with 2-Amino-2-methyl-1-propanol," *Journal of Chemical & Engineering Data*, vol. 46, no. 1, pp. 102-106, 2001.
- [157] D. R. Lide and H. V. Kehiaian, *CRC handbook of thermophysical and thermochemical data*. Crc Press, 1994.
- [158] O. Redlich and A. Kister, "Algebraic representation of thermodynamic properties and the classification of solutions," *Industrial Engineering Chemistry*, vol. 40, no. 2, pp. 345-348, 1948.

- [159] S. Lee, H.-J. Song, S. Maken, H.-C. Shin, H.-C. Song, and J.-W. Park, "Physical Solubility and Diffusivity of N₂O and CO₂ in Aqueous Sodium Glycinate Solutions," *Journal of Chemical & Engineering Data*, vol. 51, no. 2, pp. 504-509, 2006/03/01 2006.
- [160] S. Lee *et al.*, "Physical properties of aqueous sodium glycinate solution as an absorbent for carbon dioxide removal," *Journal of Chemical Engineering Data*, vol. 50, no. 5, pp. 1773-1776, 2005.